INVESTIGATING THE IN-SITU PRODUCTION AND PROCESSING OF AQUATIC FLUORESCENT ORGANIC MATTER BY FRESHWATER BACTERIA

Eva Mari Perrin BSc (Hons)

A thesis submitted in partial fullfillment of the requirements of the University of the West of England, Bristol for the degree of Doctor of Philosophy

School of Applied Sciences, University of the West of England, Bristol

2023

Abstract

Dissolved organic matter (DOM) is one of the largest reservoirs of carbon on the planet, and is ubiquitous throughout aquatic systems. It plays an essential role in global biogeochemical cycles and the transport and storage of carbon through the hydrological continuum. Intensifying anthropogenic pressures such as sewage discharge and agricultural runoff and impacting on microbial activity in freshwaters. As such, the interface between microbial activity and the processing of essential nutrients such as DOM is becoming increasingly complex, with potentially profound implications on the fate and transport of aquatic DOM. There is a need to advance our understanding of the mechanisms that underpin aquatic DOM processing my microorganisms, and the ways in which they are being impacted by anthropogenic pressures, alongside developing and implementing technological solutions to monitor this effectively through time and space.

Aquatic DOM is often 'fingerprinted' using the optical properties of its fluorescing component, aquatic fluorescent dissolved organic matter (AFOM), which is conventionally divided into 'autochthonous' (in-situ produced, labile, protein-like) and 'allochthonous' (terrestrially-derived, recalcitrant, humic-like) fractions. Peak T has conventionally been used as a biological marker for bacterial enumeration or contamination in freshwaters. To further explore the origin of bacterial-derived AFOM in freshwaters, this research utilizes findings from experimental studies enabling controlled observations of underpinning DOM processing dynamics. Through the development of a novel laboratory-based simulated freshwater model, this study provides evidence of the in-situ production of humic-like, complex AFOM from a simple bioavailable carbon substrate. The model laboratory system provides evidence that the effect of nutrients on freshwater bacterial processing can influence type of AFOM produced by bacteria. Furthermore, this study evidences a direct link between AFOM production and biological activity, underscoring the use of fluorescence as a biological marker for an upregulated metabolic state in freshwater bacteria. This research challenges current assumptions regarding the contribution of bacteria to the freshwater OM pool, and suggests that disruption of aquatic systems may be altering the balance of labile vs recalcitrant OM in aquatic systems.

In addition, the implementation of a novel fluorescence-based sensor is investigated on the River Thames and Taplow, Maidenhead, UK. A long-term (16 month) monitoring programme was undertaken, with fluorescence monitored at hourly intervals alongside conventional water quality parameters. This has highlighted the use of fluorescence as an efficient marker for in-stream biological activity, showing that this multi-channel fluorescence-based sensor can differentiate between algal and bacterial activity in the Tryptophan fluorescence region.

Acknowledgements

Firstly, I would like to extend a special thank you to my supervisor, Professor Darren Reynolds, for your support and guidance throughout my project. In particular, for being the source of new ideas and inspiration, and for teaching me that research is about both creativity and the scientific method, in equal measure (and in my case, a bit of quantum mechanics). Further thanks must go to the rest of my supervisory team; Associate Professor Robin Thorn, for invaluable support with microbiology (always delivered with an unmatched eye for detail), Dr Stephanie Sargeant, for help seeing things through the wide and wonderful lens of a biogeochemist, and Dr John Attridge, for your support and extensive technical expertise in the world of fluorosensors.

I would like to acknowledge both Chelsea Technologies Ltd. and the University of the West of England as the funders of this PhD studentship. Further thanks must also be given to the non-academic partners and stakeholders who provided guidance and collaboration through the project's duration; Chelsea Technologies Ltd, the Environment Agency, and the Westcountry Rivers Trust in particular. In addition, I am grateful to the technical and academic staff at UWE for support both in the lab and out.

To the rest of my colleagues in our research group at UWE; thank you for always lending a friendly ear, or hand, any time I needed it, often via our after-work Friday beers at the SU. In particular, Dr Bethany Fox, thank you for being a mentor since back when I was a fledgling researcher as an undergraduate student (and sorry for smashing your cuvette into tiny pieces the first time I shared your lab bench). Also, Gill, Lizzy, Alex, Becca. You all made 2K6 and 2G5 a slightly less insanity-inducing place to spend my days (and nights). Speaking of nights, it wouldn't do to go without mentioning Annie the Aqualog, often my only companion during long sleepless experiments in 2G5 spent babysitting my *Pseudomonas* flasks.

Now to my friends at UWE. You were, and still are, more than just friends; you are a community, a safety net, a source of inspiration and endless laughter, a shoulder to cry on, a network of minds with a bizarrely broad yet specific range of knowledge and skills that collectively is unstoppable at pub quizzes, you are a family. It really is something to be able to say that I have made friends who know me inside out, who will have my back no matter what, probably for the rest of my life. Thank you Buff and Marina, for your humour and vibrancy. Angeliki, the best Greek, thank you for the lockdown bike rides, film marathons with late-night *Boromir* overconsumption, and reminiscing about our respective mountains. Josie, my Welsh sister, for being a beacon of strength and for your endless wisdom, often delivered whilst sat out to sea amongst the waves. Dan, I don't think I've ever laughed as much as I do when we're sat debating something over a pint (or five). And Josh, thank you for teaching me everything you know about microbiology… and I *suppose* I should probably also express the endless

gratitude I have for our surf adventures which brought my so much joy over the PhD years and beyond. The support you have shown me both in and out of the university is something I will never take for granted. By extension, I should probably thank Freddie for the laughs and being a troublesome yet hilarious office companion (until you got banned, which was probably fair enough).

As for my friends outside of UWE, thank you for your enduring friendship through time and distance, and for your patience when sometimes it probably seemed like the PhD consumed my life a bit (it did). Fy ffrindiau Cymraeg, Hannah, Mais, Ailsa and others – diolch. A truly special thanks must go to Taz, though. I will never be able to do enough to repay you for your patience when I had low days, for all of the dinners you cooked me when I came home late from the lab, for the grounding chats, the dancing to tunes in the kitchen. Those long days in the flat through lockdown were tough in the middle of the PhD, but it was never anything a tinny on the wall or stroll over the Mound couldn't solve. Thanks also to the wider community of wonderful nature and environment lovers in Bristol. In particular to the Conham girls, Becca, Em, Charlotte and Lindsey, and by extension the River Avon itself, thank you for connecting me with the value of community, of our blue spaces in cities, of the importance of connection to others through the shared joy of water… the true meaning and sparkle behind the PhD.

Most importantly, thank you to my family for always supporting me with whatever I choose to do. Dad, in particular, for not only passing on your determination and philosophy to work hard and push through, for always questioning things and for having a passion and fascination for science and facts, for putting things into perspective and reminding me what is really valuable in life, but more importantly for being the first person to instil in me a love for our Celtic waters, which is where all of this stemmed from really. Thank you for raising me amongst the wild Welsh winds, mountains, and rivers. A love for the natural world, in particularly the water, is the reason I chose to study Environmental Science and is the reason I am where I am today.

I suppose that leads me to my final thank-you. Diolch i'r afonydd Cymru, ac y nentydd Eryri, am rhoi ysbrydoliaeth ers oeddwn yn ifanc, ac diolch i'r mor Celtaidd (Cymraeg ac Kernewek) am fod yn cysur pan mae pethau yn anodd. Diolch o fy nghalon!

Table of contents

List of figures

List of tables

Chapter 1. Introduction

1.1. Introduction

Freshwater, whilst accounting for just three per cent of all water on Earth (Firth, 1999), is integral to human activities such as agriculture and industry, as well as maintaining healthy ecosystems which are required for ecosystem services, processes and functions (Norris & Thoms, 1999). The value of freshwater resources to humanity is garnering national and international recognition, with the formation of the United Nations Sustainable Development Goals (SDGs) in 2015 recognising the restoration and protection of inland freshwater ecosystems as a priority within SDG 6: Clean Water and Sanitation in their 2030 agenda for sustainable development. Increasing pressure on freshwater resources due to urban expansion, agricultural industrialization, and population growth is placing unprecedented strain on global freshwater health and biodiversity (Darwall et al., 2018). Alongside an increased need for use and abstraction of freshwater resources, there is increased pressure from pollution sources. In 2018, the European Environment Agency report on the status of European waters found that only 40% of surface waters had Good ecological status or potential, with 38% impacted by diffuse pollution such as agriculture (Woodward et al., 2012). In England, the latest classification status assessment found that only 16% of surface waters achieved Good ecological status (Environment Agency, 2020).

At present, freshwater systems are monitored using infrequent and discrete sampling that utilises laboratory techniques, requiring lengthy wait times before data is acquired. As a result, this approach does not provide a detailed insight into the dynamism of freshwater systems, hindering our ability to identify perturbations or accurately predict future trends (Blaen et al., 2016). Such dysfunctionality cannot provide the basis for effective water quality and basin management planning. The parameters commonly relied on to inform freshwater quality information are often physicochemical measurements and macrobiological indexes. Whilst these parameters can provide basic information about the physicochemical status of a water body, or a snapshot of the community structure of aquatic macrophytes or invertebrates, there is a lack of understanding as to the underpinning microbiological dynamics of freshwater systems (Anderson et al., 2019). The development and implementation of in-situ, real-time technologies to monitor these dynamics would provide an insight into the interface between the biotic and abiotic processes which are occurring in freshwaters that ultimately form the foundations of ecosystem function within these environments.

The need for such insights has focused research in this area into further understanding organic matter (OM) processes and dynamics in aquatic systems, and utilizing its inherent fluorescing characteristics to trace OM origins and fluxes throughout the hydrological continuum. Aquatic OM is largely

heterogeneous in nature, and is influenced by the surrounding catchment characteristics such as geomorphology, soil chemistry, ecological diversity, and pollution inputs (Bright et al., 2020; Coble et al., 2014), in addition to processing by microorganisms (Battin et al., 2008). Due to the inherent fluorescence characteristics of aquatic fluorescent organic matter (AFOM), OM origins, fluxes and compositions from freshwater sources to ocean systems can be studied and also used to track pollution events (Baker, 2002; Baker et al., 2003; Carstea et al., 2010, 2014, 2016; Carstea, 2012). AFOM is classified using specific peak nomenclature, recently defined by Coble et al., 2014. This nomenclature is based upon the presence of observed fluorescence peaks aligned with optical regions associated with standard materials from known fluorescent compounds. Conventionally, AFOM has been divided into two discrete categories known as "autochthonous", which describes material affiliated with microbially-derived, protein-like compounds and "allochthonous", which refers to terrestrially-derived material present in aquatic systems which has originated from the surrounding catchments. Such material is usually present in the form of recalcitrant humic or fulvic acids.

Previous AFOM research has primarily focused on the observation of protein-like fluorescence, found within the 'Peak T' region of the fluorescence spectra, due to the presence of intracellular and extracellular proteins within wastewater (Ahmad & Reynolds, 1995; Carstea et al., 2016; Hudson et al., 2007; Reynolds, 2003; Reynolds & Ahmad, 1997; Vasel & Praet, 2002; Wu et al., 2006). More recent work has focused on exploring the relationship between AFOM and microbial enumeration in aquatic systems, derived from reported relationships between Peak T fluorescence and prevalence of pathogenic microorganisms such as *Escherichia coli* (*E. coli*) in certain environments such as groundwaters (Hudson et al., 2008; Sorensen et al., 2015, 2018, 2020). Some studies in marine environments (Kinsey et al., 2018; Shimotori et al., 2009; Yamashita et al., 2008; Yamashita & Tanoue, 2004), and more recently in freshwater environments (Berggren et al., 2020; Fox et al., 2017, 2021; Guillemette & del Giorgio, 2012; Perrin et al., 2022) have sought to investigate the relationship between AFOM signatures and microbial processing and production and have found the direct production of protein-like and humic-like AFOM. This suggests that microbes can produce AFOM in-situ which was previously considered to be allochthonous and terrestrially derived. If this is true, it could provide an insight into the role that microorganisms play in the carbon cycle, suggesting that we have until now significantly underestimated the scale of the contribution of microbes to OM production, processing and storage throughout the aquatic continuum.

Despite the presence of a vast body of literature investigating AFOM, there remains a dearth of knowledge with regards to the fundamental processes which underpin AFOM production in freshwater environments. This includes the impact of point and non-point source pollution, such as agricultural runoff, industrial waste effluents and untreated wastewater, on microbial OM processing

and the subsequent effect on AFOM characteristics. The uptake of existing fluorescence-based sensor technologies for in-situ AFOM monitoring by governmental monitoring programmes and into water quality policy, and the integration of microbial OM processing dynamics into global carbon budgets, is limited due to this lack of knowledge of the microbial-AFOM relationship. This, in turn, is hampering the potential application of this knowledge and technology for improving our understanding of the impact of increasing anthropogenic pressures on our freshwater systems globally, and therefore our ability to manage and improve ecosystems at both a national and global level.

1.1.1. Research aims

The primary aim of this research was to investigate the relationship between microbial activity and AFOM in freshwaters, with a focus on the processing of carbon and the bacterial production of AFOM under varying nutrient conditions. The specific aims of this research were:

- To develop a biological model to investigate the impact of nutrients on microbial AFOM production in a controlled freshwater laboratory system
- To further unravel the relationship between AFOM and microbial metabolism and/or enumeration
- Further investigate the production of humic-like, "allochthonous" AFOM by freshwater bacteria in-situ and consider the impact of this on the flux of carbon through the hydrological continuum
- To implement a water quality monitoring programme using a novel in-situ fluorescence-based sensor alongside standard water quality parameters
- To assess the use of fluorescence as a novel water quality parameter for monitoring microbial activity in freshwater systems

1.2. The role of freshwaters in the global carbon cycle

Fluvial environments are known to play a crucial role in the global carbon cycle, transporting, transforming and storing 200 million tonnes of terrestrial organic carbon annually, representing a significant fraction of global annual terrestrial net ecosystem production (NEP) (Battin et al., 2008; Cole et al., 2007; Dudgeon, 2015; Hotchkiss et al., 2015). Much of this exists as dissolved organic matter (DOM), one of the largest reservoirs of carbon on the planet that is ubiquitous throughout aquatic environments (Bieroza & Heathwaite, 2015; Hedges, 1992), with significant large DOM pools in surface freshwaters representing important components of fixed and bioavailable carbon (Cole et al., 2007; Trimmer et al., 2012). Aquatic DOM is largely heterogeneous and can exist in varying forms, dependent on its origin. The fixing of carbon from the atmosphere during autotrophic primary

production by plants or microbes allows carbon to enter the biosphere and helps regulate the abundance of greenhouse gases in the atmosphere (Najjar et al., 2007), as well as providing a food-web base which underpins the whole ecosystem. There are two types of DOM commonly associated with natural surface freshwaters; humic-like materials, generally considered to be high molecular-weight compounds of terrestrial origin, and proteinaceous materials which are generated in-situ by bacterial metabolic activity (usually in recycling and formation processes) and released into the surrounding water during viral lysis or grazing (Coble, 1996; Coble et al., 2014; Hudson et al., 2007, 2008; Milbrandt et al., 2010; Reynolds, 2002, 2003). The quantity of allochthonous DOM generally increases during wetter seasons when there is a larger export of soil and plant material into streams from surrounding catchments and flood plains, and the quantity of autochthonous DOM generally increases during warmer periods when primary production is higher. The type and quantity of allochthonous DOM that is present in freshwater environments is reflective of the surrounding catchment (Coble et al., 2014). Its subsequent processing and transformation is related to the composition of the heterotrophic microbial community present within the system as well as river bed morphology, sediment composition, climate, hydrology and seasonal variations which in turn influence transport rates, retention time and interaction with biologically available surfaces (Battin et al., 2008). As such, there exists a unique balance within every aquatic system whereby the type and quantity of DOM undergoes cyclical transformations as a result of physicochemical, biological, meteorological and geological processes.

1.2.1. The microbial mediation of dissolved organic matter: the 'microbial carbon pump'

The impact of microbial processing on DOM characteristics is considerable, with some 0.35 Pg y^{-1} estimated to be respired to carbon dioxide across the global fluvial network (Battin et al., 2008; Trimmer et al., 2012). As such, microbes play a critical role in the mediation of essential nutrients which underpin food webs throughout the hydrological continuum and, indeed, on a global scale. Despite how significantly the mediation of global biogeochemical cycles relies on microbial processes in freshwater ecosystems, this relationship remains unresolved and not fully characterized (Battin et al., 2008; Cole et al., 2007; Dudgeon, 2015). Fluvial environments are, by nature, inherently dynamic and subject to great spatial heterogeneity, temporal variations, and influences from anthropogenic pollution inputs (Maranger et al., 2018). For this reason, the role of inland aquatic waters is rarely explicitly included in global carbon budgets, with these environments generally only considered as a 'pipe' of carbon transport from land to ocean (Battin et al., 2008; Cole et al., 2007; Najjar et al., 2007). However, the implications of the transformations and losses that occur en-route as a result of microbial autotrophic and heterotrophic processes are largely overlooked. Worryingly, this exclusion

has led to a large 'black box' of information regarding the role microorganisms play in driving in global biogeochemical cycles. Recent literature has highlighted this dearth of knowledge, with Cavicchioli et al. (2019) emphasizing the responsibility that microbes have in mediating the fundamental nutrients which underpin the resilience of all higher organisms globally. Indeed, were it not for the 'microbial loop', allochthonous DOM sources, which are generally considered to be the main source of organic carbon for many lentic and lotic ecosystems (Sigee & Wiley, 2005), would not be remineralized into readily bioavailable forms to be consumed by higher trophic levels (Dorado-García et al., 2014).

1.2.2. Pressures on inland waters

1.2.2.1. Agriculture

Over recent decades, the availability of reactive nitrogen species has greatly increased as a result of human activities, in addition to fertilizer application – including ammonia (NH_4) and phosphate (PO_4^{3-}), resulting in runoff into surface waters within surrounding catchments (Galloway *et al.,* 2003). Nitrates and phosphates are often the limiting nutrient to primary production in surface freshwaters (Correll, 1999; Li Zweifel et al., 1993; Prieto et al., 2016), resulting in increased rates of primary production and eutrophication in nutrient loaded environments. Non-point sources such as agriculture and industry are a major source of nitrate and phosphate pollution, contributing to algal blooms and often causing hypoxic conditions (Carpenter et al., 1998). According to the EU Water Framework Directive 2018 Assessment of status and pressures of European Waters (European Environment Agency, 2019), more than 60% of surface freshwaters do not achieve 'good' ecological status, and 38% are impacted by non-point source pollution pressures. The effects of this on microbial metabolism have only recently been tested for the first time (Kominoski et al., 2018; Manning et al., 2018), with field experiments demonstrating an increased rate of whole-stream metabolism with elevated nutrient concentrations. However, key questions remain as to the impact of this on the fundamental processing, production and consumption of OM as observed in a 2017 study Fox et al. Given the long-term implications of carbon cycling in relation to ecosystem health and global climate stability, further exploration is clearly required into the impact of land-use (industrialization, urbanization, intensive agriculture) on DOM cycling by all forms of microbial life in fluvial systems (Kominoski et al., 2018). In order to understand and prepare for the response of environmental microbial communities to global change scenarios and human-induced stresses, there is a need for the development of biological model systems to gain insight into these processes at a fundamental level (Cavicchioli et al., 2019), in tandem with novel analytical instruments to monitor this in the field.

1.2.2.2. Untreated sewage

In addition to diffuse, non-point source pollution, aquatic ecosystems in the UK also face immense pressure from point-source pollution. This often comes in the form of untreated wastewater released into aquatic environments through combined sewer overflows (CSOs), or storm overflows. In England and Wales, there are currently 60,577 consented effluent discharge sites for sewage discharges (Environment Agency, 2022). Of these, 25,859 are permitted to discharge untreated or unspecified sewage-related effluents specifically from water companies. Finally, 21,877 of these are discharged directly into freshwater and tidal rivers. The introduction of untreated sewage effluent into watercourses can elevate nutrient concentrations due to their tendency to contain high levels of nitrogen and phosphorus (van Puijenbroek et al., 2019; Xie et al., 2022) contributing to algal blooms and eutrophication events. In addition, untreated sewage effluent often contains high densities of faecal coliforms such as *E. coli*, with domestic sewage containing densities as high as the region of 8 Log_{10} CFU 100 mL^{-1} (Wu et al., 2016). Other pathogenic bacteria associated with human waste include Enterococci, Streptococci and Staphylococci, constituents of a total 60 organisms known to be present in untreated sewage which can be pathogenic to humans (Wu et al., 2016). Whilst this represents a clear risk to human sanitation and hygiene, the introduction of external, non-indigenous populations of microorganisms at high densities also disrupts the existing microbial species composition and ecological structure of the water body, with specific taxonomic groups having been found to proliferate *within* sewer systems, forming a unique microbial community structure that is distinct from the receiving watercourse (Mclellan et al., 2009). As such, untreated effluent represents a multifaceted pressure in its threat to both human and ecosystem health (Wear et al., 2021; Wear & Thurber, 2015).

1.3. Aquatic fluorescent organic matter

Within DOM research, there has been investigation into exploiting the intrinsic fluorescing properties of some types of aquatic fluorescent organic matter (AFOM) in order to characterise it using fluorescence spectroscopy techniques; (Carstea et al., 2014, 2016; Coble et al., 2014; Hudson et al., 2008; Khamis et al., 2018). Aquatic organic matter fluorescence arises from complex heterogeneous compounds of various molecular weights (Aiken, 2014; Hudson et al., 2008; Leenheer & Croué, 2003) that are present in natural waters (Coble, 1996; Coble et al., 2014; Milbrandt et al., 2010; Yamashita et al., 2008). The propensity of a molecule to fluoresce is directly related to its relaxation pathways from the excited state, thereby deeming the molecular structure of high importance when determining fluorescence ability and characteristics. Molecules which have efficient or rapid relaxation pathways (such as by thermal deactivation) are less likely to fluoresce than more rigid

aromatic molecules which have fewer degrees of rotational and vibrational freedom and are more likely to return to ground state via the fluorescence pathways (Aiken, 2014).

Molecules which are highly conjugated are also more likely to fluoresce due to the smaller gap between the ground and the excited state. In addition to the molecule's propensity to fluoresce, its structure also influences its unique excitation and emission maxima wavelengths (Aiken, 2014; Lakowicz, 2006). This allows the use of its spectra to determine the relative composition and intensity of fluorophores within a sample. Through this, AFOM can be easily characterised using Excitation-Emission Matrix (EEM) fluorescence spectroscopy, whereby the fluorescing signatures of a sample are displayed as a three-dimensional contour, or 'map' of optical space. This provides a rapid, sensitive and non-destructive technique for analysing AFOM characteristics (Baker & Inverarity, 2004; Hudson et al., 2007; Lakowicz, 2006; Reynolds, 2002) by generating a visual rendering of the relative AFOM constituents within a given sample. This technique has been used extensively for analysing wastewaters, agricultural waste and industrial waste effluents, hydrocarbons and organic pollution (Baker, 2002; Baker et al., 2003; Baker & Inverarity, 2004, Hudson et al., 2007, 2008). An example of a freshwater EEM is shown in Figure 1.1.

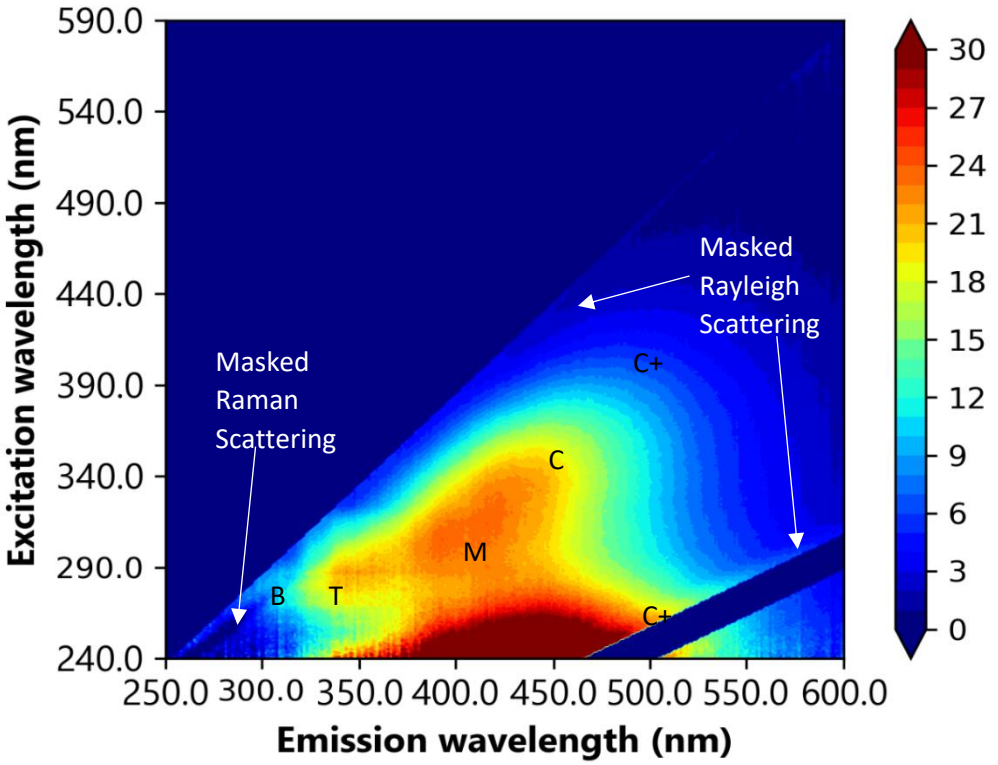

Figure 1.1. Excitation-emission matrix (EEM) from a freshwater source displaying common characterised fluorescence peaks (Coble et al., 2014) and blank-subtracted spectral features.

Both Raman and Rayleigh scatter have been masked to reduce spectral interference. Spectral scattering phenomena are often corrected for by using a blank subtraction (Hudson et al., 2007; Lakowicz, 2006; Carstea, 2012). Raman scattering is a result of the incident light causing vibrations in the covalent bonds between oxygen and hydrogen atoms in a water molecule (Hudson et al., 2007). Rayleigh scattering is a result of the reflection of the excitation energy, and can thus be seen: 1. Where emission and excitation wavelengths are equal and 2. Where the emission wavelength is double the excitation wavelength (Hudson et al., 2007). Light scattering is discussed in greater detail in section 1.4.1.

1.3.1. Peak nomenclature

The masking of spectral features using blank subtraction are a part of many other standard techniques that are used when assessing AFOM using EEM spectroscopy. One of these standard techniques is the more recent assigning of specific peak nomenclature to individual fluorescence peaks (Coble et al., 2014). Common fluorescence peaks can be seen in Figure 1.1. Peak nomenclature has historically represented a challenge due to the fact that overlapping fluorescence spectra make it difficult to identify discrete peaks, mostly owing to the composite nature of the mixture of compounds found within a given sample. As such, peak regions tend to shift along excitation and emission axes as a function of the relative distribution of compounds, in addition to matrix effects, solvent properties, and attenuation from physicochemical factors (Coble et al., 2014). Up until fairly recently, the consensus within the literature was to divide observed AFOM peaks into two discrete categories: humic-like and protein-like, based on the similarities of their optical profiles to that of material standards (Baker et al., 2003; Fellman et al., 2010; Leenheer & Croué, 2003). However, the complexity and heterogeneity of compounds within these two categories led to the development of a standardised peak nomenclature system (Coble et al., 2014), where peaks are given individual names (or letters) to classify them based on their identified excitation and emission wavelength maxima (Table 1.1).

Table 1.1. Common fluorescence peaks with associated nomenclature, wavelength peak maxima, and compound origin. Derived from Coble et al. (2014).

Peak Name	$\lambda_{ex}/\lambda_{em}$ (nm)	Fluorescence characteristics	Origin
A_B B	230/305 275/305	Tyrosine-like protein-like	Autochthonous, resembles tyrosine, possibly free/bound amino acids
A_T T	230/340 275/340	Tryptophan-like protein-like	Autochthonous, resembles tryptophan, often associated with microbial-related processes
A_M M	240/350-400 290-310/370-420	Humic-like	Allochthonous, originally identified & associated with marine environments, associated with microbial degradation processes
A_C C C+	260/400-460 320-365/420-470 250/470-504 385-420/470-505	Humic-like	Allochthonous, resembles humic acids, considered to be of terrestrial origin

1.3.2. "Protein-like" fluorescence

Protein-like fluorescence is an optical region of AFOM which is associated with microbiological activity and/or presence, and is characterised by its close resemblance to material standards of amino acids, specifically tyrosine and tryptophan. Phenylalanine is also a fluorescent amino acid but, due to its weakly fluorescent nature it is usually of little interest to DOM studies. Protein-like fluorescence is considered to sit within the optical region of the near to deep UV, with the excitation and emission maxima of tryptophan and tyrosine sitting at $\lambda_{ex}/\lambda_{em}$ 230-275/340 nm and $\lambda_{ex}/\lambda_{em}$ 230-275/305 nm respectively (Baker, 2002; Coble, 1996; Hudson et al., 2007; Wu et al., 2006; Zhu et al., 2017). These peaks are considered to have dual excitation maxima, though their usual positions within the literature are reported at λ_{ex} 275, with the λ_{ex} 230 peaks often not reported due to the interferences with instrument noise that often occurs within the deep-UV fluorescence region (Coble et al., 2014; Fox et al., 2017). The exact constituents that comprise the protein-like fluorescence region have been discussed in detail throughout the literature, with early studies having found direct correlations between protein-like AFOM intensity and the concentration of amino acids such as tyrosine and tryptophan using analytical chemistry techniques (Reynolds, 2003; Yamashita & Tanoue, 2003). However, other studies have suggested that there may be more complex compositional heterogeneity within the amino acids that make up the region, and that it may be comprised of a large composite of compounds with varying chemical structures that serve different ecological roles in natural waters (Coble et al., 2014; Maie et al., 2007).

1.3.2.1. Peak T fluorescence

Peak T fluorescence, also known as 'tryptophan-like fluorescence', is so-called due to its resemblance to the optical (fluorescence) properties of the tryptophan molecule. Due to its molecular structure – depicted in Figure 1.2 – tryptophan/Peak T is often the dominant emission profile within the protein-like fluorescence region. The relationship between Peak T and microbial presence and/or activity has received significant attention in the past 15 years (Carstea et al., 2016; Coble et al., 2014; Hudson et al., 2007, 2008; Sorensen et al., 2018). This has led to its identification as a proxy for microbial activity/presence in natural waters (Asmala et al., 2016; Sorensen et al., 2021), due to its associations with proteins which are considered indicative of microbial biomass or primary productivity. This has been further supported by statistically significant correlations seen within the literature between Peak T presence and biological oxygen demand (BOD) (Carstea et al., 2016; Hudson et al., 2007). However, recent research has challenged conventional theories on the nature of this process, further highlighting that there is much we still do not know. A 2017 study by Fox et al. found an increase in Peak T fluorescence intensity to occur without a direct correlation with cell density ubiquitously

among three monoculture species (*Escherichia coli, Pseudomonas aeruginosa, Bacillus subtillis)*. This could suggest that variations in Peak T fluorescence cannot readily be directly attributed to the enumeration of bacteria, but is more likely related to microbial activity/metabolism.

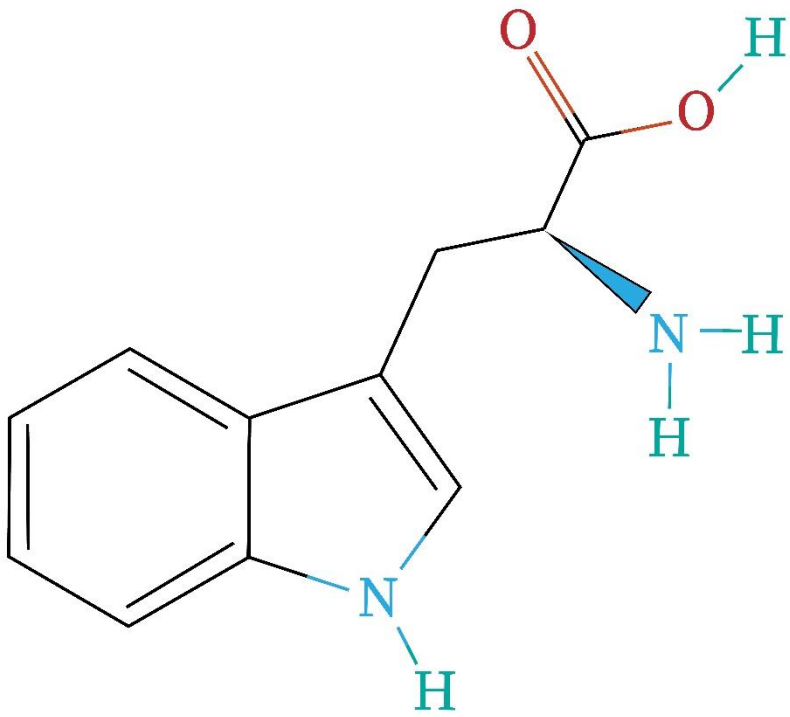

Figure 1.2. Molecular structure of the tryptophan molecule.

1.3.3. "Humic-like" fluorescence

Humic-like AFOM is generally associated with larger, more recalcitrant aromatic compounds, and is characterised as such due to its optical positioning being comparable with that of humic and fulvic acid materials (Coble, 1996; Yamashita et al., 2008; Zhu et al., 2017), although it is likely that they represent a composite mixture of compounds of varying size. Generally, they have been chemically evaluated as including compounds ranging from the 5-30 kDa range (Perminova et al., 2003), and have been named in the literature as Peaks A_C, C and C+ (Coble et al., 2014), with wavelengths at the following emission/excitation maxima: $\lambda_{ex}/\lambda_{em}$ 260/400-460, $\lambda_{ex}/\lambda_{em}$ 320-365/420-470, $\lambda_{ex}/\lambda_{em}$ 250/470-504, and $\lambda_{ex}/\lambda_{em}$ 385-420/470-505.

Outside of fluorescence-centric literature, there has been ongoing debate in recent decades pertaining to the ultimate origin and synthesis of humic substances within terrestrial environments. There lacks a commonly accepted definition of humic substances, with much debate centring around

whether humic substances are a complex entity derived from plant and animal substances, or are a unique class of compounds with characteristics without direct origin attributed to plant and animal material (Zavarzina et al., 2021). In particular, researchers are concerned with the role of extracellular secondary syntheses, and whether this plays a role in forming compounds that are entirely absent within the tissues of living organisms, or whether humic materials simply represent a less labile, more resistant constituent of the original material (Waksman, 1936; Bayeve and Wander, 2019; Lehmann and Kleber, 2015). The traditional view suggests that humic substances are simply a collection of high molecular weight macromolecules, but the new view proposed in 2015 by Lehmann and Kleber focuses on the potential of a continuum of organic fragments of varying sizes spanning from intact direct plant material to highly oxidized acids.

Despite ongoing debate pertaining to the ultimate source of humic substances in terrestrial environments, the compounds themselves are consistently viewed within the fluorescence, and freshwater, literature as being categorically of terrestrial origin, emanating from the breakdown of plant and soil material within surrounding catchments before being transported into aquatic systems during rainfall and runoff events (Hudson et al., 2007). However, recent publications have been shedding light on the nature of humic-like fluorescence in natural waters, and it is appearing increasingly likely that the binary nature of AFOM classification that has dominated the literature over the past two decades may have been misled.

The humic-like fluorescence peak is usually not associated with bacterial production, and whilst it is widely considered that most labile components of the DOM pool are generally proteinaceous and rapidly consumed in secondary production, the more recalcitrant, generally humic-like, fraction is considered to be of allochthonous origin and contributes to long-term storage, cycling/remineralization, and export to downstream ecosystems (Baker & Spencer, 2004; Coble et al., 2014; Elliott et al., 2006). However, recent research has proposed the theory that the presence of high molecular-weight, humic-like DOM in marine and terrestrial environments could be a direct consequence of *in-situ* bacterial metabolic activity (Kallenbach et al., 2016; Shimotori et al., 2010, 2012; Yamashita et al., 2004). Subsequent research by Fox et al. (2017; 2019) and Guillemette and Del Georgio (2012) further supports the notion that this may also occur in freshwater ecosystems, though this has not yet been observed to the same extent as within marine environments. If, as current evidence suggests, a portion of the DOM pool which we currently observe to be of allochthonous, terrestrial origin is bacterial in origin, this could have profound implications for the way we currently factor microbial processing in fluvial ecosystems into global carbon budgets and the role that we think they play in global carbon cycles. Any substantial changes in OM processing, degradation, or production will ultimately impact on atmospheric CO_2 concentrations and, therefore, climate. In

addition, the relative recalcitrance and/or bioavailability of fundamental organic nutrients such as DOM will alter the ways in which it is transported to organisms of higher trophic levels. The proposition that fluorescence intensity changes occur not only as a function of microbial presence, but of processing and metabolism independent of cell growth and replication, challenges our current assumptions regarding the relationship between microbes and AFOM characteristics (Fox et al., 2017; 2019) and suggests the role of bacteria in freshwater DOM processing may be underestimated.

1.4. The fluorescence process

Fluorescence constitutes one of a range of optical phenomena that sit under the collective umbrella of the term 'luminescence'. Luminescence is defined as the emission of radiation from an electronically or vibrationally excited species (Reynolds, 2014; Valeur & Berberan-Santos, 2011, 2013). Various types of luminescence exist and are classified by the excitation mode (chemiluminescence, bioluminescence, electroluminescence, photoluminescence and more). The latter – photoluminescence – is the term which encompasses both fluorescence and phosphorescence (Reynolds, 2014) and is defined as the emission of light as a result of "direct photoexcitation of the emitting species" (Braslavsky, 2007). Fluorescence as a phenomenon has been observed throughout history on many accounts, however in 1852 Sir George G. Stokes became the first to introduce the term "fluorescence" (Stokes, 1852) after observing and describing the light-emitting properties of the fluorescent fluorspar mineral, after which the phenomenon was subsequently named. Stokes also observed a phenomenon that became instrumental to our understanding of fluorescence; that is, that the light emitted by the fluorophore is consistently of a longer wavelength and lower energy than the incident light that is causing the molecule to fluoresce. This became known as Stokes' shift (Carstea et al., 2010; Reynolds, 2014; Valeur & Berberan-Santos, 2011).

The fluorescence process itself is underpinned by three fundamental steps: excitation, vibrational relaxation, and emission (Lakowicz, 2006; Reynolds, 2014). These processes are illustrated in Figure 1.2, a Jablonksi diagram that is commonly used to display a visual representation of the fluorescence process (Coble et al., 2014). A molecule enters an excited electronic state as a result of the absorption of radiation, which causes the excitation of an electron from the ground state of a molecule to an excited state, in a process called electronic transition (Reynolds, 2014). The relative delocalization of electrons in a molecule is the determinant of electronic transition, with more delocalized electrons requiring lower energy (i.e. longer wavelengths) for promotion to higher molecular orbitals. The increase in energy of the excited molecule corresponds to the energy of the absorbed photon (Equation 1.1):

$$E = h\nu = \frac{hc}{\lambda}$$

Where h is Planck's constant, nu (ν) and lambda (λ) are the frequency and wavelength of the radiation respectively, and c is the velocity of light. In order for electronic excitation to occur, E must correspond to the difference in energy between the ground electronic state and the electronically excited state in accordance with the discrete nature of quantized energy levels (Reynolds, 2014). The amount of radiation absorbed by the molecule is determined by the number of molecules in the path of the incident light, expressed through the Beer-Lambert's law (Equation 1.2):

$$I_t = I_0 \, exp^{-\epsilon cl}$$

Where I_t is the intensity of the transmitted light, I_0 is the intensity of the incident light, Є is the molar absorptivity (the propensity of the absorber to absorb light of a specified wavelength), c is the concentration of the absorber, and l is the sample path length.

After absorption and excitation have elevated the molecule to an excited electronic state, the next fundamental step in the fluorescence process is vibrational relaxation. This is a radiationless process whereby an excited molecule loses energy to the surrounding environment (for example, solvent molecules). The result of this process is that the molecule returns to a lower vibrational energy level within the same electronic state (Lakowicz, 2006; Reynolds, 2014). Vibrational relaxation is highly rapid and efficient, occurring over a timescale of picoseconds ($<10^{-12}$s), and as a result the fluorescence emission process itself usually occurs from the lowest excited state of a given vibrational energy level. Finally, fluorescence is able to occur during the return of the molecule to the original ground state, occurring over a timescale of nanoseconds ($<10^{-9}$ s). Ground state is shown in Figure 1.3 as S_0. Other forms of energy loss can occur during this period, such as internal conversion (where a molecule migrates from the ground vibrational level of an excited electronic state to a higher vibrational level of a lower electronic state) and external conversion (the loss of energy due to collision with the surrounding matrix, for example solvent molecules). Internal conversion is shown as the transition from S_2 to S_1 in Figure 1.3. The latter is often referred to as quenching, and can have an appreciable impact on the intensity of fluorescence signals. For molecules where the return to ground state via vibrational relaxation or internal conversion is improbable, and fluorescence is the most efficient means of relaxation, then the emission of a photon will occur. The wavelength of the emitted photon will be determined by the quantized difference between the excited and ground state, combined with

the effect of Stokes' shift caused by the loss of energy during the efficient decay processes described above.

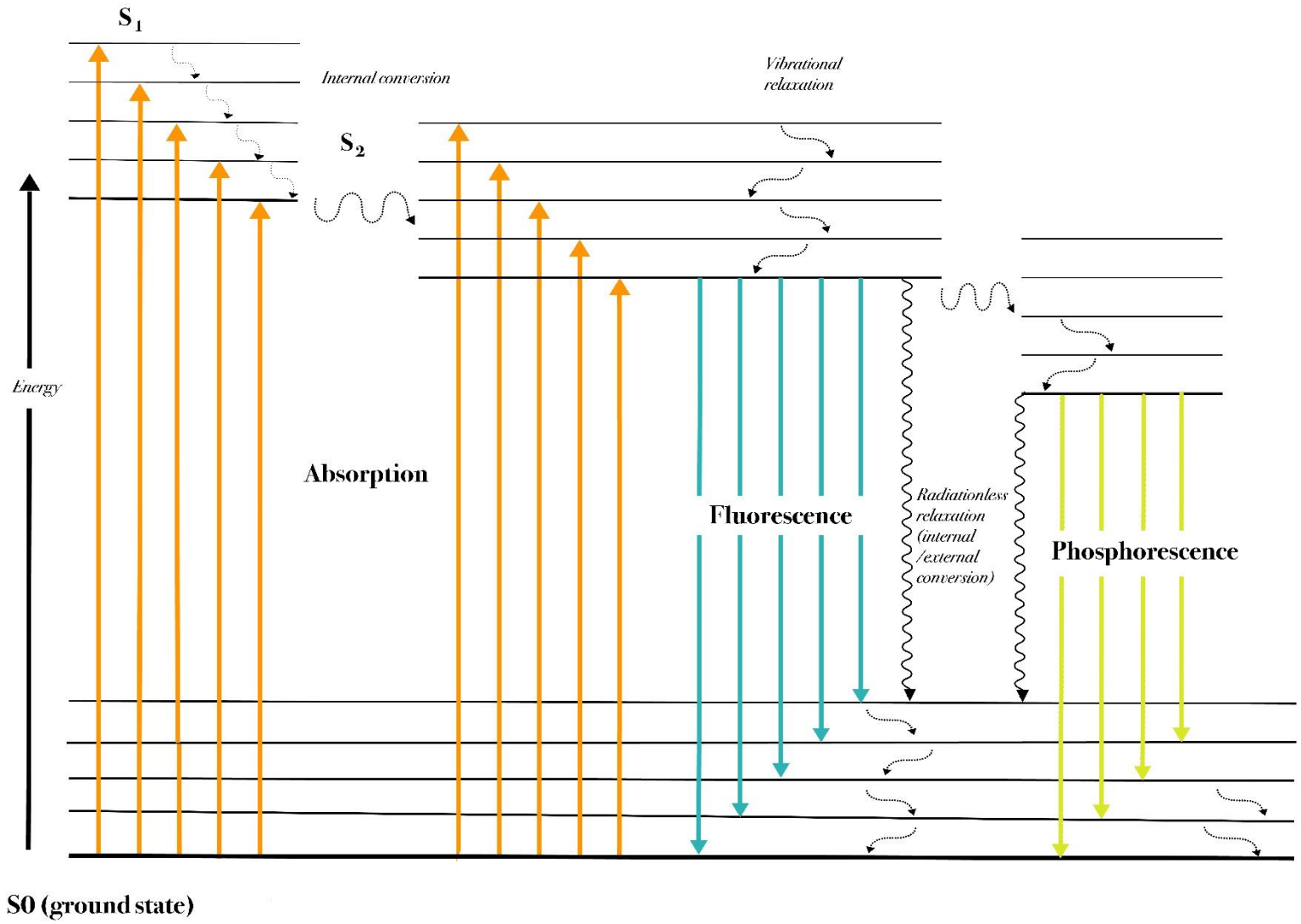

Figure 1.3. Jablonski diagram demonstrating the process of absorption, fluorescence and phosphorescence by fluorophores

1.4.1. Factors that can interfere with fluorescence signals and the fluorescence process

1.4.1.1. Light scattering

There are multiple types of radiation scattering which can occur during irradiation of a fluorophore. These can often be mistaken for, or interfere with, a fluorescence signal. As such, they are often masked using blank subtraction methods during post-processing analysis of data so as not to interfere with statistical analysis of fluorescence data. The three main forms of scattering that commonly occur are Rayleigh, Mie, and Raman (Reynolds, 2014). Rayleigh and Mie scattering are both forms of 'elastic' scattering; that is, they occur as a result of light scattering by an entity with an uneven refractive surface. This could be colloidal material, particulate matter, gas bubbles, or other forms of disruptions that are often present in natural matrices. There is no wavelength shift during this process, however the form of scattering will depend on the size of the entity in relation to the wavelength of light being scattered (Reynolds, 2014).

Raman scattering is different to Rayleigh-Mie in that it is known as an 'inelastic process', meaning that it involves some form of energy transfer resulting in the wavelength of scattered light being different to the wavelength of the incident light (Reynolds, 2014). As such, it is considered to be a less efficient process than Rayleigh-Mie scattering. Unlike the Stokes' shift which occurs during the fluorescence process, the difference in energy that occurs during Raman scattering can be either positive *or* negative, and corresponds with the difference between the two energy levels of the molecule (Bartlett et al., 1998). As such, it can be detected as a constant frequency difference when working with solvents with known spectral variability. Due to its predictability, it has been (and often still is) used as a reference point for normalising fluorescence spectra when working with aquatic fluorescence (Attermeyer et al., 2022; Baker, 2002; Baker & Inverarity, 2004; Ji et al., 2022; Lawaetz & Stedmon, 2009), although minor differences can be observed depending on the water type (i.e. fresh or seawater) (Bartlett et al., 1998).

1.4.1.2. Physicochemical effects

The physical and chemical characteristics of the matrix and/or solvent can significantly alter the characteristics and intensity of observed fluorescence signals. In the majority of cases, the intensity of the fluorescence signal is reduced or eliminated due to interaction between other chemical species which can increase the probability of the molecule returning to ground state through nonradiative pathways (Reynolds, 2014). This is known as 'fluorescence quenching'. Due to the ubiquitous nature of quenching, it is generally assumed that all environmental samples experience quenching to some

degree. However, there have been extensive studies investigating the impact of various types of quenching on DOM in natural waters.

One very common, and now well-understood, parameter that is known to cause quenching and that is also a variable in most aquatic matrices such as fresh and marine waters is pH. The pH has been found to impact the structure of the fluorophore through dissociation or protonation of acidic or basic functional groups within the fluorophore (Reynolds, 2014), causing a shift in fluorescence emission by up to 15% for pH values < 4.5, and as much as 30% at pH values > 8.3, though this is dependent on the specific fluorophore of interest (Reynolds, 2003).

Another notable quenching effect that is particularly important when analysing samples from natural waters is temperature. Most notably, temperature increase can lead to increased collision with solvent molecules within the surrounding matrix, causing the return of the fluorophore to ground state through nonradiative pathways (Baker, 2005; Lakowicz, 2006; Reynolds, 2014). Studies have specifically found that increased temperature leads to increased quenching, with protein-like fluorophores experiencing greater thermal quenching than humic or fulvic-like fluorophores, though this is believed to depend on the exposure of the fluorophore to the heat source (Baker, 2005).

Finally, photodegradation, or photobleaching, can also have an appreciable impact on fluorescence signals. Natural waters, for example, which are exposed to UV radiation can see significant changes in fluorophore characteristics depending on their irradiation period, UV intensity, and fluorophore composition (Mostofa et al., 2007). It was found that humic and fulvic acid-like DOM is more susceptible to photobleaching than protein-like DOM, and that the general impact of photodegradation sees a decrease in fluorescence intensity and a shift in emission maxima to shorter wavelengths in the blue-UV region (Coble, 1996; Mostofa et al., 2007).

1.4.1.3. Inner filter effects (IFE)

Inner filter effects (IFE) are important factors to consider when observing fluorescence spectra in natural waters. IFE occurs when the fluorescence signal is attenuated by the presence of a light-absorbing entity, for example the cuvette walls or by absorbing components within the sample matrix (Coble et al., 2014; Lakowicz, 2006). Natural waters can display significant variability in absorbance and turbidity (Bennett & Drikas, 1993). Both dissolved and particulate coloured substances in natural waters can absorb light, and in riverine environments with high turbulence and mixing potential causing the suspension of sediments in the water column, or waters with high concentrations of coloured DOM (such as peat-fed streams), there can be significant interference from absorption or scattering of emitted fluorescence (Saraceno et al., 2009). Therefore, it is often common practice when undertaking in-situ field-based fluorescence monitoring to account for these effects using

turbidity and absorbance corrections (Saraceno et al., 2017). During laboratory analysis of samples using benchtop fluorimeters, however, IFE is usually corrected for using the subtraction of a blank sample (Hudson et al., 2007; Lakowicz, 2006).

1.5. Monitoring of freshwater quality: Current state of play

1.5.1. Water quality policy and status in the UK

For over 20 years, surface water quality policy in the United Kingdom (UK) has been dictated by the assessment methods, classifications and milestones outlined within the "Directive 2000/60/EC of the European Parliament and of the Council establishing a framework for the Community action in the field of water policy, or Water Framework Directive" (WFD). Since its conception in October 2000 by the European Union (EU), the WFD has aspired towards a 'single system' of water quality management based upon the natural hydrogeological unit boundaries afforded by individual river basins, rather than bureaucratic, political or economic boundaries associated with states and countries. As such, all member states of the EU were required to develop River Basin Management Plans (RBMPs) with cross-border continuity, and abide by the objectives outlined in the WFD.

Following the exit of the UK from the European Union on 31st January 2020, many EU environmental legislations have been revoked and redrafted, including the WFD. Water quality policy in England and Wales now falls under the "Water Environment (Water Framework Directive) (England and Wales) regulations 2017", which came into force on 10th April 2017. The details of the Water Environment regulations are reflected in the classification and assessment systems that applied to the WFD, and therefore the two pieces of legislation are largely similar, including the designation of RBMPs.

The Water Environment assessment determines the classification of water bodies based on an array of physical, chemical and biological parameters which constitute two main statuses: Ecological status and Chemical status (Table 1.2). Overall status classification is determined through a variety of biological, chemical and physical water quality parameters and the presence of specific toxic pollutants. Assessments of water bodies must be carried out over at least a six-yearly cycle, with an associated RBMP developed in light of each assessment for each predetermined River Basin District alongside an official classification status. Within each assessment cycle, each water quality parameter has a specified sampling frequency. This can range from, for example, 1 survey per 6-year window for fish, to 12 samples per year for physico-chemistry. Ecological and Chemical status are then classified into a hierarchy based on water quality results. In total, there are six classifications for Ecological status: High, Good, Moderate, Poor, and Bad. Moderate and below are considered to be a 'fail' under

the WFD and Water Environment standards. For Chemical status, there are only two classifications: Pass and Fail.

The most recent round of water quality assessments in the UK was undertaken in 2019, and classification status was subsequently developed for all surface waters in 2020 based on these data. Prior to this, the previous assessment round was in 2015. Ecological status of surface freshwaters in England deteriorated between 2015 and 2020, showing a 1% decrease of the number of water bodies which met the Pass criteria. Chemical status, however, displayed a vast decrease in status, with the number of water bodies which meet the Pass criteria plummeting from 97% in 2015 to 0% in 2020. This is on account of a novel assessment method which came into place in 2019, which incorporated a wider variety of ubiquitous, persistent, bio-accumulative and toxic chemical substances into assessment criteria (Table 1.2). Individual values for classification statuses from both rounds of assessment for Ecological and Chemical statuses are available in Table 1.3.

At present, just 16% of surface freshwaters, and 14% of rivers, in England meet Good ecological status. 0% meet High status. In Wales, 40% of total water bodies and 44% of rivers meet Good, with 0% meeting High. In Scotland, 49% and 14% of total water bodies meeting Good and High respectively, and 47% and 8% of rivers meet High and Good respectively. In England, not one water body meets Good Chemical status. Rivers are consistently the lowest-scoring water body type throughout the UK (DEFRA, 2020). The UK Government's Department of Environment, Food and Rural affairs outlined in 2015 a goal to have all surface water bodies meet Good Ecological status by 2021, however this goal has since been revoked, with a new deadline outlined for 2027.

Table 1.2. Classification status components for surface freshwaters in the United Kingdom, adapted from the Environment Agency application of the UK Water Environment Legislation 2017

Status	Ecological				Chemical		
Component	Biological	Hydromorphological	Physico-chemical	Specific pollutants	Priority substances	Priority hazardous substances	Other pollutants
Element (parameter)	• Fish • Invertebrates • Angiosperms • Phytoplankto-n • Macrophytes • Macroalgae • Chironomids	• Hydromorphol-ogical regime • Morphology	• Ammonia • Total phosphorus • Phosphate • Total nitrogen • Dissolved inorganic nitrogen • Dissolved oxygen • pH • Salinity • Temperature	• Heavy metals (e.g. arsenic, copper, iron, zinc) • Glyphosphate • Cyanide • Phenol	• Herbicides, insecticides, pesticides (e.g. alachlor, atrazine, chlorfenvinph o-s, isoproturon) • Solvents (e.g. dichlorometh ane) • Polycyclic aromatic hydrocarbons (PAHs)	• Toxic PAHs (e.g. anthracene) • Toxic pesticides (e.g. endosulfan) • Mercury and associated compounds	• DDT • Industrial manufacturin g chemicals (e.g. tetrachloro-ethylene)

Table 1.3. Ecological and Chemical status classifications for surface waters in England between 2014 and 2020 (Department of Environment, Food and Rural Affairs, 2020)

	2015 (%)		2020 (%)	
	Ecological Status	Chemical Status	Ecological Status	Chemical Status
High	0	97 (P)	0	0 (P)
Good	17		16	
Moderate	63	3 (F)	64	100 (F)
Poor	17		17	
Bad	3		3	

1.5.2. Water quality monitoring using current methods

Water quality monitoring in the UK under the WFD and Water Environment assessment are largely focused around the structural bio-assessment indicators and physico-chemical parameters outlined in Table 1.2. Due to lack of regulatory requirement to integrate real-time, high-frequency in-situ measurements into water quality monitoring programmes, standard practice has involved discrete spot-sampling with laboratory-based assessment. This prevents the observation of fundamental ecosystem processes, and hinders the ability to capture pollution events as they occur in real-time. Additionally, discrete sampling provides only a 'snapshot' of water quality at a given time and location, which may not be representative of the true nature of a water body as it changes through time and space.

The standard practice of measuring the physico-chemical properties of surface waters alongside macrobiological communities has been studied extensively. For example, freshwater macroinvertebrate diversity, distribution and prevalence has been extensively investigated in relation to nutrients, heavy metals and other chemical pollutants (Dodson et al., 2000; Liess & Beketov, 2011; Pallottini et al., 2015; Xu et al., 2014). Whilst this can provide a detailed insight into the presence of specific toxic pollutants and their impact on species abundance and/or diversity of ecologically relevant invertebrate or fish communities, there is a significant lag phase between changes in chemical water quality parameters and the impact on macrobiological communities at an ecosystem scale. This can largely depend on the tolerance of specific species to environmental perturbations within their

habitat due to life cycle, feeding behaviours and other factors (Xu et al., 2014), and often the effect of pollution on individuals does not correspond to changes at a community level in a way which is readily detectable (Liess & Beketov, 2011; Pallottini et al., 2015). As such, macroinvertebrates, fish, and macrophytes, whilst providing a snapshot of the structure of an ecosystem, do not provide real-time insight into the functioning of an ecosystem.

The use of physico-chemical parameters to monitor water quality has been standard practice within environmental legislation for many years. Over the last decade, there has been significant developments in technological solutions for monitoring these parameters to greater degrees of specificity and sensitivity, with the increasing reliability of in-situ probes allowing the use of high-frequency remote telemetry equipment for intense time-series data throughput and large dataset collation at substantial temporal scales (Barker et al., 2022; Bowes et al., 2015; Geetha & Gouthami, 2017; Wade et al., 2012; Yaroshenko et al., 2020), providing the technological means of moving away from discrete spot-sampling. This high-frequency, long-term monitoring has revealed many patterns in the diurnal and seasonal variations that occur as a result of fundamental ecosystem processes in surface freshwaters (Halliday et al., 2015; Wade et al., 2012). However, limitations exist within the use of physico-chemical parameters to monitor the ecosystem health of freshwaters. For example, monitoring the concentration of harmful pollutants such as toxic industrial chemicals and nutrients provides insight into their presence, but does not provide information as to the impact of these inputs on fundamental ecosystem processes. The integration of these measurements with other parameters goes some way to uncovering their biological impacts; for example, dissolved oxygen (DO) concentration can be used to estimate variation in whole-stream metabolism (Riley & Dodds, 2013) or to monitor hypoxia-causing eutrophication events from algal blooms. However, there ultimately exists a disconnect between the information available on the biotic and abiotic functions of an ecosystem and their respective interplays.

1.5.3. The application of AFOM sensing technology for in-situ monitoring of freshwater

With fluorescence spectroscopy being increasingly employed to measure the presence and characteristics of AFOM, there have been significant technological improvements in optical sensitivity and instrument portability that have allowed fluorescence technology to be transported into the field (Baker et al., 2003; Carstea et al., 2010; Hudson et al., 2007; Sorensen et al., 2018). This has allowed the developments in real-time in-situ monitoring of water quality to extend to fluorescence, alongside other standard water quality parameters. Since the conception of portable fluorescence sensors (‘fluorosensors’), freshwater AFOM has been extensively investigated in regards to its optical properties, composition, sources, fate, and relative bioavailability/recalcitrance (Coble et al., 2014).

Much of freshwater AFOM research has focused on using Peak T to monitor microbial contamination events from wastewater effluents (Ahmad & Reynolds, 1995; Baker, 2002; Baker et al., 2003; Carstea et al., 2016; Reynolds, 2003; Sorensen et al., 2015, 2018, 2020; Vasel & Praet, 2002; Wu et al., 2006), or to examine wastewater treatment efficacy (Cohen et al., 2014). Research has also focused on using fluorescence to trace diffuse agricultural pollution in waterways (Naden et al., 2010). Fluorescence has been used to trace aquatic OM through space and time for monitoring storm events, residence time and other hydrological controls (Kothawala et al., 2014; Miller & McKnight, 2010).

More recently, a growing body of literature has been focusing on the use of AFOM to monitor microbial biogeochemical processes in freshwaters such as OM mineralisation, ecosystem metabolism and respiration, and bacterial production (Berggren et al., 2020; Guillemette et al., 2012; Kinsey et al., 2018; Sjöstedt et al., 2021). These studies have shed light on the apparent ambiguity associated between perceived allochthonous and autochthonous OM sources in freshwater systems, suggesting that the long-held belief that these two OM elements exist in a binary state may be less definitive than previously thought. They also show that AFOM can provide an insight into the underpinning ecological functioning of freshwater systems, potentially bridging the divide between the biotic and abiotic spheres by shedding light on the interface between the living and non-living world.

1.6. Summary: Key research gaps

Despite the large body of research that has been undertaken investigating fluorescence characteristics of natural waters and AFOM production by microbes, there still exists significant research gaps within the literature which need to be addressed. These include:

- The fundamental relationship between bacteria and AFOM production needs to be further investigated, in particular the use of Peak T fluorescence as a means of measuring bacterial numbers and the robustness of this method within different environments and conditions
- The impact of metabolism on bacterial AFOM production and processing has not yet been fully characterised, with some studies suggesting that fluorescence could be used as a marker for metabolic rate or activity, however this has never been specifically investigated
- The impact of pollution, in particular nutrient loading, on bacterial AFOM production and processing requires further exploration
- The ability of microbes to produce humic-like AFOM in-situ, the conditions under which they do this, and the possible implications this has on the freshwater DOM pool and its processing and transport to downstream ecosystems remains to be fully understood
- Further research is needed to investigate the potential use of longitudinal changes in AFOM in freshwaters as an in-situ water quality parameter. Furthermore, more work is needed to

understand how AFOM production and processing relates to the underpinning ecological health of freshwater ecosystems

Chapter 2. Materials and methods

2.1. Laboratory fluorescence measurements

Laboratory fluorescence spectroscopy measurements were collected using an Aqualog® (Horiba Ltd., Japan) benchtop spectrofluorometer. Methodologies pertaining to in-situ fluorescence measurements collected in the field using remote sensors are discussed in section 2.6.

2.1.1. Aqualog® spectrofluorometer and fluorescence measurements

The Aqualog® (Horiba Ltd., Japan) is a fully automated, self-contained benchtop spectrofluorometer system combining both fluorescence and absorbance measurements for acquisition of accurate and sensitive optical data. The system contains an excitation monochromator for incident light dispersal, using gratings containing 1200 grooves mm^{-1}, blazed at 250 nm excitation. The entrance and exit slits to the monochromator are set to a 5 nm bandpass. The instrument excitation range is 240-800 nm, and the emission detection range is 250-800 nm. Following excitation, sample fluorescence is directed into a multi-channel CCD detector which collects information at a 90° angle to the excitation beam to prevent bleed from the incident light. In addition, a small amount of light is directed towards the reference detector to correct for instrument and lamp variation. Absorbance data is collected using the spectral transmittance properties collected from a single-channel detector colinear to the beam.

Spectral data was collected using the Aqualog® software, which controls instrument function and sampling methodologies. The scan parameters for all analysis employed collected excitation wavelengths from 200-600 nm in 1 nm steps, and emission wavelengths were collected from 247.88 to 829.85 nm in 1.16 nm steps. An integration time of 0.5 seconds was employed. A standard 3.5 mL quartz cuvette with a 10mm pathlength was used throughout.

2.1.2. Aqualog® absorbance measurements and correction

Parallel absorbance and spectral transmittance measurements collected simultaneously during EEM spectral acquisition were used for post-processing IFE corrections within the Aqualog® software. Initially, the transmission detector signals were used to calculate the absorbance (*Abs*) and transmittance (*T*) values. Information including excitation-source intensity corrections (acquired using the reference detector) were acquired from the sample blank (I_0) and the sample being evaluated (I). The transmission (T_λ), percent transmission ($\%T_\lambda$) and absorbance values were then calculated internally using the following equations:

Equation 2.1

$$T_\lambda = \left(\frac{I}{I_0}\right)$$

Equation 2.2

$$\%T = 100 \times \left(\frac{I}{I_0}\right)$$

Equation 2.3

$$Abs = -\log(T)$$

Common practice involves using transmittance and absorbance data from the blank and sample as described above. A prerequisite required for this, however, is for the sample to fall within the Beer-Lambert linear region for the absorbance spectra associated with the collected EEM. Internal IFE corrections employed by the Aqualog® software involve measuring the absorbance spectrum of the sample for the overlapping range of both excitation and emission spectra to correct for both primary and secondary IFEs. The equation assumes the use of a 10 mm cuvette pathlength, and is applied to each individual excitation-emission wavelength coordinate of the EEM. The equation is as follows:

Equation 2.4

$$F_{ideal} = F_{obs} \times 10^{\frac{Abs_{Ex} + Abs_{Em}}{2}}$$

Where F_{ideal} is the ideal fluorescence-signal expected in the absence of the IFE effects, F_{obs} is the observed fluorescence signal, and Abs_{Ex} Abs_{Em} are the collected absorbance values present at each excitation and emission wavelength coordinates.

2.1.3. Fluorescence data analysis

2.1.3.1. Fluorescence spectra post-processing

Fluorescence data generated using the Aqualog® was blank subtracted, corrected for IFE for both excitation and emission wavelengths (as described above) and first and second-order Rayleigh scattering masked at ±10 nm $\lambda_{ex} = \lambda_{em}$ and $2\ \lambda_{ex} = \lambda_{em}$ (Coble et al., 2014). All fluorescence data generated using the Aqualog® is reported in Quinine Sulphate Units (QSU), by normalizing data to the fluorescence generated from 1 µg L^{-1} quinine sulphate in 0.105 M perchloric acid at λ_{ex} = 347.5 nm and λ_{em} = 450 nm (Kramer and Herndl, 2004). This allows for standardized quantitative analysis that is

comparable within and between studies. Instrument validation was undertaken daily using an accredited quinine sulphate standard (Starna Cells, USA), ensuring CV < 3% for all readings (n = 5) to account for changes in lamp intensity over time. Normalization factors were generated using the emission intensity of the quinine sulphate standard at 450 nm and applied to all fluorescence emission wavelength locations within the sample in order to generate normalised QSU fluorescence values.

2.1.3.2. Generating EEMs from fluorescence data

QSU fluorescence data was used to create graphical EEM matrices using a custom script written in Python™ (Python Software Foundation). The data window was cropped to λ_{ex} 240-490 nm and λ_{em} 250-500 nm, to discount fluorescence data within the deep-UV region which is heavily influenced by instrument noise. This allows for the analysis of data within the UV-visible area, the optical region associated with FDOM peaks of interest.

2.1.3.3. Peak-picking AFOM peaks

The custom Python™ script used for the generation of EEM maps was also used to isolate all emission data associated with a single excitation wavelength at the center of the peak of interest for peak-picking (Korak et al., 2014; Murphy et al., 2010). Peak-picking was then undertaken manually using Microsoft Excel, where an average value was taken across the peak emission maxima region. Emission regions for peaks of interest are highlighted in Table 1.1 (Coble et al., 2014).

2.2. Reagents and culture media

2.2.1. Bacterial growth media

All culture media was obtained from Oxoid Ltd. (Basingstoke, UK). Dehydrated culture media was reconstituted using distilled water and sterilized by autoclaving at 121°C for 15 minutes.

- Nutrient agar (NA) BO0336: a high-nutrient solid culture medium used for a wide range of microorganisms. Within this study, this was used for recovery and enumeration of *Pseudomonas aeruginosa* and all environmental isolates.
- Nutrient broth (NB) BO0210: a high-nutrient liquid culture medium used for a wide range of microorganisms. Within this study, this was used for overnight culturing of *Pseudomonas aeruginosa* and all environmental isolates.
- Membrane Lactose Glucoronide agar (MLGA) CM1031: a selective solid culture medium used for the differentiation of *Escherichia coli* and thermotolerant coliforms from non-coliforms.
- R2A agar PO0659: A low-nutrient solid medium used for general enumeration of bacteria within environmental and/or drinking water samples. Within this study, this was used for determination of heterotrophic plate counts.

- Pseudomonas cetrimide agar CM0579: A selective solid medium used for the differentiation of *Pseudomonas aeruginosa* (*P. aeruginosa*). Used here for viable colony counting of *P. aeruginosa* due to its promotion of discrete, easily enumerated bacterial colonies.

2.2.2. Development of a simulated freshwater matrix

A simulated freshwater (SFW) was developed using an adapted method from Smith et al. (2002), to provide a low-nutrient growth medium with minimal background fluorescence. This enabled the controlled introduction of elevated nutrient concentrations to investigate the impact of elevated nutrients on AFOM production and processing by bacteria. The SFW contains low concentrations of nitrate (NO_3^-; 0.3 mg L^{-1}) and phosphate (PO_4^{3-}; 0 mg L^{-1}) and no addition of dissolved organic carbon (DOC). The low-nutrient baseline media was then supplemented with higher concentrations of nitrate, phosphate and DOC, as required during experimentation. SFW reagents were prepared and dissolved at a x1000 concentration to aid in the dissolution of salts. Ionic constituents and concentrations within the SFW are outlined in Table 2.1.

All SFW prepared using this method was filter-sterilized using a 0.2 µm cellulose filter (Sartorius Stedim Biotech, Germany) into sterile glassware prior to use, due to the development of a complex background fluorescence signature when autoclaved.

Table 2.1 Anion and Cation concentrations within a Simulated Freshwater adapted from Smith et al. (2002).

Chemical constituents	Final ion concentrations (mg L^{-1})	
	Anion	Cation
$MgCl_2$	1.458	4.254
$CaCl_2$	3.209	5.672
$Ca(NO_3)_2$	0.601	1.860
$CaCO_3$	6.814	10.201
Na_2SO_4	5.288	11.046
$KHCO_3$	0.977	1.525
$NaHCO_3$	0.458	1.220

2.3. Microbial culture and enumeration

2.3.1. Laboratory bacterial cultures

The bacterial strain *Pseudomonas aeruginosa* NCIMB 8295 was obtained from the culture collection at the University of the West of England, Bristol. Cultures were stored on beads (Microbank, Pro Lab Diagnostics, Canada) at -80°C until required. Bacteria were recovered by plating onto nutrient agar and incubating at 37°C for 24 hours prior to starting each new experiment. Overnight liquid cultures

(10 mL) were obtained by inoculating nutrient broth (Oxoid™ Ltd., Basingstoke, UK) with single pure colonies and incubating for 16-18 hours at 37°C in an orbital shaker (120 rpm).

2.3.2. Isolating and culturing bacterial strains from environmental samples

Environmental bacterial strains were isolated by plating 50 µL of environmental water obtained from the Jubilee River at Taplow, Maidenhead onto R2A agar (Oxoid™ Ltd., Basingstoke, UK), and incubating at 22°C for 7 days until visible colonies had formed. Individual colonies were then isolated and streaked onto the following agar: R2A, MLGA and nutrient agar and incubated at 37°C and 22°C until visible colonies had formed. Resultant colonies were then stored as described in section 2.2.1 and recovered using the relevant media and temperature for each environmental strain.

2.3.3. Obtaining a standardized bacterial inoculum

Following overnight culturing of bacterial strains in nutrient broth, an aliquot of overnight culture (1 mL) was added to a sterile microcentrifuge tube (1.5 mL) and washed by centrifuging at 13,000 x *g* to form a pellet. The supernatant was then discarded and the pellet resuspended in sterile SFW. This process was repeated three times to remove any residual nutrients. The final resuspended pellet was standardized to an optical density measurement of 0.1 OD_{620nm} using a Jenway 6305 UV/Visible range benchtop spectrophotometer (Cole-Parmer® Ltd., USA). This standardized bacterial suspension was then used as the experimental inoculum in order to control the initial bacterial density.

2.3.4. Bacterial enumeration

Bacterial enumeration was undertaken on environmental and laboratory experimental samples using the viable colony counting technique. During laboratory monoculture experiments, experimental aliquots were diluted in phosphate-buffered saline (Oxoid™ Ltd., Basingstoke, UK) and dispensed onto nutrient agar plates using a Don Whitley WASP Touch® automated spiral plater (Don Whitley Scientific Ltd., England). Agar plates were then incubated at 37°C for 24 hours before determining the number of colony forming units (CFU) mL^{-1} using the spiral plater calculation methodology (Don Whitley Scientific Ltd., England).

Heterotrophic plate counts (HPCs) were determined from environmental samples as per the standardized methodology (Bartram *et al.,* 2013). Briefly, 50 µL aliquots were dispensed onto R2A agar plates and dispersed using a sterilized plate spreader. Plates were incubated for 7 days at 22°C and colonies were counted to calculate CFU mL^{-1}. Whilst it is known that this analysis represents only a small fraction of the viable bacterial population in an environmental sample, it is used to assess the

general bacterial content of the water and monitor trends or rapid changes in water quality or bacterial load over time (Environment Agency, 2002).

Escherichia coli (E. coli) and total thermotolerant coliforms were enumerated from environmental samples using membrane filtration. Samples (10, 50 and 100 mL) were filtered using a vacuum pump onto 0.2 µm membrane cellulose filters (Whatman® plc, Maidstone, UK). The filters were placed onto MLGA agar and incubated at 37°C for 24 hours. Colonies were then counted from the appropriate dilution factor and colony color was used to differentiate between *E. coli* and other thermotolerant coliforms, being expressed as CFU 100 mL^{-1}.

2.4. Development of a simulated freshwater model for understanding the effect of nutrients on AFOM production and processing by bacteria

A model system was developed to investigate the impacts of nutrient loading on bacterial processing of AFOM in freshwater. This employed a single-species monoculture (*P. aeruginosa*) and involved the addition of nutrients (nitrate and phosphate) and DOC in the form of glucose.

2.4.1. Nitrate, phosphate and DOC conditions

The chosen concentrations for nitrate and phosphate were informed by the EU Nitrates Directive and its constituting Water Framework Directive. Concentrations of nitrate (NO_3^-) were added at 50mg L^{-1} and concentrations of phosphate (PO_4^{3-}) were added at 0.1 mg L^{-1} to the SFW matrix. Solutions of nitrate and phosphate were prepared by the dissolution of sodium nitrate ($NaNO_3^-$) and dipotassium hydrogen orthophosphate ($KH_2PO_4^-$) respectively, in deionized water and added to the SFW prior to bacterial inoculation. DOC in the form of glucose was dosed into the model system to investigate bacterial production of AFOM from a simple, bioavailable carbon source. SFW solutions containing 0, 5 and 800 mg L^{-1} of DOC were prepared and added to the SFW prior to bacterial inoculation. A concentration of 5 mg L^{-1} of DOC represents DOC availability in many fluvial systems studied previously (Gao et al., 2017; Noacco et al., 2017) where carbon transport in rivers has been modelled. High, or excess, DOC conditions (800 mg L^{-1} glucose) were also studied. DOC levels this high, although not representative of natural systems, ensured that DOC was not a limiting factor when investigating bacterial AFOM production. This is comparable to previous laboratory-based studies that have used high-nutrient growth media with DOC concentrations in excess (Fox et al., 2017). The nutrient and DOC conditions and their associated nomenclature are outlined in Table 2.2.

Table 2.2 Nitrate, phosphate and DOC experimental conditions and their associated nomenclature. Six conditions of varying nutrients were investigated with three DOC conditions for each.

	DOC concentrations		
	0mg L^{-1} DOC	**5mg L^{-1} DOC**	**800mg L^{-1} DOC**
0mg L^{-1} PO_4^{3-} 0.3mg L^{-1} NO_3^-	*SFW0* Low nutrients, no DOC	*SFW2* Low nutrients, limited DOC	*SFW4* Low nutrients, excess DOC
0.1mg L^{-1} PO_4^{3-} 50mg L^{-1} NO_3^-	*SFW1* High nutrient, no DOC	*SFW3* High nutrient, limited DOC	*SFW5* High nutrients, excess DOC

2.4.2. Bacterial growth curves

Using a glass conical flask (500 mL), sterile SFW (250 mL) was inoculated with *Pseudomonas aeruginosa* to a density of 10^5 CFU mL^{-1} as described in section 2.3.3, this bacterial density has been previously reported to be representative of freshwater systems (Sigee & Wiley, 2005). Flasks were incubated at 37°C in an orbital shaker at 120 rpm under ambient light conditions, and aliquots (10 mL) were taken for analysis at hourly time points for the first 8 hours, and then at 12, 16, 20, 24, 36, and 48 hours thereafter. The experimental duration of 48 hours at 37°C enabled the observation of AFOM production over three phases of bacterial growth (lag, exponential and stationary). Whilst it is acknowledged that this temperature does not represent environmental conditions, this 37°C was chosen as it has been found to be the optimum growth temperature for *P. aeruginosa* (Tsuji et al., 1982). As such, this facilitated initiating the bacterial AFOM production within this model system, allowing the investigation of a range of metabolic states over a short period of time. Flasks were vented to maintain gas exchange with the environment, thus the experiment was conducted under aerobic conditions. Sample aliquots were serially diluted in sterile phosphate buffered saline (Oxoid Ltd., UK), spiral plated onto nutrient agar and the CFU mL^{-1} determined as per section 2.3.4. Each experimental condition was repeated on three independent occasions (except for SFW5, which was repeated on seven independent occasions due to high variability) using independent overnight bacterial cultures. All bacterial enumeration measurements were performed in triplicate at each time point (n=3 biological and technical replicates).

2.5. Investigating the relationship between AFOM and bacterial production

Bacterial production (BP), also known as secondary production, refers to the heterotrophic synthetization of biomass by bacteria (Cole & Pace, 1995; Fuhrman & Azam, 1980). The incorporation

of organic compounds (often those produced during primary production) by bacteria and the subsequent remineralization into metabolic end products or byproducts during bacterial respiration (BR) forms a fundamental part of the microbial loop. The measurement of bacterial production rate has, therefore, become an important method in quantifying the flow of carbon through food webs in aquatic systems. Heterotrophic metabolism is defined as the biological oxidation of organic compounds (Jurtshuk, 1996), and the incorporation of amino acids as growth substrates and their subsequent complete oxidation during respiration represent a significant part of this process. As such, measuring the rate of amino acid assimilation can be used as a means of estimating BP and BR rates, thereby providing an insight into bacterial metabolic rate.

The application of radiolabeled isotopes has long been used for tracing this activity and, therefore, is commonly used as a proxy for bacterial metabolism (Cole & Pace, 1995; Fuhrman & Azam, 1980; Marxsen, 1996; Smith & Azam, 1992). Amino acids containing hydrogen isotopes are often employed for this, notably [^{3}H]-Leucine and [^{3}H]-Thymidine (Maske et al., 2020). The leucine method measures the synthesis of proteins, and the thymidine method measures the synthesis of DNA. Due to the relatively higher sensitivity of tritiated leucine, the former method is the most commonly used and is therefore the one employed in this study.

2.5.1. Bacterial leucine incorporation assays

A method was adapted from Smith & Azam (1992) whereby [^{3}H]-Leucine was introduced into aliquots of SFW to measure the bacterial leucine incorporation rate. A final [^{3}H]-Leucine concentration of 20 nM for *Pseudomonas aeruginosa* and 25 nM for bacterial isolates (5.1 and 6.8 µL respectively) was introduced (calculated from 37 mBq mL^{-1}, PerkinElmer®, Massachusetts, USA) to a 1.7 mL aliquot of SFW experiment in sterile 2 mL screwcap microcentrifuge tubes with O-ring seals (Sarstedt, Germany). Each experiment was conducted in biological and technical triplicate (n=3) per sampling point, in addition to one 'killed' control per biological replicate at each sampling point whereby 85 µL of 100% trichloroacetic acid (TCA) was introduced to achieve a final concentration of 5% prior to incubation (Smith & Azam, 1992). Incubations were undertaken in the dark at 37°C for one hour.

Following incubation, all assays were terminated with the addition of 85 µL of 100% TCA to achieve a final concentration of 5% TCA in all samples. Samples were then vortex mixed and stored in the dark overnight. To determine the uptake of [^{3}H]-Leucine, extractions were undertaken whereby the tubes were centrifuged at 16,000 *x* g for 10 minutes and the supernatant was removed. The pellet was then resuspended and washed in 1.5 mL of 5% TCA three times. Liquid scintillation cocktail (1 mL, PerkinElmer, Massachusetts, USA) was then added to the pellet and samples were stored overnight in

the dark. Tubes were then placed into 20 mL liquid scintillation counting vials and analyzed on a liquid scintillation counter (Hidex 300 SL, Hidex Oy, Finland).

2.5.2. Bacterial leucine incorporation and bacterial production data analysis and calculations

Bacterial leucine incorporation values were calculated from the raw data obtained from the scintillation counter using the following equation (Smith & Azam, 1992):

Equation 2.5

$$\frac{(d - d_c)4.5\ x\ 10^{-13}}{SA} = a$$

Where d is the disintegrations per minute (dpm) obtained directly from the scintillation counter, d_c is the dpm from the killed control, and 4.5 x 10^{-13} represents the conversion from dpm to Curies (Ci) (1 dpm = 4.5 x 10^{-1} Ci). SA is the specific activity of the [^{3}H]-Leucine (Ci mmol^{-1}).

The following equation was then undertaken to calculate bacterial production, where the production of Equation 2.5, a, was used for Equation 2.6:

Equation 2.6

$$\left(\frac{a}{tv}\right)\ 1000 = BP$$

Where t is the incubation time (h) and v is the sample volume (mL).

2.5.3. Bacterial growth curves

A sterile flask (500 mL) was inoculated with 250 mL of SFW containing a bacterial isolate monoculture. Isolates were cultured using methodology described in Section 2.3.2, and two isolates were chosen for this experiment based on survival rates in simulated freshwater. Isolates were grown up in overnight culture before being washed, resuspended and standardized as described in section 2.3.3. In order to observe bacterial leucine incorporation in the most representative freshwater model, the SFW3 (Table 2.2) condition was used, containing high nutrients (0.1 mg L^{-1} phosphate and 50 mg L^{-1} nitrate) and limited DOC (5 mg L^{-1} in the form of glucose). Flasks were incubated at 37°C in an orbital incubator shaking at 120 rpm. Aliquots were removed from the flask for analysis of bacterial leucine incorporation, bacterial enumeration, and fluorescence at the following time points: 0, 4, 8, 24 and 48 hours. Flasks were vented to maintain gas exchange; thus, the experiment was conducted under aerobic conditions. Bacterial enumeration was undertaken as described in section 2.3.4.

2.6. Long-term in-situ monitoring of the River Thames at Taplow, Maidenhead

A novel fluorescence-based sensor was deployed at the river Thames at Taplow, Maidenhead between July 2021 and November 2022. This section pertains to sensor installation, sampling location and discrete sampling procedure. For information regarding sensing system hardware specifications, refer to Chapter 5.

2.6.1. Discrete sampling of a freshwater system

Discrete samples were taken over a 1-month period between August 2021 and November 2022 every two weeks. Samples were collected from the concrete structure shown in Figure 2.3 using a telescopic sampling rod, approximately 2 m from the riverbank. Samples were collected in sterile 50 mL Falcon tubes to ensure no microbial contamination was present. For filtered samples, a sterile 50 mL syringe was used, and samples were filtered in the field immediately after collection at both 0.22 µm and 0.45 µm. Samples were stored on ice in a cooler box during transport to the laboratory, before being analyzed within 4 hours of collection for microbiological, fluorescence and chemical laboratory analyses (all of which are detailed in the preceding methodologies).

2.6.2. Installation of the V-Lux fluorosensor on the River Thames at Taplow, Maidenhead

The Chelsea Technologies Ltd. fluorosensor was installed for long-term deployment at a monitoring station on the River Thames at Taplow, Maidenhead, (N 51° 32’ 27”, W 0° 41’ 40”). The monitoring station was situated approximately 30 m directly perpendicular to the sampling location, shown in Figure 2.1. The water body is a heavily engineered river system, surrounded by immediate deciduous woodland and draining a number of nearby urban areas within its catchment. The sensor was installed in a permanent location using a custom-built stainless-steel flow cell (Chelsea Technologies Ltd.) which allowed water to pass through the sample chamber whilst preventing the bleed of any ambient light into the chamber, shown in Figure 2.2. The flow cell was connected to a rotor pump using braided hose tubing which ran towards the river at the sampling location shown in Figure 2.1. Prior to installation, a turbidity offset algorithm was applied to the V-Lux to account for changes in light scattering which may occur inside the flow cell (Chelsea Technologies Ltd.). The sensor collected a sample at hourly intervals, during which time the rotor pump would fill the flow cell with river water before pumping the water back into the river. In-between pumping times, water was fully emptied from the cell to prevent the sensor from permanently sitting in water, thereby limiting the risk of biofouling. The sensor was removed from the flow cell once every two weeks for cleaning and maintenance, whereby the sample window was wiped with 100% ethanol.

Figure 2.1 Sampling and pump tubing location on the River Thames at Taplow, Maidenhead in January (left) and May (right), and the location of the pump tubing attached to the concrete structure from where river water was pumped up to the monitoring station (below).

Figure 2.2 Chelsea Technologies V-Lux fluorosensor (Chelsea Technologies Ltd.) in a custom-built stainless-steel flow cell at the monitoring station in on the River Thames at Taplow, Maidenhead. Flow cell, V-Lux sensor and piping through which water was pumped directly to and from the water body are shown.

2.6.3. *In-situ* physicochemical measurements

In addition to the V-Lux sensor, a YSI multiparameter EXO3 sonde (Xylem Analytics, UK) was deployed for the in-situ measurements of the following parameters: turbidity, pH, conductivity, dissolved oxygen, chlorophyll-a, and ammonium. The sonde was installed inside a water trough where water from the river was pumped from the same location as described in section 2.6 using the same pumping regime as the V-Lux.

2.6.4. Sensor and sonde data collection

Both the V-Lux and the multiparameter sonde were digitized via a remotely accessed telemetry communication system, or radio telemetry unit (RTU) portable real-time monitoring system (MCE-ESNET2, Meteor Communications Ltd., Hertfordshire, UK). Data was accessed and collected via the MeteorCloud™ system (Meteor Communications Ltd.), where it could be viewed for real-time analysis and for downloading of historical datasets. The ESNET2 system also controlled the powering of the sensors to allow for controlled power cycling at each one-hour pumping and sampling interval.

Chapter 3. The in-situ production of aquatic fluorescent organic matter in a simulated freshwater laboratory model

3.1. Introduction

Dissolved organic matter (DOM) is one of the largest reservoirs of carbon on the planet, representing a source of both fixed and bioavailable carbon that is ubiquitous throughout aquatic environments (Cole et al., 2007; Hedges, 1992; Trimmer et al., 2012). In freshwater systems, DOM is a largely heterogeneous mixture of organic compounds, the type and quantity of which is representative of surrounding catchment characteristics, as well as being influenced by processes such as photodegradation and *in-situ* microbial processing (Coble, 1996; D'Andrilli et al., 2019; Yamashita & Tanoue, 2003). DOM is conventionally divided into two categories; 1. allochthonous material, which represents carbon that has been transported into the fluvial system from surrounding terrestrial environments, and considered to represent complex, high molecular-weight humic and fulvic organic carbon and 2. autochthonous material, representing carbon that has been generated within the fluvial system by microbial processes and is regarded as simpler, proteinaceous and lower molecular-weight in nature (Baker & Spencer, 2004; Hudson et al., 2007; Leenheer & Croué, 2003).

A fraction of DOM in aquatic environments exhibits fluorescence properties, and this is known as aquatic fluorescent organic matter (AFOM). AFOM can be analysed using fluorescence spectroscopy, providing a rapid and sensitive means of investigating the processing and transport of carbon in aquatic systems. AFOM is classified using specific peak nomenclature (Coble et al., 2014), based on the presence of observed fluorescence peaks which appear within optical regions associated with known organic compounds. AFOM associated with microbially-derived compounds is known as 'autochthonous'. Peaks within this region have been named Peaks T ($\lambda_{ex}/\lambda_{em}$ 275/340) and B ($\lambda_{ex}/\lambda_{em}$ 275/305), which fluoresce in the same optical regions as tryptophan and tyrosine, which are essential amino acids. This is also known as 'protein-like' AFOM. AFOM associated with terrestrially-derived compounds is known as 'allochthonous', and includes peaks known as Peak C ($\lambda_{ex}/\lambda_{em}$ 320-365/420-470), Peak C+ ($\lambda_{ex}/\lambda_{em}$ 385-420/470-505), and Peak M ($\lambda_{ex}/\lambda_{em}$ 290-310/370-420). Despite this binary classification, some peaks have been reported to occur as a result of both autochthonous and allochthonous processes, such as Peak M in marine environments (Milbrandt et al., 2010).

Much of the work on AFOM in freshwater systems has focused on utilizing Peak T fluorescence as a tool for microbial enumeration, derived from reported relationships between Peak T fluorescence intensities and primary productivity (Hudson et al., 2007; 2008) or microbial enumeration (Sorensen et al., 2015; 2018). Previous studies have sought to investigate the origins of AFOM and its relationship with microbial processing in marine systems (Kinsey et al., 2018; Shimotori et al., 2010; Yamashita et

al., 2008) and, more recently, in surface waters such as lakes (Berggren et al., 2020; Guillemette & del Giorgio, 2012). These have suggested that AFOM in the humic-like optical region can be produced as a direct result of aquatic microbial activity. Recent studies (Fox et al., 2017; 2019) employing laboratory-based model systems to investigate the origin of freshwater AFOM produced by bacteria *in-situ* have provided further evidence to support this. Furthermore, this work has suggested that Peak T fluorescence is associated with microbial metabolism and activity, and is not a reliable indicator for specific cell enumeration as has been previously reported.

Despite recent advances, there is still a dearth of knowledge surrounding the role played by freshwater microbes within in-situ AFOM processing (Anderson et al., 2019). Inland freshwaters are known to play a disproportionately large role in global carbon cycling, despite covering less than 4% of the Earth's surface (Cole et al., 2007; Downing, 2008; Tranvik et al., 2009). Furthermore, the inherent complexity of microbial AFOM processing is compounded by anthropogenically-induced perturbations, particularly agricultural activities, which often lead to nutrient loading as a result of runoff from cultivated land surrounding a river catchment. Over recent decades, the availability of nutrients such as reactive nitrogen and phosphorus species has greatly increased in surface waters, with 38% of European freshwaters impacted by non-point source pollution such as agricultural land-use (Woodward et al., 2012). Recent field-based studies have observed increases in ecosystem respiration and ultimately carbon loss within surface waters as a result of nutrient loading (Kominoski et al., 2018; Manning et al., 2018). There is, however, a need to develop laboratory models to support these field-based studies. Previous approaches for characterizing microbial AFOM production within environmental water matrices (Guillemette and Del Georgio, 2012; Fox et al., 2019) are limited by complex background fluorescence signatures, or the utilization of high-nutrient growth media which do not represent nutrient concentrations observed in the field (Fox et al., 2017; 2019). Therefore, existing models are of limited use for investigating the effects of controlled nutrient loading on microbial AFOM production.

The work undertaken here seeks to develop and utilize a laboratory-based model for the investigation of nutrient loading on in-situ bacterial AFOM processing within freshwater systems. A simulated freshwater (SFW) matrix, adapted from Smith et al. (2002), was developed, standardized and used throughout the study. In contrast to previous laboratory-based studies (Fox et al., 2017; 2018; 2021), the SFW matrices contains concentrations of ionic constituents found within oligotrophic fresh waters (Smith et al., 2002), i.e. contains a low baseline concentration of nitrate, phosphate and dissolved organic carbon (DOC) in the form of glucose. Importantly, the developed SFW exhibited low background fluorescence, unlike many studies which utilize environmental freshwaters (Berggren et al., 2020; Fox et al., 2018; Kominoski et al., 2018). The main aim of this work was to observe the origin

of AFOM via bacterial processing as a function of nutrient availability using a single-species freshwater model system.

3.2. Results

3.2.1. AFOM processing over 48 hours

By using glucose as the sole carbon source, it was possible to investigate the bacterial production of AFOM over a 48-hour period. At 0 h, all inoculated SFW cultures under all conditions (SFW 0-5) exhibited minimal fluorescence properties (< 5 QSU). Complex fluorescence signatures were produced under all six experimental conditions, whereby the dominant fluorescence peaks present at the end of the 48-hour incubation period were Peaks T, C and C+ (Figure 3.1, Table 3.1). Notably, the production of these AFOM peaks was observed within both high and low nutrient conditions (SFW0 and SFW1) containing no glucose-DOC, albeit at low fluorescence intensities (< 50 QSU).

Table 3.1. Fluorescence intensities at 48 hours for all peaks (T, C and C+) under all conditions (SFW0-5). Fluorescence intensities are reported in Quinine Sulfate Units (QSU). Variation (n=3 biological and technical replicates) is also provided in the form of standard deviation (denoted by ±).

	No DOC		5 mgL^{-1} DOC		800 mgL^{-1} DOC	
	Low Nutrient	High Nutrient	Low Nutrient	High Nutrient	Low Nutrient	High Nutrient
	QSU (48h)	QSU (48h)	QSU (48h)	QSU (48h)	QSU (48h)	QSU (48h)
T	6.5 (±3.7)	11.3 (±2.4)	56 (±4.1)	51.8 (±1.1)	45.5 (±1.3)	58 (±14.6)
C	14.8 (±0.13)	21.5 (±10.2)	81.5 (±66.4)	162.7 (±38)	449 (±164)	332.6 (±364)
C+	6.2 (±1.9)	28.6 (±13.3)	599.7 (±530.3)	1215.8 (±193.8)	592 (±212.2)	612.7 (±303.3)

Viable bacterial cell counts of extracted samples show that the exponential phase of bacterial growth consistently occurred between 6 and 12 hours under all experimental conditions as shown in Figure 3.2. This corresponds to observed increases in the intensities of all AFOM peaks under all conditions (SFW0-5).

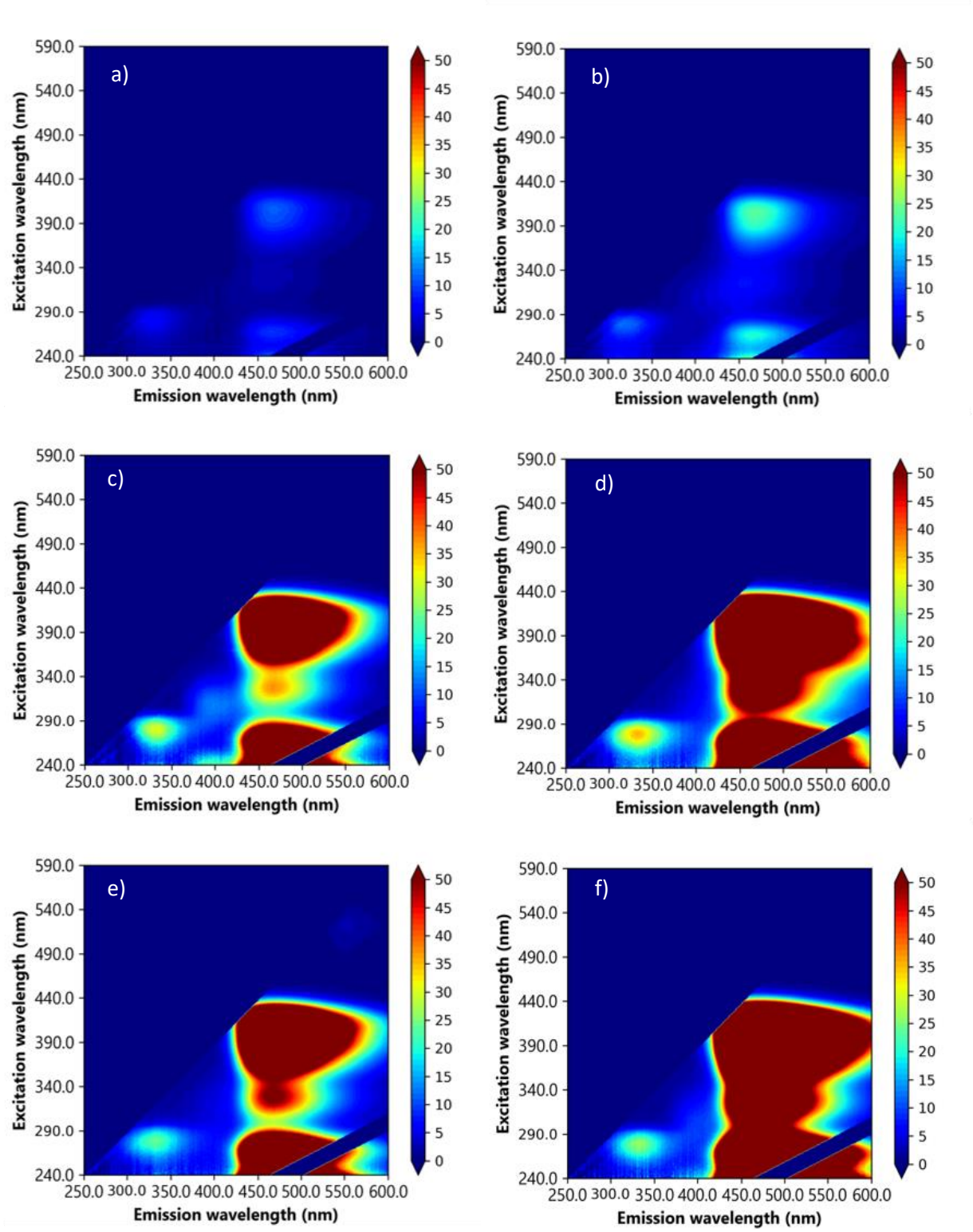

Figure 3.1. Excitation-emission matrices (EEMs) of *Pseudomonas aeruginosa* monoculture in simulated freshwater after a 48-hour incubation period, under the following experimental conditions: a) oligotrophic, no additional carbon (SFW0), b) high nutrient, no carbon (SFW1), c) oligotrophic, limited carbon (SFW2), d) high nutrient, limited carbon (SFW3), e) oligotrophic, excess carbon (SFW4) and f) high nutrient, excess carbon (SFW5).

In all conditions, except SFW2 (low nutrients, limited DOC), bacterial cell replication continued until 16 h as shown in Figure 3.2c. Upon inoculation of all samples, at 0 h, no significant difference was observed in viable counts (CFU mL^{-1}) providing confidence that inoculum density was stable between the different experimental conditions. Between 0 and 6 h, a lag phase was observed during which viable cell counts remained within the 5 Log_{10} CFU mL^{-1} region for all conditions. However, during exponential growth, cell numbers increased by between 1 and 2 Log, ranging between 1-7 x 10^5 CFU mL^{-1} at the beginning of the growth phase, to 5 x 10^6 – 5 x 10^7 CFU mL^{-1} at the end of the growth phase. During this time, the rate of growth of the bacterial communities can be seen to diverge as a function of nutrient and DOC conditions. Within high nutrient, excess carbon conditions, (SFW5) significantly higher CFU mL^{-1} values (6.7 x 10^5 CFU mL^{-1}) were observed after 5 hours ($p < 0.01$) when compared to all other experimental conditions (SFW0-4). From 8 hours of incubation, both the low and high nutrient conditions with no DOC (SFW0-1) had significantly lower cell counts ($p < 0.05$) than all other conditions (SFW2-5). In addition, significant differences in cell numbers were observed between limited DOC (SFW2-3) and excess DOC (SFW4-5) conditions ($p < 0.05$). Whilst differences in cell number were found to be significantly affected by the provision of DOC in the system, the availability of nitrate and phosphate was not found to result in significantly higher cell numbers ($p > 0.05$), suggesting that the community is not limited by nitrate or phosphate within this experimental system.

The fluorescence intensities of all peaks under all conditions (SFW0-5) varies over the experimental time period of 48 hours. The fluorescence peaks mimic the lag phase for 0 to 6 hours before increasing in concert with the exponential growth phase of the *P. aeruginosa* community studied. Peak T fluorescence exhibited the largest increase in intensity between 6 and 16 hours. For low nutrient conditions with 0, limited and excess DOC (SFW0, SFW2 and SFW4), increases of 778% for Peak T, 65% for Peak C and 22382% for Peak C+ were observed. For high nutrient conditions, under the same DOC conditions (SFW 1, SFW3 and SFW5) increases of 756% for Peak T, 216% for Peak C and 682% for Peak C+ were observed. After 16 hours, the observed fluorescence intensities plateaued after increases of 52%, 10% and 2% for conditions with low nutrients and excess DOC conditions (SFW0, 2 and 4) for Peaks T, C and C+. For high nutrient conditions (SFW1, 3 and 5) the observed increases were 12%, 0% and 20% for Peaks T, C and C+ respectively.

In a time-series of all fluorescence peaks over the entire experimental period (0-48 h), it was found that there was a significant change in fluorescence intensity over time for the majority of peaks investigated across all of the experimental conditions. For low nutrient, no DOC conditions (SFW0), Peaks T and C were found to significantly change over the experimental duration ($p < 0.01$). However, Peak C+ was not seen to significantly change over the experiment ($p > 0.05$). For high nutrient, no DOC conditions (SFW1), no peaks were found to change significantly over the experimental period ($p >$

0.05). For low nutrient conditions with limited DOC (SFW2), Peaks T and C were found to change significantly ($p < 0.05$), however Peak C+ was not ($p > 0.05$). All other conditions (SFW3-5) were found to display significant changes over the experimental duration ($p < 0.05$).

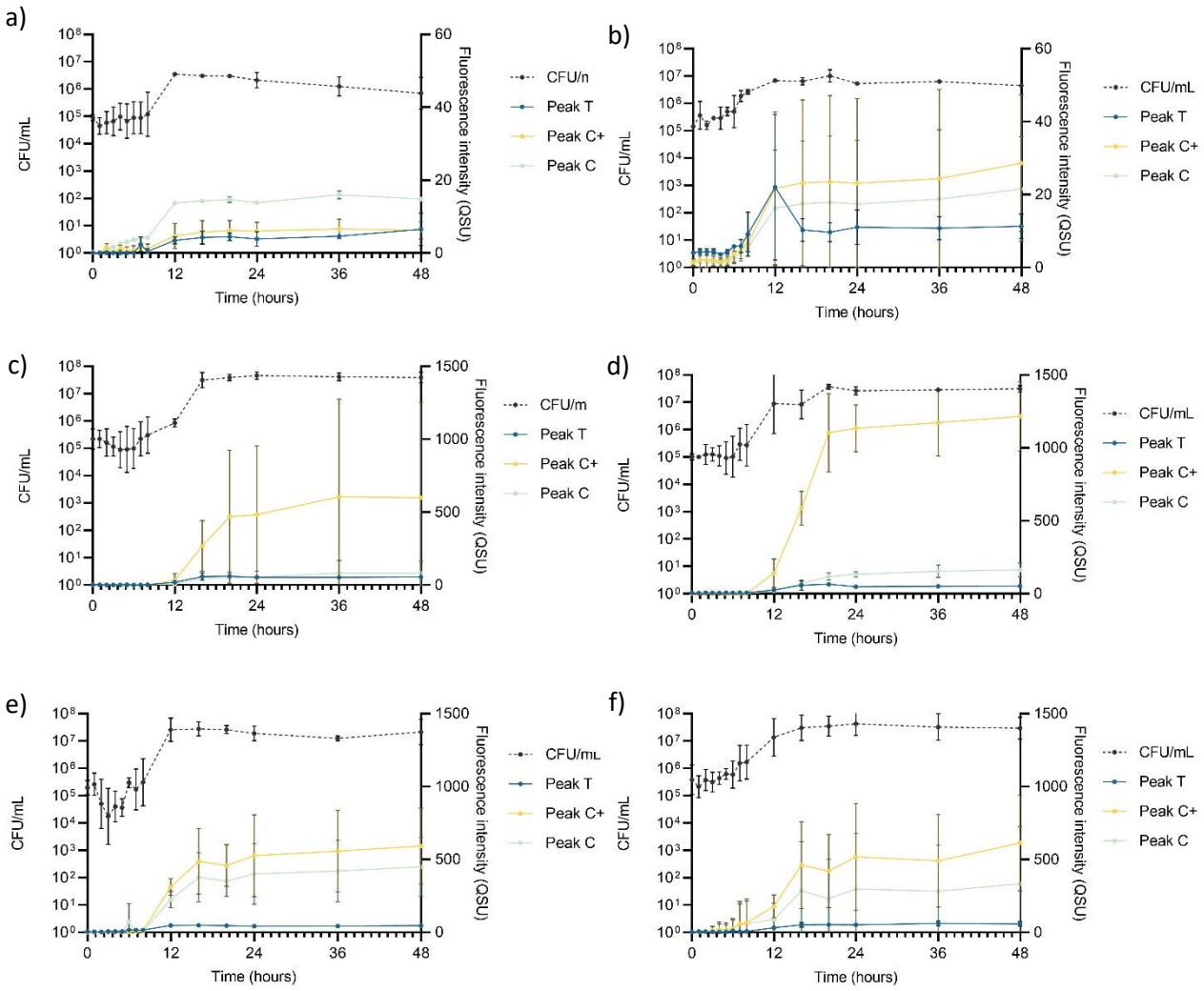

Figure 3.2. *Pseudomonas aeruginosa* growth curve data showing cell numbers (CFU mL^{-1}) relative to fluorescence intensity over 48 hours for Peaks T, C and C+ for the following experimental conditions (n = 3 biological and technical replicates): a) low nutrient, no DOC (SFW0), b) high nutrient, no DOC (SFW1), c) low nutrient, limited DOC (SFW2), d) high nutrient, limited DOC (SFW3), e) low nutrient, excess DOC (SFW4) and f) high nutrient, excess DOC (SFW5).

The relationship between individual fluorescence peaks varies significantly throughout the experimental duration. Under high nutrient conditions and zero DOC (SFW1), low nutrient conditions and limited DOC (SFW2) and high nutrient conditions and excess DOC (SFW5) there are no significant differences ($p > 0.05$) observed between Peaks C and C+, suggesting that the production of this AFOM is interrelated. In contrast, for low nutrient, zero DOC (SFW0), Peak C fluorescence intensity is seen to

decrease by 1.2 QSU (± 0.8) over the final 24 hours (late stationary phase), whilst Peak C+ decreases by only 0.4 QSU (± 0.3), resulting in a divergence between these two peaks at the end of the experimental period. This was found to be statistically significant ($p < 0.05$). For high nutrient conditions, limited DOC (SFW3) the relationship between Peaks C and C+ are statistically different, where the greatest increase in Peak C+ is observed between 36 and 48 hours, increasing by 42.3 QSU (± 9.4) whilst Peak C increases by 7.8 QSU (± 5.3) ($p < 0.05$). For all other conditions (SFW3 and SFW4), there remains no significant difference between these peaks over the experimental duration. The relationship between Peak T and C/C+ also varies, with only low nutrient, zero DOC (SFW0) displaying a significant difference between Peaks T and C throughout the experimental period ($p < 0.05$) for all but the first 2 hours. High nutrient, limited DOC (SFW3), display the most significant differences between all peaks, where the difference is over 1000 QSU between Peak C+ and Peaks T and C ($p < 0.05$; Figure 3.2). For Peaks T and C+, this significant difference is present throughout the experimental period ($p < 0.05$). For high nutrient, excess DOC (SFW5), the variation observed between the three biological replicates was found to be substantially higher than was seen under all other conditions. For Peaks C and C+, there was found to be a mean of 332.6 ± 364.0 and 612.7 ± 303.3 QSU, respectively at 48 hours. Comparatively, there is less variability between biological replicates for low nutrient, no DOC conditions (SFW0), with means of 14.8 QSU for Peak C and 6.2 QSU for Peak C+, and standard deviations of 0.1 for Peak C and 1.9 for Peak C+. Observed variability was determined to be a result of inherent biological variation. Lower variability (determined by standard deviation) was observed in conditions that comprised of lower nutrient conditions.

3.2.2. Effects of DOC and nutrients (NO_3^- and PO_4^{3-}) on AFOM production and processing

To compare directly the effect of altering nutrient regimes on AFOM processing, fluorescence data was normalized to bacterial enumeration to account for the changing density of viable cells during the growth curve period (Figure 3.3). For this, QSU data was enumeration-corrected to every 10^6 CFU and the data logged for all conditions for comparison (expressed as $f_{QSU/CFU}$). For the experimental time period, the relationship between viable cell numbers and Peaks T, C and C+ fluorescence is not linear for any of the conditions studied (Figure 3.3). Large fluctuations occurring in per-cell fluorescence ($f_{QSU/CFU}$) over the duration of the experiment were observed. Under all experimental conditions, the period of greatest variation in $f_{QSU/CFU}$ occurs between 0 and 12 h. An increase in per cell fluorescence can initially be seen under all conditions, with maximum fluorescence intensities being reached during the first 8 h of the experiment. This coincides with the beginning of the bacterial exponential growth phase as seen in Figure 3.2, which occurs between 6 and 12 h, during which the bacterial growth rate is at its highest. In high nutrient conditions with limited DOC (SFW 3), Peak C+ reaches its maximum $f_{QSU/CFU}$ at 16 hours, and in high nutrient conditions with excess DOC (SFW5), Peak C+ reaches its

maximum $f_{QSU/CFU}$ at 12 hours. A sharp decrease in $f_{QSU/CFU}$ is then observed until 12 h in conditions containing zero and excess DOC (SFW0, SFW1, SFW4 and SFW5, Figures 3.3a, 3.3b, 3.3e and 3.3f) for all peaks except for Peak C in SFW5. Under limited carbon conditions (SFW2 and SFW3, figure 3.3c and 3.3d), $f_{QSU/CFU}$ continues to decrease until 16 and 24 h for low and high nutrient conditions respectively. Whilst the $f_{QSU/CFU}$ remains low for the remaining duration of the experimental period, all conditions (with the exception of SFW3), experience a gradual increase during the final 24 h of the experiment coinciding with the late stationary phase of the bacterial community.

$f_{QSU/CFU}$ is influenced by the availability of nutrients and DOC in the system. Table 3.1 shows the influence of the experimental conditions on the ratio of Peaks T, C and C+. The relative contribution of each fluorescence peak to the total fluorescence observed as a function of nutrients and DOC is shown. In conditions with zero and limited DOC, higher nutrient availability was found to result in more Peak T production, with a higher ratio of Peak T relative to Peaks C and C+. Under excess DOC conditions, however, increased nutrient availability was found to reduce the production of Peak T relative to Peaks C and C+, with the latter peaks accounting for a larger proportion of the total fluorescence. For experimental conditions containing zero DOC, the maximum $f_{QSU/CFU}$ for Peak T in high nutrient conditions was substantially higher (102.3, ± 20.5) in comparison to low nutrient conditions. When DOC is limited, the $f_{QSU/CFU}$ for Peak T was elevated by 255.9 (± 45.7) in low nutrient conditions compared to higher nutrient conditions. Interestingly, for conditions containing excess DOC, the $f_{QSU/CFU}$ for Peak T associated with high nutrients was significantly less (1116.6 ± 257.8) when compared to low nutrient conditions ($p < 0.01$). For Peaks C and C+, conditions with no DOC show that the addition of nutrients results in a decrease in fluorescence intensity of 61.8 (± 36.7*)* $f_{QSU/CFU}$ for Peak C and 374.2 (± 196.6*)* $f_{QSU/CFU}$ for Peak C+. However, for high nutrients and excess DOC conditions, higher fluorescence intensities for Peak C are observed in the high nutrient conditions. This equates to an additional $f_{QSU/CFU}$ of 228.8 (± 168.2).

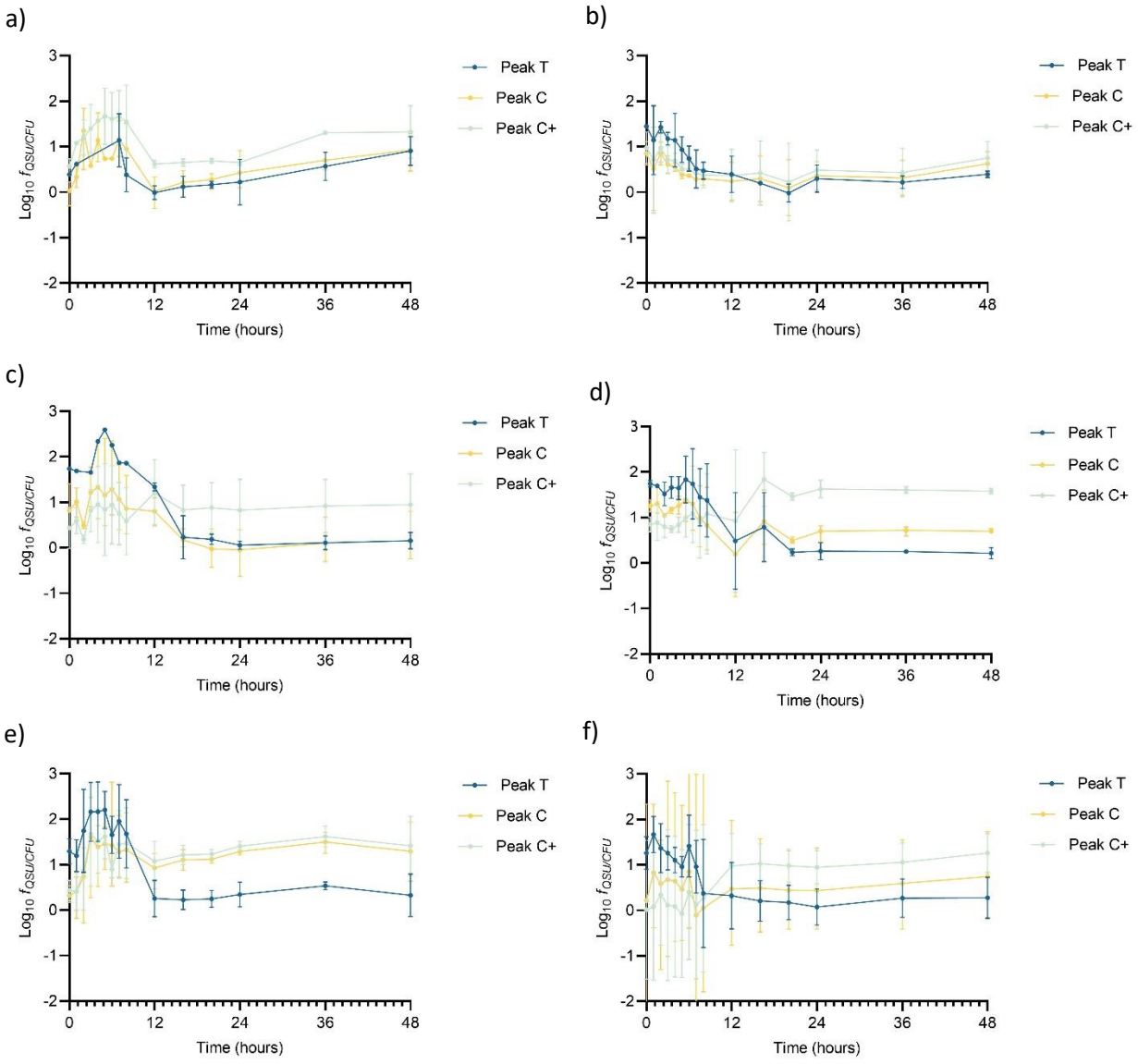

Figure 3.3. Peaks T, C and C+ fluorescence data corrected for bacterial cell enumeration, displaying Log10 QSU per 10^6 CFU (fQSU/CFU) for *Pseudomonas aeruginosa* growth curve data under the following experimental conditions (n=3 biological and technical replicates): 3a) low nutrient, no DOC (SFW0), 3b) high nutrient, no DOC (SFW1), 3c) low nutrient, limited DOC (SFW2), 3d) high nutrient, limited DOC (SFW3), 3e) low nutrient, excess DOC (SFW4) and 3f) high nutrient, excess DOC (SFW5). Error bars denote standard deviation.

3.3. Discussion

3.3.1. AFOM processing over 48 hours

The data presented here demonstrates that under all conditions, *P. aeruginosa* is capable of producing a complex range of AFOM including Peaks T, C and C+, in a simulated freshwater model system. This includes the production of materials that fluoresce in both the autochthonous (protein-like) and allochthonous (humic-like) optical regions. Furthermore, material that has conventionally been assigned as autochthonous and allochthonous have been produced within this biological model in all DOC conditions. The production of this material relative to the bacterial cell numbers in the system was shown to vary over time, commensurate with the stage of biological growth occurring in the community.

It has been previously shown that bacterial communities are capable of producing semi-labile humic-like material from *in-situ* incubation experiments within marine systems (Koch et al., 2014), consistent with the theory of the microbial carbon pump (Jiao et al., 2011). This has been characterized, using molecular techniques such as ultra high-resolution mass spectrometry, as consisting of higher molecular-weight material generated from biologically labile substrates such as glucose (Koch et al., 2014). More recently, model freshwater studies have shown the production of optically active compounds that are fluorescent in the high molecular-weight, humic-like region using high-carbon, high-nutrient microbiological growth media (Fox *et al.,* 2017; 2019). In support of this study, the data presented here clearly demonstrates that *P. aeruginosa* is capable of producing AFOM peaks commonly considered to be allochthonous in nature, from a low-nutrient base media containing no additional nitrate, phosphate or DOC. This suggests that whilst the capacity of bacteria to produce complex AFOM in-situ is enhanced by the availability of a labile, low molecular weight carbon source (glucose) and an abundance of nutrients, they are also capable of utilizing very minimal concentrations of essential nutrients to demineralize and/or utilize carbon derived from the microbial community to produce fluorescing material. It is notable that conditions containing no introduced glucose-DOC still produced substantial fluorescence signatures over the experimental period (that is, 11.3, 21.5 and 28.6 QSU for Peaks T, C and C+ in high nutrient, no DOC conditions at 48 h) which, whilst lower than the 58, 332.6 and 612.7 QSU for Peaks T, C and C+ seen in high nutrient, excess DOC conditions, still represents a significant increase in fluorescence over the experimental period. It is likely that this occurred as a result of DOC delivered into the system from the microbial inoculum in the form of bacterial biomass which was utilized by the community as an organic substrate to generate fluorescing compounds. The introduction of bioavailable DOC from the microbial community may have occurred

as a result of a number of factors; for example, cell death and subsequent cell lysis, or the export of compounds such as iron-scavenging siderophores into the system.

Data presented in Figure 3.3 clearly demonstrates that the relationship between AFOM peaks and cell density is not correlated for any conditions within this model system. The intensity of the AFOM produced per bacterial cell varies both throughout the experimental period and between different conditions of nutrients and carbon. By observing these dynamics over time (at hourly intervals between 0 and 8 h) variations in $f_{QSU/CFU}$ are observed between all experimental conditions studied. Peak T was observed in all conditions and always displays an increase in fluorescence intensity between 8 and 16 hours. This suggests that whilst DOC and nutrient availability heavily influences the maximum intensity of the fluorescence peaks produced, ultimately it does not affect the pattern of AFOM production over time. There are large fluctuations observed in $f_{QSU/CFU}$ during the first 12-hour period of all experiments, with Peak T reaching its maximum $f_{QSU/CFU}$ between 0 and 7 h in all conditions, before sharply decreasing thereafter. The sharp increase in maximum $f_{QSU/CFU}$ during the first several hours of the experiment suggests that an increase in Peak T fluorescence intensity may represent a precursor to the start of the exponential growth phase, indicating the upregulated metabolic state the bacterial community is undergoing prior to cell replication. This variable relationship between $f_{QSU/CFU}$ of Peak T, and the increase seen in the $f_{QSU/CFU}$ prior to a period of rapid cell multiplication, strongly supports the use of Peak T as a marker for an active bacterial population under model conditions, as has been evidenced in recent literature (Fox et al., 2017; 2019). As such, this model highlights the complexity of the relationship between bacterial activity and observed fluorescence, underscoring the fact that whilst Peak T presents a useful tool for monitoring microbial presence in surface waters, there may be challenges associated with using this technique as a direct enumerator for bacterial cells as has been previously reported (Sorensen et al., 2015; 2018), particularly within dynamic systems which are heavily influenced by nutrient influxes. It is also of note that the method used to enumerate bacterial cells in this study, the viable count method, does likely not account for every cell present within the system. That is, this method represents only the number of actively growing/dividing cells present within the system. Therefore, whilst methodological consistency ensures relative accuracy within the study, it is likely that not all cells present within the system will be represented in the bacterial cell numbers data, though they may still be contributing to the observed fluorescence signatures.

Peak C/C+ fluorescence also exhibits a non-linear relationship with bacterial cell density over the duration of the experimental period. Following the initial fluctuation in $f_{QSU/CFU}$ between 0 and 12 to 16 h, the $f_{SU/CFU}$ can be seen to increase, gradually, for the duration of the experiment for all conditions except for high nutrient and limited DOC. This could possibly be caused by the persistence of

compounds that comprise Peak C/C+ FOM within the system (i.e. are not acted upon by the bacterial population). This is supported by previous literature which demonstrates the microbial production of less labile, higher molecular weight material (known to fluoresce in the Peak C/C+ region) albeit in the marine environment, from a simple glucose carbon substrate, which exhibited persistence for up to two years (Kinsey et al., 2018). Our data shows the *in-situ* production of Peaks C and C+ within a freshwater matrix, and their subsequent accumulation and persistence within the system throughout the experimental duration of 48 h. Material that fluoresces in this region has conventionally been associated with allochthonous material that is transported into surface waters from the surrounding catchment, rather than as a result of the direct in-situ production by microorganisms. Whilst the in-situ production of this material has previously been seen in marine environments, this study is the first to show this phenomenon in a controlled laboratory environment using a representative simulated freshwater matrix. Further work is required to determine the relative recalcitrance of the presumed higher molecular weight FOM that is produced, by monitoring the fluorescence in this region over longer periods of time and in the presence of a more diverse microbial community. Recent literature has suggested that the origin of Peak C+ is partly derived from extracellular microbial products (Sorensen et al., 2020; Fox et al., 2021). However, to date, the overwhelming consensus is that Peaks C and C+ in freshwater environments are associated with material that is allochthonous in origin (Coble et al., 2014).

3.3.2. Effects of DOC and nutrients (NO_3^- and PO_4^{3-}) on AFOM production and processing

The concentration of DOC, nitrate and phosphate was found to have an impact on the production and processing of AFOM by the bacterial community within the SFW models studied here. The data presented in Table 3.1 shows that higher concentrations of DOC resulted in higher maximum $f_{CFU/QSU}$ values (sum of Peaks T, C and C+). For all low nutrient conditions, the sum of the maximum $f_{QSU/CFU}$ is higher with increasing DOC conditions. Similarly, for high nutrient conditions incremental increases of the maximum $f_{CFU/QSU}$ are observed. This shows that with higher DOC availability, bacteria are capable of producing increased quantities of AFOM per bacterial cell. This suggests that carbon availability represents a limiting factor to AFOM production within the model system studied. This further supports the notion that AFOM observed in the natural environment will be a direct consequence of the activity of the bacterial cells present and the quantity and availability of a carbon substrate from which to produce AFOM.

Whilst increased DOC availability results in overall increases to the maximum $f_{QSU/CFU}$, there are substantial differences in the relative contribution of each of the studied peaks to the f_{total}. Moreover, the DOC concentration appears to have an influence on the effect of nutrient additions on AFOM

production. In experimental conditions containing no added DOC and 5 mg L^{-1} DOC, the addition of nutrients results in an increase in Peak T fluorescence and a decrease in Peaks C and C+. However, in high nutrient and excess DOC conditions, there is a substantial decrease in Peak T fluorescence, and an increase in the production of Peaks C and C+, in comparison to the observed fluorescence exhibited in low nutrient, excess DOC conditions. This suggests that when the availability of carbon substrate in the system is a limiting factor, the production of Peak T takes precedent within the system. Peak T is considered to represent intracellular structural and functional compounds such as amino acids, which are essential for cell growth and replication (Coble et al., 2007) and therefore may take priority when carbon is limited, or in high demand, to the bacteria within the system. However, when carbon is available in excess, additional nutrient resources may be diverted to the production of higher molecular weight compounds such as Peaks C and C+. A possible theory to explain this may be that the community is producing a pool of more recalcitrant compounds to store carbon whilst DOC is available in excess, though further work would be needed to confirm this postulation. Conversely, when DOC is available in excess but nutrient resources are limited, the ability to produce these higher molecular-weight compounds may be compromised, leading to an excess production of smaller, simpler proteinaceous material. By providing a nutrient-limited baseline which can be incrementally manipulated to study the effects of controlled nitrate, phosphate and DOC loading on the system, it has been demonstrated that the availability of these nutrients has a significant impact on the fluorescence production by the bacterial species present within our controlled model system. This further supports previous findings that fluorescence intensity measurements cannot be used as a surrogate measure of bacterial enumeration. When monitoring fluorescence within natural systems, it may be important to consider the effect of changing environmental conditions such as nutrient and DOC availability on the intensity and ratios of fluorescence peaks present to obtain an insight into the functioning of a system.

The DOC availability within the system is also seen to influence the normalized fluorescence intensity per bacterial cell ($f_{QSU/CFU}$). Greater variations were observed in high-nutrient, excess DOC conditions than in any other experimental condition (Figure 3.2) in relation to Peaks C and C+. This is possibly because organic matter produced by *P. aeruginosa* is known to fluoresce in the Peak C+ region which also corresponds to the observed fluorescence properties of the siderophore pyoverdine (Wasserman, 1965). Pyoverdine is an extracellular iron-scavenging metabolite, and is strongly pigmented (Meyer, 2000). It is possible that the rapid production of Peak C+ shown in our data can be attributed to the production and exporting of pyoverdine from the bacterial cells. The production of pigmented, water-soluble extracellular siderophores by *Pseudomonas* species has long been known to be influenced by a range of environmental factors (Cornelis et al., 2002). The differential expression of these

fluorescent pigments as a result of external factors such as nutrient availability could suggest that under high-nutrient conditions, external factors controlling the rate of fluorescence production may be affecting the system, resulting in the variability seen only within the high-nutrient, excess DOC conditions. The variability in the expression of fluorescent pigments by bacteria as a result of nutrient and DOC availability further highlights the complexities associated with using fluorescence intensity as a predictor for bacterial enumeration, but could support its application as a useful biomarker for a metabolically active microbial population, particularly in relation to its responses to changing environmental conditions in natural waters. The observed high variations in Peak C/C+ fluorescence intensities within the high nutrient, excess DOC conditions could be attributed to metabolic differences between independent biological populations of the same species. Observed variations between individual fluorescence measurements within experimental repeats are much lower, eliminating instrumental variability. Therefore, we postulate that the variations in exported humic-like AFOM are driven by metabolic variations between discrete populations of *P. aeruginosa.* This is further supported by the $f_{QSU/CFU}$ data which demonstrates that the measured fluorescence values are independent of cell numbers. In addition, whilst pyoverdine fluoresces in the humic-like region, it is not considered to represent humic-like material. Siderophores are usually considered a group of low molecular weight compounds, often between 500 – 1500 Daltons (Da) (Hider and Kong, 2010). Pyoverdine has a molecular weight of 1335.4 Da which, whilst still considered to be low molecular weight, does represent a higher molecular weight than glucose, at 180 Da. This suggests the possible production of higher molecular weight compounds (pyoverdine) from a simple and labile carbon source (glucose) is occurring.

3.4. Conclusions

- In this model system, *P. aeruginosa* is capable of producing a range of AFOM including Peaks T, C and C+ from basic constituents within a simulated freshwater model. This includes the production of material which fluoresces in the allochthonous region, which is conventionally associated with higher molecular weight material. *P. aeruginosa* is capable of producing this under all conditions, both from a simple carbon source (glucose) and where no introduced glucose-DOC is available. A possible mechanism may include the demineralization of inorganic carbon and the utilization of carbon derived from the microbial inoculum to produce AFOM.
- The relationship between fluorescence intensity and bacterial cell number is not linear over the experimental time studied. During times of known upregulated metabolism, e.g. the exponential phase of the bacterial growth curve, higher $f_{QSU/CFU}$ is observed. This suggests that the production of AFOM increases during times of metabolic upregulation and supports the

concept that fluorescence intensity represents a useful marker for microbial community activity rather than as an enumerator.

- Both fluorescence intensity and fluorescence peak ratios are influenced by the concentration of nitrate, phosphate and DOC within the system. Whilst higher DOC concentrations result in higher total fluorescence, this also influences the response of the bacterial community to the introduction of nutrients. This suggests that caution should be taken when attempting to use inherent fluorescence intensity as a predictor for the direct enumeration of bacteria within natural systems which are influenced by changing conditions.

Chapter 4. Investigating microbial AFOM production and metabolism using radiolabelled isotopes

4.1. Introduction

Fluorescence has long been used as a technique for monitoring the presence of organic matter in freshwaters (Carstea et al., 2010, 2014, 2016; Hudson et al., 2007; Khamis et al., 2018; Reynolds, 2002, 2003), with focus on tracing DOM through space and time to monitor storm events, residence times and other hydrological controls (Kothawala et al., 2014; Miller & McKnight, 2010). In addition, it has been used to monitor the efficacy of sewage treatment and detecting microbial contamination in surface and groundwaters (Baker, 2002; Baker & Inverarity, 2004; Reynolds & Ahmad, 1997; Sorensen et al., 2018). Throughout this research, there has been a continuous decoupling of the two 'main' forms of AFOM – protein-like and humic-like – with the former considered to be microbially-derived, autochthonous material and the latter considered to be allochthonous material imported into surface waters from the breakdown of plant material within the surrounding catchment. Due to its association with amino acids found in bacterial cells, protein-like AFOM has been extensively used to monitor the presence of bacteria, specifically *E. coli*, for detecting sewage contamination (Ahmad & Reynolds, 1995; Reynolds, 2003; Sorensen et al., 2015, 2018, 2020).

A growing body of literature in recent years has, however, begun exploring the use of protein-like AFOM for monitoring microbial activity in freshwater systems. These studies have employed fluorescence as a means of understanding underpinning biogeochemical processes which occur in freshwater systems, such as ecosystem metabolism and respiration, bacterial production, and carbon demand (Berggren et al., 2020; Kinsey et al., 2018b; Sjöstedt et al., 2021). These studies have found, for example, links between DOM turnover and bacterial production and respiration rates in subarctic lakes. In addition, there have been several recent laboratory-based studies where the relationship between fluorescence and microbial growth/cell number has been explored (Fox et al., 2017, 2018, 2021; Perrin et al., 2022). These studies have found a non-linear relationship between fluorescence and cell number, suggesting caution should be taken when using fluorescence to infer the inherent presence of bacteria in surface freshwaters where there are a number of external inputs and a diverse microbial community. These findings point towards the potential application of fluorescence as a measurement for an active microbial population, rather than cell number alone.

One finding, explored in Chapter 3, suggests that the increase in AFOM production per bacterial cell, during times of increased growth rate (such as the exponential growth phase within bacterial growth curves) and in conditions more conducive to increased growth rate (such as those with high

concentrations of nutrients), could occur as a result of upregulated metabolic activity. However, these conclusions remain speculative as they are based on data relating to cell numbers and AFOM production alone. To date, no studies have observed the direct relationship between AFOM production, cell number, and metabolism. Enhancing our understanding of this relationship will not only shed light on the underpinning processes which dictate the nature of AFOM production and consumption, but will also inform the use of fluorescence as a water quality parameter for measuring ecosystem processes in-situ. Whilst current methods of water quality monitoring focus on structural parameters such as invertebrate and macrophyte diversity, and physico-chemical attributes, real-time processes, such as ecosystem metabolism and respiration, are able to notice changes in water quality more rapidly, and provide more information about how these changes are influencing the wider system.

It is clear that more work is needed in assessing the role that bacterial activity plays in the production of AFOM and its characteristics in order to inform the mechanisms which underpin DOM processing. The work described in this chapter explores the relationship between bacterial AFOM processing and cell number as a function of bacterial production, calculated using bacterial leucine incorporation rates. This approach provides an in-depth insight into the metabolic rate of bacteria throughout a complete growth curve analysis, providing a direct comparison of AFOM production, growth rate, and metabolism across a number of bacterial species, from both laboratory and environmental sources, to determine whether AFOM production could act as a marker for biological metabolism in freshwater systems.

4.2. Results: AFOM production over 48 h

Four bacterial strains (*Pseudomonas aeruginosa, Escherichia coli,* Isolate 7, Isolate 15) were investigated over a 48 h period in simulated freshwater (SFW) to establish the relationships between fluorescence production and processing, bacterial production rates and enumeration (Figure 4.1). Peaks T, C and C+ were all found to be present within each bacterial strain studied (Table 4.1), at varying degrees of intensity. Peak T fluorescence was found to be the dominant peak present across growth curves from all bacterial strains isolated from the River Thames, with Isolate 7 displaying the highest Peak T intensity at 9.552 (±0.599) QSU, and both *E. coli* and Isolate 15 displaying lower intensities at 3.527 (±2.660) QSU and 3.103 (±0.243) QSU respectively. Peaks C and C+ were also present in all environmental isolates but at lower intensities (< 0.5 QSU for all environmental isolates).

Overall fluorescence intensity across all peaks was highest for the laboratory strain, *P. aeruginosa*, with fluorescence peak intensities ranging from between ten-fold and one thousand-fold higher than the environmental isolates. It is already understood, from data discussed in Chapter 3, that *P.*

aeruginosa exhibits high fluorescence intensities when processing AFOM in SFW, in particular the Peak C+ region, which was the most intense fluorescence peak present within this growth curve for this strain at 629.912 (±21.129) QSU at 48 h. However, it is of note that data presented in Table 4.1 outlines raw fluorescence intensity data at 48 h without considering the effect of cell density. As such, more intense fluorescence signals from *P. aeruginosa* were likely to have occurred as a result of higher cell densities for this strain, shown in Figure 4.2.

Table 4.1 Fluorescence intensities at 48 h for Peak T, C and C+ for all bacterial strains investigated (n=3 biological and technical replicates). Fluorescence intensities are reported in QSU (quinine sulphate units). Variation is also provided in the form of SD (denoted ±).

	Pseudomonas aeruginosa	***Escherichia coli***	**Isolate 15**	**Isolate 7**
T	30.655 (±2.660)	3.527 (±0.591)	3.103 (±0.243)	9.552 (±0.599)
C	83.144 (±3.324)	0.47 (±0.327)	0.132 (±0.049)	0.379 (±0.04)
C+	629.912 (±21.129)	0.162 (±0.068)	0.055 (±0.013)	0.296 (±0.034)

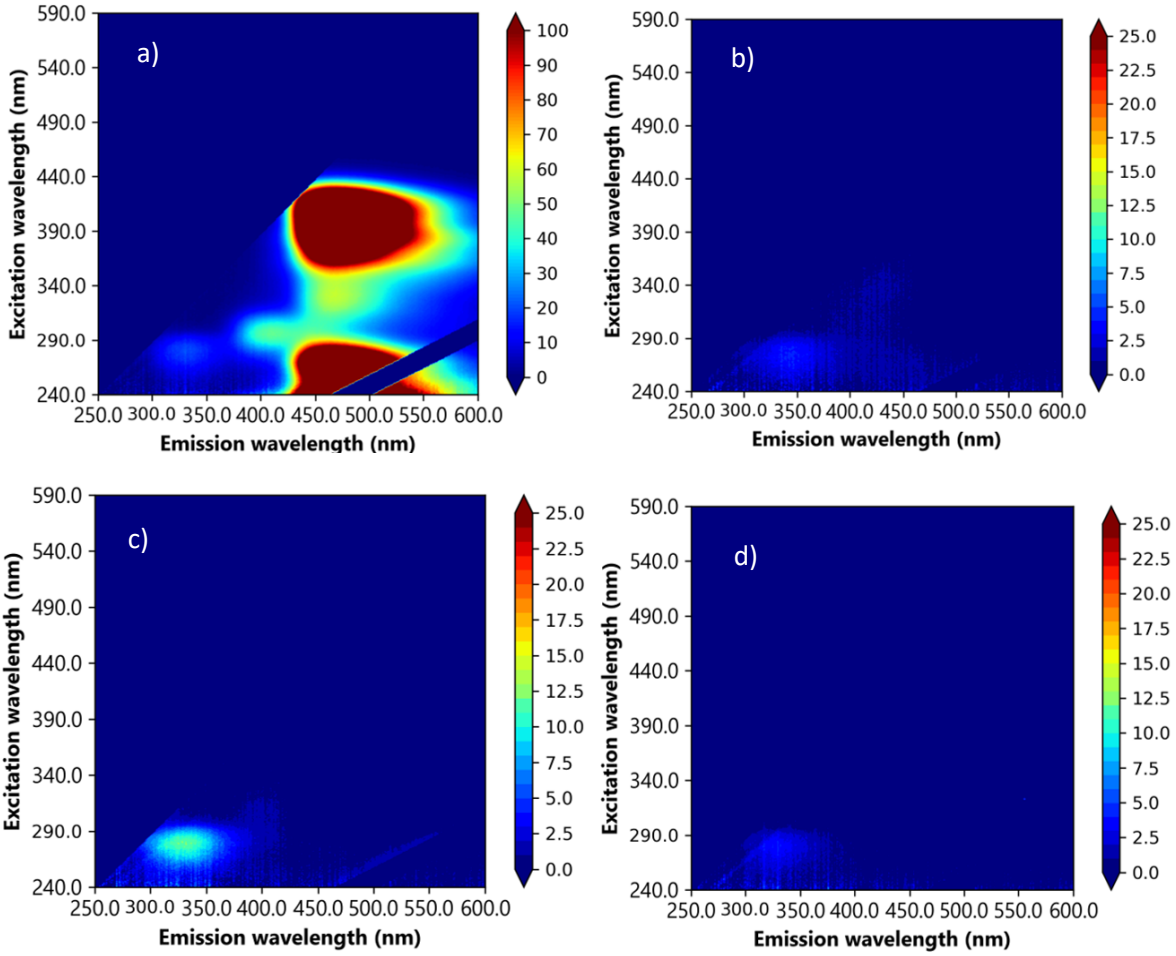

Figure 4.1. Excitation-emission matrices (EEMs) showing AFOM production after 48 h for four bacterial strains: a) *Pseudomonas aeruginosa,* b) *Escherichia coli,* c) Isolate 7 and d) Isolate 15.

Radiolabelled tritiated leucine, or [^{3}H]-Leucine, was used to measure bacterial leucine incorporation (BLI) and therefore estimate bacterial production (BP) for all strains of bacteria. Growth curves were undertaken over a 48 h period, with BLI measured in tandem with fluorescence and cell number. Parameters were measured at the following time points: 0, 4, 8, 24 and 48 h. For *P. aeruginosa* growth curves, an additional time point was investigated at 12 h due to the occurrence of a known increase rate of growth during this time period, as seen in Chapter 3. SFW conditions containing 0.1 mg L^{-1} phosphate, 50 mg L^{-1} nitrate and 5 mg L^{-1} dissolved organic carbon in the form of glucose (SFW3, described in Table 2.2) were chosen to undertake this work due to the nature of the conditions providing adequate nutrients and carbon to allow the phenomenon of AFOM production and processing to take place, whilst remaining representative of environmental conditions.

4.2.1. *Pseudomonas aeruginosa*

P. aeruginosa was selected as a model organism with which to first investigate the relationship between AFOM production, cell number and bacterial production (BP). This strain has been previously characterised in terms of growth dynamics and AFOM production in a range of nutrient environments in Chapter 3. Thus, it was considered a reasonable organism with which to begin investigating this method.

Initial results in Figure 4.2 show the relationship between cell number and BP over the 48-hour experimental period. Both cell number and BP follow a classical 'growth curve' pattern, with cell number displaying an initial decrease post-inoculum (as is also seen in Chapter 3), where CFU mL^{-1} drops from 1.5 x 10^5 CFU mL^{-1} to 3.5 x 10^4 CFU mL^{-1} between hours 0 and 4, before increasing to a maximum of 8.9 x 10^6 CFU mL^{-1} at hour 24. Cell number then decreases to 1.8 x 10^6 CFU mL^{-1} at hour 48. Over the duration of the growth curve, BP follows a similar pattern, but reaches maximum at hour 12, 12 hours prior to the maximum cell number value recorded. Following this, BP begins to decrease, preceding the decrease in cell number. Whilst not significant, there is a positive relationship (R^2 = 0.657, $p > 0.05$) between cell number and BP.

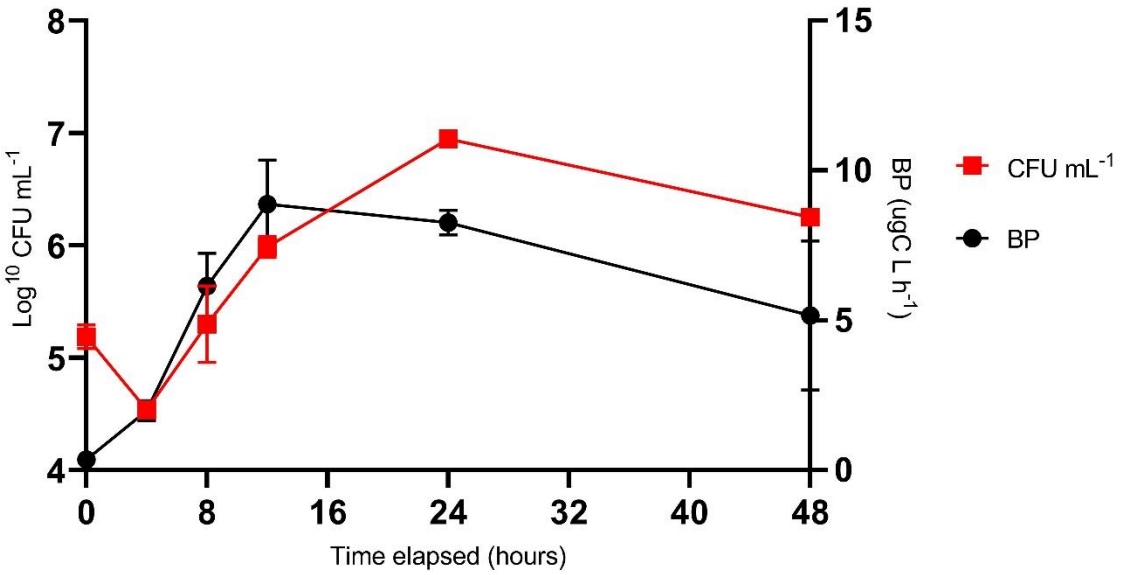

Figure 4.2 Cell number (CFU mL^{-1}) and bacterial production (µg C L h^{-1}) over a 48 h growth curve period for *Pseudomonas aeruginosa* (n=3 biological and technical replicates). Error bars denote standard deviation.

Despite the initial positive relationship between cell number and BP, normalised data (Figure 4.3) which depicts BP as a function of cell number (expressed as µg C 10^6 CFU L h^{-1}) and cell number as a function of growth rate (the increase in CFU mL^{-1} per hour throughout the growth curve period, expressed as CFU mL hr^{-1}) found a negative correlation between the two datasets. Whilst this was not found to be significant (R^2 = -0.371, p > 0.05), it is clear that when data is normalised to account for cell number and rate of cell replication, the relationship between cell number and BP becomes inverse. In this instance, the rate of BP is higher in the first 8 hours of the growth curve, reaching its maximum at 4 h, suggesting an increase in metabolic rate and activity during the exponential phase of the bacterial growth curve.

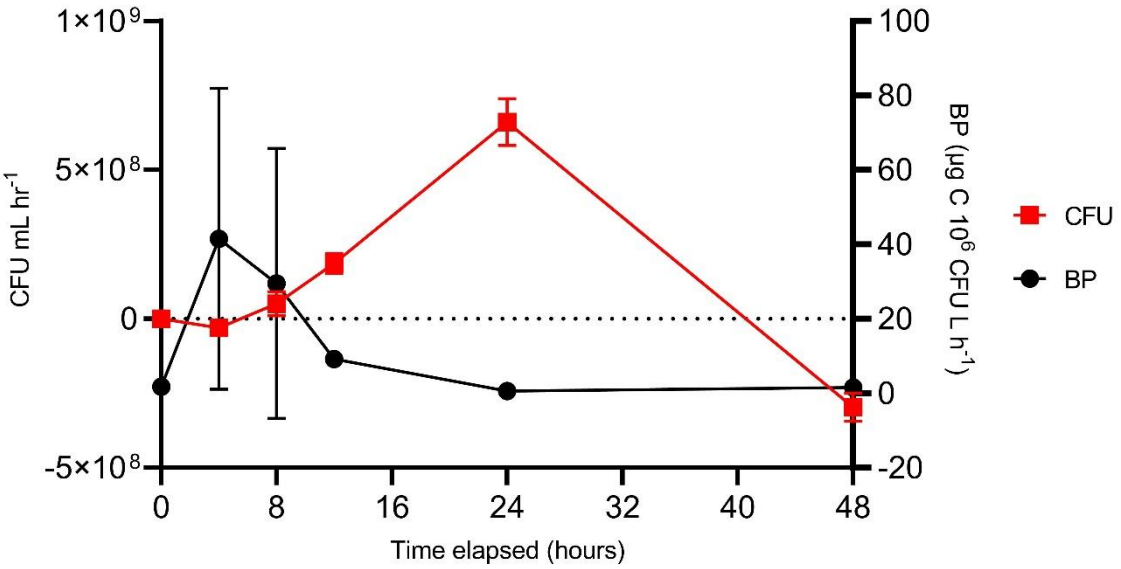

Figure 4.3 Cell number depicting the increase in cells per hour (CFU mL h^{-1}), and bacterial production normalised to the number of cells present (µg C 10^6 CFU h^{-1}) over a 48 h growth curve period (n=3 biological and technical replicates). Error bars denote standard deviation.

Figure 4.4 shows the relationship between fluorescence and normalised BP for Peaks T, C and C+. Peaks T and C both reach their maximum rate of fluorescence increase at 4 h. This is in-line with BP values, where the highest rate per cell also occurs at 4 h. Peak T then decreases until 8 h, and Peak C decreases until 12 h, before both begin to gradually increase again until the final measured time point at 48 h. Both Peak T (R^2 = 0.5291, p > 0.05), and Peak C (R^2 = 0.5319, p > 0.05), were found to have a positive correlation with BP per cell, although neither were found to be significant. Peak C+ displayed an increase in fluorescence between 0 and 12 h, reaching its maximum rate of fluorescence increase at 12 h. The rate then decreases between 12 and 24 h, before increasing again over the last 24 h up

until the final measured time point at 48 h. There was found to be a non-significant negative correlation between BP and Peak C+ (R^2 = 0.1731, p > 0.05).

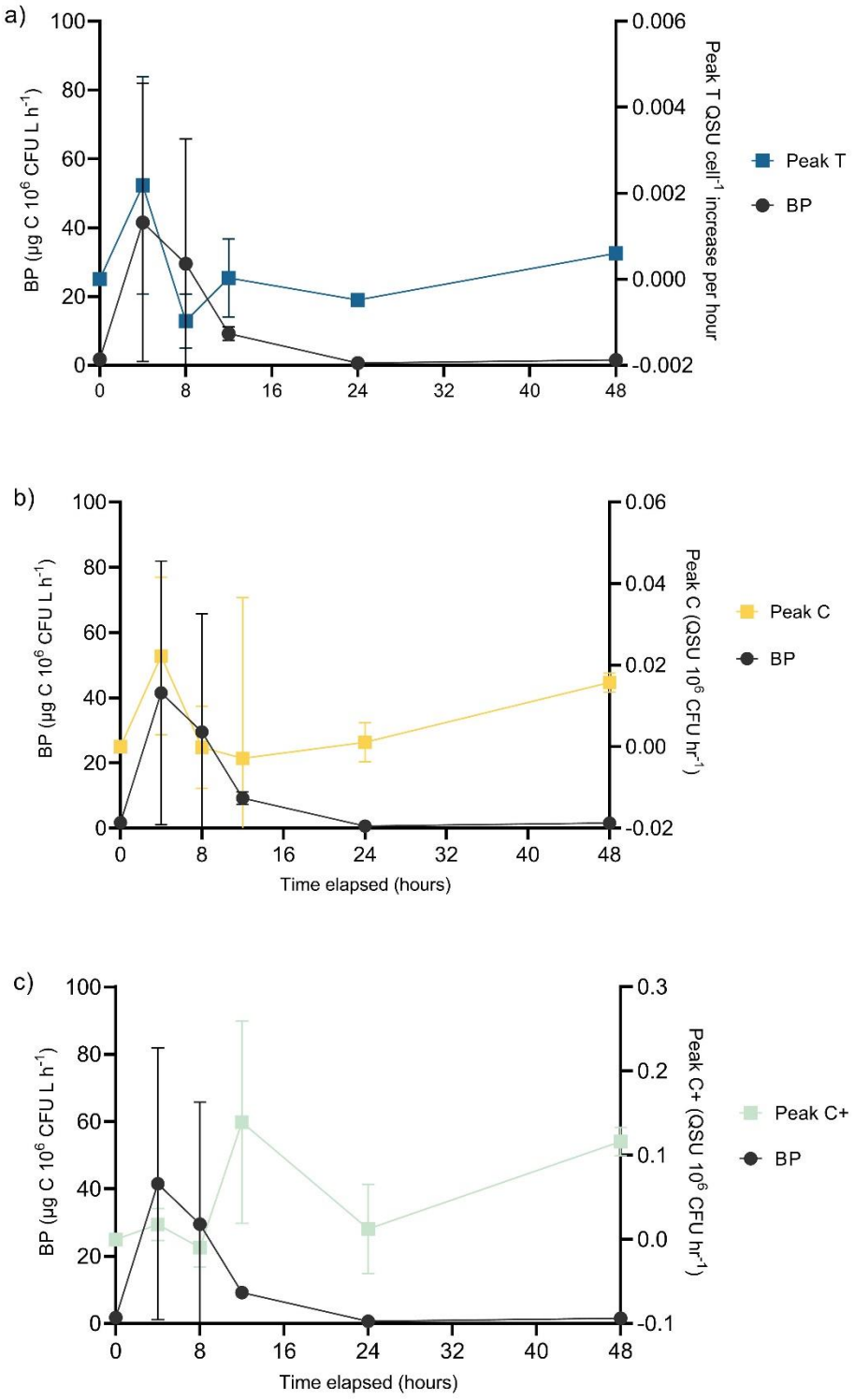

Figure 4.4 Fluorescence (expressed as the increase in QSU per cell per hour, QSU 10^6 CFU hr^{-1}) for Peaks T, C and C+ and bacterial production (expressed as µg C per 10^6 cells L h^{-1}) over a 48 h growth curve period for *Pseudomonas aeruginosa* (n=3 biological and technical replicates). Error bars denote standard deviation.

4.2.2. Escherichia coli

To investigate the processing of AFOM in model systems by environmental bacteria, strains were selected which were able to proliferate both within a high-nutrient broth at 37°C so as to obtain a high-density overnight inoculum prior to beginning the experiments, and also within the SFW high nutrient, 5mg L^{-1} DOC variant medium to ensure growth within the experiments.

Initial results in Figure 4.5 showing raw uncorrected data display a classical growth curve pattern for *E. coli*. Cell numbers increase over the first 8 h of the exponential growth phase of the growth curve, reaching a maximum of 3.8 x 10^5 CFU mL^{-1}. Cell numbers then gradually decrease over the remaining period of the growth curve. Whilst the BP reaches its peak earlier (4 h), the pattern is similar to data from *P. aeruginosa* in that the BP appears to precede cell number data, reaching its peak before cell numbers, before decreasing for the remainder of the growth curve.

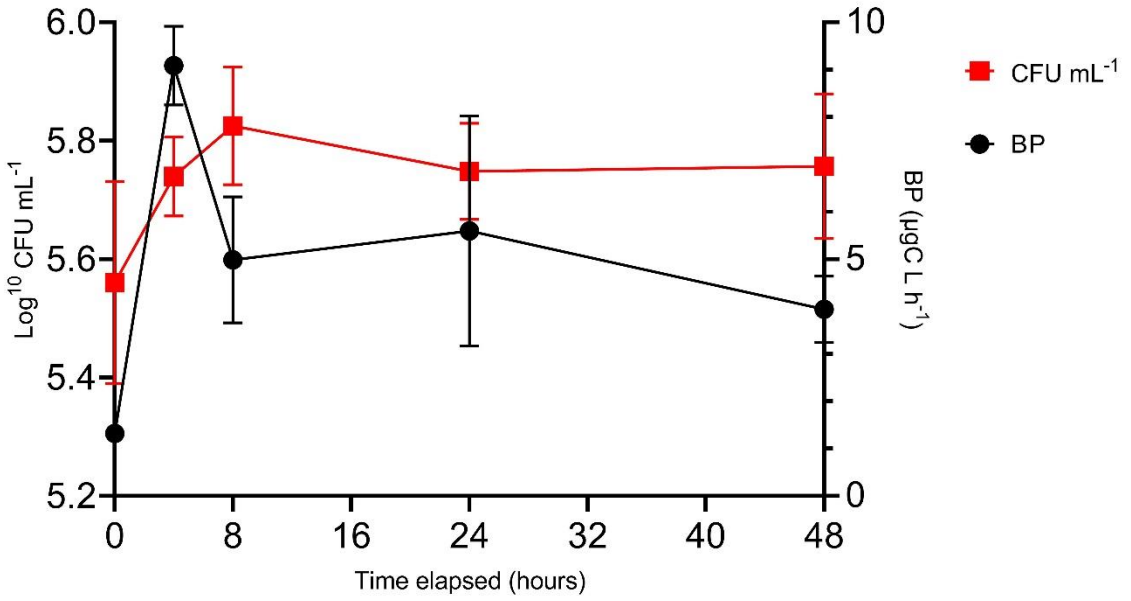

Figure 4.5 Cell number (CFU mL^{-1}) and bacterial leucine incorporation (µg C L h^{-1}) over a 48 h growth curve period for *Escherichia coli* (n=3 biological and technical replicates). Error bars denote standard deviation.

Figure 4.6 shows BP normalised to cell number, and cell number expressed as a rate of increase per hour. Unlike data displayed in the *P. aeruginosa* normalised growth curve (Figure 4.3), where the maximum rate of cell increase occurs at 24 h (20 h later than the maximum increase in BP), *E. coli* instead displays a shift towards the beginning of the growth curve period for cell number increase. BP does not appear to display much change following normalisation to cell number (Figure 4.6), possibly

due to the smaller increase and decrease in CFU over the growth curve period that is displayed by *E. coli* in comparison to *P. aeruginosa.*

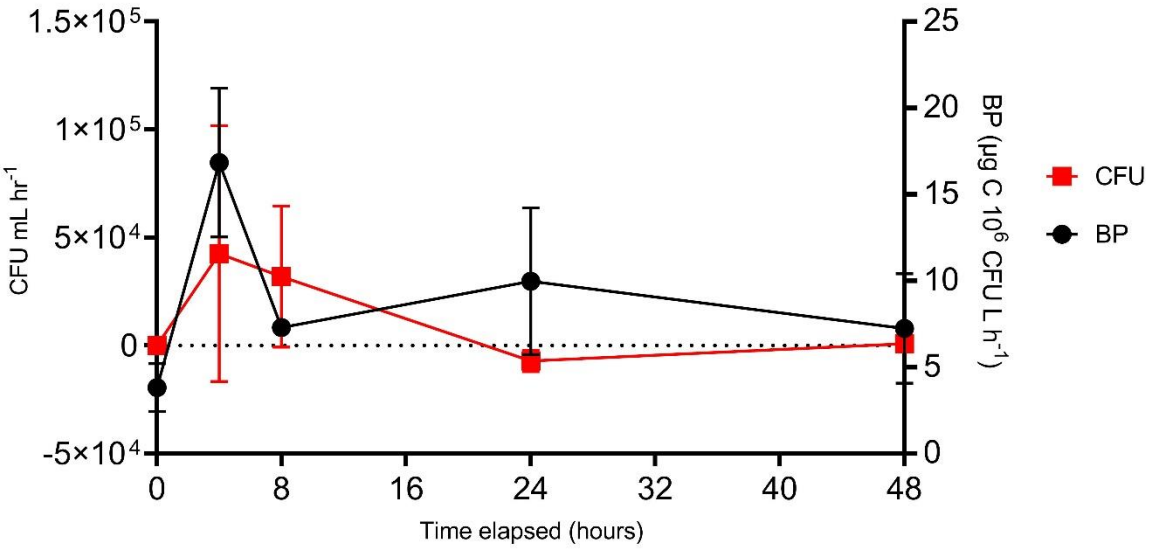

Figure 4.6 Cell number depicting the increase in cells per hour (CFU mL h^{-1}), and bacterial production normalised to the number of cells present (µg C 10^6 CFU h^{-1}) over a 48 h growth curve period for *Escherichia coli* (n=3 biological and technical replicates). Error bars denote standard deviation.

The relationship between BP and fluorescence Peaks T, C and C+ for *E. coli* is shown in Figure 4.7. The highest period of increase in fluorescence intensity occurs between 0 and 4 h for all peaks, corresponding with the greatest increase in BP value. Peak T increases by 1.27 QSU 10^6 CFU^{-1} during this time, before decreasing by 0.13 QSU 10^6 CFU^{-1} between 4 and 8 h. A smaller increase of 0.1 QSU 10^6 CFU^{-1} is then seen between 8 and 24 h, before a final decrease between 24 and 48 h. This pattern of fluorescence intensity change over the growth period occurs in tandem with BP values, represented by a significant correlation between Peak T and BP for *E. coli* (R^2 0.8255, $p < 0.05$). Peak C follows a similar trajectory to Peak T for all time points except for the final measured 24 h of the experiment. Peak C reaches its maximum QSU increase at 4 h, where there is an increase of 0.038 QSU 10^6 CFU^{-1} before decreasing by 0.02 QSU 10^6 CFU^{-1} between 4 and 8 h. An increase in fluorescence intensity is then seen for the remainder of the experimental period between 8 and 48 h. Peak C and BP are seen to have a slightly positive, yet non-significant, correlation ($R^2 = 0.4360$, $p > 0.05$). Peak C+ also reaches its highest value at 4 h, seeing an increase of 1.09 QSU 10^6 CFU^{-1} before decreasing between 4 and 8 h by 0.005 QSU 10^6 CFU^{-1} in a similar trajectory to Peaks T and C. However, following this decrease, Peak C+ remains low for the duration of the experimental period, seeing no further significant increase

in fluorescence intensity. A significant correlation was seen between Peak C+ and BP ($R^2 = 0.8048$, $p < 0.05$).

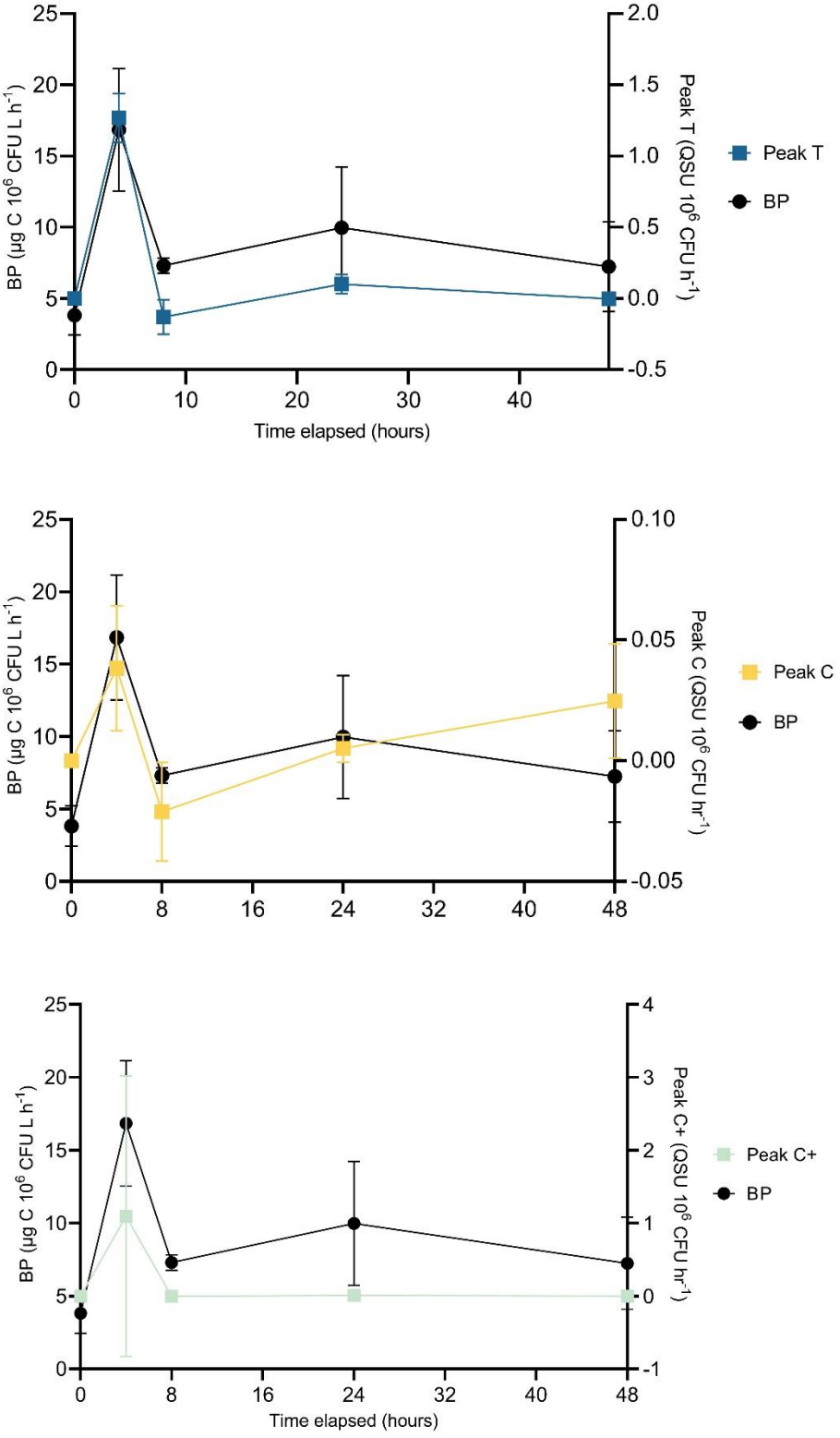

Figure 4.7 Fluorescence (expressed as the increase in QSU per cell per hour, QSU 10^6 CFU hr^{-1}) for Peaks T, C and C+ and bacterial production (expressed as µg C per 10^6 cells L h^{-1}) over a 48 h growth curve period for *Escherichia coli* (n=3 biological and technical replicates). Error bars denote standard deviation.

4.2.3. Isolate 7

Uncorrected data showing BP and CFU mL^{-1} show a largely similar pattern throughout the duration of the growth curve period, apart from 0-4 h (Figure 4.8). An initial drop in CFU mL^{-1} occurs between 0 and 4 h, suggesting a shock to the inoculum upon introduction to the SFW matrix, possibly causing rapid cell death prior to the beginning of the exponential growth phase. This is not reflected in the BP values, however, where despite the initial drop in bacterial load, the BP begins to increase immediately between 0-4 h. However, this activity rate is seen to be slower than the following 4 hours, suggesting an upregulation in metabolism due to a shock to the bacterial cells post-inoculation. Both CFU and BP reach their maximum at 24 h, before decreasing back to near their initial 0 h values at 48 h. Despite this, their relationship was non-significant ($R^2 = 0.7380$, $p > 0.05$).

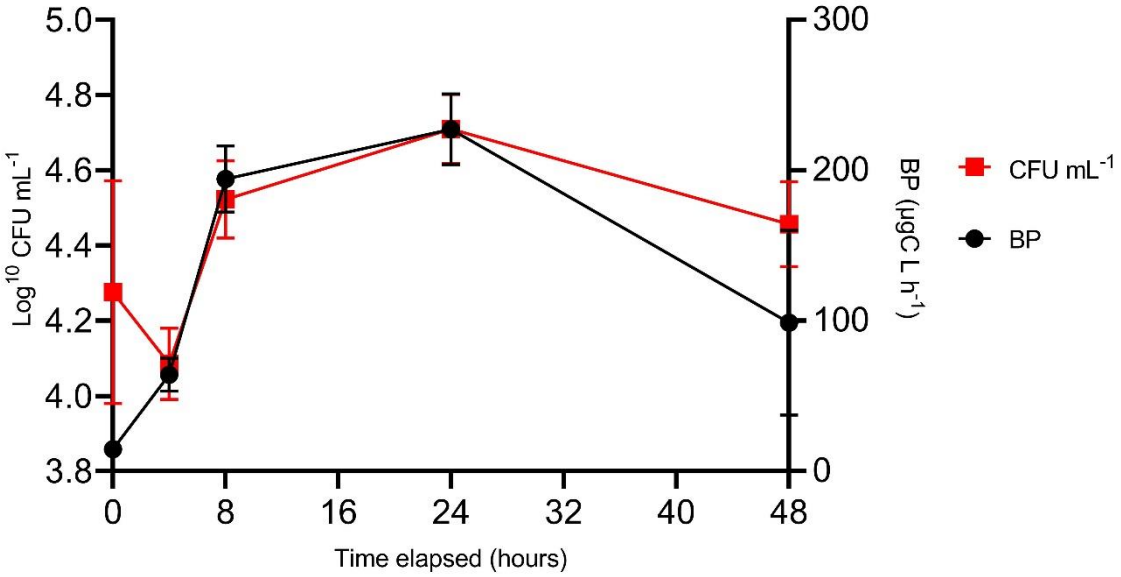

Figure 4.8 Cell number (CFU mL^{-1}) and bacterial production (µg C L h^{-1}) over a 48 h growth curve period for Isolate 7 (n=3 biological and technical replicates). Error bars denote standard deviation.

Figure 4.9 shows corrected CFU and BP data, with BP expressed per 10^6 CFU mL^{-1} and CFU expressed as a rate of change per hour. Both BP and CFU have shifted towards the beginning of the growth curve period, with the highest values for both still falling on the same hour, but now hour 8 rather than hour 24 as in Figure 4.8. Both values then rapidly decrease in tandem with one another between 8 and 48 h to the end of the growth curve period. Despite this, there was found to be a weaker correlation between these values following normalisation ($R^2 = 0.1593$, $p > 0.05$), likely skewed due to the initial drop in cell numbers which does not occur for BP data.

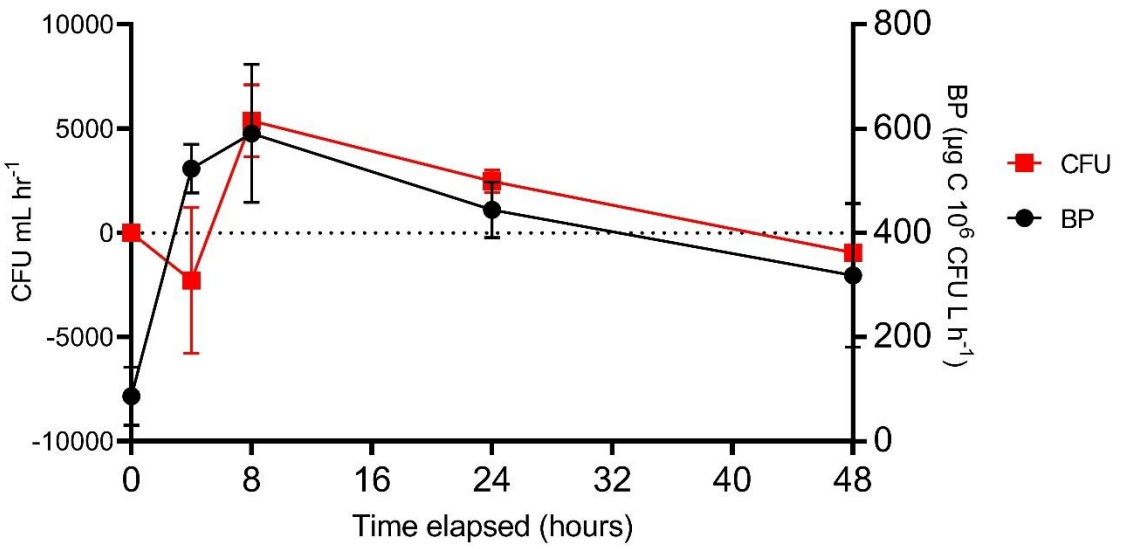

Figure 4.9 Cell number depicting the increase in cells per hour (CFU mL h^{-1}), and bacterial production normalised to the number of cells present (µg C 10^6 CFU h^{-1}) over a 48 h growth curve period for Isolate 7 (n=3 biological and technical replicates). Error bars denote standard deviation.

Normalised fluorescence values shown in Figure 4.10 show a weaker relationship with BP than cell number, or fluorescence values from previous bacterial strains discussed in this chapter. All fluorescence peaks reach their maximum QSU value at 4 h, before decreasing up until 8 h then increasing gradually over the remainder of the experimental period to 48 h. This is in contrast to the BP values, which rapidly increase from 0-8 h where they reach their peak before decreasing for the remainder of the experimental period. No peaks were found to have a significant correlation with BP for this bacterial strain, with Peak T having a correlation of $R^2 = 0.1573$ ($p > 0.05$), Peak C having a correlation of $R^2 = 0.0050$ ($p > 0.05$), and Peak C+ having a correlation of $R^2 = 0.0029$ ($p > 0.05$).

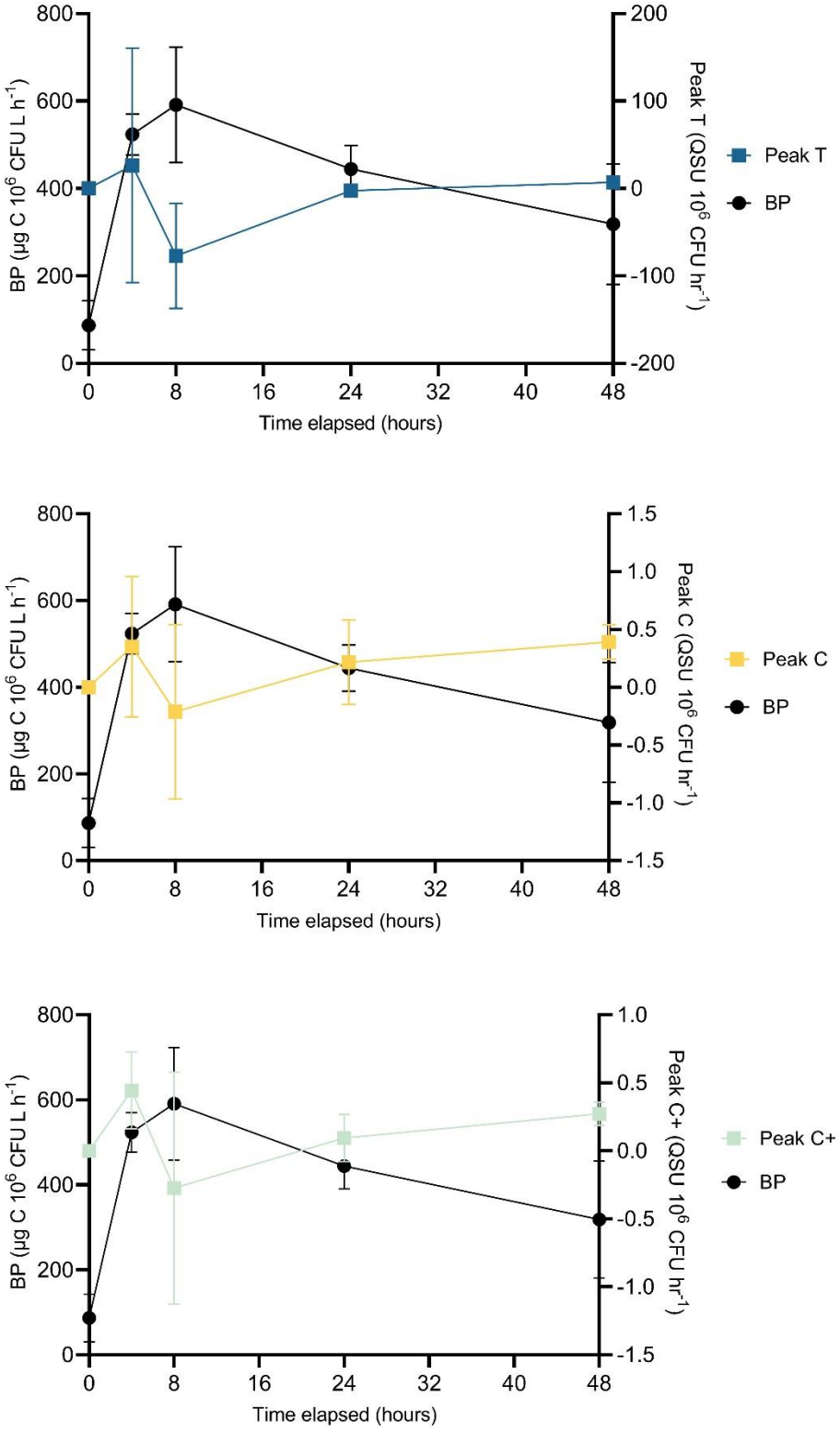

Figure 4.10 Fluorescence (expressed as the increase in QSU per cell per hour, QSU 10^6 CFU hr^{-1}) for Peaks T, C and C+ and bacterial production (expressed as µg C per 10^6 cells L h^{-1}) over a 48 h growth curve period for Isolate 7 (n=3 biological and technical replicates). Error bars denote standard deviation.

4.2.4. Isolate 15

Raw data for BP and CFU (Figure 4.11) shows a general downward trend for both parameters over the experimental period, with cell numbers and BP values decreasing from 4 and 8 h respectively. This is in contrast to all other bacterial strains investigated in this study, in that the growth pattern does not reflect a classical growth curve structure over the experimental period. A possible explanation for this could be that the growth curve occurs over a shorter time period, with the system entering the death phase earlier than other bacterial strains investigated, resulting in a trajectory of cell death from early on in the growth curve.

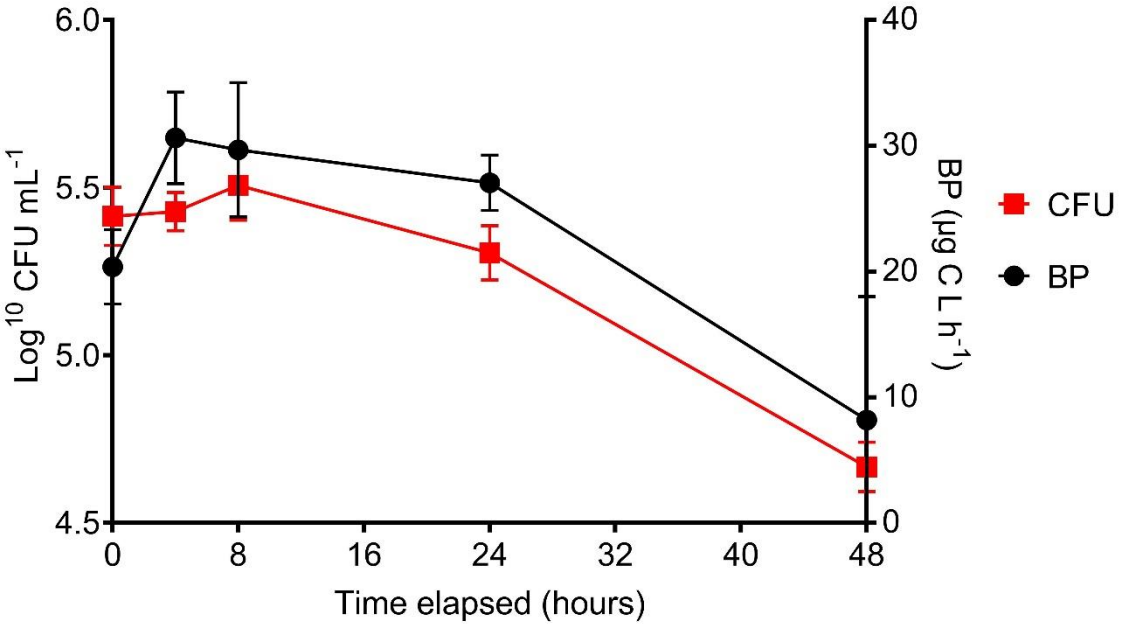

Figure 4.11 Cell number (CFU mL^{-1}) and bacterial production (µg C L h^{-1}) over a 48 h growth curve period for Isolate 15 (n=3 biological and technical replicates). Error bars denote standard deviation.

A minor increase in cell number is observed between 4-8 h, where cell number increases from 2.7 x 10^5 and 3.3 x 10^5 CFU mL^{-1}. Following the peak in cell numbers at 8 h, cell numbers then drop for the remainder of the experimental period by nearly a 1-Log reduction. BP values follow a similar trend, but precede cell number by reaching the highest value at 4 H before gradually decreasing throughout the remainder of the experimental period in line with CFU values. A significant positive correlation was found between CFU and BP for this bacterial strain (R^2 = 0.8191, p = < 0.05), ascertaining that despite the 4 h difference in the highest value for BP and CFU, the two parameters follow a very similar pattern of minor increase before a large decrease in value over the growth curve period.

Data displayed in Figure 4.12, showing BP normalised to CFU and CFU expressed as an increase per hour, shows a considerable diversion between the two parameters over the period studied. Whilst both parameters increase slightly between hours 0 and 4, CFU continues to increase rapidly up to its highest value at 8, before decreasing between 8-24 h then increasing very slightly before 24-48 h. In contrast, BP displays a slight decrease after its highest point at 4 h, before increasing gradually over the remainder of the experimental period between 8 and 48 h. No significant correlation was found between these two parameters when data was normalised ($R^2 = 0.3912$, $p > 0.05$).

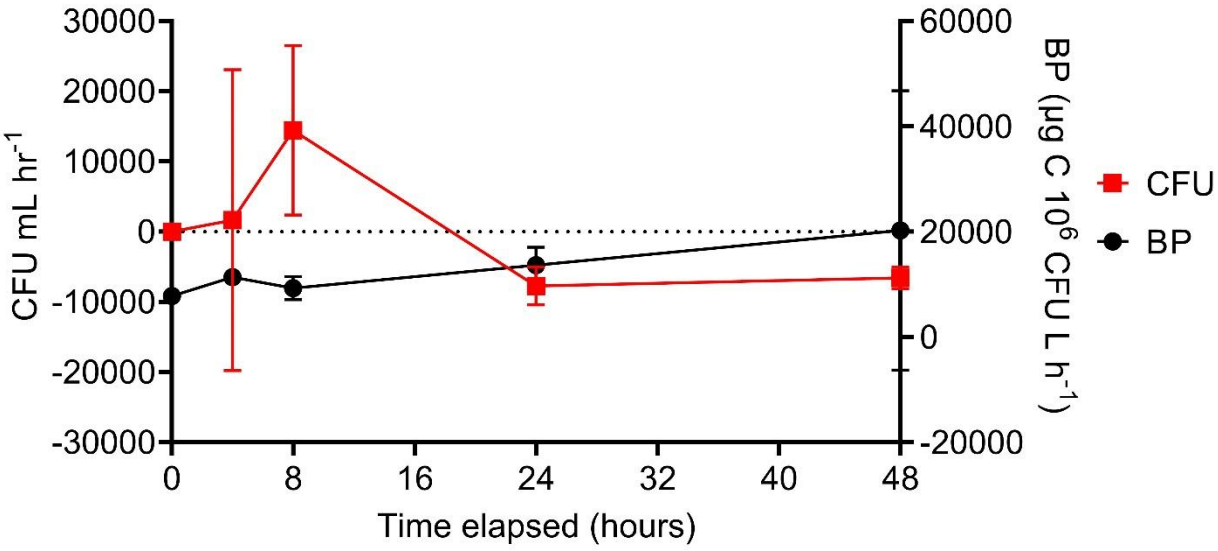

Figure 4.12 Cell number depicting the increase in cells per hour (CFU mL h^{-1}), and bacterial production normalised to the number of cells present (µg C 10^6 CFU h^{-1}) over a 48 h growth curve period for Isolate 15 (n=3 biological and technical replicates). Error bars denote standard deviation.

Data shown in Figure 4.13 displays the relationship between normalised QSU per cell expressed as a function of increase per hour, and BP normalised to cell number. Fluorescence peaks appear to increase steadily over the experimental duration, between 4 and 24 h. Prior to this, all peaks display a slight drop (< 5 QSU) in fluorescence intensity between 0 and 4 h, possibly due to the rapid uptake of AFOM through secondary production upon inoculation into the SFW media. This is supported by the BP data, which shows an upregulation in BP at 4 h. Following the initial drop in AFOM production, all peaks steadily increase until the end of the experimental period. This occurs in tandem with the BP data which also increases steadily. The relationship between Peak T and BP was found to be significant here ($R^2 = 0.8050$, $p < 0.05$), however Peaks C and C+ do not display significant correlations with BP ($R^2 = 0.0699$, $p > 0.05$ and $R^2 = 0.2446$, $p > 0.05$ respectively).

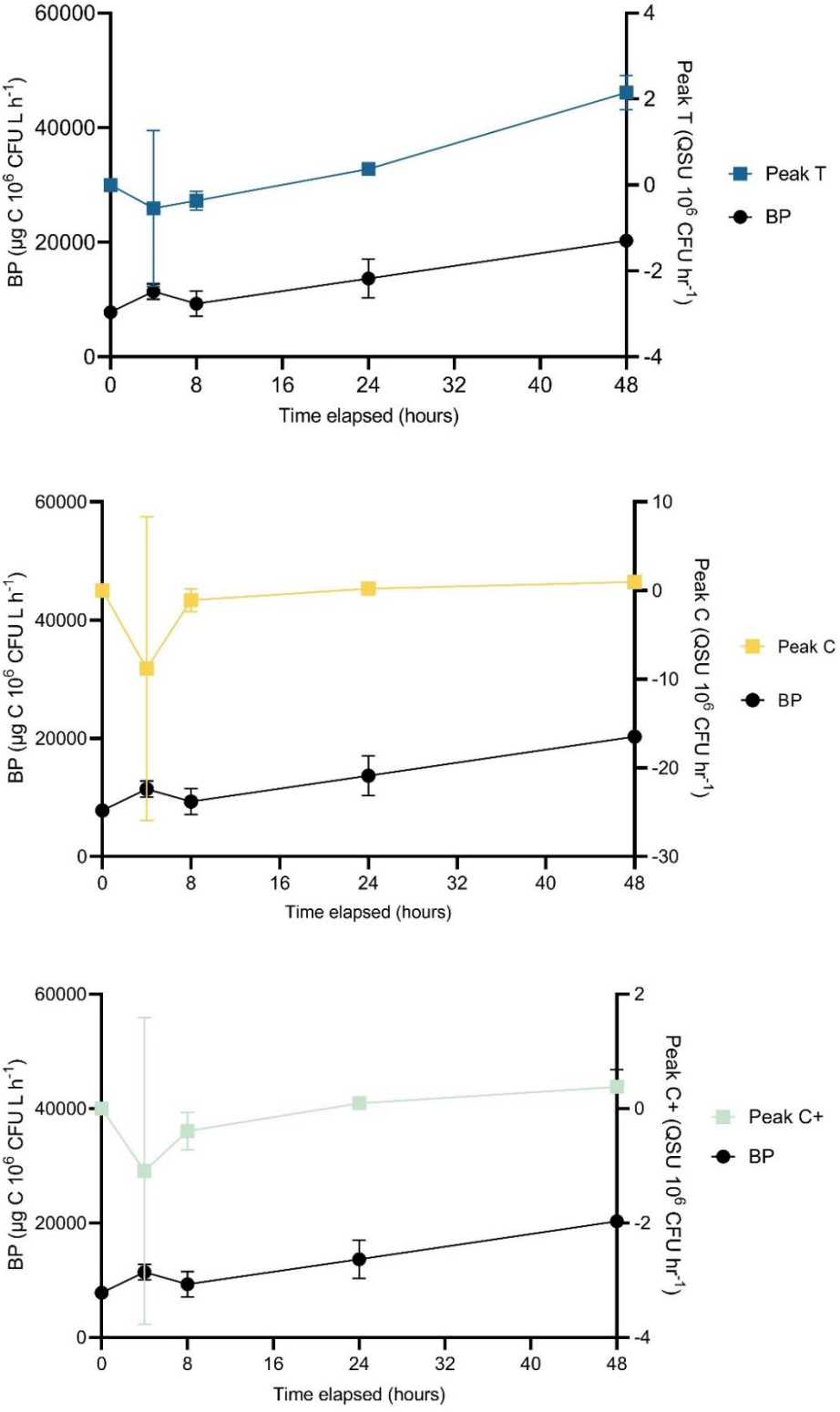

Figure 4.13 Fluorescence (expressed as the increase in QSU per cell per hour, QSU 10^6 CFU hr^{-1}) for Peaks T, C and C+ and bacterial production (expressed as µg C per 10^6 cells L h^{-1}) over a 48 h growth curve period for Isolate 15 (n=3 biological and technical replicates). Error bars denote standard deviation.

4.3. Discussion

At present, the binary

classification system between allochthonous and autochthonous AFOM dictates that protein-like AFOM is sourced from the presence of bacterial cells and generated *in-situ* by microbial metabolic processes, and that humic-like AFOM is imported into aquatic systems from the breakdown of plant materials within surrounding catchments (Hudson et al., 2007, 2008; Reynolds, 2002). Whilst a large body of literature exists pertaining to the characterisation of organic matter, there is still a significant dearth of knowledge regarding specific microbial-OM interactions and the pathways involved in the production, processing and breakdown of AFOM in freshwaters. One of these knowledge gaps relates to the relationship between AFOM and microbial activity and/or presence, with protein-like AFOM often used within fluorescence literature as a surrogate for cell number (Fox et al., 2021; Reynolds & Ahmad, 1997; Sorensen et al., 2015, 2018, 2020). By directly assessing the relationship between microbial AFOM production and processing over time, cell number, and bacterial production using tritiated leucine incorporation techniques, this work was able to provide an insight into the hypothesis that fluorescence acts as a proxy for an active microbial population, as has been stipulated in recent literature (Fox et al., 2017, 2018, 2021; Perrin et al., 2022).

4.3.1. Bacterial cell growth and bacterial production

The work demonstrated in this chapter (Figures 4.2, 4.3, 4.5, 4.6, 4.8, 4.9, 4.11, 4.12) clearly displays a positive relationship between cell number and bacterial production, calculated from measuring the incorporation of tritiated leucine, or [^{3}H]-Leucine, into bacterial cells. Figures in which non-normalised data is shown, i.e. Log^{10} CFU mL^{-1} alongside bacterial leucine incorporation rates expressed as µg C L h^{-1}, demonstrate that the pattern of growth reflects that of a classical bacterial growth curve. It is known that bacterial production can be used to estimate bacterial growth rates through its direct relationship with the synthesis of cellular material during cell replication (Bastviken & Tranvik, 2001; Kirchman, 2001; Jurtshuk, 1996). As such, the relationship seen between these two parameters likely stems from upregulated metabolic rate which often precedes the increase in cell numbers (Kirchman, 2001; Jurtshuk, 1996). In some cases, specifically for *P. aeruginosa* and *E. coli* growth curves, the bacterial production rate can be seen to peak 4 h prior to the highest cell numbers over the growth curve experimental period. This supports the notion that bacterial production is providing an insight into the upregulated metabolic rate that precedes the production of increased bacterial numbers.

Interestingly, the normalisation of data appears to have a different effect on the relationship between BP and cell number in each bacterial strain investigated. Data from all bacterial strains was normalised, whereby BP values where normalised to cell density, and cell density is expressed as a function of increase per hour, providing a value which is more closely comparable with BP in that it is expressed as a rate-like value rather than a cumulative value. For *P. aeruginosa* and Isolate 7 growth curves, the normalization of BP values resulted in a shift of the 'peak' BP value – that is, the point of the growth

curve at which the BP rate was highest – towards the beginning of the experimental time period. In both instances, this changed the relationship between cell density and BP, resulting in weaker correlations, with the R^2 value for *P. aeruginosa* decreasing from 0.657 to 0.0561 following normalisation. For Isolate 7, the R^2 value decreased from 0.7380 to 0.1593 following normalisation.

A possible explanation for the diversion between BP and cell number following normalisation could be that prior to normalising BP values to account for cell density, higher values are likely reflecting the presence of a higher number of cells within the system. As such, there is more likely to be a correlation between these two values. Following normalisation, the shift of the highest BP rate towards the beginning of the growth curve often causes this to fall within the exponential growth phase of the bacterial growth curve. This suggests that the BP values are more reflective of an active microbial population that is dividing and multiplying during exponential growth, rather than simply a higher presence of cells, as non-normalised data may suggest. In particular, the inverse relationship between cell number and BP values seen in Figure 4.3 suggests that a microbial population may be more active in assimilating biomass prior to growth and reproduction during times of stress, such as in the early hours post-inoculation. In this model system, this is highly likely due to the low nutrient and carbon content that is present within the SFW matrix when compared with the high-nutrient overnight broth media in which the bacterial strains were initially cultivated. This hypothesis is supported by the raw, uncorrected data (Figure 4.2 and 4.8) from both *P. aeruginosa* and Isolate 7, where CFU mL^{-1} values can be seen to drop by 0.7 and 0.2-Log respectively between 0-4 h of the experimental growth period, before beginning to increase rapidly into exponential growth. During this time, both bacterial strains see a rapid increase in activity, shown through BP values, despite cell death.

Whilst *P. aeruginosa* displayed the highest peak intensity for all AFOM peaks out of the four bacterial strains studied, it did not display the highest bacterial production rate of all the strains investigated. In fact, normalised bacterial production rate was substantially lower than other strains at between 2 and 16 µg C 10^6 CFU L h^{-1}. A potential explanation for this could be the substantially higher cell numbers that were present in the *P. aeruginosa* system, rising to 1 x 10^7 CFU mL^{-1}; 2-Log higher than any other bacterial strain investigated. Due to the minimal nature of the SFW medium used for this study, a limited quantity of essential nutrients such as carbon, nitrate and phosphate exist with which to undertake secondary production. From work undertaken in Chapter 3, and published in Perrin *et al*. (2022), it is known that dissolved organic carbon represents a limiting factor to growth and AFOM production in this system. As such, the higher number of bacterial cells present in the *P. aeruginosa* system compared with the three other bacterial strains studied could have resulted in higher competition for available resources, thereby limiting the potential for secondary bacterial production.

For the remaining two bacterial strains, *E. coli* and Isolate 15, uncorrected data (rather than corrected) shows BP preceding bacterial growth. Data for *E. coli* shows that both corrected and uncorrected data exhibits similar patterns for BP, with the highest value remaining at 4 h and the overall pattern of change throughout the experimental period being very similar for both corrected and uncorrected datasets. For Isolate 15, a significant positive correlation was found between BP and cell number (R^2 = 0.8191, $p < 0.05$), whereby despite an initial diversion between these two parameters between 0-4 h, the remainder of the growth curve period shows a drastic decrease for both values, with cell numbers decreasing by 0.8-Log and bacterial production rate decreasing by two-thirds (Figure 4.11). A potential explanation for this finding could be that unlike all other bacterial strains investigated in this study, Isolate 15 displays relatively very low bacterial production rates throughout the experimental period, with its maximum BP value being at around one-tenth of other strains. This, coupled with the very low levels of bacterial growth over time, suggests that the overall activity of this strain is very low. In addition, the significant positive correlation between cell number and bacterial production rate for the non-normalised data shown in Figure 4.11 results in a flat line in BP values for the normalised data.

4.3.2. Bacterial AFOM processing and bacterial production

Fluorescence data from all bacterial strains shows a considerable difference between the intensity of the fluorophores produced by the laboratory strain *P. aeruginosa* and the environmental isolate strains investigated (Figure 4.1). Fluorescence peak intensity was between 1 and 3-Log fold higher for *P. aeruginosa* for all fluorescence peaks investigated (Peaks T, C and C+). Peaks T, C and C+ were present in all bacterial strains investigated, with Peak T being the dominant AFOM peak in all environmental strains, and Peak C+ being the dominant AFOM peak in the *P. aeruginosa* laboratory strain. The only other strain to present fluorescence in the Peak C region that is visible within the EEM is *E. coli*, but this is not the dominant peak.

Despite differences in fluorescence intensities and AFOM signatures across the four bacterial strains studied, a unifying factor between all strains is the increased variability which is seen during the early stages of the growth curves, which subsequently decreases over the final 24-36 hours. This is commensurate with data described in Chapter 3, in which *P. aeruginosa* sees higher variation within the exponential growth phase of the bacterial growth curve. From the data presented in Figures 4.4, 4.7, 4.10 and 4.13 shows that this is a ubiquitous trait for fluorescence across different bacterial strains. This suggests that following a system shock (for example, the introduction into a different environment following inoculation), or during times of upregulated metabolism such as the exponential phase of the bacterial growth curve, the relationship between microbes and fluorescence breaks down. This may suggest that in natural freshwater systems, system changes which promote

increased biological activity may not only cause a shift in AFOM peak intensities but make the AFOM response more unpredictable. This supports hypotheses from Chapter 3, shedding light on the direct relationship between increased biological activity and variability in fluorescence.

4.3.2.1. Pseudomonas aeruginosa

Fluorescence and bacterial production data from the *P. aeruginosa* system shows a positive correlation between normalised BP data and fluorescence intensity, expressed as an increase in QSU cell per hour. Unlike normalised cell number data discussed above, which shows an inverse relationship with BP, fluorescence data shows that during times of increase BP activity, AFOM production is also higher, in particular for Peaks T and C. Though these relationships were not found to be significant, the time points during which AFOM production was at its highest (4 h for Peaks T and C) were also the times were bacterial production was at its highest (Figure 4.4). Interestingly, raw cell number data from the uncorrected growth curve (Figure 4.2) shows that this also coincides with a decrease in cell number from 1 x 10^5 CFU mL^{-1} to 5 x 10^4 CFU mL^{-1}; i.e. over half a log decrease. This suggests that AFOM production and bacterial production rates not only increase in tandem with one another, but independently of cell number, possibly during a period of metabolic upregulation post-inoculum.

Peak C+ does not increase in tandem with bacterial production rates, but several hours later, with its highest time point occurring at 12 h. This suggests that whilst Peak T (and potentially Peak C) may represent OM associated with an actively growing population within this system, Peak C+ may represent OM which is produced at a slower pace and remains within the system for longer periods of time.

4.3.2.2. Escherichia coli

E. coli is often used as an indicator organism for pathogenic contamination, particularly for faecal contamination from untreated sewage or agricultural pollution (Hudson et al., 2007; Reynolds & Ahmad, 1997; Sorensen et al., 2021). It was therefore an important organism to include in this study due to its contextual relevance, both within the literature and in real-world applications. *E. coli* has a known propensity for producing intense AFOM signals (Fox et al., 2017), particularly in the Peak T/Tryptophan-like fluorescence region, with handheld fluorometers having been found to detect fluorescence from bacterial loads as low as 7 CFU mL^{-1} (Wildeboer et al., 2010). However, there are a number of limitations associated with the use of fluorescence as a biomarker for 'counting' *E. coli*. These include the fact that whilst *E. coli* is known to produce fluorescence, AFOM production is not exclusive to *E. coli*, exemplified by the clear in-situ production of AFOM over a 48-hour period in the same conditions for four bacterial strains shown in Figure 4.1, in which *E. coli* is seen to produce only

the third-most intense AFOM signal for Peak T, the often-used fluorescence peak for monitoring this species (Sorensen et al., 2018; Wildeboer et al., 2010). As such, this data shows it is not possible to attribute the presence of AFOM (in the form of any fluorescence peak) to the exclusive presence of *E. coli* alone. Additionally, recent studies have found reason to suggest that the use of handheld, in-situ fluorometers may serve better purpose for monitoring the presence of an active microbial population of *E. coli* amongst other bacterial species, rather than specific enumeration of *E. coli* (Fox et al., 2018, 2021, 2022). Despite this, there have been no studies to date which specifically investigate the direct relationship between *E. coli* fluorescence and activity, and as such this was an important factor to consider within this study.

Data investigating the *E. coli* bacterial strain found the strongest correlations between AFOM production and bacterial production rates over the experimental time period out of all bacterial strains investigated. In particular, a significant correlation was found between Peak T fluorescence per cell, expressed as an increase per hour, and normalised bacterial production rate ($R^2 = 0.8255$, $p < 0.05$). In addition the highest point of AFOM production and BP rate, at 4 h (Figure 4.7), occurs in tandem with an immediate increase in cell number upon inoculation into the SFW media (Figure 4.5). However, whilst cell numbers continue to increase into the exponential phase of the bacterial growth curve up to 8 h (Figure 4.5), both the rate of AFOM production and BP experience a decrease. This suggests that rather than representing a continuously increasing number of cells in the system, AFOM production and processing by *E. coli* may represent periods of upregulated microbial activity, potentially following a shock to cells after inoculation. This is in contrast to the aforementioned studies which have pointed towards the use of Peak T fluorescence for *E. coli* enumeration in freshwaters, and suggests a closer relationship between Peak T fluorescence and an actively metabolising system of microbes, possibly containing *E. coli.*

Whilst no significant correlation was found between Peak C and BP, it is possible to see visually from Figure 4.7 that the period between 0 and 4 h represents an increase in AFOM production and BP in tandem with one another. Peak C+ does, however, represent a significant correlation with BP ($R^2 = 0.8048$, $p < 0.05$). Whilst Peak T intensity displays a decrease towards the end of the experimental period between 24 and 48 h, Peak C displays an increase and Peak C+ does not display any change. This supports the theory that Peak T represents more bioavailable and labile OM which is consumed in secondary production, whilst Peaks C and C+ represent more recalcitrant compounds which remain and accumulative within a system over time.

4.3.2.3. Isolate 7

Isolate 7 data shows the weakest relationship between fluorescence intensity and BP values over the growth curve period. Fluorescence intensity for Isolate 7 experiences an immediate peak between 0 and 4 h, before a sharp decrease between 4 and 8 h. After this, fluorescence intensity increases for the remainder of the bacterial growth curve period. Here, the spike in fluorescence precedes the peak BP rate by 4 hours. The only period during the growth curve in which there is a relationship between fluorescence intensity and BP is during the first 4 hours, at which point both fluorescence intensity and BP are increasing. After this, the relationship is inverse throughout the growth curve period. The increase in fluorescence intensity which occurs throughout the final 36 hours of the growth curve suggests that despite a decrease in cell number and activity, shown by BP, AFOM remains within the system. This is true for all fluorescence peaks, and suggests that the fluorescence being detected is coming from extracellular metabolites or exudates, possibly excreted during cell death.

4.3.2.4. Isolate 15

The fluorescence signatures seen over time in the Isolate 15 growth curve are unique in that this is the only strain to display an initial decrease in fluorescence intensity for all peaks, before a gradual increase over the remainder of the experimental period. Whilst this represents an initial negative relationship with BP (which shows an increase between 0-4 h before a decrease between 4-8 h), the remainder of the experimental period shows a relationship between fluorescence intensity and BP as both steadily rise up to 48 h. This increase in fluorescence intensity and BP occurs in spite of a decrease in cell number post-8 h. This suggests that despite cell death, a level of activity remains within the system. This could be explained by an increase in activity occurring within the small population of microbes that remain during the cell death of the majority. As other bacterial cells within the system die, it is possible that the total viable cell density is decreasing, but the minority which are left are metabolising faster, possibly during the breakdown of cell matter from those that are dying. Future work for this could include studying the system for a longer time period to determine whether the system was able to reach an equilibrium whereby cell multiplication again outweighs cell death.

4.4. Conclusions

- Three fluorescence peaks were produced by all four bacterial strains investigated at varying intensities. This includes Peak T, conventionally viewed as autochthonous, and Peaks C and C+, conventionally viewed as allochthonous. This shows that bacteria are capable of producing a variety of fluorescence peaks *in-situ* in a nutrient limited, simulated freshwater environment, including those conventionally presumed to be terrestrially-derived humic-like compounds

- Bacterial production (BP) values displayed correlative relationships with cell number where no unit normalisation has taken place. When data normalisation was undertaken to correct for the effects of increased cell number on BP rate, the positive relationship between BP and cell number breaks down, in some cases resulting in a directly negative correlation. This shows that bacterial processing is occurring independently, and in spite of, bacterial cell reproduction in this system.
- Correlations are seen between BP values and fluorescence intensities. Whilst this was not significant for all fluorescence peaks for all bacterial strains investigated, is it clear that there is a stronger relationship between AFOM and bacterial activity, than between AFOM and cell number. Not only does this underscore the hypothesis that fluorescence can be used as an effective maker for upregulated metabolism in freshwater systems, it suggests that increased processing of OM occurs during times of upregulated metabolism. This may be important when considering the impact of anthropogenic inputs into freshwater systems and the impact that this may have on metabolism and, therefore, the processing and transport of OM through the hydrological continuum by freshwater microorganisms.
- *E. coli* fluorescence intensity, in particular, was found to correlate strongly with BP. This was in spite of the historical use of Peak T for the direct enumeration of *E. coli* in freshwaters.

Chapter 5. The implementation of a novel fluorescence-based sensor on the River Thames at Taplow, Maidenhead, UK.

5.1. Introduction

Monitoring the quality of freshwater systems globally is of great interest and significance. In particular, water quality concerns surrounding industrial, agricultural and sewage-related pressures in aquatic ecosystems are beginning to gain recognition alongside a backdrop of increasing societal demands and associated global environmental challenges (Arndt et al., 2022). Requirements for water quality monitoring regimes and strategies have historically been driven by policy regulation. The UK's exit from the European Union on the 31st January 2020 resulted in the uprooting, and subsequent reform, of national water quality monitoring legislation (discussed in detail in section 1.5.1) which has previously fallen under the EU Water Framework Directive. The resulting piece of legislation – England and Wales' Water Environment regulations – went some way to address the issues arising from anthropogenic pollution currently experienced by the UK's waterways, including specific policies on improving the monitoring and management of combined sewer overflow (CSO) use. As such, the need for effective monitoring of these parameters is of great national importance in the UK at this time.

Current standard water quality monitoring techniques used for freshwater systems are often time consuming and costly. Discrete sampling is often the main method used, focusing on specific locations of interest at sparse spatial scales, with samples being collected monthly or even yearly, providing little temporal resolution. Laboratory analysis is often undertaken for monitoring the presence of microbial contamination or nutrient concentrations, requiring lengthy wait times for assays and incubation as well as high costs of laboratory consumables and human labour. These techniques, whilst useful for ground-truthing due to their accuracy, are unable to capture the dynamism of freshwater systems through time and space. As such, important pollution events are often missed, with reported data providing only a 'snapshot' of water quality rather than an accurate portrayal of ecological health. Furthermore, many of the standard parameters used only provide insight into structural qualities of an ecosystem; for example, physico-chemical parameters, which represent only the abiotic characteristics, or species diversity of macrophytes, fish and invertebrates, which require substantial changes in water quality over long periods of time to present discernible changes (Liess & Beketov, 2011; Pallottini et al., 2015).

Understanding the quality of freshwaters is paramount for the preservation and enhancement of both ecosystem and human health. A prerequisite for the understanding of freshwater systems is an ability to effectively monitor them in intelligent and efficient ways. The use of in-situ, high-resolution

monitoring techniques have been shown to be effective in influencing public perception and understanding of freshwater systems, as well as having tangible impacts on stakeholder engagement, demonstrating changes both in immediate practice by polluters as well as in policymaker decision at a legislative level (Jordan & Cassidy, 2022). The application of this technology for freshwater quality monitoring is not new, with physical and chemical measurements such as pH, turbidity, dissolved oxygen and electrical conductivity having seen significant technological improvements in recent decades with regards to in-situ sensors. However, whilst these parameters can provide insight into the chemical status of a water body, they do not provide in-depth information regarding the impact of this on fundamental underpinning ecosystem processes.

Fluorescence technologies have been used in the past for monitoring storm events, OM transportation, and pollution inputs into freshwater systems (Baker et al., 2003; Baker & Inverarity, 2004; Carstea et al., 2010, 2014, 2016; Hudson et al., 2007; Sorensen et al., 2015, 2018). Humic-like fluorescence has historically been considered to be allochthonous and used to trace OM runoff from terrestrial ecosystems. Protein-like fluorescence has been used to provide insight into the density of faecal-contamination indicator organisms such as *E. coli* (Sorensen et al., 2015, 2018, 2020, 2021). However, there has been some recent literature suggesting that not only could bacterial activity be responsible for the production of humic-like fluorescing compounds (Berggren et al., 2020; Fox et al., 2017; Guillemette & del Giorgio, 2012; Koch et al., 2014; Yamashita & Tanoue, 2004), but protein-like fluorescence may in fact represent an active microbial population rather than cell enumeration alone (Fox et al., 2021).

There is clearly a dearth of knowledge surrounding the application of fluorescence-based sensors for the real-time, in-situ monitoring of ecosystem processes and responses to pollution inputs such as nutrient loading. In addition, existing fluorescence sensing technology commonly observes single-channel fluorescence readings per sensor unit, and requires external post-processing to correct for IFE impacts, quenching, and to normalise reported data to standardised units such as QSU in order to quantitatively compare fluorescence data across time and space. This chapter explores the implementation of a novel fluorescence-based sensor which is the first iteration of its kind, employing three fluorescence channels alongside turbidity and absorbance measurements to undertake built-in corrections and data normalization. Alongside a long-term in-situ deployment of the novel fluorescence sensor, regular discrete sampling was also undertaken to replicate common water quality monitoring practice and ultimately investigate the use of in-situ fluorescence technology as a new water quality parameter for monitoring ecosystem health in freshwaters.

5.1.1. Chelsea Technologies Ltd. V-Lux sensor

The Chelsea Technologies Ltd. V-Lux is a fluorescence-based sensor that was developed and implemented over the duration of this project (Figure 5.1). The sensor allows for greater functionality than previous iterations in that it contains five internal reporting optical channels, whereas previous iterations have supported only a single channel. The sensor contains three fluorescence channels – Tryptophan, Chlorophyll, and CDOM – alongside both absorbance and turbidity channels. Unit standardisation is reported in QSU to facilitate intra- and inter-comparability throughout study locations and over time. Internal corrections are also undertaken to account for absorbance and turbidity interference which can result in non-linearity in the relationship between fluorescence intensity and fluorophore concentration. The V-Lux is small and compact, with a diameter of 45 mm and a length of 130 mm ensuring the portability of the unit. The unit is robust, with a wide range of operating conditions (-4°c to 55°c, 600 m depth) and a sapphire window with surrounding copper bezels to limit biofouling. These features, in addition to the unit's technological compatibility with remote radio telemetry units, make it attractive for in-situ remote deployments and online data collection.

Figure 5.1. Image of the V-Lux sensor (Chelsea Technologies Ltd., UK). Used with permission of its creator.

5.1.1.1. V-Lux sensor optical channels and output

The details provided in Table 5.1 outline the optical parameters and the associated wavelength regions that are monitored by the V-Lux. The sensor contains five optical channels; absorbance, turbidity and three fluorescence channels (Tryptophan, CDOM, Chlorophyll). Unit standardization is reported in Quinine Sulphate Units (QSU) to facilitate comparison within and between studies. This allows the direct comparison between data collected by different V-Lux units, data collected within different field site locations, and comparison between V-Lux and benchtop studies undertaken using laboratory-based benchtop spectrofluorometers. As reported by the V-Lux, 1 QSU is equivalent to the recorded fluorescence intensity on an Aqualog® (Horiba, Japan) spectrofluorometer of 1 ppb quinine sulphate standard in 0.1 M perchloric acid (Starna Cells, USA) at $\lambda_{ex}/\lambda_{em}$ 347.5/450 nm. The data presented from the V-Lux is reported as an average of the emission spectrum detected by the instrument within the prescribed wavelengths of the emission filter, relative to a 280 nm excitation from the UV LED.

Table 5.1 Optical parameters and associated wavelengths monitored by the V-Lux fluorosensor (Chelsea Technologies Ltd., UK).

Parameter	Excitation λ (nm)	Emission λ (nm)	Dynamic Range	Sensitivity
Chlorophyll fluorescence	280	682 ± 15	0-700 µg L^{-1} (chlorophyll-a)	0.01 µg L^{-1}
Tryptophan fluorescence	280	365 ± 25	0-600 QSU 1-1200 µg L^{-1} (tryptophan)	0.02 QSU 0.04 µg L^{-1}
CDOM fluorescence	280	450 ± 25	0-600 QSU 0-800 µg L^{-1}	0.02 QSU 0.04 µg L^{-1}
Absorbance	280	-	0-3.5 OD	0.002 OD
Turbidity	860	860	0-1000 FNU	0.01 NU

5.1.1.2. V-Lux optical design

Figure 5.2 outlines the optical structure of the V-Lux sensor. Internally, the unit contains two LED bulbs; an infrared (IR) and ultraviolet (UV) source. For fluorescence measurements, the incident light at 280 nm is generated from the UV source and reflected off the first dichroic filter and directed towards the sample chamber through the sapphire window. The subsequently generated fluorescence by the fluorophores within the sample is collected back through the window and past the same dichroic lens. The light then reaches a second set of three dichroic lenses, which separate out the light into three specific wavelengths of interest, starting with the longest wavelength (chlorophyll). Each wavelength is ultimately channeled to a Silicon Photomultiplier (SiPM) which detects the intensity of the fluorescence generated. Figure 5.2 shows the internal structure of the polyaromatic hydrocarbon

(PAH) variant of the V-Lux, though the principal is the same when applied to the tryptophan variant as used within this study.

To collect absorbance measurements, optical transmission is measured using a UV-enhanced absorbance photodiode parallel to the excitation window. A reference photodiode is used to monitor the output of the UV LED and accounts for drift in output as well as acting as a reference for optical transmission measurements. The IR LED is used to generate incident light at 860 nm for turbidity measurements. The light passes through an aperture to direct the excitation beam into the sample chamber. Any scattering of light caused by interaction between the beam and suspended particulate matter is then detected by the UV-enhanced photodiode.

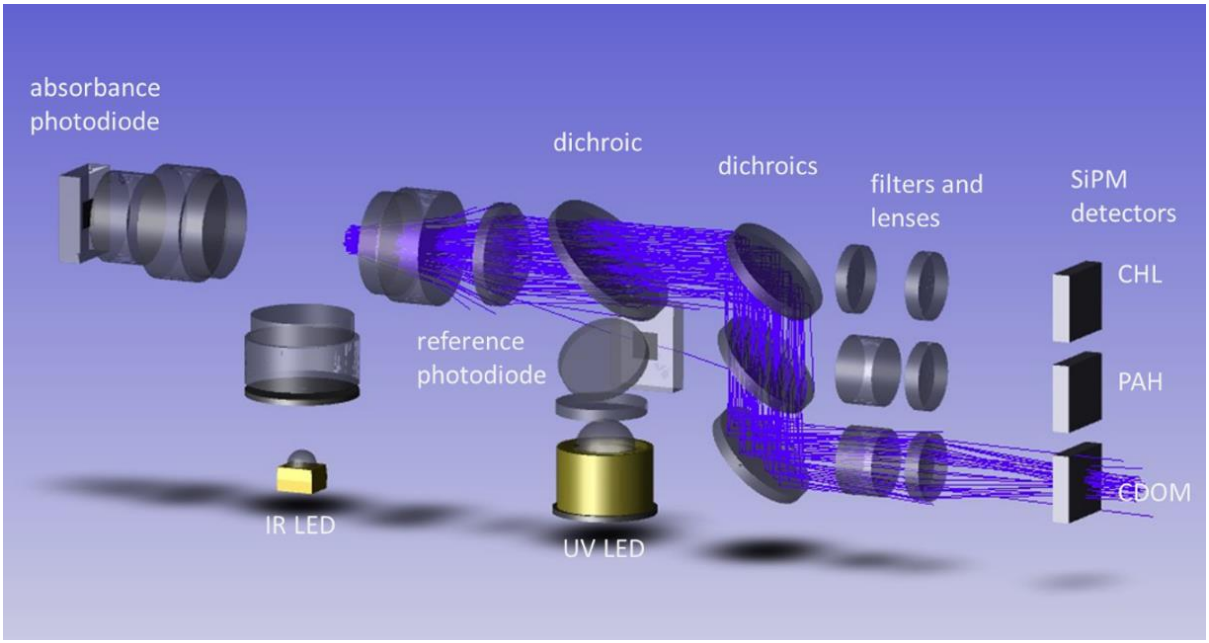

Figure 5.2 Internal structure of the V-Lux sensor showing the exemplary detection path for CDOM. Used with permission of its creator (Chelsea Technologies Ltd.).

5.1.1.3. Absorbance and turbidity internal corrections

There are a number of factors which can cause interference with observed fluorescence characteristics. The V-Lux contains internal features to mitigate for these effects; for example, high quality filters which prevent the elevated signal arising from scattered light from the excitation beam reaching the detector, and a careful selection of emission wavelength regions and bandpass to minimize interference from Raman scattering.

As discussed in section 1.4.1.3, absorbance and turbidity are two common factors which can cause attenuation of fluorescence signal, introducing non-linearity into the relationship between fluorescence intensity and fluorophore concentration. As such, in field-based scenarios such as in-situ

deployments in surface waters, where there may be considerable suspended matter within the water column and/or color from dissolved species, it is essential to consider these factors and correct for them where possible. The V-Lux contains internal algorithms to correct for this using independent, simultaneous turbidity and absorbance measurements which are applied to the measured fluorescence output.

5.2. Long-term in-situ fluorescence monitoring using the Chelsea Technologies V-Lux

Figure 5.3 displays data from the in-situ deployment of the Chelsea Technologies V-Lux fluorescence-based sensor on the River Thames at Taplow, Maidenhead between July 2021 and November 2022. Whilst the cleaning of the instrumentation was undertaken fortnightly, it is possible to see the times at which instrument cleaning fell upon a pumping cycle and therefore coincided with an automated fluorescence reading from the instrument. Data from all fluorescence peaks is seen to cease between 02/02/2022 and 14/02/2022 due to a failure in SDi12 connection between the V-Lux sensor and the telemetry unit. Fluorescence data is not seen to be affected by the cleaning of the instrumentation, suggesting that in this context, biofouling does not appear to be an issue for this instrument. This is likely due to the sensor housing and pumping cycle, whereby contact with river water is only made during the 5-minute pumping cycle at hourly intervals, mitigating for the potential biofouling that may occur were the sensor to permanently reside within the water.

Fluorescence events occur periodically over the measured time period, with individual fluorescence peaks undergoing events both independently and in tandem with one another. Table 5.2 shows average fluorescence data for each month between July 2021 and November 2022 for Chlorophyll, Tryptophan and CDOM. For CDOM, Average monthly fluorescence intensity values see increases above an average of 70 QSU per month during October and November 2021, in February 2022, and the following year in November 2022. Tryptophan fluorescence intensity increases over 40 QSU during the months of July-August 2021, October 2021, April-May 2022, July 2022, and September-November 2022. Chlorophyll fluorescence intensity remains low (< 3 QSU) throughout the time period studied, except for April and May, where fluorescence intensity increases to > 8 QSU. No statistically significant correlations were found between monthly averages of fluorescence intensity data for any peaks (p > 0.05).

Data from the sensor shown in Figure 5.3 is relatively noisy due to the high frequency of data collection (hourly) but also due to the potential overlapping of fluorescence spectra, and therefore trending of fluorescence intensity data over time, caused by similarities in optical regions, particularly for Tryptophan and CDOM channels (Figure 5.3a). These similarities occur due to the single excitation wavelength used for all fluorescence channels, a result of the UV LED bulb employed within the V-Lux

which generates incident light at 280 nm. As such, the known excitation maxima for these fluorescence regions (outlined in Table 1.1) is not the same as the excitation region investigated using the V-Lux sensor.

Table 5.2 Average monthly data from the Chelsea Technologies Ltd V-Lux fluorescence sensor on the River Thames at Taplow, Maidenhead, showing Chlorophyll, Tryptophan and CDOM data between July 2021 and November 2022. All data are reported in QSU. ± denotes standard deviation.

	Chlorophyll		**Tryptophan**		**CDOM**	
	Average	±	Average	±	Average	±
Jul-21	2.54	0.48	40.03	2.18	57.41	11.75
Aug-21	2.73	1.17	40.43	3.42	51.03	4.22
Sep-21	2.03	0.32	36.97	1.87	45.35	2.41
Oct-21	2.33	0.61	40.67	2.23	74.96	15.51
Nov-21	2.19	0.77	35.84	2.95	75.07	17.87
Dec-21	1.92	0.54	30.56	3.78	65.20	9.37
Jan-22	1.93	0.65	24.51	1.97	64.13	13.84
Feb-22	2.40	0.63	27.56	2.61	70.32	11.19
Mar-22	2.27	0.59	28.56	4.41	69.39	14.82
Apr-22	8.62	8.78	40.67	13.28	45.19	7.40
May-22	13.61	7.71	55.47	18.94	44.01	11.31
Jun-22	2.54	0.56	37.96	1.54	45.99	2.08
Jul-22	2.85	1.08	40.00	5.00	43.74	2.51
Aug-22	2.27	0.46	39.64	1.59	46.24	3.93
Sep-22	2.00	0.33	40.35	1.76	57.14	5.17
Oct-22	1.81	0.40	42.81	2.51	60.51	9.67
Nov-22	3.08	0.63	45.02	3.03	100.40	16.06

To remove interference from potentially overlapping fluorescence spectra and data trending, data normalisation was undertaken to investigate the ratio of Tryptophan:CDOM fluorescence and CDOM:Tryptophan fluorescence. This allows data to be investigated where Tryptophan fluorescence intensity increases independently of an increase in CDOM fluorescence intensity (Figure 5.3b) and where CDOM fluorescence intensity increases independently of an increase in Tryptophan fluorescence intensity (Figure 5.3c). In addition to reducing potential interference from spectral overlap, this data allows the isolation of events which occur where increases of fluorescence intensity occur due to the increase in the concentration of specific types of OM. Several events occur over the duration of the measured time period where fluorescence peaks increase in isolation from one another. During the period between April and June 2022, Tryptophan increases independently of

CDOM from 30.156 QSU on 15/04/2022 to a maximum of 80.262 QSU on 01/05/2022 before decreasing again to 36.362 on 14/06/2022. This represents the only duration over the measured time period in which Tryptophan fluorescence intensity is higher than CDOM fluorescence, with a Tryptophan:CDOM ratio of 1.57.

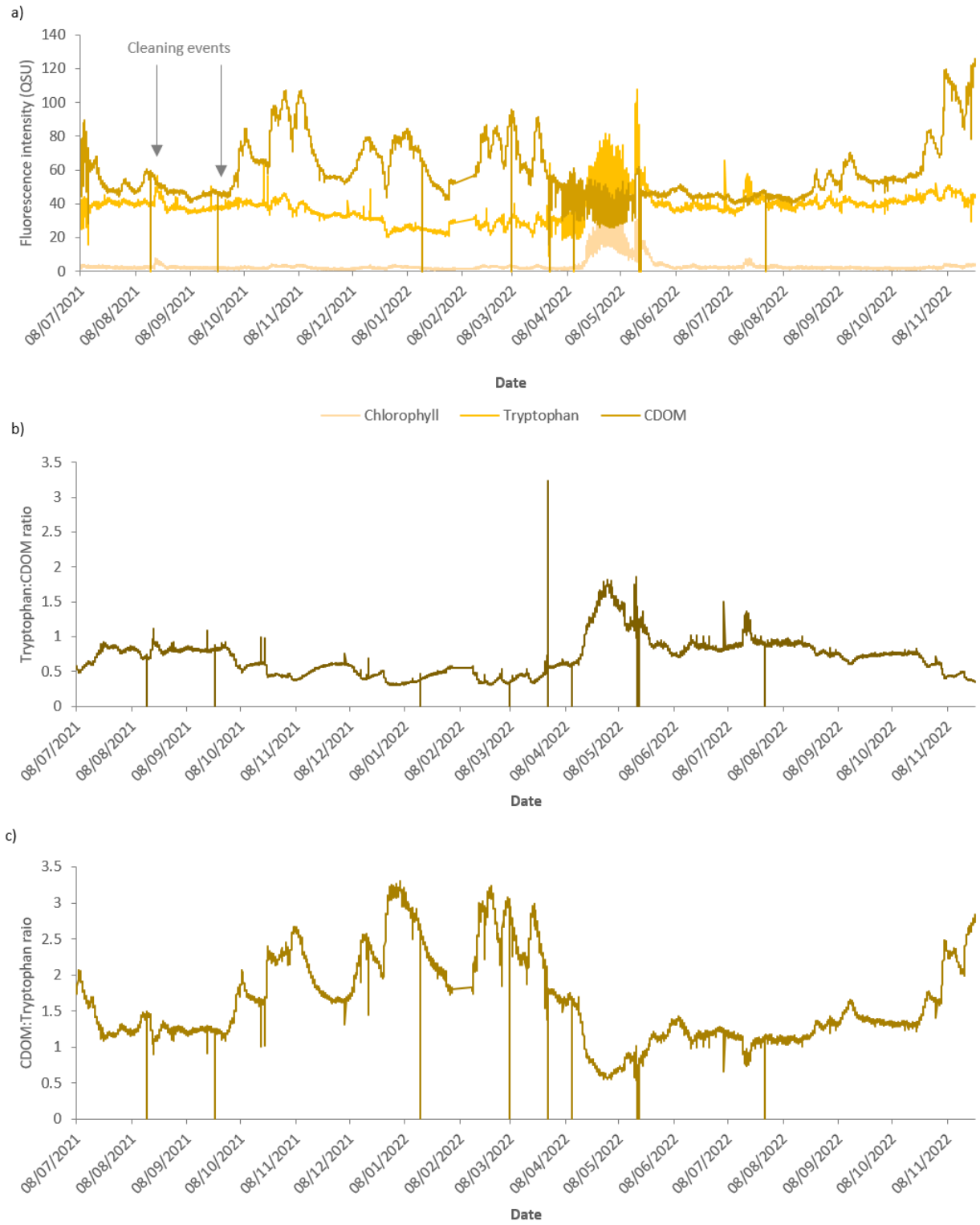

Figure 5.3 High-frequency, in-situ monitoring on the River Thames at Taplow, Maidenhead using the Chelsea Technologies V-Lux fluorescence-based sensor. Data collection was undertaken at 1-hour intervals, showing: a) Chlorophyll, tryptophan and CDOM fluorescence, b) Tryptophan:CDOM ratio, and c) CDOM:Tryptophan ratio. Data is presented in Quinine Sulphate Units. Data is shown from July 2021-November 2022. Empty (0 QSU) data points are due to the cleaning of instrumentation falling on the time of a pumping cycle and collection of a fluorescence reading by the sensor.

Figure 5.4 shows a high-resolution graph of data collected between 15/04/2022 and 16/05/2022, displaying fluorescence intensity data from Chlorophyll, Tryptophan and CDOM channels from the Chelsea Technologies V-Lux sensor. In addition to being the largest increase in Tryptophan fluorescence intensity over the measured time period, it also shows an increase in Chlorophyll fluorescence intensity. For the only time during the study period, Chlorophyll and Tryptophan fluorescence intensities are seen to correlate with one another more strongly than CDOM and Tryptophan fluorescence intensities, suggesting the presence of an algal bloom.

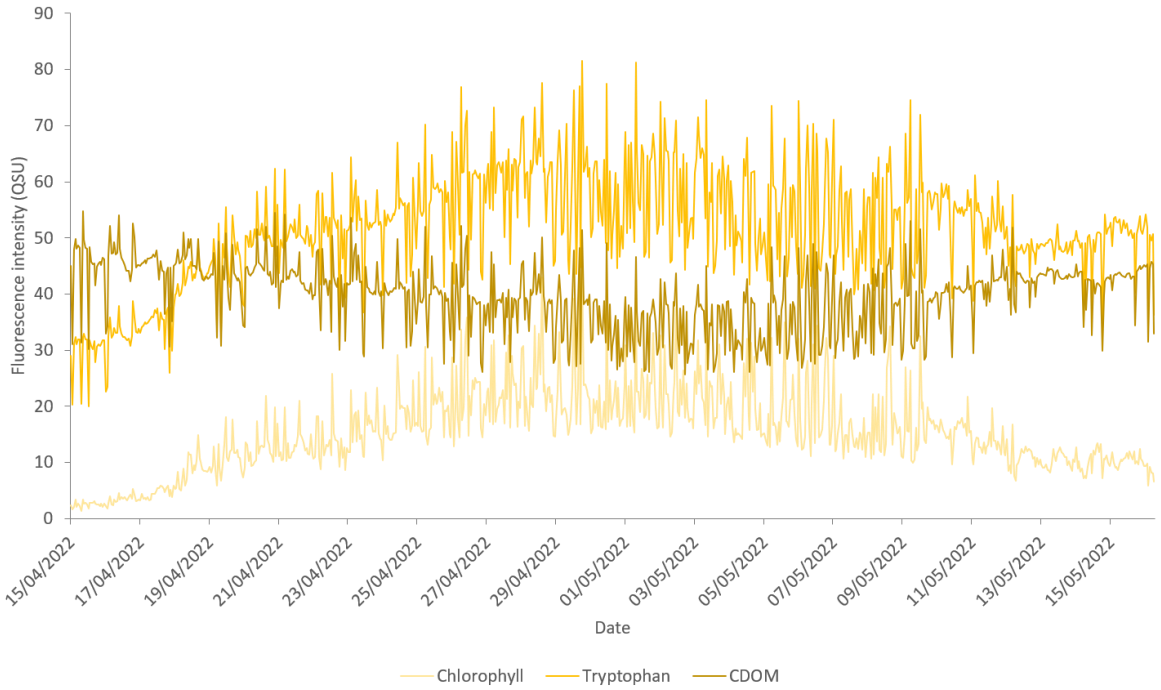

Figure 5.4 High-resolution data of the Chelsea Technologies Ltd. V-Lux fluorescence sensor, showing Tryptophan, CDOM and Chlorophyll channels between 15/04/2022 and 16/05/2022 on the River Thames at Taplow, Maidenhead.

The noise from the Tryptophan, Chlorophyll and CDOM peaks from the sensor during this time period is also seen to increase when compared to the noise from other months during the sampling period, seen comparatively in Figure 5.3.

In addition to the major algal bloom event in April and May 2022, another, smaller, algal bloom event appears to occur in July 2022, seen in high-resolution in Figure 5.5. During this period, both Chlorophyll and Tryptophan peaks increase (CDOM data has been omitted from this graph so as to focus more clearly on the relationship between Chlorophyll and Tryptophan, the specific peaks of interest during this event). Chlorophyll fluorescence intensity increases from 1.98 QSU on 16/07/2022 to a maximum

of 7.78 QSU on 19/07/2022, before decreasing to 2.5 QSU on 22/07/2022. Tryptophan fluorescence intensity visibly tracks the same pattern as Chlorophyll fluorescence intensity during this time. Tryptophan fluorescence intensity increases from 37.8 QSU on 16/07/2022 to a maximum of 53.04 QSU on 19/07/2022. However, Tryptophan fluorescence intensity remains elevated in reference to its previous state prior to the algal bloom event, initially decreasing to around 40 QSU for several days, before undergoing a secondary peak between 25/07/2022 and 26/07/2022, reaching a maximum of 47.12 QSU on 26/07/2022. During this period, Figure 5.5 shows a clear divergence between the two peaks, before finally converging again from 31/07/2022 onward.

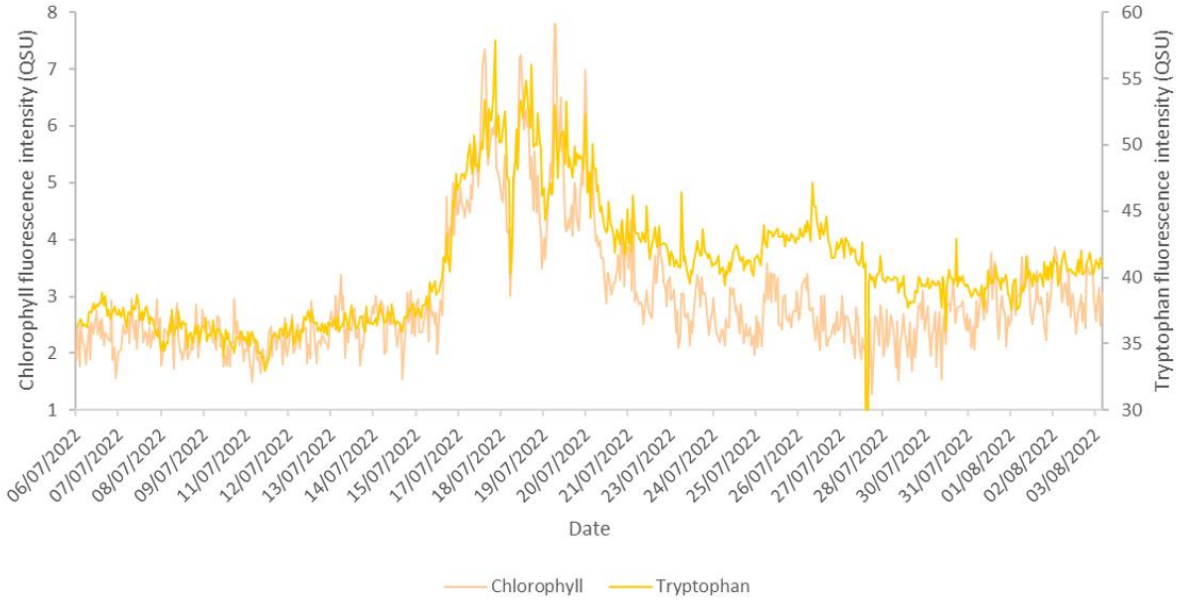

Figure 5.5 Fluorescence intensity data for Chlorophyll and Tryptophan channels from the V-Lux sensor on the River Thames at Taplow, Maidenhead between 06/07/2022 and 03/08/2022.

Whilst the increase in Tryptophan occurring in tandem with Chlorophyll clearly points towards the occurrence of an algal bloom event, the subsequent spike in Tryptophan independent of Chlorophyll could suggest an increase in microbial activity that can be attributed to bacteria, rather than algae.

To further explore the relationship between fluorescence parameters, in particular Tryptophan and Chlorophyll/CDOM, a generalised additive model (GAM) was used to analyse the relationship between parameters collected over the measured time period to account for periods of temporal change using

an automatic smoothness selection method, known as a spline, to estimate non-linear trends in the time-series data (Figure 5.6).

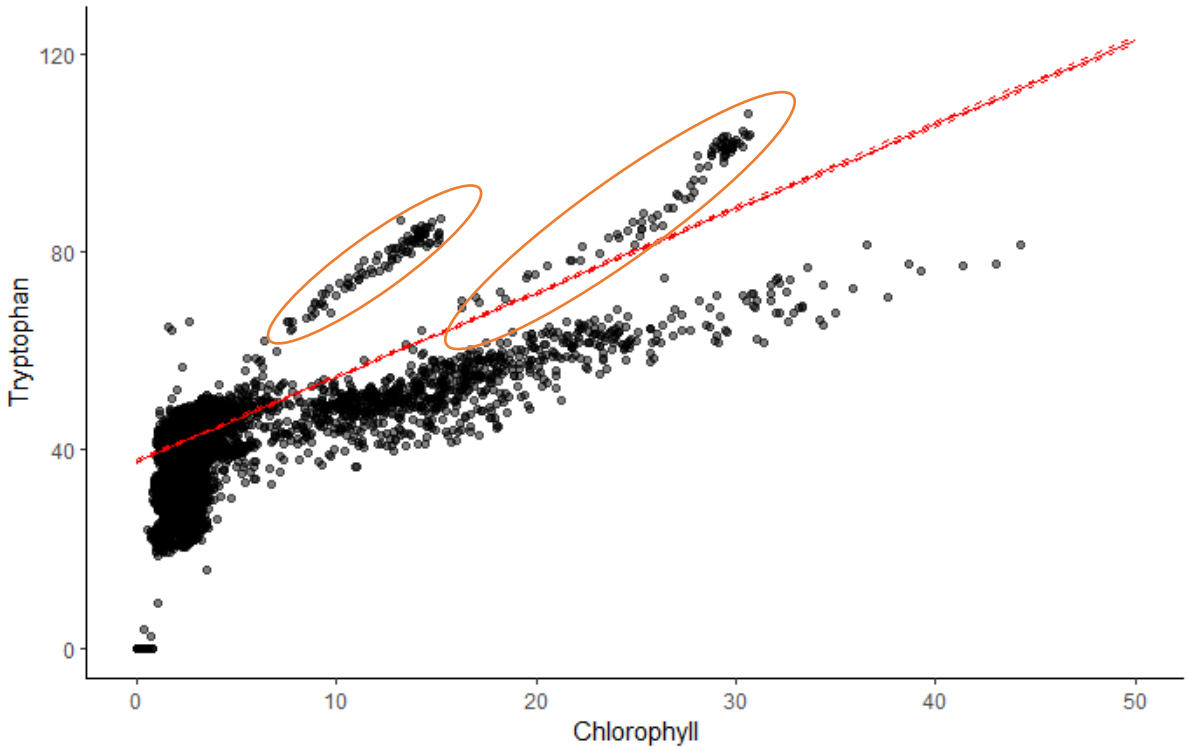

Figure 5.6 Fluorescence intensity data for Tryptophan and Chlorophyll channels from the V-Lux sensor on the River Thames at Taplow, Maidenhead showing a non-linear General Additive Model.

Results from the model show a significant correlation (p <0.001) between Tryptophan and Chlorophyll when accounting for the influence of time on the two parameters over the measured time period (R^2 = 0.807). The general trend displays a positive correlation between the two parameters, however distinct regions are visible where clusters of data points form at higher Tryptophan-Chlorophyll ratios (highlighted in orange), showing increased Tryptophan fluorescence relative to Chlorophyll, likely denoting specific events which may have occurred as a result of a shift in the origin of the Tryptophan-like fluorescence signal.

The model also showed significant correlations (p <0.001) between Tryptophan and CDOM (Figure 5.7). Interestingly, these two parameters were not as strongly correlated (R^2 = 0.559) as Tryptophan and Chlorophyll, with two distinct groups, or patterns, presenting clearly in the data (highlighted in orange). One pattern shows an increase in Tryptophan at a quicker rate than the increase in CDOM, and one shows an increase in CDOM at a quicker rate than the increase in Tryptophan, likely reflecting the ratio changes seen in Figure 5.3b and 5.3c.

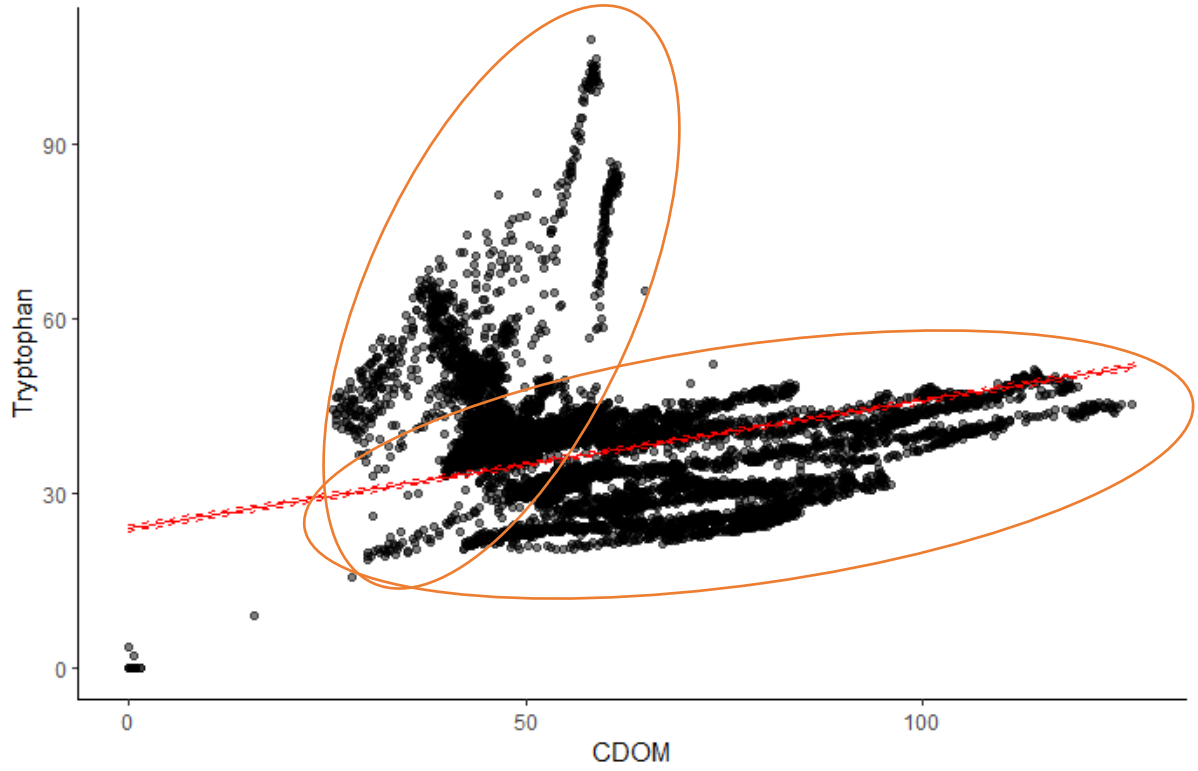

Figure 5.7 Fluorescence intensity data for Tryptophan and Chlorophyll channels from the V-Lux sensor on the River Thames at Taplow, Maidenhead showing a non-linear General Additive Model.

In addition to physico-chemical data collected from the water quality sonde, river flow data was obtained from the Centre for Ecology and Hydrology National River Flow Archive (NRFA) to investigate the potential impact of hydrology on the fluorescence signals observed. Figure 5.8 shows mean daily hydrological flow data between July 2021 and September 2022, the most recent available data in the NRFA database. Flow data over this time period was seen to vary between 2.75 m^3/s and 9.88 m^3/s, but more commonly remaining within the 5-7 m^3/s range. Figure 5.9 shows the correlation between the monthly average data of flow and fluorescence intensity for CDOM and Tryptophan. Neither correlations were significant ($p > 0.05$), suggesting that fluorescence changes over time are not directly attributed to hydrological influences on a monthly basis.

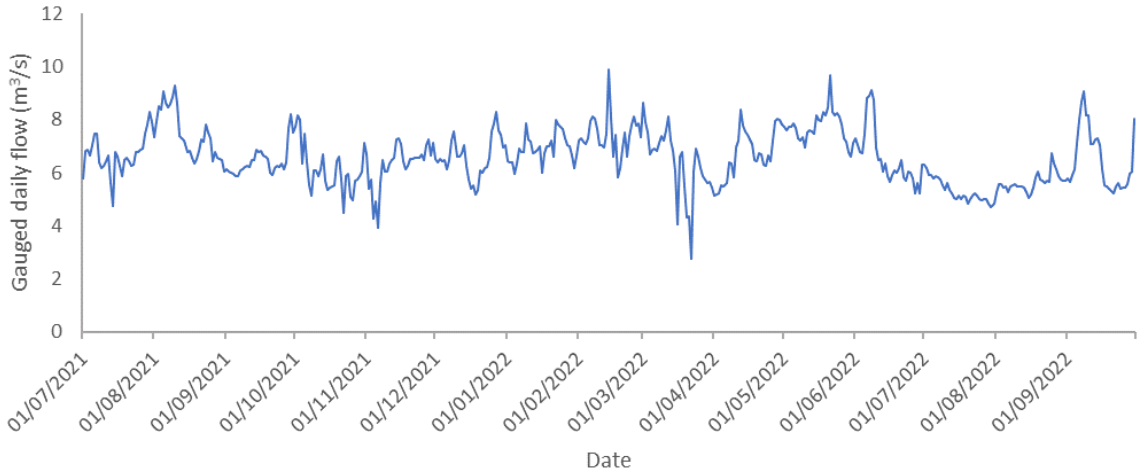

Figure 5.8 Hydrological river flow data showing mean gauged daily flow in m^3/s at Taplow Pumping Station, Jubilee River, Maidenhead. Data was acquired from the Centre for Ecology and Hydrology National River Flow Archive.

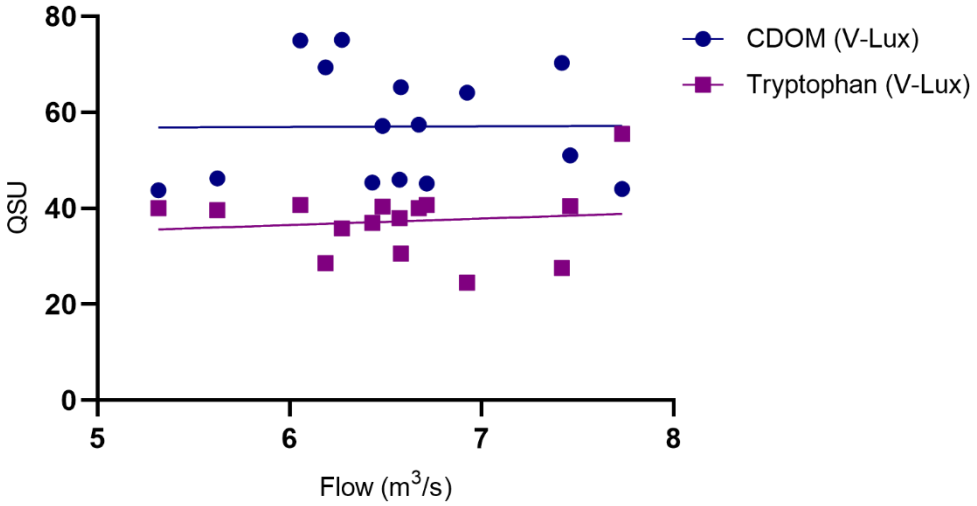

Figure 5.9 Monthly averages for V-Lux Tryptophan and CDOM fluorescence intensity (QSU) and hydrological flow data (m^3/s).

Despite there being no statistically significant correlation between fluorescence and flow date when observing monthly averages, it is possible to pick out some events in the flow data presented which explain other individual events that can be seen throughout the real-time monitoring data. For example, the point at which flow data is lowest throughout the reported time period occurs in late March and early April 2022. Temperature data displayed in 5.11b corroborates that a weather event occurred during this time in which rainfall, and therefore flow, was low and temperature was rapidly increasing with the onset of spring. This occurs at the same time as the beginning of the algal bloom period seen in Figures 5.3 and 5.4.

5.2.1. Long-term in situ sensing of physicochemical data using a water quality sonde

Water quality measurements were made on an hourly basis between August 2021 and November 2022 for the following parameters: pH, dissolved oxygen, conductivity, ammonium, temperature, and turbidity (Figures 5.10 and 5.11).

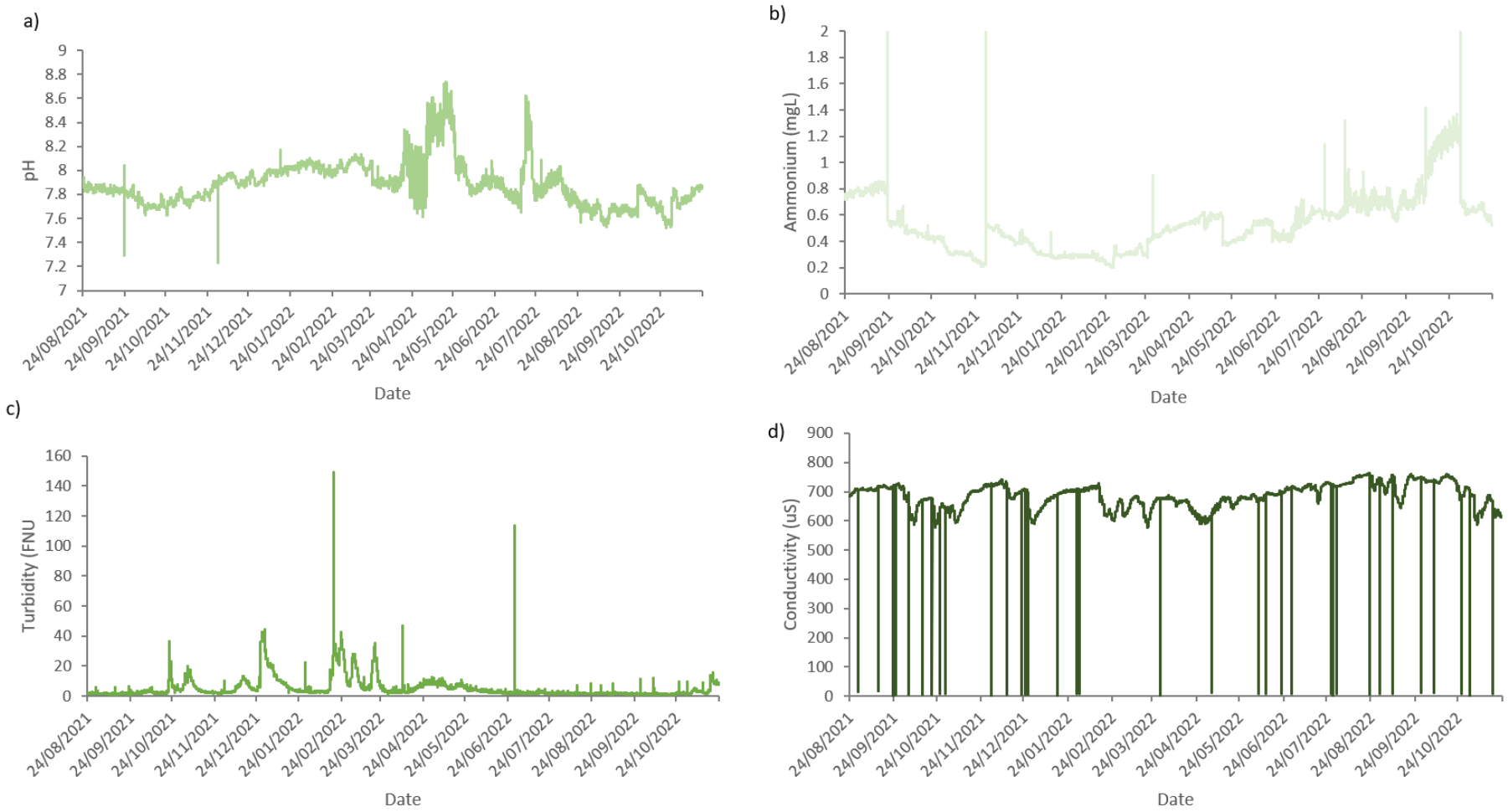

Figure 5.10 Data collected between August 2021 and November 2022 showing pH, Ammonium, Turbidity and Conductivity from the EXO2 sonde on the River Thames at Taplow, Maidenhead.

a)

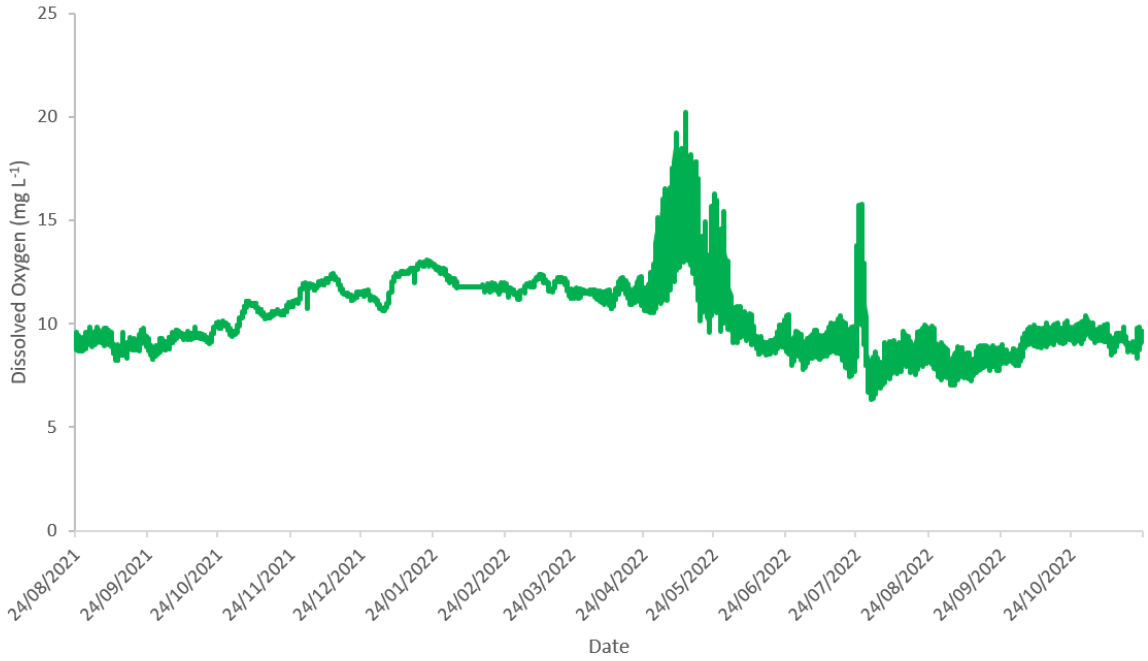

b)

Figure 5.11 Data collected between August 2021 and November 2022 showing a) temperature and b) dissolved oxygen on the River Thames at Taplow, Maidenhead.

Physico-chemical data appears to remain relatively stable throughout the sampling period, with some parameters displaying a vast increase during the period of April and May 2022. This is known from fluorescence data collected (displayed in Figures 5.3 and 5.4) to be an algal bloom, and it is possible to see a reaction to this event from the physico-chemical parameters. pH data displays an average value of 7.88 (±0.19) over the measured period, however the month of April displays an average of 7.93 (±0.12) and May displays an average of 8.27 (±0.24). Over the period measured during the beginning of June, the average pH then decreases to nearer the total average (Figure 5.10a). This shows that not only does the pH increase during the algal bloom period, but the variability is also substantially higher, particularly in May, which is consistent with the fluorescence data which also shows higher variation during this period (Figures 5.3 and 5.4).

Interestingly, turbidity, ammonia and conductivity do not show changes that are as notable during this period. However, these three parameters have a less stable baseline, and appear to be more substantially influenced by discrete, short-term events than pH. Over the April and May 2022 period, ammonia readings show a gradual increase in concentration from 0.44 mg L^{-1} on 01/04/2022 to a maximum of 0.62 mg L^{-1} on 16/05/2022, before rapidly decreasing to 0.37 mg L^{-1} on the 25/05/2022. This occurs in line with other parameters, including the period where the chlorophyll fluorescence is seen to decrease. However, the decrease in ammonium occurs at a much faster rate than other parameters. Turbidity also shows a gradual increase over this time, from 2.87 FNU on 01/04/2022 to a maximum of 12.26 FNU on 07/05/2022 before gradually decreasing over the remainder of the May period. This pattern seen within the turbidity data occurs in contrast to other turbidity events which are seen to occur of the measured time period; for example, an increase from 3.91 FNU on 23/12/2021 to 42.68 FNU on 28/12/2021, before decreasing again to 4 FNU over a 17-day period. This may be explained by a decrease in conductivity which is also seen during this period, where conductivity readings decrease from 708 µS on 23/12/2021 to 604 µS on 28/12/2021. The decreasing conductivity that also occurs during this period suggests that the spike in turbidity could be explained by a sudden rainfall event transporting particulate material from the surrounding catchment into the system. A conductivity drop is not seen during the algal bloom period of April and May 2022, however, further confirming that the gradual increase in turbidity seen during this time is consistent with the steadier development of a biological bloom rather than the sudden vast input of allochthonous material.

Dissolved oxygen concentration (Figure 5.11a) also shows an increase over the April-May algal bloom period. Dissolved oxygen was seen to have a total average of 10.42 mg L^{-1} (±1.79) which increased to 12.70 mg L^{-1} (±2.01) in April and 12.51 mg L^{-1} (±2.27) in May. This is consistent with the data which suggests a major algal bloom event occurs during this time, which would feasibly result in an increase

in the availability is dissolved oxygen due to increased primary productivity and O_2 production. Following this, dissolved oxygen concentration begins to decrease, suggesting the retrospective increase in secondary productivity which occurs as bacterial communities consume algal biomass, utilizing much of the excess available dissolved oxygen. Indeed, whilst the chlorophyll fluorescence intensity is seen to return to baseline levels following the bloom event, tryptophan concentration remains slightly elevated.

Turbidity, ammonium, conductivity and temperature see very discrete spikes or dips over the measured time period, which appear to be independent of general baseline trends. These occur during a very discrete period – only one measured time point – and occur in tandem with one another. For example, at 10:04 am on 01/12/2021, data displays 0.22 mg L^{-1} for ammonium, 2.05 FNU for turbidity, 726.85 µS for conductivity, and 6.59°C for temperature. One hour later, at 11:04 am on 01/12/2021, these parameters read 2.22 mg L^{-1} for ammonium, 10.2 FNU for turbidity, 0.45 µS for conductivity, and 11.25°C for temperature. The following hour, all parameters has returned to levels representative with those measured at 10:04 am the same day. The discrete nature of these events, in addition to the extreme changes in parameters, suggests that they are not a result of reliable physical, chemical or biological events. Rather, it is likely that they are an artefact of a reading being taken at the same time as a pumping cycle, causing temporary interference with instrumentation reliability.

5.3. Discrete sampling

Discrete samples were taken, initially on a weekly, then on a twice-monthly basis over the measured time period. Samples were collected from the water body as detailed in Section 2.6.2. The following parameters were measured: microbiological (*Escherichia coli*, total coliforms, and heterotrophic plate counts) nutrients (nitrate, phosphate, dissolved organic carbon), and fluorescence excitation-emission matrices (EEMs).

5.3.1. Fluorescence excitation-emission matrix (EEM) and peak-picking data from benchtop spectrofluorometric analysis

Excitation-emission matrices (EEMs) were collected for both filtered and unfiltered samples so as to examine the impact of filtration on fluorescence signature and intensity, as this has previously been reported to influence optical characteristics and can provide an insight as to the intra- or extracellular nature of the observed AFOM. Figure 5.12 displays peak-picking data for Peak T, C and C+ (both filtered and unfiltered) collected from the water body between July 2021 and October 2022.

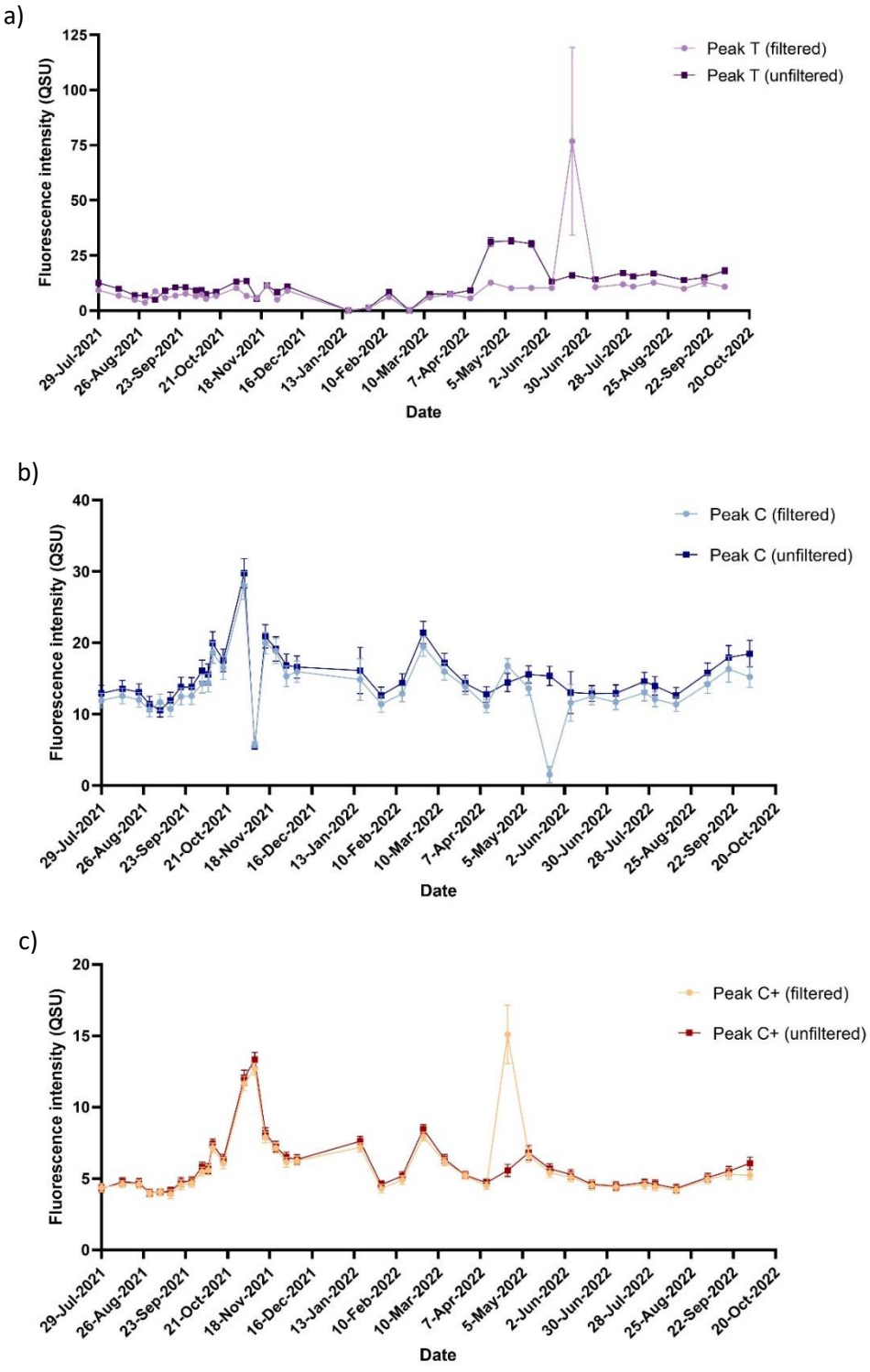

Figure 5.4 Fluorescence peak-picking data from the River Thames at Taplow, Maidenhead showing Peaks T, C and C+ (filtered and unfiltered) between July 2021 and October 2022 (n=3 experimental and technical replicates). Error bars denote standard deviation.

In general, the trends of filtered and unfiltered AFOM appear to track each other closely over the measured time period for all three fluorescence peaks measured (T, C and C+). For Peak T data, the fluorescence intensity of filtered samples was rarely higher than the fluorescence intensity of unfiltered samples, with the average ratio of unfiltered:filtered fluorescence intensity being 1.45 (±0.53) over the measured time period. On several occasions, however, the ratio dips below 1, indicating that filtered samples are exhibiting higher fluorescence intensity than unfiltered samples. Samples taken on 15/11/2021 and 22/11/2021 show an unfiltered:filtered ratio of 0.95 and 0.99 respectively. Additionally, a sample taken on 20/06/2022 shows a ratio of 0.21, albeit with a more substantial standard deviation value. Samples measured between 25/04/2022 and 23/05/2022 display the highest ratio of unfiltered to filtered, with ratios between 2.45 and 3.91. This is consistent with data from Figure 5.4, where there is believed to be a substantial algal bloom occurring. Interestingly, filtered Peak T fluorescence remains very low during this time, suggesting that the majority of the measured fluorescence is attributed to the presence of microbial cells present within the sample. Other than these major events, Peak T fluorescence intensity appears to remain relatively steady over the measured time period, with 31 out of 37 samples remaining between 5 and 17 QSU for unfiltered samples, and 36 out of 37 samples remaining between 3 and 13 QSU for filtered samples.

Peak C data also displays a reliable ratio between unfiltered and filtered samples, with an average ratio of 1.31 (±1.45) for unfiltered:filtered samples over the measured time period. This ratio dips below 1 two times; first, on 06/09/2021 (0.9) and again on 25/04/2022 (0.86). The latter time point is consistent with the algal bloom event which occurs during this time, where unfiltered Peak C fluorescence intensity sees a gradual increase between 12.78 and 15.56 QSU before gradually decreasing again to 12.9 over the period of two months. Filtered Peak C fluorescence intensity, however, displays a sharp increase at the beginning of the algal bloom period before undergoing a sharp decrease, dropping from 13.6 to 1.53 QSU before returning to 11.6 QSU over a one-month period. This drastic drop in filtered fluorescence at the end of the algal bloom period may suggests that some of the Peak C fluorescence at this time point may have been tied up in cellular matter, perhaps from a microbial bloom which happens after the algal bloom. Samples taken between 18/10/2021 and 15/11/2021 show both unfiltered and filtered fluorescence increasing from 16.51 and 17.55 QSU respectively to 28.04 and 29.73 QSU respectively, before dropping to 5.74 and 5.45 QSU respectively. Both filtered and unfiltered fluorescence then increase, back to 19.95 and 20.91 respectively. This coincides with an increase in CDOM, measured on the V-Lux, seen in Figure 5.3a, and also a decrease in conductivity and increase in turbidity, seen in Figures 5.10c and 5.10d, which suggest that a rainfall event had cause an increase in allochthonous organic matter import into the system.

Data for Peak C+ is consistent with data for Peak C in this regard, where a substantial increase in fluorescence intensity for both filtered and unfiltered fluorescence is observed in the months of October and November 2021. However, interestingly, Peak C+ does not display the same rapid decrease in fluorescence intensity following the spike. Additionally, Peak C+ displays a smaller ratio between unfiltered and filtered fluorescence intensity, with an average ratio of 1.02 (±0.11). This ratio only drops below 0 during one sample taken on 25/04/2022. This occurs during the algal bloom event of April and May 2022, and may suggest a sudden increase of intracellular AFOM, possibly from algal biomass.

To further explore the fluorescence peak-picking data, analysis was undertaken to investigate the relationship between fluorescence data acquired by the Aqualog benchtop spectrofluorometer and the in-situ V-Lux fluorescence sensor. Figure 5.13 displays the relationship between in-field fluorescence measurements using the V-Lux and peak-picking data obtained using the Aqualog from discrete samples. The relationship between Peak C and CDOM (Figure 5.13a) has a significant positive correlation (p <0.001, R^2 = 0.5608). The relationship between Peak T and Tryptophan (Figure 5.13b) also has a significant correlation (p <0.0001, R^2 = 0.7899). Whilst this data relates to monthly averages throughout the measured time period (July 2021 – October 2022) show a clear relationship can be seen between the two methods of fluorescence data acquisition, with a particularly strong correlation present between V-Lux Tryptophan and Aqualog Peak T data. It is important to consider factors which may impact the relationship between these two measurements, such as increased interference with fluorescence signals in the environment due to scattering and biofouling of the sensor window. Considering the impact of these potential interferences to in-situ fluorescence data, discrepancies between field and laboratory measurements of data are expected.

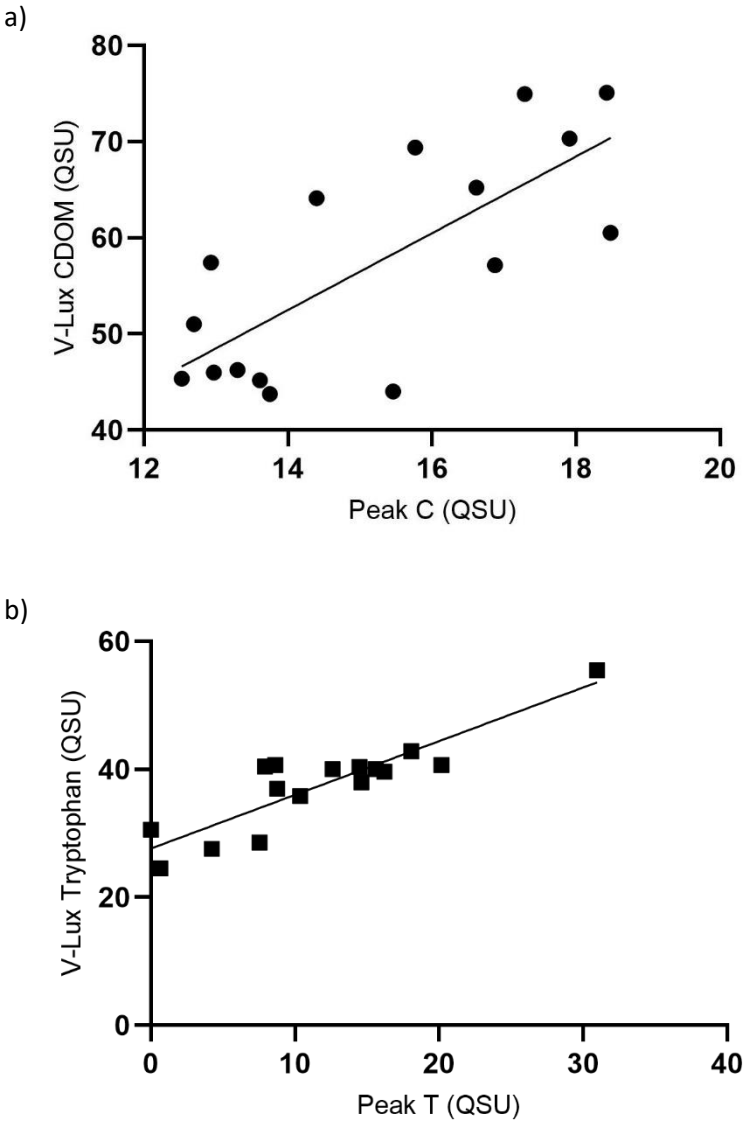

Figure 5.5 Correlation between laboratory peak picking measurements and field V-Lux sensor measurements, showing monthly averages of fluorescence (QSU) for a) CDOM and Peak C and b) Tryptophan and Peak T.

Figures 5.14 and 5.15 show Excitation-Emission Matrices (EEMs) from selected sampling weeks throughout the measured time period between July 2021 and September 2022. Here, it is possible to see visually the impact of filtration on the fluorescence intensities and characteristics, in addition to the change in fluorescence intensity over time throughout the year. As is possible to see within the peak-picked data shown in Figure 5.13, there is general similarities in peak morphology and shape, visually, between filtered and unfiltered samples throughout the measured time period, however the intensity is seen to change in some samples. In 5.14b and 5.14c, for example, the Peak T 'shoulder' can be seen to be less potent in the filtered sample than in the unfiltered sample, reflected in the peak-picked data showing lower Peak T fluorescence QSU intensities for filtered samples on these dates (Figure 5.8a). In 5.15f and 5.15g, it is possible to see a clear, discrete T-Peak in the unfiltered sample, which is almost entirely removed when the sample was filtered. These samples were taken during the algal bloom event of April and May 2022, suggesting the particularly strong Peak T region in these samples may represent a shape and intensity associated with the presence of algal cells which are removed during sample filtration.

Interestingly, the morphological characteristics of the fluorescence peaks can be seen to change over the months. For example, Figure 5.14d shows a very distinct shape of peak morphology, with notably less fluorescence in the deep-UV region below 260 nm. This is in contrast to 5.15e, for example, which has less distinct peak morphology, particularly in this region. An influx of external allochthonous DOM from the surrounding catchment could explain instances where observed humic-like peaks are higher than peak T in some samples. It is known that DOM, in particular humic-like AFOM, does not exist as discrete fluorescent compounds but rather as a composite of many types. An influx would likely cause the bleeding of more discrete fluorescence peaks into other areas due to a wider variety of fluorescing species being present within the measured sample.

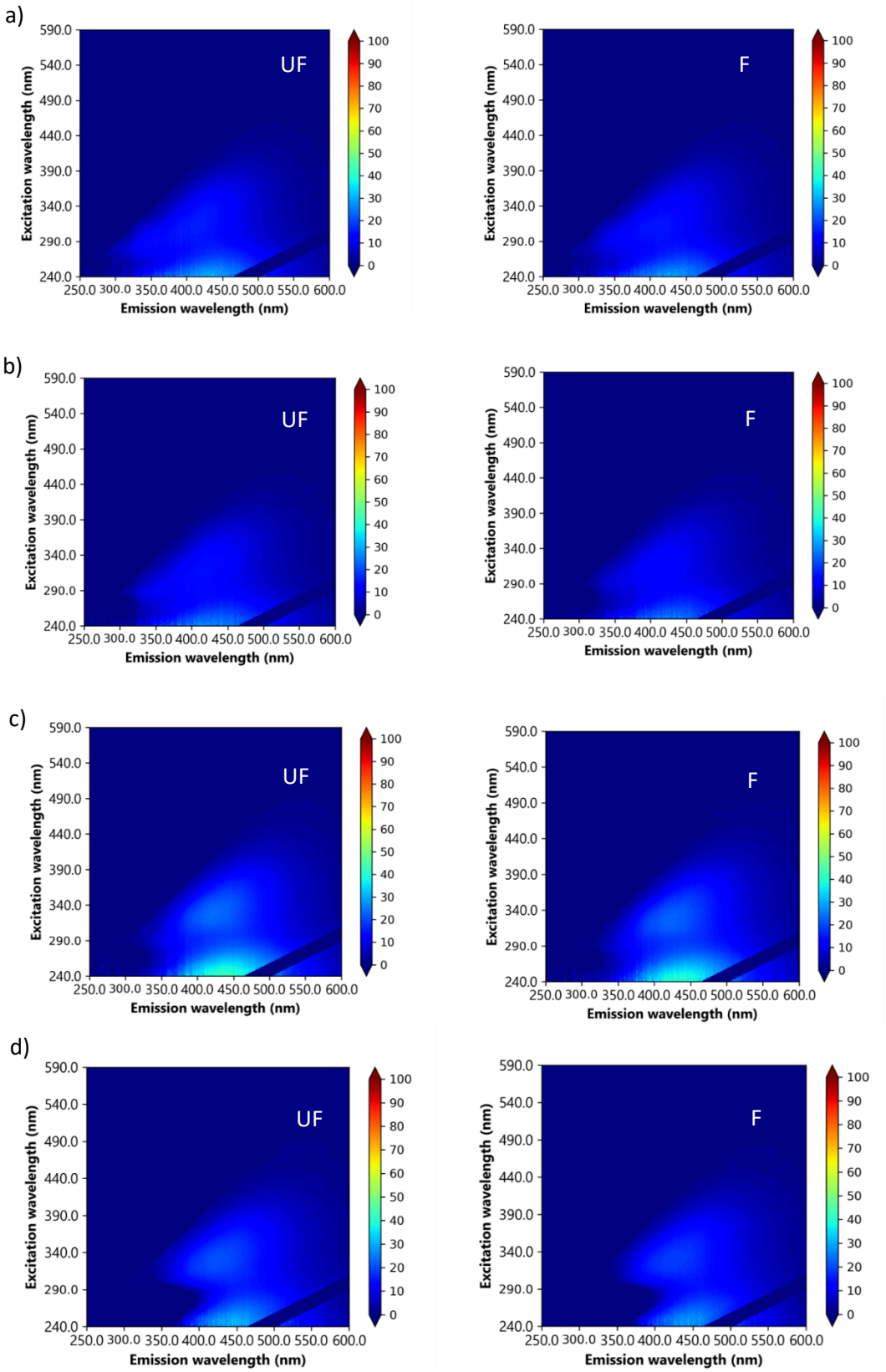

Figure 5.6 Excitation-Emission Matrices (EEMs) from the River Thames at Taplow, Maidenhead showing filtered (F) and unfiltered (UF) samples from: a) 20/07/2021, b) 13/09/2021, c) 15/11/2021 and d) 17/01/2022.

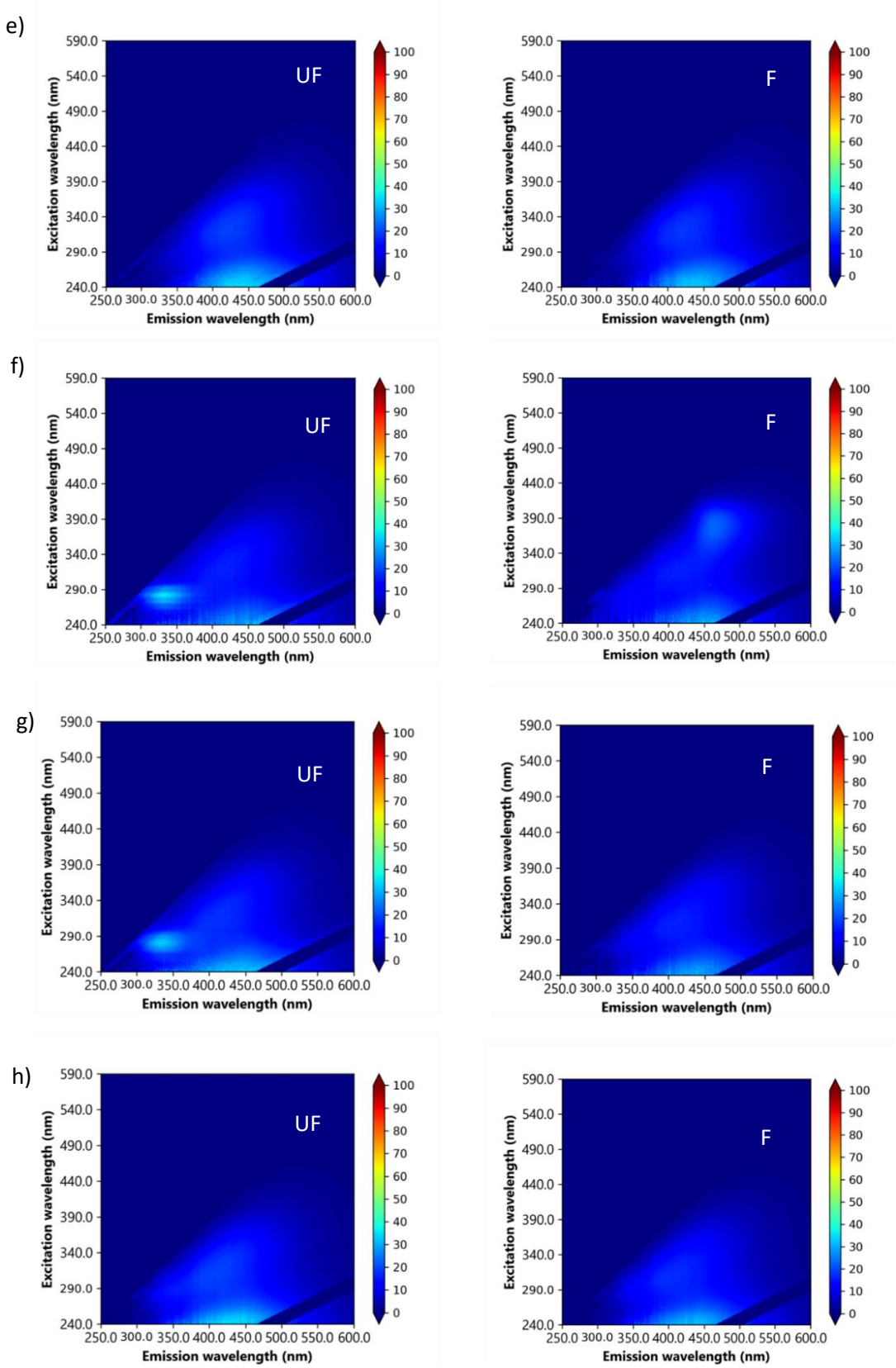

Figure 5.7 Excitation-Emission Matrices (EEMs) from the River Thames at Taplow, Maidenhead showing filtered (F) and unfiltered (UF) samples from: e) 14/03/2022, f) 24/04/2022, g) 23/05/2022 and h) 05/09/2022.

5.3.2. Microbiological data

Samples were collected weekly, then twice monthly, for microbiological analysis of the following: *Escherichia coli* (*E. coli*), non-*E.coli* coliforms, and heterotrophic plate counts. Figure 5.16 displays data between July 2021 and October 2022.

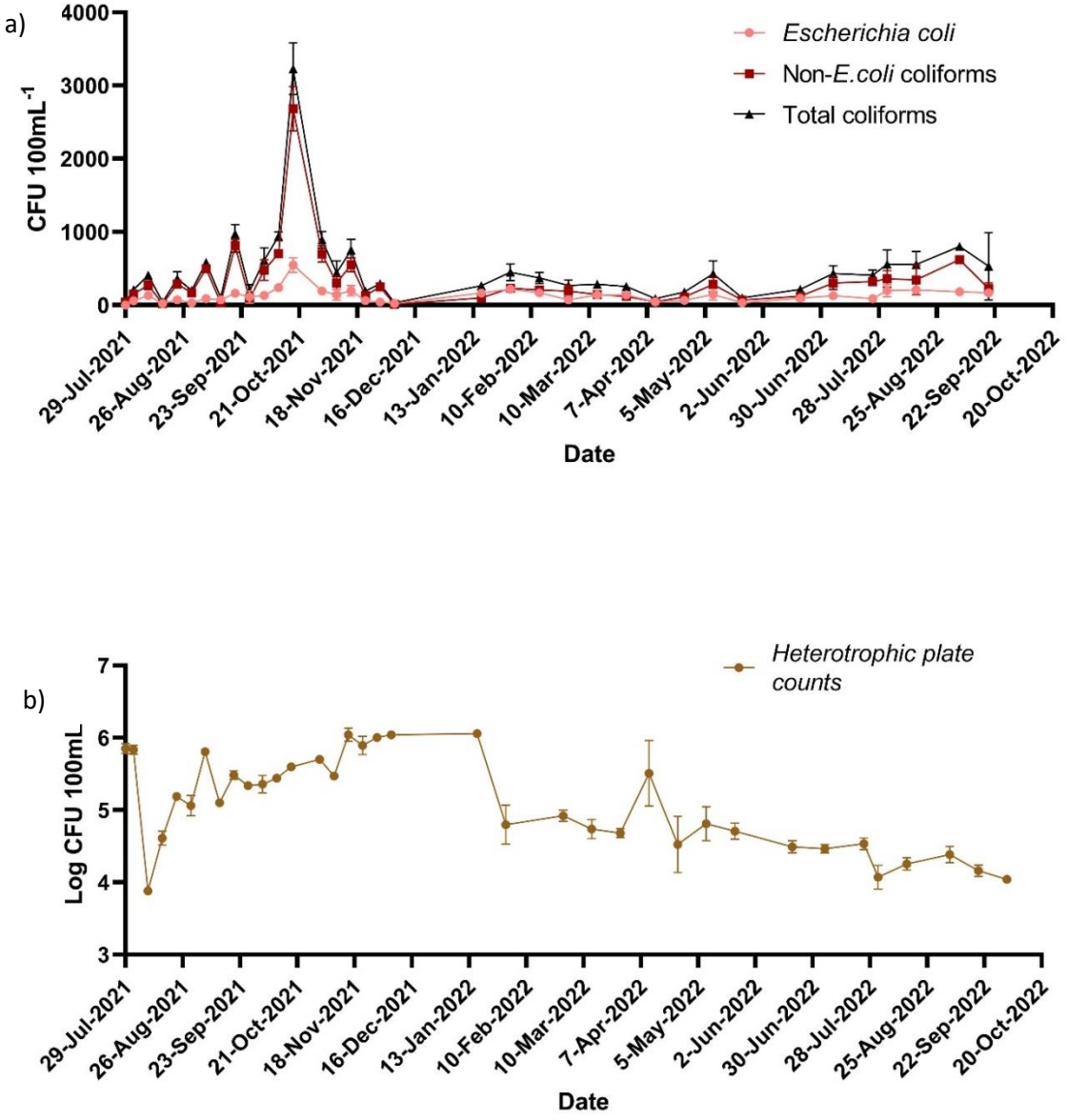

Figure 5.8 Microbiological data showing a) Escherichia coli (E. coli), non-E. coli coliforms, and total coliforms and b) heterotrophic plate counts (HPCs) from the River Thames at Taplow, Maidenhead between July 2021 and October 2022 (n=3 biological and technical replicates). Error bars denote standard deviation.

E. coli, non-*E. coli* and total coliform data shows variation throughout the measured time period, with several significant spikes in bacterial numbers (Figure 5.16a). *E. coli* data appears to be less variable than non-*E. coli* (and therefore total coliform) data. *E. coli* data ranges between 20 (±20) and 546 (±100) CFU 100mL^{-1}, whereas non-*E. coli* coliforms varies between 13 (±11) and 810 (±90) CFU 100mL^{-1}. There is variability between July and December 2021 during which several spikes in non-*E. coli* coliforms are seen, where *E. coli* data follows a similar pattern but with less variation. For example, an event which occurs on 27/09/2021 sees an increase of 777 CFU 100mL^{-1} for non-*E.coli* coliforms, but only an increase of 93 CFU 100mL^{-1} for *E. coli*. Whilst all coliforms increase at this time, the increase is much greater for non-*E. coli* coliforms, suggesting an event in which other forms of coliforms may have been introduced into the system.

Several other events occur over the measured time period where all coliforms increase, but non-*E. coli* coliforms increase more than *E. coli*. For example, over the summer period of 2022, between July and September. During this time, non-*E. coli* coliforms increase from 66 (±25) to 620 (±28) CFU 100mL^{-1} over a period of 3 months, before beginning to decline again in September. *E. coli* numbers follow a similar pattern, increasing form 30 (±17) to 209 (±28) CFU 100mL^{-1} over the same period. This increase in cell numbers occurs in tandem with an increase in temperature (Figure 5.11b), suggesting it is a result of a natural increase in cell numbers occuring as a result of warming conditions within the system during the summer time. Other instances of cell number increase, however, do not occur in tandem with temperature increase and therefore may be explained by an input into the system.

Figure 5.17 displays data from discrete samples showing the relationship between the fluorescence intensities of Peak T, C and C+ (filtered and unfiltered) and the density of *E. coli.* Interestingly, Peak T displays the weakest correlation with *E. coli*, with an R^2 value of 0.00005 for unfiltered samples and 0.2 for filtered samples. Peak C displayed an R^2 value of 0.31 for unfiltered samples and 0.2 for filtered samples, and Peak C+ displayed an R^2 value of 0.28 for unfiltered samples and 0.09 for filtered samples. Peaks C and C+ both show similar correlations with *E. coli*, in addition to both showing stronger correlations for unfiltered samples than filtered samples.. For Peak T, however, there is a higher descrepancy between the correlation of filtered and unfiltered samples, with the relationship between *E. coli* and unfiltered Peak T showing nearly no correlation, but *E. coli* and filtered Peak T showing a stronger correlation of R^2 0.2.

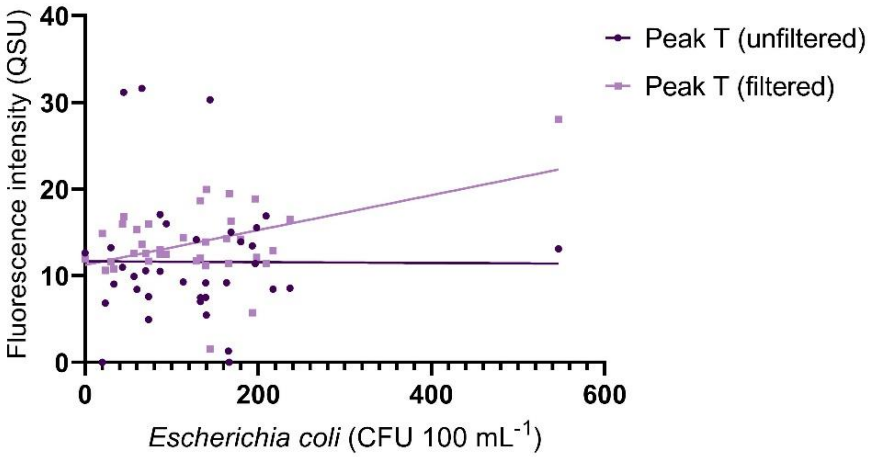

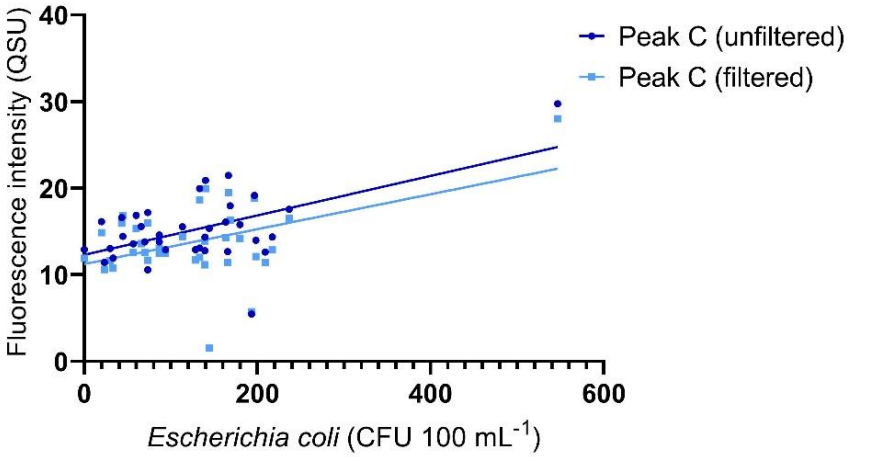

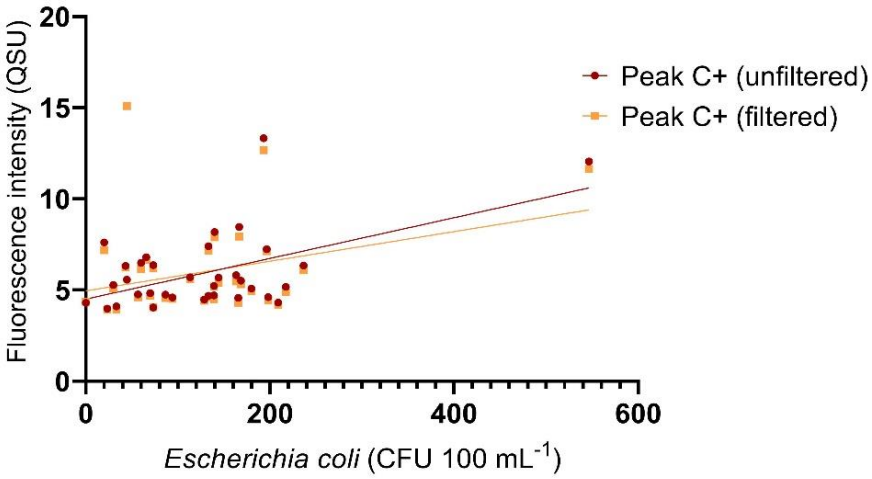

Figure 5.9 *Escherichia coli* (CFU 100 mL^{-1}) and fluorescence intensity (QSU) for; a) Peak T, b) Peak C and c) Peak C+, showing filtered and unfiltered fluorescence samples.

5.4. Discussion

In this study, a novel fluorescence-based sensor has been applied to a freshwater system alongside a water quality sonde to perform hourly measurements of a number of fluorescence and physicochemical parameters over a 16-month period. In addition to this, frequent discrete samples have been collected for benchtop laboratory fluorescence measurements and microbiological data. Advances in handheld fluorometry technology has, in recent years, made in-situ monitoring of fluorescence a possibility (Carstea et al., 2016; Khamis et al., 2018; Old et al., 2019a; Sorensen et al., 2015, 2018, 2021). However, much of this data has focused on specific case studies, such as nutrient transport of faecal contamination, and there are still few studies exploring long-term monitoring with an extensive suite of biological, physicochemical and fluorescence characteristics in tandem with one another. This work addresses this by utilising a novel five-channel fluorescence-based sensor alongside standard water quality parameters on the River Thames at Taplow, Maidenhead, UK, with the view to highlighting the potential of fluorescence as a novel water quality parameter.

5.4.1. Water quality monitoring: physico-chemical, microbiological and fluorescence characteristics of the River Thames at Taplow, Maidenhead

Several events occur over the measured time period which are detected by the range of water quality parameters that are measured. In general, Tryptophan and CDOM measurements reflect one another throughout the measured time period, often displaying similar troughs and peaks as they respond to water quality events. This is possibly due to the fluorescence regions which are investigated with the V-Lux sensor, which employs a single-excitation 280 nm bulb for all incident light. As a result, it is possible that some bleeding of fluorescence spectra may occur, resulting in spectral overlap. To disentangle this, ratios of CDOM:Tryptophan and Tryptophan:CDOM were observed. Using the Tryptophan:CDOM ratio (Figure 5.3) it is clearer to pick out individual events which may indicate microbial processing, activity or presence without interference from CDOM. Figure 5.3 illustrates that there are many events that occur during which CDOM increases independently of Peak T, with CDOM fluorescence intensity showing a higher average and higher contribution to the overall fluorescence than Tryptophan. This suggests that the majority of AFOM in this system can be attributed to inputs of allochthonous material of terrestrial origin (Coble et al., 2014; Hudson et al., 2007), with more discrete events being seen to occur which contribute to smaller, though noticeable, increases in microbially-derived AFOM. Additionally, the winter months between November and April see higher CDOM:Tryptophan ratios, likely to have occurred due to an increase in delivery of allochthonous material from the surrounding catchment into the system. The summer months see a higher Tryptophan:CDOM ratio, suggesting an increase in temperature, evident in Figure 5.11b, is resulting

in upregulated metabolic activity and potentially a higher bacterial load in the system. These ratios point towards the usefulness of multi-parameter fluorescence-based sensors for monitoring the contribution of various organic matter sources to the total DOM pool. The flow data presented in Figures 5.8 and 5.9 further supports this claim, suggesting that whilst flow can be a useful tool to support an enhanced understanding of environmental variables in a dynamic system, in the case of the data presented here is does not appear to be directly contributing to the fluorescence signature observed – rather, helping to explain the biological mechanisms behind the changes in fluorescence.

In addition to the potential for spectral overlap which may occur from the composite AFOM being detected by the Tryptophan and CDOM channels in the V-Lux sensor, the emerging knowledge that bacterial activity can contribute to perceived higher molecular-weight AFOM with humic-like optical properties (Berggren et al., 2020; Fox et al., 2017, 2021; Guillemette & del Giorgio, 2012; Perrin et al., 2022; Shimotori et al., 2009), further discussed in Chapters 3 and 4, may explain some of the smaller increases seen in both Tryptophan and CDOM, such as those between June and July 2022 (Figure 5.3a), particularly during the summer months where microbial secondary production due to warmer temperatures is higher and terrestrial input is lower due to decreased rainfall. This data highlights that the use of ratios can be useful to remove noise and identify events pertaining to specific fluorescence peaks, it is also imperative to assess this alongside the raw, individual data values so as not to oversee other potential events.

In addition to the relationship between CDOM and Tryptophan, several events occur over the measured time period where observing the relationship between Chlorophyll and Tryptophan highlights the dynamics occurring within the system. The increase in both Chlorophyll and Tryptophan together, which occurred in April and May 2022, clearly denotes an algal bloom event, and suggests that the measured increase in Tryptophan intensity is a product of algal, rather than bacterial, biomass. This is further supported by evidence presented in Figure 5.6, where though a general positive relationship can be seen between Chlorophyll and Tryptophan (also found to be significant), distinct regions showing 'spikes' in Tryptophan suggest discrete events in which bacterial-derived Tryptophan dominates the Tryptophan-like fluorescence profile. Though it is known that Tryptophan can be used to assess algal presence (Yin et al., 2020), it is a more commonly used metric for assessing the presence of pathogenic bacteria such as *E. coli* in freshwaters (Sorensen et al., 2015, 2018, 2021). The close relationship between Chlorophyll and Tryptophan fluorescence during the algal bloom periods, however, highlights the importance of dual measurements so as to account for the potential contribution of both algae and bacteria to this AFOM. This is further highlighted during the algal bloom of July 2022 (Figure 5.5), during which both Chlorophyll and Tryptophan increase in tandem, followed by a small 'shoulder' of Tryptophan fluorescence which occurs in isolation to the Chlorophyll

fluorescence (potentially shown further as one of the discrete regions in Figure 5.6). This could be attributed to an increase in bacterial secondary production during the decomposition of algal biomass which occurs following an algal bloom; a phenomenon which, at large scales, can contribute to the rapid development of hypoxic conditions in surface waters (Bai et al., 2017). This may denote both an increase in bacterial activity (in the form of respiration), and an increase in bacterial cell number.

When considering these data, it is important to account for the potential impact of temperature variations on observed fluorescence signals through increased collisional quenching. This has been explored at depth in numerous studies (Baker 2005, Lakowicz, Reynolds, 2014, Carstea 2014), with the general conclusion that temperature correction algorithms, whilst difficult to develop due to the highly variable range of the impacts that temperature can exert on different fluorophores alongside the combined effects of other environmental variables, should be applied. It is recommended that caution be taken with this, and if possible, corrections should be applied through an internal algorithm within the sensor (Carstea 2014, Khamis 2015).

The Chelsea Technologies V-Lux sensor employed in this study does not utilize internal corrections for temperature. As such, it is possible that temperature changes are exerting some impact on the observed fluorescence intensities. It is expected that due to increased collisional quenching, this would result in a decrease in fluorescence intensity during times of increased temperatures. There is therefore the possibility that increases in ecosystem metabolism which may be occurring during summer months, which may result in increased production of fluorophores (particularly tryptophan-like fluorescence), are not being captured to their full extent by the by the V-Lux fluorosensor. However, data collected using the Aqualog benchtop spectrofluorometer using samples of comparable temperatures, does not show a statistically significant increase in fluorescence intensity during the summer months where temperature is seen to increase.

In addition to exploring the in-situ fluorescence data, these observed patterns can be further disentangled using the microbiological data available. Heterotrophic plate count (HPC) data, whilst known to represent only a fraction of viable microorganisms within a given water sample (Gensberger et al., 2015), can provide an insight into general trends in cell density of microorganisms over time. A sample taken on 25/07/2022 shows approximately a two-fold increase in HPCs (Figure 5.16b) from samples taken two weeks before and after, suggesting that the small Tryptophan ‘shoulder’ may occur as a result of a bacterial bloom. Interestingly, *E. coli* data does not show any significant peak during this time in the same way that HPC data does (Figure 5.16a), but shows a general incline over the summer months which is likely attributed to more favourable conditions for growth as the water temperature increases, evidenced in Figure 5.11. Benchtop laboratory measurements of Peaks T, C

and C+ during these algal bloom periods show that during the April and May 2022 algal bloom event, unfiltered Peak T fluorescence intensity rose sharply whilst filtered Peak T fluorescence remained low. It is known that filtration of water samples can discern between intracellular and extracellular fluorescence (Fox et al., 2021; Herlemann et al., 2014). This data therefore suggests that during the algal bloom period, the production of intracellular AFOM may have taken precedent over the export of extracellular fluorescing metabolites within the microbial community, particularly for proteinaceous material. This may point towards a higher representation of intracellular material within the algal AFOM pool, potentially highlighting the use of the filtration technique as a tool for providing information about the presence of different microorganisms, and the contribution of different microbes to the community. This highlights the importance of coupling ground truthing, on-site analysis with a multi parameters approach to fluorescence analysis (such as couple Tryptophan and Chlorophyll measurements) to disentangle the biological processing dynamics that are occurring.

Significant biological events such as algal blooms are also seen to cause increased variability, or noise, within the data. Figures 5.3, 5.5, 5.10 and 5.11 all show increased variability during the algal bloom period of April and May 2022. This is true for both fluorescence and physico-chemical data. During an algal bloom period, increased metabolic activity would have occurred as a result of both primary and secondary production by microorganisms within the system as cells grow and multiply. This may explain the increased variability in the data, as microbial activity, and the subsequent AFOM response, becomes harder to predict. This has been seen previously in data from Chapters 3 and 4, in which the growth rate and AFOM characteristics become more variable within systems with conditions more favourable to growth; that is, those with higher nutrient and DOC availability. It is possible that the fluorescence response is more difficult to predict in these scenarios.

The relationship between *E. coli* cells and filtered and unfiltered fluorescence data from benchtop spectrofluorometric measurements shows, interestingly, that *E. coli* has a stronger correlation with Peaks C and C+ fluorescence than with Peak T fluorescence. This is not in agreement with data from previous literature which has suggested that Peak T fluorescence can be used to monitor the presence and density of *E. coli* in freshwaters (Sorensen et al., 2021). Where Peak T does correlate with fluorescence intensity, the correlation was found to be weak, though slightly stronger for filtered Peak T samples than for unfiltered Peak T samples. This suggests that Peak T fluorescence represents intracellular material more closely than it represents extracellular material, potentially suggesting that where Peak T and *E. coli* do correlate, Peak T is not directly detecting cellular material, but potentially extracellular exudates. It is worth noting that the system in which this study was undertaken represents a lowland river with various inputs from anthropogenic activities such as treated and untreated sewage, and agricultural and industrial effluents, and therefore is likely to have a significant

total microbial load. Therefore, *E. coli* likely represents a very small fraction of the total bacterial population that is present, which may explain the weak correlation between cell number and Peak T fluorescence. The stronger correlation seen between *E. coli* and Peak C/C+ could highlight the potential use of Peak C/C+, or other humic-like fluorescence regions, as being related to biological presence or activity. This is in agreement with previous data seen in this thesis (Chapters 3 and 4) which show the clear in-situ production of these fluorescence peaks by microorganisms from a simple, labile carbon source. Other explanations for the stronger relationship between Peak C/C+ and *E. coli* could be the relationship with precipitation events, which are known to not only introduce humic-like compounds into the system from the surrounding catchment but also can correlate with the use of combined sewer overflows, often containing faecal coliforms.

5.5. Conclusions

- In-situ fluorescence spectroscopy can be an effective tool to monitor biological events over a long time period in freshwater systems, particularly when coupled with discrete samples and physico-chemical measurements to ground-truth the data.
- Relationships between Tryptophan and CDOM and Tryptophan and Chlorophyll statistically show overall positive relationships between these parameters over the measured time period. However, it is clear that during distinct events, such as bacterial upregulation, algal blooms or the input of allochthonous material into the system during the winter months, it is possible to pick out distinct patterns within the data.
- A combination of Chlorophyll and Tryptophan measurements are useful when monitoring biological activity in freshwaters so as to disentangle the impacts of algal blooms on Tryptophan fluorescence, which can be significant.
- It is more difficult to predict the fluorescence response by microbes during time of increased growth, or metabolic upregulation. During this time, fluorescence signatures become noisier and more variable. This is a finding that is echoed in Chapters 3 and 4 of this thesis.
- *E. coli* data was found to correlate very weakly (non-significant) with Peak T, and slightly more strongly with Peaks C/C+. This suggests that the use of Peak T as a marker for the presence and density of *E. coli* should be done with caution, and may point towards the use of more humic-like peaks as an effective biomarker for biological processes or presence, rather than the terrestrial input of allochthonous material only.

Chapter 6. Final Discussion and Conclusions

6.1. Synopsis

The main aim of this research was to investigate the origin, production and processing of bacterial AFOM in freshwaters. Specifically, the work sought to develop a laboratory model in which this could be investigated in a controlled environment, before applying this new knowledge to a field study using a novel fluorescence-based sensor. The basis of this work stemmed from the lack of clarity within existing literature surrounding the relationship between bacterial presence/activity, and freshwater AFOM characteristics. Much of the research to date has focused on the relationship between cell presence and Peak T fluorescence intensity (Sorensen et al., 2015, 2018, 2021), however some recent publications have also pointed towards the use of Peak T as a marker for an active microbial population, rather than a measure of cell number alone (Fox et al., 2018, 2021), however, to date the direct relationship between bacterial activity and fluorescence production and processing had not been investigated. In addition, recent literature has begun challenging the conventional notion of the 'autochthonous' and 'allochthonous' binary classification system which is often assigned to AFOM. Some studies have recently suggested that allochthonous, humic-like AFOM may be produced in-situ as a function of microbial processes, rather than imported directly into the catchment (Berggren et al., 2020; Fox et al., 2021; Guillemette & del Giorgio, 2012; Shimotori et al., 2009, 2012). This required further investigation, in particular as a function of changing freshwater conditions, which had not yet been investigated. As such, one of the prime focuses of this work was to investigate the production of AFOM by freshwater bacteria in-situ as a function of changing nutrient conditions, a factor which is known to be impacting freshwater quality at an increasingly alarming rate (Bechtold et al., 2012; Blaen et al., 2016; Manning et al., 2018; Old et al., 2019b; Woodward et al., 2012).

To further disentangle the phenomenon of in-situ processing and production of AFOM by bacteria in freshwater, a model laboratory-based system was developed to allow the underpinning dynamics to be studied without the influence of background fluorescence or elevated baseline nutrient concentrations. A minimal simulated freshwater (SFW) medium was developed, adapted from Smith et al. (2002), containing all essential ionic constituents for growth of microbes in freshwater, with limited nitrate, phosphate and dissolved organic carbon (DOC) availability. Six conditions of nutrient concentrations were developed so as to investigate microbial production and processing of AFOM as a function of nutrient concentrations, as detailed in Chapter 3 using *Pseudomonas aeruginosa*. This work has highlighted the clear production of a range of AFOM peaks, including those previously considered to be of allochthonous, terrestrial origin, such as Peaks C and C+. This has implications for the contribution of bacteria to the freshwater organic matter (OM) pool, suggesting that bacteria may produce, in-situ, compounds which are more recalcitrant in nature and may persist within the

environment in an extracellular form. Understanding the contribution of bacteria to the freshwater OM pool is key to understanding global biogeochemical cycling, and carbon transport and storage throughout the hydrological continuum (Baker & Spencer, 2004; Bieroza & Heathwaite, 2015; Carstea et al., 2010; Coble et al., 2014; Elliott et al., 2006; Mostofa et al., 2007; Saraceno et al., 2009; Weigelhofer et al., 2020).

Work undertaken in Chapter 3 found that the relationship between fluorescence and cell number was non-linear over time. This was interesting due to the historical notion in the literature that fluorescence, in particular Peak T, represents intracellular compounds and can be used to monitor the presence and density of bacterial cells in freshwater systems (Carstea et al., 2016; Elliott et al., 2006; Sorensen et al., 2018). During periods of presumed metabolic upregulation, such as the exponential growth period of the bacterial growth curve (known to be so due to the frequent monitoring of viable cell numbers), a higher fluorescence per cell was observed. In addition, it was found that all fluorescence peaks (T, C and C+) were influenced by the concentration of nutrients (nitrate, phosphate and DOC) in the system. It was found that higher DOC concentrations indicate higher total fluorescence, showing the immediate, in-situ utilization of available labile carbon for the production of more complex organic molecules. In addition, nutrient concentrations were found to substantially impact the relative contribution of each fluorescence peak to the total fluorescence, particularly as a function of changing DOC conditions. For example, conditions containing both no additional DOC and an additional 5 mg L^{-1} DOC were found to produce more Peak T fluorescence relative to Peaks C and C+ upon the addition of nitrates and phosphates, whereas higher DOC conditions (800 mg L^{-1}) were found to produce more Peak C and C+ relative to Peak T when higher nutrient concentrations were introduced. This suggests that the availability of DOC, nitrate, and phosphate, and more importantly the ratio of these nutrients, influences which form of AFOM production takes precedent within a system.

These results underscore the complexities associated with using fluorescence intensity as a direct proxy for cell number, particularly within dynamic systems which may be influenced by the influx of nutrients of other pollutants. Instead, this work highlights the potential application of fluorescence Peaks T, C and C+ as potential markers for biological activity, indicating an upregulated metabolic rate in freshwater systems. In addition, the work sheds light on the influence of nutrient concentrations on bacterial AFOM production, suggesting that the influx of anthropogenic pollutants into freshwaters may be altering the role that bacteria play as the mediators of carbon in freshwater systems.

In order to further investigate the postulation formed in Chapter 3 that fluorescence acts as a marker for an upregulated metabolic state within a bacterial community, further investigation was

undertaken in Chapter 4 to directly measure the activity of a range of different bacterial species in a model freshwater system, and its relationship with fluorescence and cell number. Data in Chapter 3 was not able to directly ascertain the link between fluorescence production and biological activity, beyond assumptions that were made from the observed increase in fluorescence per cell which occurred during the presumed metabolic upregulation during the exponential phase of the bacterial growth curve. Work undertaken in Chapter 4, therefore, sought to investigate this link directly by calculating bacterial production (BP) measurements through the incorporation of radiolabelled [^{3}H]-Leucine assays alongside fluorescence and viable cell counts. Four bacterial strains were investigated, one of which was the *P. aeruginosa* strain employed in Chapter 3, with the remaining three strains having been isolated and cultivated from the River Thames and Taplow, Maidenhead. The same SFW system was employed as in Chapter 3, with only one condition being investigated which contained the most relevant conditions to a standard freshwater environment. The results from this work supported data from Chapter 3 in showing that all bacterial strains investigated were able to produce fluorescence in both the conventionally 'autochthonous' and 'allochthonous' optical regions (Peaks T, C and C+), bolstering the theory that bacteria can contribute to a large portion of the AFOM pool, including humic-like AFOM, from in-situ production in freshwaters. Results from the BP work showed that BP was found to 'peak' at its highest rate prior to the peak of cell number (4 h prior in the case of *P. aeruginosa* and *Escherichia coli*), suggesting this was indicating the upregulation in metabolism which often precedes an increase in cell number during cell growth and replication (Kirchman, 2001; Jurtshuk, 1996).

All strains investigated in Chapter 4 were seen to have a higher variability in fluorescence intensity (shown by higher standard deviation values) during the exponential growth phase of the growth curve, than at any other time throughout the experiment. This is commensurate with data from Chapter 3, which also found there to be higher variability between experimental repeats (both technical and biological) during the exponential growth curve period. This suggests that at times of upregulated metabolic activity, it is more difficult to predict the fluorescence response by microorganisms. This finding is particularly relevant for field-based fluorescence applications, where fluorescence intensity may be used to directly monitor biological contamination. Positive correlations were found between BP and fluorescence intensity for *P. aeruginosa* and for *E. coli*, with the former being non-significant and the latter being significant ($p < 0.05$). Data from both of these strains shows that 'peak' QSU times corresponded with 'peak' BP times during the growth curve. Interestingly, these peak times were shown to coincide with a substantial decrease in cell number, suggesting that BP and AFOM production increase in tandem with one another, independently of cell number. The other strains investigated, whilst not showing as strong correlations between BP and QSU, do point towards a

stronger relationship between BP and QSU than between cell number and QSU. This is an important finding, as it supports the use of fluorescence as a marker for an active microbial population, as has been hypothesised throughout this work, rather than as a direct enumerator for bacterial cell numbers.

The water quality monitoring study which was undertaken in Chapter 5 of this work sought to apply the use of fluorescence for monitoring biological activity into the field utilizing a novel fluorescence-based sensor developed by Chelsea Technologies Ltd on the River Thames at Taplow, Maidenhead. The aim of this chapter was to understand how in-situ fluorescence monitoring can be used in the future as a novel and meaningful water quality parameter. The fluorescence sensor, alongside a water quality sonde undertaking physico-chemical measurements, sampled at hourly intervals between July 2021 and November 2022. This is the first five-channel fluorescence-based sensor to contain multiple optical channels (Tryptophan, Chlorophyll and CDOM) alongside internal measurements and corrections for absorbance and turbidity. The sensor was found to perform well under the deployment conditions (a custom flow cell with hourly pumping intervals directly from the freshwater system). Additionally, the sensor performed well at monitoring biological activity within the system, with a clear response from both the Chlorophyll and Tryptophan channels during an algal bloom event. Additionally, the use of the multi-channel V-Lux allowed the differentiation between algal- and bacterial-derived Tryptophan signals, with one algal bloom event showing a clear, independent Tryptophan peak occurring after a peak in Chlorophyll, suggesting an upregulation in bacterial activity during the breakdown and respiration of algal biomass. This was further supported by an increase in Heterotrophic Plate Counts (HPCs) during this time. Sensor data also further confirmed the findings from Chapters 3 and 4 which suggested that the fluorescence response by microbes becomes less reliable, and more variable, during times of upregulated metabolic activity. Another interesting finding from this study showed a stronger correlation between *E. coli* and humic-like fluorescence (Peaks C and C+) than between *E. coli* and Peak T. This is contextually relevant due to Peak T commonly being used to monitor the presence and abundance of *E. coli* in freshwater systems (Sorensen et al., 2018).

Results displayed in Chapter 5 highlight the value of fluorescence-based in-situ sensing for improving our understanding of the source and origin of AFOM in aquatic systems. Through investigating the relationships between fluorescence parameters, in particular through understanding the ratios between different parameters obtained through using a multi-channel instrument with standardised units of measurement, it was possible to clearly identify the sources of different types of AFOM present within the system and their changes over time. In particular, it has been demonstrated that it is possible to identify periods of enhanced microbial activity that occur within a lowland river system, and relate this specifically to either algal or bacterial biomass.

This research has shown that data from simplified laboratory models can help to explain the ultimate origin of AFOM in freshwater systems, and be used to contextualise the potential sources of AFOM within the field. The findings have shown that under increased nutrient conditions – a common pressure facing freshwater systems – fluorescence intensity increases in laboratory scenarios. Further laboratory models have shown the increase in fluorescence intensity can be attributed to upregulated, or enhanced, microbial activity. This was then translated into a real-world scenario in the field, with a multi-channel fluorescence sensor displaying clear information regarding the source of AFOM. The contribution of this work to the improved understanding of the role of microbial processes in AFOM processing in freshwaters has underscored the use of fluorescence as being a dynamic parameter that can assess microbial activity through time, in particular through looking at the relationships between multiple fluorophores using data collected from a single, standardised instrument. This work has proven the functionality and value in using a novel five-channel fluorescence-based sensor to monitor microbial activity in freshwater systems, whilst highlighting what information fluorescence can provide regarding the underpinning processing of AFOM in aquatic systems.

6.2. Conclusions

The key objectives of this research were the following:

- To develop a biological model to investigate the impact of nutrients on microbial AFOM production in a controlled freshwater laboratory system
- To further unravel the relationship between AFOM and microbial metabolism and/or enumeration
- Investigate the production of humic-like, “allochthonous” AFOM by freshwater bacteria and consider the impact of this on the flux of carbon through the hydrological continuum
- To implement a water quality monitoring programme using a novel in-situ fluorescence-based sensor alongside standard water quality parameters
- To assess the use of fluorescence as a novel water quality parameter for monitoring microbial activity in freshwater systems

This work, underscored by the above objectives, has culminated in a number of conclusive findings which have contributed to the development of new knowledge within this field of study. These are as follows:

6.2.1. The in-situ production of a range of AFOM from a simple, labile carbon source

This research provides the first evidence of the in-situ production of a range of complex AFOM, including AFOM that is presumed to be high molecular-weight and is often associated with terrestrially-derived, humic-like molecules, from a simple, labile carbon source (glucose). This sheds light on the previously-overlooked role of bacteria in the freshwater carbon cycle, suggesting they may play a direct and substantial role in the production of less bioavailable, more recalcitrant AFOM that may contribute to long-term carbon storage and transport to downstream ecosystems. This finding also underscores the potential for humic-like AFOM, such as Peaks C/C+, to be used as biological markers where previously Peak T, or Tryptophan-like, fluorescence was considered to be the only appropriate fluorescence marker for in-situ biological activity.

6.2.2. The influence of nutrients on in-situ AFOM production

Secondly, this research has shown that bacterial AFOM production and processing is influenced by the concentrations of nitrate, phosphate, and DOC within the system. Specifically, increased DOC availability results directly in increased total fluorescence intensity per bacterial cell, and increased nitrate and phosphate concentrations result in changes in the relative contribution of each fluorescent peak to the total fluorescence. This results in the preferential production of differing forms of AFOM dependent on the nutrient status of the system.

6.2.3. AFOM production is directly related to upregulated biological activity

Thirdly, this work has, for the first time, directly examined the link between biological activity and AFOM production and processing, and found that the relationship between fluorescence and cell number is weaker than the relationship between fluorescence and bacterial activity. It has been shown that fluorescence per cell increases during times of upregulated metabolic activity, highlighting the use of fluorescence as a marker for an active microbial population rather than for cell enumeration alone.

6.2.4. The implementation of a novel five-channel in-situ fluorescence sensor

Finally, the work presented demonstrates the implementation and use of a novel in-situ fluorescence sensor for monitoring biological activity and water quality in a lowland UK river. This work has shown that a multi-channel fluorescence sensor can be successfully used to monitor major biological events of both algal and bacterial origin in real-time over a long-term deployment. This technology platform,

combined with the use of a water quality sonde and discrete monitoring of microbiological parameters, presents a novel means of monitoring water quality and biological activity in freshwater systems.

6.3. Recommendations for future work

The work presented in this thesis has contributed new knowledge regarding the relationship between bacterial activity and AFOM production and processing. It has provided direct evidence for the relationship between bacterial production and AFOM processing in a number of bacterial strains, and evidenced that nutrient loading in freshwater environments can impact this process substantially. However, there are a number of knowledge gaps that remain. Firstly, the model laboratory system that has been produced would benefit from a more representative bacterial community inoculum. Work undertaken in this thesis has focused on individual monoculture species at a time, but for a true representation of biological processing, a mixed microbial community must be investigated which utilizes a variety of bacteria, algae, and cyanobacteria that are representative of those found in freshwaters. Little is still known with regards to the algal production and processing of AFOM and its contribution to the fluorescence pool, and whilst some work presented in Chapter 5 of this thesis was able to touch upon the algal-bacterial dynamics in freshwaters, this could be explored further, particularly in regards to bacterial secondary processing of algal-derived organic exudates. In addition, all work undertaken in this thesis investigated bacterial AFOM processing in planktonic form only. Very little is known about the contribution of biofilms towards AFOM processing, despite biofilms in the hyporheic zone and on suspended aggregates in the water column contributing substantially towards the total bacterial population of freshwater systems. As such, future work could include the investigation of a mixed-model system including a diverse microbial community of bacteria and algae in both planktonic and biofilm form, perhaps involving a simulated hyporheic flow system. In addition, further changes could be made towards the development of a more environmentally representative SFW model. This may include investigating bacterial AFOM production under ambient environmental temperature conditions, rather than stimulating production using 37°C conditions.

It would also be of merit to investigate the continued processing of AFOM over a longer experimental period (i.e. weeks) to determine the relative recalcitrance of the material produced. A limitation of the work presented within this thesis is the lack of data pertaining to the processing of AFOM beyond a 48 h time period, but data that is available shows much of the humic-like AFOM (Peaks C and C+) that is produced in the model systems persists in the system over time, whilst Peak T often decreases towards the end of the experimental period. This suggests that some of the material produced represents more recalcitrant, less biologically-available material that is produced in-situ from more labile carbon, however in order to verify this experimentally, longer experimental study periods would

be required. The theory that freshwater bacteria are capable of producing higher molecular-weight, recalcitrant molecules from a simple bioavailable carbon source, suggested in this work from the in-situ development of distinct AFOM peaks within the humic-like optical region, also requires further investigation in order to be verified experimentally. A potential route for this could be to directly measure the material produced, using an analytical technique such as, for example, Fourier-transform ion cyclotron resonance mass spectrometry (FT-ICR-MS), a technique which allows the analysis of the composition and concentration of ions at very low concentrations. This would provide an insight into the molecular weight of the AFOM being produced, ascertaining whether the microbial community are producing higher molecular-weight material from lower molecular-weight carbon.

Within this work, in-situ fluorescence has been investigated using a novel fluorescence-based sensor with five channels (three fluorescence channels: Tryptophan, Chlorophyll and CDOM, alongside turbidity and absorbance). This investigation took place in a single location on a long-term basis, on the River Thames at Taplow, Maidenhead. The sensor and monitoring system were located externally to the river, in a separate system with a flow cell into which water was pumped from the river on an hourly basis. As such, the sensor was not submerged in river water permanently, thereby reducing the risk of biofouling. The use of an indoor monitoring set-up with a flow cell and pumping system may not be convenient for deployments in, for example, remote locations where there is no permanent infrastructure or access to mains power. For future deployments, it is therefore important to test that the sensor hardware, including V-Lux, sonde and Meteor system, is fully operational within a remote context under solar power. In addition, testing the necessary cleaning regime will be important, as biofouling may occur more frequently when deployment is undertaken permanently within a river system. Furthermore, to thoroughly test the capabilities of the V-Lux sensor with regards to monitoring the quality of freshwater systems as a function of inputs such as treated and untreated sewage discharges, nutrient inputs and industrial effluents, a network of sensor systems must be developed using two or more monitoring units. This could involve, for example, a two-unit system monitoring upstream and downstream of a known pollution source, or a larger-scale operation utilizing multiple systems along the length of a river at a catchment scale. This would provide an insight into the processing and transformation of DOM from young, labile OM in small headwater streams, to highly processed OM in lowland systems that has undergone transformation and experienced various terrestrial inputs. Additionally, whilst this work has sought to shed light on the use of in-situ fluorescence monitoring to measure biological activity in freshwaters, no direct measurements of biological activity have been made in this field-based study. Future work may incorporate the use of [^{3}H]-Leucine incorporation bacterial production assays in order to directly measure biological activity

and its relationship with fluorescence intensity changes over time at high temporal and spatial resolution.

Chapter 7. References

Ahmad, S. R., & Reynolds, D. M. (1995). Synchronous fluorescence spectroscopy of wastewater and some potential constituents. *Water Research*, *29*(6), 1599–1602. https://doi.org/10.1016/0043-1354(94)00266-A

Aiken, G. (2014). Fluorescence and Dissolved Organic Matter. *Aquatic Organic Matter Fluorescence*, 35–74. https://doi.org/10.1017/CBO9781139045452.005

Anderson, T. R., Rowe, E. C., Polimene, L., Tipping, E., Evans, C. D., Barry, C. D. G., Hansell, D. A., Kaiser, K., Kitidis, V., Lapworth, D. J., Mayor, D. J., Monteith, D. T., Pickard, A. E., Sanders, R. J., Spears, B. M., Torres, R., Tye, A. M., Wade, A. J., & Waska, H. (2019). Unified concepts for understanding and modelling turnover of dissolved organic matter from freshwaters to the ocean: the UniDOM model. *Biogeochemistry 2019 146:2*, *146*(2), 105–123. https://doi.org/10.1007/S10533-019-00621-1

Arndt, J., Kirchner, J. S., Jewell, K. S., Schluesener, M. P., Wick, A., Ternes, T. A., & Duester, L. (2022). Making waves: Time for chemical surface water quality monitoring to catch up with its technical potential. *Water Research*, *213*, 118168. https://doi.org/10.1016/J.WATRES.2022.118168

Asmala, E., Kaartokallio, H., Carstensen, J., & Thomas, D. N. (2016). Variation in riverine inputs affect dissolved organic matter characteristics throughout the estuarine gradient. *Frontiers in Marine Science*, *2*(JAN), 125. https://doi.org/10.3389/FMARS.2015.00125/BIBTEX

Attermeyer, K., Harjung, A., Schelker, J., & Weigelhofer, G. (2022). Experimental evaluation of the role of inorganic phosphorus for terrestrial carbon degradation in stream hyporheic zones. *Freshwater Biology*. https://doi.org/10.1111/FWB.13980

Bai, L., Cao, C., Wang, C., Xu, H., Zhang, H., Slaveykova, V. I., & Jiang, H. (2017). Toward Quantitative Understanding of the Bioavailability of Dissolved Organic Matter in Freshwater Lake during Cyanobacteria Blooming. *Environmental Science and Technology*, *51*(11), 6018–6026. https://doi.org/10.1021/ACS.EST.7B00826/ASSET/IMAGES/LARGE/ES-2017-00826E_0004.JPEG

Baker, A. (2002). Fluorescence Excitation−Emission Matrix Characterization of River Waters Impacted by a Tissue Mill Effluent. *Environmental Science and Technology*, *36*(7), 1377–1382. https://doi.org/10.1021/ES0101328

Baker, A. (2005). Thermal fluorescence quenching properties of dissolved organic matter. *Water Research*, *39*(18), 4405–4412. https://doi.org/10.1016/J.WATRES.2005.08.023

Baker, A., & Inverarity, R. (2004). Protein-like fluorescence intensity as a possible tool for determining river water quality. *Hydrological Processes*, *18*(15), 2927–2945. https://doi.org/10.1002/hyp.5597

Baker, A., Inverarity, R., Charlton, M., & Richmond, S. (2003). Detecting river pollution using fluorescence spectrophotometry: case studies from the Ouseburn, NE England. *Environmental Pollution*, *124*(1), 57–70. https://doi.org/10.1016/S0269-7491(02)00408-6

Baker, A., & Spencer, R. G. M. (2004). Characterization of dissolved organic matter from source to sea using fluorescence and absorbance spectroscopy. *Science of the Total Environment*, *333*(1–3), 217–232. https://doi.org/10.1016/j.scitotenv.2004.04.013

Barker, L. J., Fry, M., Hannaford, J., Nash, G., Tanguy, M., & Swain, O. (2022). Dynamic High Resolution Hydrological Status Monitoring in Real-Time: The UK Water Resources Portal. *Frontiers in Environmental Science*, *10*, 811. https://doi.org/10.3389/FENVS.2022.752201/BIBTEX

Bartlett, J. S., Voss, K. J., Sathyendranath, S., & Vodacek, A. (1998). Raman scattering by pure water and seawater. *Applied Optics*, *37*(15), 3324. https://doi.org/10.1364/AO.37.003324

Bastviken, D., & Tranvik, L. (2001). The Leucine Incorporation Method Estimates Bacterial Growth Equally Well in Both Oxic and Anoxic Lake Waters. *Applied and Environmental Microbiology*, *67*(7), 2916. https://doi.org/10.1128/AEM.67.7.2916-2921.2001

Battin, T. J., Kaplan, L. A., Findlay, S., Hopkinson, C. S., Marti, E., Packman, A. I., Newbold, J. D., & Sabater, F. (2008). Biophysical controls on organic carbon fluxes in fluvial networks. *Nature Geoscience*, *1*(2), 95–100. https://doi.org/10.1038/ngeo101

Bechtold, H. A., Marcarelli, A. M., Baxter, C. v., & Inouye, R. S. (2012). Effects of N, P, and organic carbon on stream biofilm nutrient limitation and uptake in a semi-arid watershed. *Limnology and Oceanography*, *57*(5), 1544–1554. https://doi.org/10.4319/lo.2012.57.5.1544

Bennett, L. E., & Drikas, M. (1993). The evaluation of colour in natural waters. *Water Research*, *27*(7), 1209–1218. https://doi.org/10.1016/0043-1354(93)90013-8

Berggren, M., Gudasz, C., Guillemette, F., Hensgens, G., Ye, L., & Karlsson, J. (2020a). Systematic microbial production of optically active dissolved organic matter in subarctic lake water. *Limnology and Oceanography*, *65*(5), 951–961. https://doi.org/10.1002/lno.11362

Berggren, M., Gudasz, C., Guillemette, F., Hensgens, G., Ye, L., & Karlsson, J. (2020b). Systematic microbial production of optically active dissolved organic matter in subarctic lake water. *Limnology and Oceanography*, *65*(5), 951–961. https://doi.org/10.1002/LNO.11362

Bieroza, M. Z., & Heathwaite, A. L. (2015). Seasonal variation in phosphorus concentration–discharge hysteresis inferred from high-frequency in situ monitoring. *Journal of Hydrology*, *524*, 333–347. https://doi.org/10.1016/J.JHYDROL.2015.02.036

Blaen, P. J., Khamis, K., Lloyd, C. E. M., Bradley, C., Hannah, D., & Krause, S. (2016). Real-time monitoring of nutrients and dissolved organic matter in rivers: Capturing event dynamics, technological opportunities and future directions. *Science of the Total Environment*, *569–570*, 647–660. https://doi.org/10.1016/J.SCITOTENV.2016.06.116

Bowes, M. J., Jarvie, H. P., Halliday, S. J., Skeffington, R. A., Wade, A. J., Loewenthal, M., Gozzard, E., Newman, J. R., & Palmer-Felgate, E. J. (2015). Characterising phosphorus and nitrate inputs to a rural river using high-frequency concentration–flow relationships. *Science of The Total Environment*, *511*, 608–620. https://doi.org/10.1016/J.SCITOTENV.2014.12.086

Braslavsky, S. E. (2007). Glossary of terms used in photochemistry 3rd edition: (IUPAC Recommendations 2006). *Pure and Applied Chemistry*, *79*(3), 293–465. https://doi.org/10.1351/PAC200779030293/PDF

Bright, C. E., Mager, S. M., & Horton, S. L. (2020). Catchment-scale influences on riverine organic matter in southern New Zealand. *Geomorphology*, *353*, 107010. https://doi.org/10.1016/J.GEOMORPH.2019.107010

Carpenter, S. R., Caraco, N. F., Correll, D. L., Howarth, R. W., Sharpley, A. N., & Smith, V. H. (1998). NONPOINT POLLUTION OF SURFACE WATERS WITH PHOSPHORUS AND NITROGEN. *Ecological Applications*, *8*(3), 559–568. https://doi.org/10.1890/1051-0761

Carstea, E. M., Baker, A., Bieroza, M., & Reynolds, D. (2010). Continuous fluorescence excitation-emission matrix monitoring of river organic matter. *Water Research*, *44*(18), 5356–5366. https://doi.org/10.1016/J.WATRES.2010.06.036

Carstea, E. M., Baker, A., & Savastru, R. (2014). Comparison of river and canal water dissolved organic matter fluorescence within an urbanised catchment. *Water and Environment Journal*, *28*(1), 11–22. https://doi.org/10.1111/WEJ.12062

Carstea, E. M., Bridgeman, J., Baker, A., & Reynolds, D. M. (2016). Fluorescence spectroscopy for wastewater monitoring: A review. *Water Research*, *95*, 205–219. https://doi.org/10.1016/J.WATRES.2016.03.021

Cavicchioli, R., Ripple, W. J., Timmis, K. N., Azam, F., Bakken, L. R., Baylis, M., Behrenfeld, M. J., Boetius, A., Boyd, P. W., Classen, A. T., Crowther, T. W., Danovaro, R., Foreman, C. M., Huisman, J., Hutchins, D. A., Jansson, J. K., Karl, D. M., Koskella, B., Mark Welch, D. B., … Webster, N. S. (2019). Scientists' warning to humanity: microorganisms and climate change. *Nature Reviews Microbiology*, *17*(9), 569–586. https://doi.org/10.1038/s41579-019-0222-5

Coble, P. G. (1996). Characterization of marine and terrestrial DOM in seawater using excitation-emission matrix spectroscopy. *Marine Chemistry*, *51*(4), 325–346. https://doi.org/10.1016/0304-4203(95)00062-3

Coble, P. G., Spencer, R. G. M., Baker, A., & Reynolds, D. M. (2014). Aquatic Organic Matter Fluorescence. In *Aquatic Organic Matter Fluorescence*. https://doi.org/10.1017/cbo9781139045452.006

Cohen, E., Levy, G. J., & Borisover, M. (2014). Fluorescent components of organic matter in wastewater: Efficacy and selectivity of the water treatment. *Water Research*, *55*, 323–334. https://doi.org/10.1016/J.WATRES.2014.02.040

Cole, J. J., Prairie, Y. T., Caraco, N. F., McDowell, W. H., Tranvik, L. J., Striegl, R. G., Duarte, C. M., Kortelainen, P., Downing, J. A., Middelburg, J. J., & Melack, J. (2007). Plumbing the global carbon cycle: Integrating inland waters into the terrestrial carbon budget. *Ecosystems*, *10*(1), 171–184. https://doi.org/10.1007/s10021-006-9013-8

Cole, J., & Pace ML. (1995). Why measure bacterial production? A reply to the comment by Jahnke and Craven. *Limnology and Oceanography*, *40*, 441–444.

Correll, D. L. (1999). Phosphorus: a rate limiting nutrient in surface waters. *Poultry Science*, *78*(5), 674–682. https://doi.org/10.1093/PS/78.5.674

D'Andrilli, J., Junker, J. R., Smith, H. J., Scholl, E. A., & Foreman, C. M. (2019). DOM composition alters ecosystem function during microbial processing of isolated sources. *Biogeochemistry*, *142*(2), 281–298. https://doi.org/10.1007/s10533-018-00534-5

Darwall, W., Bremerich, V., de Wever, A., Dell, A. I., Freyhof, J., Gessner, M. O., Grossart, H. P., Harrison, I., Irvine, K., Jähnig, S. C., Jeschke, J. M., Lee, J. J., Lu, C., Lewandowska, A. M., Monaghan, M. T., Nejstgaard, J. C., Patricio, H., Schmidt-Kloiber, A., Stuart, S. N., … Weyl, O. (2018). The Alliance for Freshwater Life: A global call to unite efforts for freshwater biodiversity science and conservation. *Aquatic Conservation: Marine and Freshwater Ecosystems*, *28*(4), 1015–1022. https://doi.org/10.1002/AQC.2958

Dodson, S. I., Arnott, S. E., & Cottingham, K. L. (2000). THE RELATIONSHIP IN LAKE COMMUNITIES BETWEEN PRIMARY PRODUCTIVITY AND SPECIES RICHNESS. *SYNTHESIS EMPHASIZING NEW IDEAS TO STIMULATE RESEARCH IN ECOLOGY Ecology*, *81*(10), 2662–2679. https://doi.org/10.1890/0012-9658

DOM transformations in stream biofilms shown by fluorescence spectroscopy | Request PDF. (n.d.). Retrieved March 16, 2021, from https://www.researchgate.net/publication/258624658_DOM_transformations_in_stream_biofilms_shown_by_fluorescence_spectroscopy

Dorado-García, I., Medina-Sánchez, J. M., Herrera, G., Cabrerizo, M. J., & Carrillo, P. (2014). Quantification of Carbon and Phosphorus Co-Limitation in Bacterioplankton: New Insights on an Old Topic. *PLOS ONE*, *9*(6), e99288. https://doi.org/10.1371/JOURNAL.PONE.0099288

Downing, J. A. (2008). Emerging global role of small lakes and ponds: little things mean a lot. *Limnetica*, *29*(1), 9–24. https://doi.org/10.23818/limn.29.02

Dudgeon, D. (2015). Freshwater Biology – sustaining excellence in a world of change. *Freshwater Biology*, *60*(9), 1737–1739. https://doi.org/10.1111/FWB.12631

Elliott, S., Lead, J. R., & Baker, A. (2006). Characterisation of the fluorescence from freshwater, planktonic bacteria. *Water Research*, *40*(10), 2075–2083. https://doi.org/10.1016/J.WATRES.2006.03.017

Fellman, J. B., Hood, E., & Spencer, R. G. M. (2010). Fluorescence spectroscopy opens new windows into dissolved organic matter dynamics in freshwater ecosystems: A review. *Limnology and Oceanography*, *55*(6), 2452–2462. https://doi.org/10.4319/LO.2010.55.6.2452

Firth, P. (1999). The importance of water resources education for the next century. *Journal of the American Water Resources Association*, *35*(3), 487–492. https://doi.org/10.1111/J.1752-1688.1999.TB03605.X

Fox, B. G., Thorn, R. M. S., Anesio, A. M., Cox, T., Attridge, J. W., & Reynolds, D. M. (2018). Microbial processing and production of aquatic fluorescent organic matter in a model freshwater system. *Water (Switzerland)*, *11*(1). https://doi.org/10.3390/w11010010

Fox, B. G., Thorn, R. M. S., Anesio, A. M., & Reynolds, D. M. (2017). The in situ bacterial production of fluorescent organic matter; an investigation at a species level. *Water Research*, *125*, 350–359. https://doi.org/10.1016/J.WATRES.2017.08.040

Fox, B. G., Thorn, R. M. S., Dutta, T. K., Bowes, M. J., Read, D. S., & Reynolds, D. M. (2022). A case study: The deployment of a novel in situ fluorimeter for monitoring biological contamination within the urban surface waters of Kolkata, India. *Science of the Total Environment*, *842*. https://doi.org/10.1016/J.SCITOTENV.2022.156848

Fox, B. G., Thorn, R. M. S., & Reynolds, D. M. (2021). Laboratory In-Situ Production of Autochthonous and Allochthonous Fluorescent Organic Matter by Freshwater Bacteria. *Microorganisms 2021, Vol. 9, Page 1623*, *9*(8), 1623. https://doi.org/10.3390/MICROORGANISMS9081623

Fuhrman, J. A., & Azam, F. (1980). Bacterioplankton Secondary Production Estimates for Coastal Waters of British Columbia, Antarctica, and California. *Applied and Environmental Microbiology*, *39*(6), 1085–1095. https://doi.org/10.1128/AEM.39.6.1085-1095.1980

Gao, Y., Yang, T., Wang, Y., & Yu, G. (2017). Fate of river-transported carbon in china: implications for carbon cycling in coastal ecosystems. *Http://Dx.Doi.Org/10.1002/Ehs2.1265*, *3*(3). https://doi.org/10.1002/EHS2.1265

Geetha, S., & Gouthami, S. (2017). Internet of things enabled real time water quality monitoring system. *Smart Water 2017 2:1*, *2*(1), 1–19. https://doi.org/10.1186/S40713-017-0005-Y

Gensberger, E. T., Gössl, E. M., Antonielli, L., Sessitsch, A., & Kostić, T. (2015). Effect of different heterotrophic plate count methods on the estimation of the composition of the culturable microbial community. *PeerJ*, *2015*(3). https://doi.org/10.7717/PEERJ.862/SUPP-2

Guillemette, F., & del Giorgio, P. A. (2012). Simultaneous consumption and production of fluorescent dissolved organic matter by lake bacterioplankton. *Environmental Microbiology*, *14*(6), 1432–1443. https://doi.org/10.1111/J.1462-2920.2012.02728.X

Guillemette, F., microbiology, P. del G.-E., & 2012, undefined. (2012). Simultaneous consumption and production of fluorescent dissolved organic matter by lake bacterioplankton. *Wiley Online Library*, *14*(6), 1432–1443. https://doi.org/10.1111/j.1462-2920.2012.02728.x

Halliday, S. J., Skeffington, R. A., Wade, A. J., Bowes, M. J., Gozzard, E., Newman, J. R., Loewenthal, M., Palmer-Felgate, E. J., & Jarvie, H. P. (2015). *High-frequency water quality monitoring in an urban catchment: hydrochemical dynamics, primary production and implications for the Water Framework Directive; High-frequency water quality monitoring in an urban catchment: hydrochemical dynamics, primary production and implications for the Water Framework Directive*. https://doi.org/10.1002/hyp.10453

Hedges, J. I. (1992). Global biogeochemical cycles: progress and problems. *Marine Chemistry*, *39*(1–3), 67–93. https://doi.org/10.1016/0304-4203(92)90096-S

Herlemann, D. P. R., Manecki, M., Meeske, C., Pollehne, F., Labrenz, M., Schulz-Bull, D., Dittmar, T., & Jürgens, K. (2014). Uncoupling of Bacterial and Terrigenous Dissolved Organic Matter Dynamics in Decomposition Experiments. *PLOS ONE*, *9*(4), e93945. https://doi.org/10.1371/JOURNAL.PONE.0093945

Hotchkiss, E. R., Hall, R. O., Sponseller, R. A., Butman, D., Klaminder, J., Laudon, H., Rosvall, M., & Karlsson, J. (2015). Sources of and processes controlling CO2 emissions change with the size of streams and rivers. *Nature Geoscience 2015 8:9*, *8*(9), 696–699. https://doi.org/10.1038/ngeo2507

Hudson, N., Baker, A., & Reynolds, D. (2007). Fluorescence analysis of dissolved organic matter in natural, waste and polluted waters—a review. *River Research and Applications*, *23*(6), 631–649. https://doi.org/10.1002/RRA.1005

Hudson, N., Baker, A., Ward, D., Reynolds, D. M., Brunsdon, C., Carliell-Marquet, C., & Browning, S. (2008). Can fluorescence spectrometry be used as a surrogate for the Biochemical Oxygen

Demand (BOD) test in water quality assessment? An example from South West England. *Science of the Total Environment*, *391*(1), 149–158. https://doi.org/10.1016/j.scitotenv.2007.10.054

Ji, X., Liu, K., Zhu, Q. Q., Zhang, J., & Yang, G. P. (2022). Spatio-temporal variation of Dissolved Organic Matter (DOM) in the Bohai Sea and the Yellow Sea. *Journal of Marine Systems*, *234*, 103777. https://doi.org/10.1016/J.JMARSYS.2022.103777

Jordan, P., & Cassidy, R. (2022). Perspectives on Water Quality Monitoring Approaches for Behavioral Change Research. *Frontiers in Water*, *4*, 101. https://doi.org/10.3389/FRWA.2022.917595/BIBTEX

Khamis, K., Bradley, C., & Hannah, D. M. (2018). Understanding dissolved organic matter dynamics in urban catchments: insights from in situ fluorescence sensor technology . *Wiley Interdisciplinary Reviews: Water*, *5*(1), e1259. https://doi.org/10.1002/wat2.1259

Kinsey, J. D., Corradino, G., Ziervogel, K., Schnetzer, A., & Osburn, C. L. (2018). Formation of chromophoric dissolved organic matter by bacterial degradation of phytoplankton-derived aggregates. *Frontiers in Marine Science*, *4*(JAN), 430. https://doi.org/10.3389/FMARS.2017.00430/BIBTEX

Kirchman, D. (2001). Measuring bacterial biomass production and growth rates from leucine incorporation in natural aquatic environments. *Methods in Microbiology*, *30*, 227–237. https://doi.org/10.1016/S0580-9517(01)30047-8

Koch, B. P., Kattner, G., Witt, M., & Passow, U. (2014). Molecular insights into the microbial formation of marine dissolved organic matter: Recalcitrant or labile? *Biogeosciences*, *11*(15), 4173–4190. https://doi.org/10.5194/bg-11-4173-2014

Kominoski, J. S., Rosemond, A. D., Benstead, J. P., Gulis, V., & Manning, D. W. P. (2018). Experimental nitrogen and phosphorus additions increase rates of stream ecosystem respiration and carbon loss. *Limnology and Oceanography*, *63*(1), 22–36. https://doi.org/10.1002/lno.10610

Korak, J. A., Dotson, A. D., Summers, R. S., & Rosario-Ortiz, F. L. (2014). Critical analysis of commonly used fluorescence metrics to characterize dissolved organic matter. *Water Research*, *49*, 327–338. https://doi.org/10.1016/J.WATRES.2013.11.025

Kothawala, D. N., Stedmon, C. A., Müller, R. A., Weyhenmeyer, G. A., Köhler, S. J., & Tranvik, L. J. (2014). Controls of dissolved organic matter quality: evidence from a large-scale boreal lake survey. *Global Change Biology*, *20*(4), 1101–1114. https://doi.org/10.1111/GCB.12488

Lakowicz, J. R. (2006). Principles of fluorescence spectroscopy. *Principles of Fluorescence Spectroscopy*, 1–954. https://doi.org/10.1007/978-0-387-46312-4/COVER

Lawaetz, A. J., & Stedmon, C. A. (2009). Fluorescence intensity calibration using the Raman scatter peak of water. *Applied Spectroscopy*, *63*(8), 936–940. https://doi.org/10.1366/000370209788964548

Leenheer, J. A., & Croué, J.-P. (2003). Peer Reviewed: Characterizing Aquatic Dissolved Organic Matter. *Environmental Science & Technology*, *37*(1), 18A-26A. https://doi.org/10.1021/es032333c

Liess, M., & Beketov, M. (2011). Traits and stress: Keys to identify community effects of low levels of toxicants in test systems. *Ecotoxicology*, *20*(6), 1328–1340. https://doi.org/10.1007/S10646-011-0689-Y/TABLES/4

Li Zweifel, U., Norrman, B., & Hagstrom, A. (1993). Consumption of dissolved organic carbon by marine bacteria and demand for inorganic nutrients. *MARINE ECOLOGY PROGRESS SERIES Mar. Ecol. Prog. Ser*, *101*, 23–32.

Maie, N., Scully, N. M., Pisani, O., & Jaffé, R. (2007). Composition of a protein-like fluorophore of dissolved organic matter in coastal wetland and estuarine ecosystems. *Water Research*, *41*(3), 563–570. https://doi.org/10.1016/J.WATRES.2006.11.006

Manning, D. W. P., Rosemond, A. D., Gulis, V., Benstead, J. P., & Kominoski, J. S. (2018). Nutrients and temperature additively increase stream microbial respiration. *Global Change Biology*, *24*(1), e233–e247. https://doi.org/10.1111/gcb.13906

Maranger, R., Jones, S. E., & Cotner, J. B. (2018). Stoichiometry of carbon, nitrogen, and phosphorus through the freshwater pipe. *Limnology and Oceanography Letters*, *3*(3), 89–101. https://doi.org/10.1002/LOL2.10080

Marxsen, J. (1996). Measurement of bacterial production in stream-bed sediments via leucine incorporation. *MICROBIOLOGY ECOLOGY ELSEWIER FEMS Microbiology Ecology*, *2*, 13–325. https://doi.org/10.1111/j.1574-6941.1996.tb00128.x

Maske, H., Hatzenpichler, R., Braissant, O., Ch, O. B., Astasov-Frauenhoffer, M., Waltimo, T., & Bonkat, G. (2020). *A Review of Methods to Determine Viability, Vitality, and Metabolic Rates in Microbiology*. https://doi.org/10.3389/fmicb.2020.547458

Mclellan, S. L., Huse, S. M., Mueller-Spitz, S. R., Andreishcheva, E. N., & Sogin, M. L. (n.d.). *Diversity and population structure of sewage derived microorganisms in wastewater treatment plant influent*. https://doi.org/10.1111/j.1462-2920.2009.02075.x

M., E. (2012). Fluorescence Spectroscopy as a Potential Tool for In-Situ Monitoring of Dissolved Organic Matter in Surface Water Systems. *Water Pollution*. https://doi.org/10.5772/28979

Milbrandt, E. C., Coble, P. G., Conmy, R. N., Martignette, A. J., & Siwicke, J. J. (2010). Evidence for the production of marine fluorescence dissolved organic matter in coastal environments and a possible mechanism for formation and dispersion. *Limnology and Oceanography*, *55*(5), 2037–2051. https://doi.org/10.4319/LO.2010.55.5.2037

Miller, M. P., & McKnight, D. M. (2010). Comparison of seasonal changes in fluorescent dissolved organic matter among aquatic lake and stream sites in the Green Lakes Valley. *Journal of Geophysical Research: Biogeosciences*, *115*(G1), 0–12. https://doi.org/10.1029/2009JG000985

Mostofa, K. M. G., Yoshioka, T., Konohira, E., & Tanoue, E. (2007). Photodegradation of fluorescent dissolved organic matter in river waters. *Undefined*, *41*(5), 323–331. https://doi.org/10.2343/GEOCHEMJ.41.323

Murphy, K. R., Butler, K. D., Spencer, R. G. M., Stedmon, C. A., Boehme, J. R., & Aiken, G. R. (2010). Measurement of dissolved organic matter fluorescence in aquatic environments: An interlaboratory comparison. *Environmental Science and Technology*, *44*(24), 9405–9412. https://doi.org/10.1021/ES102362T/SUPPL_FILE/ES102362T_SI_001.PDF

Naden, P. S., Old, G. H., Eliot-Laize, C., Granger, S. J., Hawkins, J. M. B., Bol, R., & Haygarth, P. (2010). Assessment of natural fluorescence as a tracer of diffuse agricultural pollution from slurry spreading on intensely-farmed grasslands. *Water Research*, *44*(6), 1701–1712. https://doi.org/10.1016/J.WATRES.2009.11.038

Najjar, R. G., Jin, X., Louanchi, F., Aumont, O., Caldeira, K., Doney, S. C., Dutay, J. C., Follows, M., Gruber, N., Joos, F., Lindsay, K., Maier-Reimer, E., Matear, R. J., Matsumoto, K., Monfray, P., Mouchet, A., Orr, J. C., Plattner, G. K., Sarmiento, J. L., … Yool, A. (2007). Impact of circulation on export production, dissolved organic matter, and dissolved oxygen in the ocean: Results from Phase II of the Ocean Carbon-cycle Model Intercomparison Project (OCMIP-2). *Global Biogeochemical Cycles*, *21*(3), 3007. https://doi.org/10.1029/2006GB002857

Noacco, V., Wagener, T., Worrall, F., Burt, T. P., & Howden, N. J. K. (2017). Human impact on long-term organic carbon export to rivers. *Journal of Geophysical Research: Biogeosciences*, *122*(4), 947–965. https://doi.org/10.1002/2016JG003614

Norris, R. H., & Thoms, M. C. (1999). What is river health? *Freshwater Biology*, *41*(2), 197–209. https://doi.org/10.1046/j.1365-2427.1999.00425.x

Old, G. H., Naden, P. S., Harman, M., Bowes, M. J., Roberts, C., Scarlett, P. M., Nicholls, D. J. E., Armstrong, L. K., Wickham, H. D., & Read, D. S. (2019a). Using dissolved organic matter fluorescence to identify the provenance of nutrients in a lowland catchment; the River Thames, England. *Science of the Total Environment*, *653*, 1240–1252. https://doi.org/10.1016/J.SCITOTENV.2018.10.421

Pallottini, M., Goretti, E., Gaino, E., Selvaggi, R., Cappelletti, D., & Céréghino, R. (2015). Invertebrate diversity in relation to chemical pollution in an Umbrian stream system (Italy). *Comptes Rendus Biologies*, *338*(7), 511–520. https://doi.org/10.1016/J.CRVI.2015.04.006

Perminova, I. v., Frimmel, F. H., Kudryavtsev, A. v., Kulikova, N. A., Abbt-Braun, G., Hesse, S., & Petrosyan, V. S. (2003). Molecular weight characteristics of humic substances from different environments as determined by size exclusion chromatography and their statistical evaluation. *Environmental Science and Technology*, *37*(11), 2477–2485. https://doi.org/10.1021/ES0258069/ASSET/IMAGES/LARGE/ES0258069F00003.JPEG

Perrin, E. M., Thorn, R. M. S., Sargeant, S. L., Attridge, J. W., & Reynolds, D. M. (2022). The in situ Production of Aquatic Fluorescent Organic Matter in a Simulated Freshwater Laboratory Model. *Frontiers in Microbiology*, *13*, 435. https://doi.org/10.3389/FMICB.2022.817976/BIBTEX

Peter Jurtshuk, Jr. (1996). Bacterial Metabolism. *Medical Microbiology*. https://www.ncbi.nlm.nih.gov/books/NBK7919/

Prieto, A., Barber-Lluch, E., Herna´ndez, M., Herna´ndez-Ruiz, H., Marti´nez, S., Marti´nez-Garci´a, M., Garci´a, G., Ferna´ndez, E., Ferna´ndez, F., & Teira, E. (2016). Assessing the role of phytoplankton-bacterioplankton coupling in the response of microbial plankton to nutrient additions. *J. Plankton Res*, *38*(1), 55–63. https://doi.org/10.1093/plankt/fbv101

Reynolds, D. M. (2002). The differentiation of biodegradable and non-biodegradable dissolved organic matter in wastewaters using fluorescence spectroscopy. *Journal of Chemical Technology and Biotechnology*, *77*(8), 965–972. https://doi.org/10.1002/JCTB.664

Reynolds, D. M. (2003). Rapid and direct determination of tryptophan in water using synchronous fluorescence spectroscopy. *Water Research*, *37*(13), 3055–3060. https://doi.org/10.1016/S0043-1354(03)00153-2

Reynolds, D. M. (2014). The Principles of Fluorescence. *Aquatic Organic Matter Fluorescence*, 3–34. https://doi.org/10.1017/CBO9781139045452.004

Reynolds, D. M., & Ahmad, S. R. (1997). Rapid and direct determination of wastewater BOD values using a fluorescence technique. *Water Research*, *31*(8), 2012–2018. https://doi.org/10.1016/S0043-1354(97)00015-8

Riley, A. J., & Dodds, W. K. (2013). Whole-stream metabolism: Strategies for measuring and modeling diel trends of dissolved oxygen. *Freshwater Science*, *32*(1), 56–69. https://doi.org/10.1899/12-058.1/ASSET/IMAGES/LARGE/I2161-9565-32-1-56-F07.JPEG

Saraceno, J. F., Pellerin, B. A., Downing, B. D., Boss, E., Bachand, P. A. M., Saraceno, J. F. ;, Pellerin, B. A. ;, Downing, B. D. ;, Boss, E. ;, Bachand, P. A. M. ;, Bergamaschi, B. A., Saraceno, J. F., Pellerin, B. A., Downing, B. D., Bachand, P. A. M., & Bergamaschi, B. A. (2009). High-Frequency in Situ Optical Measurements During a Storm Event: Assessing Relationships Between Dissolved Organic Matter, Sediment Concentrations, and Hydrologic Processes. *J. Geophys. Res*, *114*, 0–09. https://doi.org/10.1029/2009JG000989

Saraceno, J. F., Shanley, J. B., Downing, B. D., & Pellerin, B. A. (2017). Clearing the waters: Evaluating the need for site-specific field fluorescence corrections based on turbidity measurements. *Limnology and Oceanography: Methods*, *15*(4), 408–416. https://doi.org/10.1002/LOM3.10175

Shimotori, K., Omori, Y., & Hama, T. (2009). Bacterial production of marine humic-like fluorescent dissolved organic matter and its biogeochemical importance. *Aquatic Microbial Ecology*, *58*(1), 55–66. https://doi.org/10.3354/AME01350

Shimotori, K., Omori, Y., & Hama, T. (2010). Bacterial production of marine humic-like fluorescent dissolved organic matter and its biogeochemical importance. *Aquatic Microbial Ecology*, *58*(1), 55–66. https://doi.org/10.3354/ame01350

Shimotori, K., Watanabe, K., & Hama, T. (2012). Fluorescence characteristics of humic-like fluorescent dissolved organic matter produced by various taxa of marine bacteria. *Aquatic Microbial Ecology*, *65*(3), 249–260. https://doi.org/10.3354/ame01552

Sigee, D. C., & Wiley, J. (2005). Freshwater Microbiology: Biodiversity and Dynamic Interactions of Microorganisms in the Aquatic Environment. *Freshwater Microbiology: Biodiversity and Dynamic Interactions of Microorganisms in the Aquatic Environment*, 1–524. https://doi.org/10.1002/0470011254

Sjöstedt, J., Lapierre, J. F., Yamashita, Y., & Baltar, F. (2021). Editorial: Microbial Utilization and Transformation of Dissolved Organic Matter in Aquatic Environments–From Streams to the Deep Ocean. *Frontiers in Microbiology*, *12*, 997. https://doi.org/10.3389/FMICB.2021.668560/BIBTEX

Smith, D. C., & Azam, F. (1992). A simple, economical method for measuring bacterial protein synthesis rates in seawater using 3H-leucine 1. *Marine Microbial Food Webs*, *6*(2), 107–114.

Smith, E. J., Davison, W., & Hamilton-Taylor, J. (2002). Methods for preparing synthetic freshwaters. *Water Research*, *36*(5), 1286–1296. https://doi.org/10.1016/S0043-1354(01)00341-4

Sorensen, J. P. R., Baker, A., Cumberland, S. A., Lapworth, D. J., MacDonald, A. M., Pedley, S., Taylor, R. G., & Ward, J. S. T. (2018). Real-time detection of faecally contaminated drinking water with tryptophan-like fluorescence: defining threshold values. *Science of the Total Environment*, *622–623*, 1250–1257. https://doi.org/10.1016/J.SCITOTENV.2017.11.162

Sorensen, J. P. R., Diaw, M. T., Pouye, A., Roffo, R., Diongue, D. M. L., Faye, S. C., Gaye, C. B., Fox, B. G., Goodall, T., Lapworth, D. J., MacDonald, A. M., Read, D. S., Ciric, L., & Taylor, R. G. (2020). In-situ fluorescence spectroscopy indicates total bacterial abundance and dissolved organic carbon. *Science of the Total Environment*, *738*. https://doi.org/10.1016/J.SCITOTENV.2020.139419

Sorensen, J. P. R., Lapworth, D. J., Marchant, B. P., Nkhuwa, D. C. W., Pedley, S., Stuart, M. E., Bell, R. A., Chirwa, M., Kabika, J., Liemisa, M., & Chibesa, M. (2015). In-situ tryptophan-like fluorescence: A real-time indicator of faecal contamination in drinking water supplies. *Water Research*, *81*, 38–46. https://doi.org/10.1016/J.WATRES.2015.05.035

Sorensen, J. P. R., Nayebare, J., Carr, A. F., Lyness, R., Campos, L. C., Ciric, L., Goodall, T., Kulabako, R., Curran, C. M. R., MacDonald, A. M., Owor, M., Read, D. S., & Taylor, R. G. (2021). In-situ fluorescence spectroscopy is a more rapid and resilient indicator of faecal contamination risk in drinking water than faecal indicator organisms. *Water Research*, *206*. https://doi.org/10.1016/J.WATRES.2021.117734

Tranvik, L. J., Downing, J. A., Cotner, J. B., Loiselle, S. A., Striegl, R. G., Ballatore, T. J., Dillon, P., Finlay, K., Fortino, K., Knoll, L. B., Kortelainen, P. L., Kutser, T., Larsen, Soren., Laurion, I., Leech, D. M., McCallister, S. L., McKnight, D. M., Melack, J. M., Overholt, E., … Weyhenmeyer, G. A. (2009). Lakes and reservoirs as regulators of carbon cycling and climate. *Limnology and Oceanography*, *54*(6part2), 2298–2314. https://doi.org/10.4319/lo.2009.54.6_part_2.2298

Trimmer, M., Grey, J., Heppell, C. M., Hildrew, A. G., Lansdown, K., Stahl, H., & Yvon-Durocher, G. (2012). River bed carbon and nitrogen cycling: State of play and some new directions. In *Science of the Total Environment* (Vol. 434, pp. 143–158). Sci Total Environ. https://doi.org/10.1016/j.scitotenv.2011.10.074

Tsuji, A., Kaneko, Y., Takahashi, K., Ogawa, M., & Goto, S. (1982). The Effects of Temperature and pH on the Growth of Eight Enteric and Nine Glucose Non-Fermenting Species of Gram-Negative Rods. *Microbiology and Immunology*, *26*(1), 15–24. https://doi.org/10.1111/J.1348-0421.1982.TB00149.X

Valeur, B., & Berberan-Santos, M. N. (2011). A brief history of fluorescence and phosphorescence before the emergence of quantum theory. *Journal of Chemical Education*, *88*(6), 731–738. https://doi.org/10.1021/ED100182H

Valeur, Bernard., & Berberan-Santos, M. Nuno. (2013). *Molecular Fluorescence : principles and applications*. 569. https://www.wiley.com/en-us/Molecular+Fluorescence%3A+Principles+and+Applications%2C+2nd+Edition-p-9783527328376

van Puijenbroek, P. J. T. M., Beusen, A. H. W., & Bouwman, A. F. (2019). Global nitrogen and phosphorus in urban waste water based on the Shared Socio-economic pathways. *Journal of Environmental Management*, *231*, 446–456. https://doi.org/10.1016/J.JENVMAN.2018.10.048

Vasel, J. L., & Praet, E. (2002). On the use of fluorescence measurements to characterize wastewater. *Water Science and Technology*, *45*(4–5), 109–116. https://doi.org/10.2166/WST.2002.0564

Wade, A. J., Palmer-Felgate, E. J., Halliday, S. J., Skeffington, R. A., Loewenthal, M., Jarvie, H. P., Bowes, M. J., Greenway, G. M., Haswell, S. J., Bell, I. M., Joly, E., Fallatah, A., Neal, C., Williams, R. J., Gozzard, E., & Newman, J. R. (2012). Hydrology and Earth System Sciences Hydrochemical processes in lowland rivers: insights from in situ, high-resolution monitoring. *Hydrol. Earth Syst. Sci*, *16*, 4323–4342. https://doi.org/10.5194/hess-16-4323-2012

Wear, S. L., Acuña, V., McDonald, R., & Font, C. (2021). Sewage pollution, declining ecosystem health, and cross-sector collaboration. *Biological Conservation*, *255*. https://doi.org/10.1016/J.BIOCON.2021.109010

Wear, S. L., & Thurber, R. V. (2015). Sewage pollution: Mitigation is key for coral reef stewardship. *Annals of the New York Academy of Sciences*, *1355*(1), 15–30. https://doi.org/10.1111/NYAS.12785

Wildeboer, D., Amirat, L., Price, R. G., & Abuknesha, R. A. (2010). Rapid detection of Escherichia coli in water using a hand-held fluorescence detector. *Water Research*, *44*(8), 2621–2628. https://doi.org/10.1016/J.WATRES.2010.01.020

Woodward, G., Gessner, M. O., Giller, P. S., Gulis, V., Hladyz, S., Lecerf, A., Malmqvist, B., McKie, B. G., Tiegs, S. D., Cariss, H., Dobson, M., Elosegi, A., Ferreira, V., Graça, M. A. S., Fleituch, T., Lacoursière, J. O., Nistorescu, M., Pozo, J., Risnoveanu, G., … Chauvet, E. (2012). Continental-scale effects of nutrient pollution on stream ecosystem functioning. *Science*, *336*(6087), 1438–1440. https://doi.org/10.1126/SCIENCE.1219534/SUPPL_FILE/WOODWARD_ET_AL_DATA_TABLES_S1_AND_S2-SCIENCE.XLSX

Wu, J., Pons, M. N., & Potier, O. (2006). Wastewater fingerprinting by UV-visible and synchronous fluorescence spectroscopy. *Water Science and Technology*, *53*(4–5), 449–456. https://doi.org/10.2166/WST.2006.149

Wu, S., Carvalho, P. N., Müller, J. A., Manoj, V. R., & Dong, R. (2016). Sanitation in constructed wetlands: A review on the removal of human pathogens and fecal indicators. *Science of the Total Environment*, *541*, 8–22. https://doi.org/10.1016/J.SCITOTENV.2015.09.047

Xie, Y., Liu, X., Wei, H., Chen, X., Gong, N., Ahmad, S., Lee, T., Ismail, S., & Ni, S. Q. (2022). Insight into impact of sewage discharge on microbial dynamics and pathogenicity in river ecosystem. *Scientific Reports 2022 12:1*, *12*(1), 1–12. https://doi.org/10.1038/s41598-022-09579-x

Xu, M., Wang, Z., Duan, X., & Pan, B. (2014). Effects of pollution on macroinvertebrates and water quality bio-assessment. *Hydrobiologia*, *729*(1), 247–259. https://doi.org/10.1007/S10750-013-1504-Y

Yamashita, Y., Jaffé, R., Maie, N., & Tanoue, E. (2008). Assessing the dynamics of dissolved organic matter (DOM) in coastal environments by excitation emission matrix fluorescence and parallel factor analysis (EEM-PARAFAC). *Limnology and Oceanography*, *53*(5), 1900–1908. https://doi.org/10.4319/LO.2008.53.5.1900

Yamashita, Y., & Tanoue, E. (2003). Chemical characterization of protein-like fluorophores in DOM in relation to aromatic amino acids. *Marine Chemistry*, *82*(3–4), 255–271. https://doi.org/10.1016/S0304-4203(03)00073-2

Yamashita, Y., & Tanoue, E. (2004). In situ production of chromophoric dissolved organic matter in coastal environments. *Geophysical Research Letters*, *31*(14). https://doi.org/10.1029/2004GL019734

Yaroshenko, I., Kirsanov, D., Marjanovic, M., Lieberzeit, P. A., Korostynska, O., Mason, A., Frau, I., & Legin, A. (2020). Real-Time Water Quality Monitoring with Chemical Sensors. *Sensors (Basel, Switzerland)*, *20*(12), 1–22. https://doi.org/10.3390/S20123432

Yin, H., Wang, Y., Yang, Y., Huang, J., & Xu, Z. (2020). Tryptophan-like fluorescence as a fingerprint of dry-weather misconnections into storm drainage system. *Environmental Sciences Europe*, *32*(1), 1–14. https://doi.org/10.1186/S12302-020-00336-3/FIGURES/7

Zhu, G., Bian, Y., Hursthouse, A. S., Peng Wan, ·, Katarzyna Szymanska, ·, Ma, J., Wang, · Xiaofeng, & Zhao, Z. (2017). Application of 3-D Fluorescence: Characterization of Natural Organic Matter in Natural Water and Water Purification Systems. *Journal of Fluorescence*, *27*, 2069–2094. https://doi.org/10.1007/s10895-017-2146-7

Appendix I

Perrin, E. M., Thorn, R. M. S., Sargeant, S. L., Attridge, J. W., & Reynolds, D. M. (2022). The in situ Production of Aquatic Fluorescent Organic Matter in a Simulated Freshwater Laboratory Model. *Frontiers in Microbiology*, *13*, 435. https://doi.org/10.3389/FMICB.2022.817976/BIBTEX

frontiers in Microbiology

ORIGINAL RESEARCH
published: 24 February 2022
doi: 10.3389/fmicb.2022.817976

The *in situ* Production of Aquatic Fluorescent Organic Matter in a Simulated Freshwater Laboratory Model

*Eva M. Perrin[1], Robin M. S. Thorn[1], Stephanie L. Sargeant[1], John W. Attridge[2] and Darren M. Reynolds[1]**

[1]*Centre for Research in Biosciences, University of the West of England, Bristol, United Kingdom,* [2]*Chelsea Technologies Ltd., East Molesey, United Kingdom*

Dissolved organic matter (DOM) is ubiquitous throughout aquatic systems. Fluorescence techniques can be used to characterize the fluorescing proportion of DOM, aquatic fluorescent organic matter (AFOM). AFOM is conventionally named in association with specific fluorescence "peaks," which fluoresce in similar optical regions as microbially-derived proteinaceous material (Peak T), and terrestrially-derived humic-like compounds (Peaks C/C+), with Peak T previously being investigated as a tool for bacterial enumeration within freshwaters. The impact of anthropogenic nutrient loading on the processing of DOM by microbial communities is largely unknown. Previous laboratory studies utilizing environmental freshwater have employed growth media with complex background fluorescence, or very high nutrient concentrations, preventing the investigation of AFOM production under a range of more representative nutrient concentrations within a matrix exhibiting very low background fluorescence. We describe a laboratory-based model with *Pseudomonas aeruginosa* that incorporates a low fluorescence growth matrix consisting of a simulated freshwater (SFW), representative of low-hardness freshwater systems allowing controlled nutrient conditions to be studied. The effects of microbial processing of DOM as a function of available nitrogen, phosphorous, and dissolved organic carbon (DOC) in the form of glucose were investigated over 48 h at highly resolved time increments. The model system demonstrates the production of a range of complex AFOM peaks in the presence and absence of DOC, revealing no linear relationship between cell numbers and any of the peaks for the bacterial species studied, with AFOM peaks increasing with microbial cell number, ranging from 55.2 quinine sulfate units (QSU) per 10^6 cells to 155 QSU per 10^6 cells ($p < 0.05$) for Peak T during the exponential growth phase of *P. aeruginosa* under high nutrient conditions with 5 mg L^{-1} DOC. Nutrient and DOC concentration was found to cause differential production of autochthonous- or allochthonous-like AFOM, with lower DOC concentrations resulting in higher Peak T production relative to Peaks C/C+ upon the addition of nutrients, and high DOC concentrations resulting in higher Peak C/C+ production relative to Peak T. Our results show the production of allochthonous-like AFOM from a simple and non-fluorescent carbon source, and provide uncertainty in the

OPEN ACCESS

Edited by:
Christian Lønborg, Aarhus University, Denmark

Reviewed by:
Birgit Koehler, Swedish University of Agricultural Sciences, Sweden
Marc Tedetti, UMR7294 Institut Méditerranéen d'océanographie (MIO), France

***Correspondence:**
Darren M. Reynolds
darren.reynolds@uwe.ac.uk

Specialty section:
This article was submitted to Aquatic Microbiology, a section of the journal Frontiers in Microbiology

Received: *18 November 2021*
Accepted: *31 January 2022*
Published: *24 February 2022*

Citation:
Perrin EM, Thorn RMS, Sargeant SL, Attridge JW and Reynolds DM (2022) The in situ Production of Aquatic Fluorescent Organic Matter in a Simulated Freshwater Laboratory Model. Front. Microbiol. 13:817976. doi: 10.3389/fmicb.2022.817976

use of Peak T as a reliable surrogate for specific bacterial enumeration, particularly in dynamic or nutrient-impacted environments, pointing toward the use of fluorescence as an indicator for microbial metabolism.

Keywords: dissolved organic matter, freshwater, microbial processing, nutrient loading, fluorescence

INTRODUCTION

Dissolved organic matter (DOM) is one of the largest reservoirs of carbon on the planet, representing a source of both fixed and bioavailable carbon that is ubiquitous throughout aquatic environments (Hedges, 1992; Cole et al., 2007; Trimmer et al., 2012). In freshwater systems, DOM is a largely heterogeneous mixture of organic compounds, the type and quantity of which is representative of surrounding catchment characteristics, as well as being influenced by processes such as photodegradation and *in situ* microbial processing. DOM is conventionally divided into two categories; allochthonous material, which represents carbon that has been transported into the fluvial system from surrounding terrestrial environments, is considered to represent complex, high molecular-weight humic and fulvic organic carbon, and autochthonous material represents carbon that has been generated within the fluvial system by microbial processes is regarded as simpler, proteinaceous, and lower molecular-weight in nature (McKnight et al., 2001; Leenheer and Croué, 2003; Baker and Spencer, 2004; Hudson et al., 2007).

A fraction of DOM in aquatic environments exhibits fluorescence properties, and this is known as aquatic fluorescent organic matter (AFOM). AFOM can be analyzed using fluorescence spectroscopy, providing a rapid and sensitive means of investigating the processing and transport of carbon in aquatic systems. AFOM is classified using specific peak nomenclature (Coble et al., 2014), based on the presence of observed fluorescence peaks which appear within optical regions associated with known organic compounds. AFOM associated with microbially-derived compounds is known as "autochthonous." Peaks within this region have been named Peaks T ($\lambda_{ex}/\lambda_{em}$ 275/340) and B ($\lambda_{ex}/\lambda_{em}$ 275/305), which fluoresce in the same optical regions as tryptophan and tyrosine, essential amino acids. This is also known as "protein-like" AFOM. AFOM associated with terrestrially-derived compounds is known as "allochthonous," and includes peaks known as Peak C ($\lambda_{ex}/\lambda_{em}$ 320–365/420–470), Peak C+ ($\lambda_{ex}/\lambda_{em}$ 385–420/470–505), and Peak M ($\lambda_{ex}/\lambda_{em}$ 290–310/370–420). Despite this binary classification, some peaks have been reported to occur as a result of both autochthonous and allochthonous processes, such as Peak M in marine environments (Milbrandt et al., 2010).

Much of the work on AFOM in freshwater systems has focused on utilizing Peak T fluorescence as a tool for microbial enumeration, derived from reported relationships between Peak T fluorescence intensities and primary productivity (Hudson et al., 2007, 2008) or microbial enumeration (Sorensen et al., 2015, 2018). Previous studies have sought to investigate the origins of AFOM and its relationship with microbial processing in marine systems (Yamashita and Tanoue, 2004; Yamashita et al., 2008; Shimotori et al., 2010; Kinsey et al., 2018) and, more recently, in surface waters such as lakes (Guillemette and del Giorgio, 2012; Berggren et al., 2020). These have suggested that AFOM in the humic-like optical region can be produced as a direct result of aquatic microbial activity. Recent studies (Fox et al., 2017, 2018) employing laboratory-based model systems to investigate the origin of freshwater AFOM produced by bacteria *in situ* have provided further evidence to support this. Furthermore, this work has suggested that Peak T fluorescence is associated with microbial metabolism and activity, and is not a reliable indicator for specific cell enumeration as has been previously reported.

Despite recent advances, there is still a dearth of knowledge surrounding the role played by freshwater microbes within *in situ* AFOM processing (Anderson et al., 2019). Inland freshwaters are known to play a disproportionately large role in global carbon cycling, despite covering less than 4% of the Earth's surface (Cole et al., 2007; Downing, 2008; Tranvik et al., 2009). Furthermore, the inherent complexity of microbial AFOM processing is compounded by anthropogenically-induced perturbations, particularly agricultural activities, which often lead to nutrient loading as a result of runoff from cultivated land surrounding a river catchment. Over recent decades, the availability of nutrients such as reactive nitrogen and phosphorus species has greatly increased in surface waters, with 38% of European freshwaters impacted by non-point source pollution such as agricultural land-use (Woodward et al., 2012; European Environment Agency, 2018). Recent field-based studies have observed increases in ecosystem respiration and ultimately carbon loss within surface waters as a result of nutrient loading (Kominoski et al., 2018; Manning et al., 2018). There is, however, a need to develop laboratory models to support these field-based studies. Previous approaches for characterizing microbial AFOM production within environmental water matrices (Guillemette and del Giorgio, 2012; Fox et al., 2018) are limited by complex background fluorescence signatures, or the utilization of high-nutrient growth media which do not represent nutrient concentrations observed in the field (Fox et al., 2017, 2018). Therefore, existing models are of limited use for investigating the effects of controlled nutrient loading on microbial AFOM production.

The work undertaken here seeks to develop and utilize a laboratory-based model for the investigation of nutrient loading on *in situ* bacterial AFOM processing within fresh water systems. A simulated freshwater (SFW) matrix, adapted from Smith et al. (2002), was developed, standardized, and used throughout the study. In contrast to previous laboratory-based studies (Fox et al., 2017, 2018, 2021), the SFW matrices contains concentrations of ionic constituents found within oligotrophic fresh waters (Smith et al., 2002), i.e., contains a low baseline concentration of nitrate, phosphate, and dissolved organic carbon (DOC) in the form of glucose. Importantly, the developed SFW exhibited low background

TABLE 1 | Anion and cation concentrations within the SFW, adapted from Smith et al. (2002).

Chemical constituents	Final ion concentrations (mg L^{-1})	
	Anion	Cation
$MgCl_2$	1.458	4.254
$CaCl_2$	3.209	5.672
$Ca(NO_3)_2$	0.601	1.860
$CaCO_3$	6.814	10.201
Na_2SO_4	5.288	11.046
$KHCO_3$	0.977	1.525
$NaHCO_3$	0.458	1.220

TABLE 2 | Nitrate, phosphate, and dissolved organic carbon (DOC) experimental conditions and their associated nomenclature.

	DOC concentrations		
	0 mg L^{-1} DOC	5 mg L^{-1} DOC	800 mg L^{-1} DOC
0 mg L^{-1} PO_4^{3-} 0.3 mg L^{-1} NO_3^-	*SFW0* Low nutrient, no DOC	*SFW2* Low nutrient, limited DOC	*SFW4* Low nutrient, excess DOC
0.1 mg L^{-1} PO_4^{3-} 50 mg L^{-1} NO_3^-	*SFW1* High nutrient, no DOC	*SFW3* High nutrient, limited DOC	*SFW5* High nutrient, excess DOC

Six conditions of varying nutrients were investigated, with both oligotrophic and high-nutrient conditions observed with three different DOC conditions for each.

fluorescence, unlike many studies which utilize environmental freshwaters (Fox et al., 2018; Kominoski et al., 2018; Berggren et al., 2020). The main aim of this study was to observe the origin of AFOM *via* bacterial production and processing as a function of nutrient availability using a single species freshwater model system.

MATERIALS AND METHODS

Simulated Freshwater Media

Simulated freshwater was developed using an adapted method from Smith et al. (2002) and is detailed in **Table 1**. The SFW contains low concentrations of nitrate and phosphate (0 mg L^{-1} $P0_4^{3-}$ and 0.3 mg L^{-1} NO_3^-) and no addition of glucose-DOC. By starting with a baseline low concentration of these nutrients in the initial SFW, subsequent higher quantities of nitrates, phosphates, and DOC can be introduced in their desired concentration. This facilitates the investigation of both low and high nutrient conditions, unlike previous studies which have used growth media with very high baseline nutrient concentrations. All SFW prepared using this method was filter-sterilized using a 0.2 µm cellulose filter (Sartorius Stedim Biotech, Germany) prior to use and all glassware sterilized by autoclaving at 121°C for 15 min. **Table 1** outlines the concentrations of all ions present within the SFW. Growth curve experimental conditions are detailed in the section "Bacterial Growth Curve Experimental Conditions."

Nitrate, Phosphate, and DOC Conditions

Concentrations of nitrate (NO_3^-) and phosphate (PO_4^{3-}) were added to the SFW matrix at concentrations of 50 and 0.1 mg L^{-1}, respectively. Stock solutions of nitrate and phosphate were prepared by the dissolution of sodium nitrate ($NaNO_3^-$) and dipotassium hydrogen orthophosphate ($KH_2PO_4^-$), respectively in deionized water and added to the SFW prior to bacterial inoculation. The chosen concentrations for nitrate and phosphate were informed by the EU Nitrates Directive and its constituting Water Framework Directive (Directive 2000/60/EC of the European Parliament and of the Council of 23 October 2000 establishing a framework for community action in the field of water policy, 2000), whereby these concentrations are deemed to be high and of concern.

Dissolved organic carbon in the form of glucose was dosed into the model system to investigate bacterial production of AFOM from a simple, bioavailable carbon source. SFW solutions containing 0, 5, and 800 mg L^{-1} of DOC were prepared and added to the SFW prior to bacterial inoculation. A concentration of 5 mg L^{-1} of DOC represents DOC availability in many fluvial systems studied previously (Gao et al., 2017; Noacco et al., 2017) where carbon transport in rivers has been modeled. High, or excess, DOC conditions (800 mg L^{-1} glucose) were also studied. DOC levels this high, although not representative of natural systems, ensured that DOC was not a limiting factor when investigating bacterial AFOM production. This is comparable to previous laboratory-based studies that have used high-nutrient growth media with DOC concentrations in excess (Fox et al., 2017). In addition, 0 mg L^{-1} DOC was used to investigate bacterial AFOM production under conditions with no additional DOC source, therefore a total of three DOC conditions were investigated. The six experimental conditions investigated are outlined in **Table 2**, with the associated nomenclature used to refer to these conditions during the study.

Inoculum Preparation

Pseudomonas aeruginosa (NCIMB 8295) was selected for study within the model system due to the ubiquitous nature of this species in the freshwater environment (Sigee, 2004; Elliott et al., 2006; Fox et al., 2017). For culture preparation, 10 ml of nutrient broth was inoculated with a single colony derived from a fresh plate culture. Cultures were incubated for 18–24 h at 37°C, shaking at 120 rotations per minute (RPM). Prior to inoculation, bacterial cells were washed three times in SFW by centrifuging at 13,000 ×× *g* for 3 min to form a pellet. The supernatant was then removed and the pellet resuspended in sterile SFW to remove any residual nutrients. Bacterial cell densities (CFU ml^{-1}) were standardized using optical density measurements at 620 nm.

Bacterial Growth Curve Experimental Conditions

Using a glass conical flask (500 ml), sterile SFW (250 ml) was inoculated with *P. aeruginosa* to a density of 10^5 CFU ml^{-1}, this bacterial density has been previously reported to be representative of freshwater systems (Sigee, 2004). Flasks were incubated at 37°C shaking at 120 RPM under ambient light conditions, and aliquots (10 ml) were extracted for analysis

at hourly time points for the first 8 h, and then at 12, 16, 20, 24, 36, and 48 h thereafter. The experimental duration of 48 h at 37°C enabled the observation of AFOM production over three phases of bacterial growth (lag, exponential, and stationary). While it is acknowledged that this temperature does not represent environmental conditions, this 37°C was chosen as it has been found to be the optimum growth temperature for *P. aeruginosa* (Tsuji et al., 1982). As such, this facilitated initiating the bacterial AFOM production with this model system, allowing the investigation of a range of metabolic states over a short period of time. Flasks were vented to maintain gas exchange with the environment, thus the experiment was conducted under aerobic conditions. Sample aliquots were serially diluted in sterile phosphate-buffered saline (Oxoid Ltd., United Kingdom) and plated onto nutrient agar *via* spiral plating (Don Whitley Scientific Ltd., England). Plates were incubated at 37°C for 24 h and viable colonies counted to calculate the CFU ml^{-1}. Each experimental condition was repeated on three independent occasions (except for SFW5, which was repeated on seven independent occasions due to high variability) using separate overnight bacterial cultures. All fluorescence and bacterial enumeration measurements were performed in triplicate at each time point.

Fluorescence Measurements

Inoculated SFW (3 ml) was collected for fluorescence excitation-emission matrices (EEMs) at each time point using an Aqualog® (Horiba Ltd., Japan). The following scan parameters were employed: excitation wavelengths from 200 to 600 nm in 1 nm steps, and emission wavelengths from 247.88 to 829.85 nm in 1.16 nm steps and an integration time of 0.5 s. A 3 ml microquartz cuvette with a 10 mm pathlength was used throughout. Spectra were blank-subtracted using the fluorescent spectra of a fresh SFW sample. EEMs of filter-sterilized SFW were collected to determine whether any background fluorescence was present prior to inoculation of the experiment. In addition, control experiments were undertaken alongside this study with sterile SFW under all six nutrient conditions. From this, the SFW media were found to be non-fluorescent, with <5 QSU present after 48 h under any experimental conditions. Inoculated SFW at 0 h of the experiment showed fluorescence intensities of 2.2 QSU (±2) for Peak T, 0.9 QSU (±0.8) for Peak C, and 0.6 QSU (±0.5) for Peak C+.

Fluorescence Data Analysis

Raw fluorescence data were processed through a custom Python™ script (Python Software Foundation) to normalize data to QSU and generate EEM maps. The data window was cropped to λ_{ex} 240–490 nm and λ_{em} 250–500 nm, to discount fluorescence data within the deep-UV region which is heavily influenced by instrument noise. This allows for the analysis of data within the UV–visible area, the optical region associated with FDOM peaks of interest. PARAFAC was attempted within this study, however, the simple nature of the growth matrix and single-species biological culture limited its application. As such, no robust model (CORCONDIA >90%) was identified which could adequately explain the dataset. This is likely due to the dominance of the main fluorescence peaks, Peaks T and C+. Instead, peak-picking, an established method (Asmala et al., 2016) used for identifying specific fluorescence peaks, was undertaken. For this, cross-sections of emission values at a set excitation wavelength were obtained using the custom Python™ script, and the mean fluorescence intensity of the peaks was calculated. Peak regions were: Peak T ($\lambda_{ex}/\lambda_{em}$ 275/340), Peak C ($\lambda_{ex}/\lambda_{em}$ 340/420–470), and Peak C+ ($\lambda_{ex}/\lambda_{em}$ 400/470–505). Collected absorbance and transmittance data were used to correct spectra for inner-filter effects (Aqualog®) for both excitation and emission wavelengths, and first and second order Rayleigh Scattering was masked. All fluorescence data are reported in quinine sulfate units (QSU), acquired by normalizing data to the fluorescence generated from 1 µg L^{-1} quinine sulfate at λ_{ex} = 347.5 nm and λ_{em} = 450 nm (Kramer and Herndl, 2004; Mostofa et al., 2013). This allows for standardized quantitative analysis that is comparable within and between studies.

Statistical Analysis

Statistical analysis of all data was conducted using GraphPad Prism version 9.2.0 for Windows (GraphPad Software, San Diego, CA, United States). A time-series analysis of all time points was undertaken using mixed-effects modeling whereby the significance of the fixed effect was assessed using ANOVA ($p < 0.05$ regarded as significant). This enabled statistical comparison of fluorescence intensity between peaks and between nutrient and DOC conditions over time.

RESULTS

AFOM Processing Over 48 h

By using glucose as the sole carbon source, it was possible to investigate the bacterial production of AFOM over a 48 h period. At time zero, all inoculated SFW cultures under all conditions (SFW0-5, see **Table 2**) exhibited minimal fluorescence properties (< 5 QSU). Complex fluorescence signatures were produced under all six experimental conditions (SFW0–5), where the dominant fluorescence Peaks T, C, and C+ were present at the end of the 48 h incubation period (see **Figure 1**; **Table 3**). Notably, the production of these AFOM peaks was observed within both high and low nutrient conditions (SFW0 and SFW1) containing no glucose-DOC, albeit at low fluorescence intensities (< 50 QSU) as shown in **Figures 1A, 2A** and **Table 4**.

Viable bacterial cell counts of extracted samples show that the exponential phase of bacterial growth consistently occurred between 6 and 12 h under all experimental conditions as shown in **Figure 2**. This corresponds to observed increases in the intensities of all AFOM peaks under all conditions (SFW0–5). In all conditions, except SFW2 (low nutrients, limited DOC), bacterial cell replication continued until 16 h as can be deduced from **Figure 2C**. Upon inoculation of all samples, at 0 h, no significant difference was observed in viable counts (CFU ml^{-1}) providing confidence that inoculum density was stable between the different experimental conditions. Between 0 and 6 h, a lag phase was observed

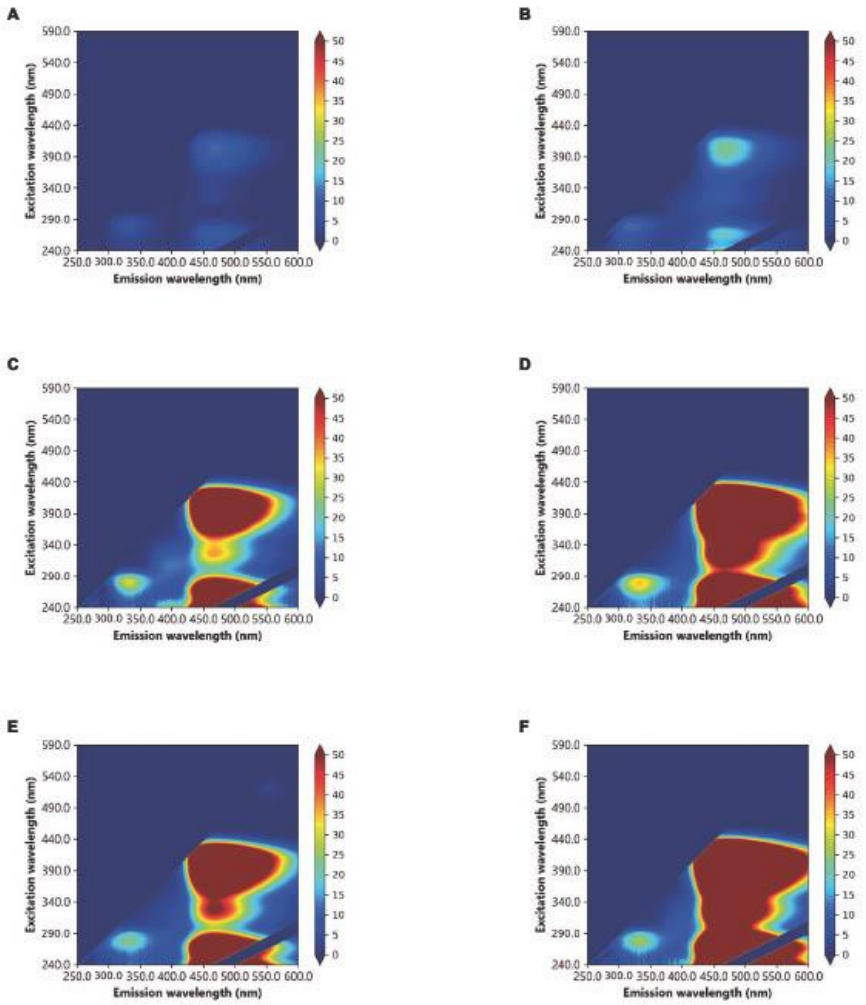

FIGURE 1 | Excitation-emission matrices (EEMs) of *Pseudomonas aeruginosa* monoculture in simulated freshwater (SFW) after a 48 h incubation period, under the following experimental conditions: **(A)** oligotrophic, no carbon (SFW0), **(B)** high nutrient, no carbon (SFW1), **(C)** oligotrophic, limited carbon (SFW2), **(D)** high nutrient, limited carbon (SFW3), **(E)** oligotrophic, excess carbon (SFW4), and **(F)** high nutrient, excess carbon (SFW5). Color bars are displayed in quinine sulfate units (QSU), where 1 QSU = 1 μg L^{-1} quinine sulfate solution.

during which viable cell counts remained within the range of 5 Log_{10} CFU ml^{-1} for all conditions. However, during exponential growth, cell numbers increased by between 1 and 2 Log, ranging between $1–7 \times 10^5$ CFU ml^{-1} at the beginning of the growth phase, and $5 \times 10^6–5 \times 10^7$ CFU ml^{-1} at the end of the growth phase. During this time, the growth rate of the bacterial communities can be seen to diverge as a function of nutrient and DOC conditions. Within high nutrient, excess carbon conditions, (SFW5) significantly higher CFU ml^{-1} values (6.7×10^5 CFU ml^{-1}) were observed after 5 h ($p < 0.01$) when compared to all other experimental conditions (SFW0–4). From 8 h of incubation, both the low and high nutrient conditions with no DOC (SFW0–1) had significantly lower cell counts ($p < 0.05$) than all other conditions (SFW2–5).

TABLE 3 | Fluorescence intensities at 48 h for all peaks (T, C, and C+) under all conditions (SFW0–5).

	No DOC		5 mg L^{-1} DOC		800 mg L^{-1} DOC	
	Low nutrient	High nutrient	Low nutrient	High nutrient	Low nutrient	High nutrient
	QSU (48 h)	QSU (48 h)	QSU (48 h)	QSU (48 h)	QSU (48 h)	QSU (48 h)
T	6.5 (±3.7)	11.3 (±2.4)	56 (±4.1)	51.8 (±1.1)	45.5 (±1.3)	58 (±14.6)
C	14.8 (±0.13)	21.5 (±10.2)	81.5 (±66.4)	162.7 (±36)	449 (±164)	332.6 (±364)
C+	6.2 (±1.9)	26.6 (±13.3)	599.7 (±530.3)	1215.8 (±193.8)	592 (±212.2)	612.7 (±303.3)

Fluorescence intensities are reported in quinine sulfate units (QSU). Variation is also provided in the form of SD (denoted by ±).

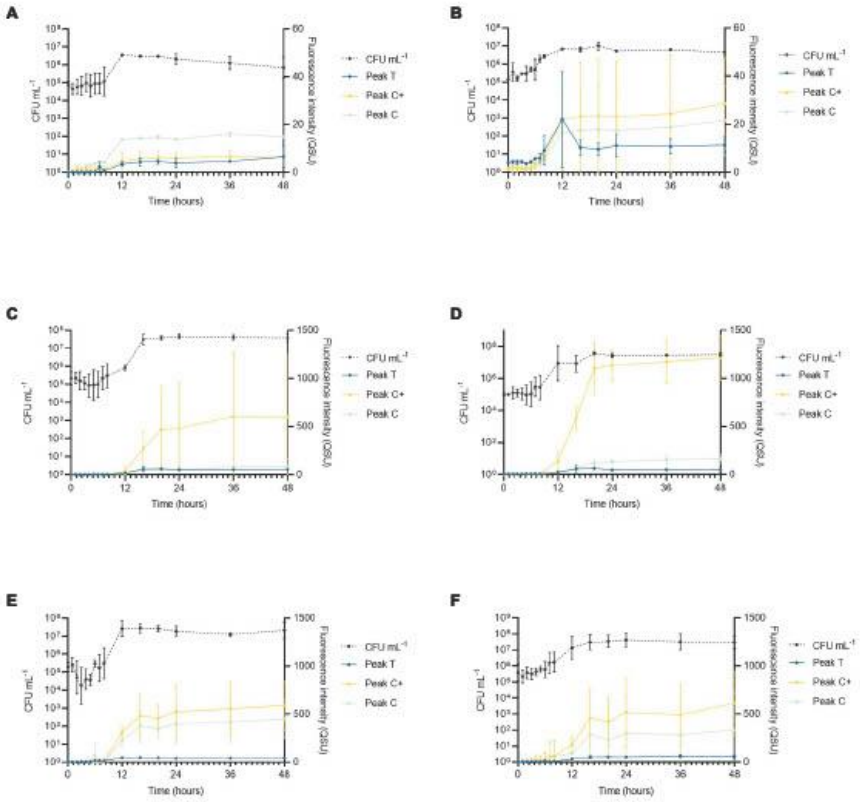

FIGURE 2 | *Pseudomonas aeruginosa* growth curve data showing cell numbers (CFU ml^{-1}) relative to fluorescence intensity over 48 h for Peaks T, C, and C+ for the following experimental conditions ($n = 3$ biological and technical replicates): **(A)** low nutrient, no DOC (SFW0), **(B)** high nutrient, no DOC (SFW1), **(C)** low nutrient, limited DOC (SFW2), **(D)** high nutrient, limited DOC (SFW3), **(E)** low nutrient, excess DOC (SFW4), and **(F)** high nutrient, excess DOC (SFW5).

In addition, significant differences in cell numbers were observed between limited DOC (SFW2–3) and excess DOC (SFW4–5) conditions ($p < 0.05$); while differences in cell number were found to be significantly affected by the provision of DOC in the system, the availability of nitrate and phosphate was not found to result in significantly higher cell numbers ($p > 0.05$), suggesting that the community is not limited by nitrate or phosphate within this experimental system.

TABLE 4 | Fluorescence intensities showing total fluorescence (f_{total}) normalized per 10^6CFU.

	No DOC				5 mgL^{-1} DOC				800 mgL^{-1} DOC			
	Low nutrient		High nutrient		Low nutrient		High nutrient		Low nutrient		High nutrient	
	$f_{QSU/CFU}$	%	$f_{QSU/CFU}$	%	$f_{QSU/CFU}$	%	$f_{QSU/CFU}$	%	$f_{QSU/CFU}$	%	$f_{QSU/CFU}$	%
T	50.2 (±34.4)	8	152.6 (±14.7)	49	391.8 (±507.5)	40	647.7 (±480.1)	47	1346.3 (±170.8)	51	229.7 (±211.3)	10
C	128.6 (±52.5)	20	66.8 (±37.8)	22	346.5 (±402.0)	36	251.8 (±145.2)	19	693.2 (±22.7)	26	929.6 (±2052.8)	42
C+	462.2 (±261.2)	72	88.1 (±48.5)	28	237.0 (±212.0)	24	465.9 (±271.7)	34	623.2 (±313.9)	23	1069.3 (±2300.6)	48
f_{total}	641.1		307.4		975.3		1365.3		2662.8		2228.7	

The f_{total} is defined as the sum of Peaks T, C, and C+ at each time point, with all time points over the experimental duration added together for each experimental condition, and is reported in $f_{QSU/CFU}$. The relative contribution of individual peaks to the f_{tot} is also shown in the form of a percentage value.

The fluorescence intensities of all peaks under all conditions (SFW0–5) vary over the experimental time period of 48 h. The fluorescence peaks mimic the lag phase for 0–6 h before increasing in concert with the exponential growth phase of the *P. aeruginosa* community studied. Peak T fluorescence exhibited the largest increase in intensity between 6 and 16 h. For low nutrient conditions with 0, limited and excess DOC (SFW0, SFW2, and SFW4), increases of 778% for Peak T, 65% for Peak C, and 22,382% for Peak C+ were observed. For high nutrient conditions, under the same DOC conditions (SFW 1, SFW3, and SFW5) increases of 756% for Peak T, 216% for Peak C, and 682% for Peak C+ were observed. After 16 h, the observed fluorescence intensities plateaued after increases of 52, 10, and 2% for conditions with low nutrients and excess DOC conditions (SFW0, 2, and 4) for Peaks T, C, and C+. For high nutrient conditions (SFW1, 3, and 5), the observed increases were 12, 0, and 20% for Peaks T, C, and C+, respectively.

In a time-series analysis of all fluorescence peaks over the entire experimental period (0–48 h), it was found that there was a significant change in fluorescence intensity over time for the majority of peaks investigated across all of the experimental conditions. For low nutrient, no DOC conditions (SFW0), Peaks T and C were found to significantly change over the experimental duration ($p < 0.01$). However, Peak C+ was not seen to significantly change over the experiment ($p > 0.05$). For high nutrient, no DOC conditions (SFW1), no peaks were found to change significantly over the experimental period ($p > 0.05$). For low nutrient conditions with limited DOC (SFW2), Peaks T and C were found to change significantly ($p < 0.05$); however, Peak C+ was not ($p > 0.05$). All other conditions (SFW3-5) were found to display significant changes over the experimental duration ($p < 0.05$).

The relationship between individual fluorescence peaks varies significantly throughout the experimental duration. Under high nutrient conditions and zero DOC (SFW1), low nutrient conditions and limited DOC (SFW2), and high nutrient conditions and excess DOC (SFW5), there are no significant differences ($p > 0.05$) observed between Peaks C and C+, suggesting that the production of this AFOM is interrelated. In contrast, for low nutrient, zero DOC (SFW0), Peak C fluorescence intensity is seen to decrease by 1.2 QSU (± 0.8) over the final 24 h (late stationary phase), while Peak C+ decreases by only 0.4 QSU (± 0.3), resulting in a divergence between these two peaks at the end of the experimental period. This was found to be statistically significant ($p < 0.05$). For high nutrient conditions, limited DOC (SFW3), the relationship between Peaks C and C+ is statistically different, where the greatest increase in Peak C+ is observed between 36 and 48 h, increasing by 42.3 QSU (± 9.4) while Peak C increases by 7.8 QSU (± 5.3; $p < 0.05$). For all other conditions (SFW3 and SFW4), there remains no significant difference between these peaks over the experimental duration. The relationship between Peak T and C/C+ also varies, with only low nutrient, zero DOC (SFW0) displaying a significant difference between Peaks T and C throughout the experimental period ($p < 0.05$) for all but the first 2 h. High nutrient, limited DOC (SFW3), display the

most significant differences between all peaks, where the difference is over 1,000 QSU between Peak C+ and Peaks T and C ($p < 0.05$; **Figure 2**). For Peaks T and C+, this significant difference is present throughout the experimental period ($p < 0.05$). For high nutrient, excess DOC (SFW5), the variation observed between the three biological replicates was found to be substantially higher than was seen under all other conditions. For Peaks C and C+, there was found to be a mean of 332.6 and 612.7 QSU, and a SD of 364 and 303.3, respectively, at 48 h. Comparatively, there is less variability between biological replicates for low nutrient, no DOC conditions (SFW0), with means of 14.8 QSU for Peak C and 6.2 QSU for Peak C+, and SDs of 0.1 for Peak C and 1.9 for Peak C+. Observed variability was determined to be a result of inherent biological variation which is discussed further in "Discussion." Lower SD was observed in conditions that comprised of lower nutrient conditions.

Effects of DOC and Nutrients (NO_3^- and PO_4^{3-}) on AFOM Production and Processing

To compare directly the effect of contrasting nutrient regimes on AFOM processing, QSU fluorescence data were normalized to bacterial enumeration to account for the changing density of viable cells during the growth curve period (**Figure 3**). For this, QSU data were enumeration-corrected to every 10^6 CFU and the data logged for all conditions for comparison

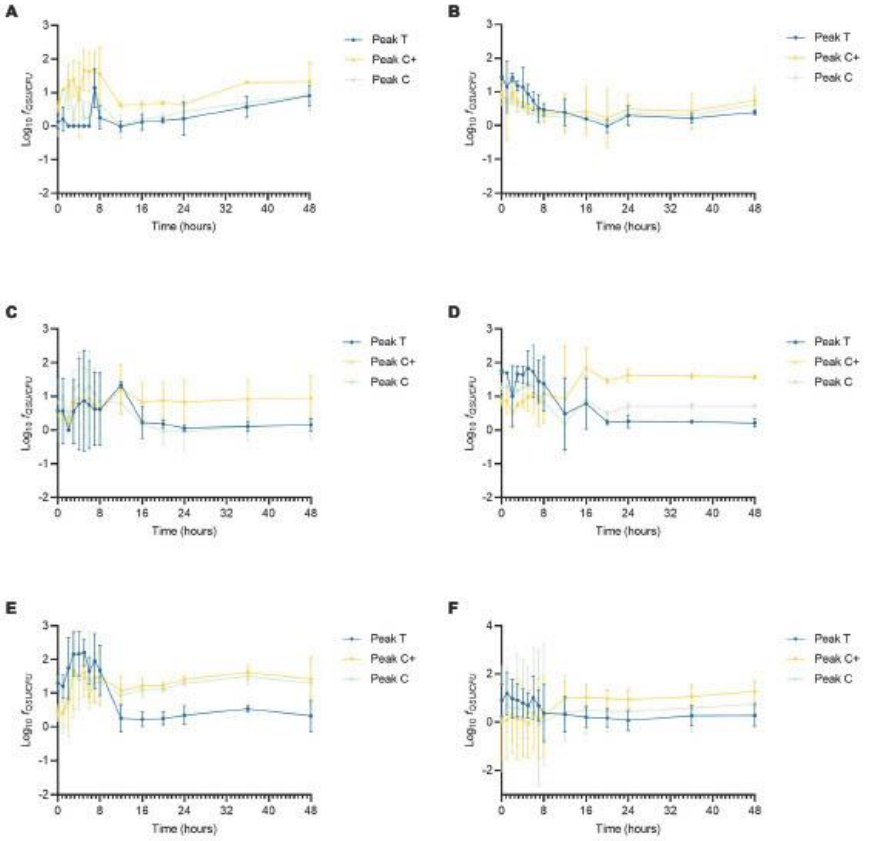

FIGURE 3 | Peaks T, C, and C+ fluorescence data corrected for enumeration, displaying Log_{10} QSU per 10^6 CFU ($f_{QSU/CFU}$) for *Pseudomonas aeruginosa* growth curve data under the following experimental conditions ($n = 3$ biological and technical replicates): **(A)** low nutrient, no DOC (SFW0), **(B)** high nutrient, no DOC (SFW1), **(C)** low nutrient, limited DOC (SFW2), **(D)** high nutrient, limited DOC (SFW3), **(E)** low nutrient, excess DOC (SFW4), and **(F)** high nutrient, excess DOC (SFW5).

(expressed as $f_{QSU/CFU}$). For the experimental time period, the relationship between viable cell numbers and Peaks T, C, and C+ fluorescence is not linear for any of the conditions studied (**Figure 3**). Large fluctuations occurring in per-cell fluorescence ($f_{QSU/CFU}$) over the duration of the experiment were observed. Under all experimental conditions, the period of greatest variation in $f_{QSU/CFU}$ occurs between 0 and 12 h. An increase in per cell fluorescence can initially be seen under all conditions, with maximum fluorescence intensities being reached during the first 8 h of the experiment. This coincides with the beginning of the bacterial exponential growth phase as seen in **Figure 2**, which occurs between 6 and 12 h, during which the bacterial growth rate is at its highest. In high nutrient conditions with limited DOC (SFW 3), Peak C+ reaches its maximum $f_{QSU/CFU}$ at 16 h, and in high nutrient conditions with excess DOC (SFW5), Peak C+ reaches its maximum $f_{QSU/CFU}$ at 12 h. A sharp decrease in $f_{QSU/CFU}$ is then observed until 12 h in conditions containing zero and excess DOC (SFW0, SFW1, SFW4, and SFW5, **Figures 3A,B,E,F**) for all peaks except for Peak C in SFW5. Under limited carbon conditions (SFW2 and SFW3, **Figures 3C,D**), $f_{QSU/CFU}$ continues to decrease until 16 and 24 h for low and high nutrient conditions, respectively. While the $f_{QSU/CFU}$ remains low for the remaining duration of the experimental period, all conditions (with the exception of SFW3), experience a gradual increase during the final 24 h of the experiment coinciding with the late stationary phase of the bacterial community.

$f_{QSU/CFU}$ is influenced by the availability of nutrients and DOC in the system. **Table 4** shows the influence of the experimental conditions on the ratio of Peaks T, C, and C+. The relative contribution of each fluorescence peak to the total fluorescence observed as a function of nutrients and DOC is shown. In conditions with zero and limited DOC, higher nutrient availability was found to result in more Peak T production, with a higher ratio of Peak T relative to Peaks C and C+. Under excess DOC conditions, however, increased nutrient availability was found to reduce the production of Peak T relative to Peaks C and C+, with the latter peaks accounting for a larger proportion of the total fluorescence. For experimental conditions containing zero DOC, the maximum $f_{QSU/CFU}$ for Peak T in high nutrient conditions was substantially higher (102.3, ±20.5) in comparison to low nutrient conditions. When DOC is limited, the $f_{QSU/CFU}$ for Peak T was elevated by 255.9 (±45.7) in low nutrient conditions compared to higher nutrient conditions. Interestingly, for conditions containing excess DOC, the $f_{QSU/CFU}$ for Peak T associated with high nutrients was significantly less (1116.6 ± 257.8) when compared to low nutrient conditions ($p < 0.01$). For Peaks C and C+, conditions with no DOC show that the addition of nutrients results in a decrease in fluorescence intensity of 61.8 (± 36.7) $f_{QSU/CFU}$ for Peak C and 374.2 (±196.6) $f_{QSU/CFU}$ for Peak C+. However, for high nutrients and excess DOC conditions, higher fluorescence intensities for Peak C are observed in the high nutrient conditions. This equates to an additional $f_{QSU/CFU}$ of 228.8 (±168.2).

DISCUSSION

AFOM Processing Over 48 h

The data presented here demonstrate that under all conditions, *P. aeruginosa* is capable of producing a complex range of AFOM including Peaks T, C, and C+, in a SFW model system. This includes the production of materials that fluoresce in both the autochthonous (protein-like) and allochthonous (humic-like) optical regions. Furthermore, material that has conventionally been assigned as autochthonous and allochthonous have been produced within this biological model in low and available DOC conditions. The production of this material relative to the bacterial cell numbers in the system was shown to vary over time, commensurate with the stage of biological growth occurring in the community.

It has been previously shown that bacterial communities are capable of producing semi-labile humic-like material from *in situ* incubation experiments within marine systems (Koch et al., 2014), consistent with the theory of the microbial carbon pump (Jiao et al., 2011). This has been characterized, using molecular techniques such as ultra-high-resolution mass spectrometry, as consisting of higher molecular-weight material generated from biologically labile substrates such as glucose (Koch et al., 2014). More recently, model freshwater studies have shown the production of optically active compounds that are fluorescent in the high molecular-weight, humic-like region using high-carbon, and high-nutrient microbiological growth media (Fox et al., 2017, 2018). In support of this study, the data presented here clearly demonstrate that *P. aeruginosa* is capable of producing AFOM peaks commonly considered to be allochthonous in nature, from a low-nutrient base media containing no additional nitrate, phosphate, or DOC. This suggests that while the capacity of bacteria to produce complex AFOM *in situ* is enhanced by the availability of a labile, low molecular weight carbon source (glucose), and an abundance of nutrients, they are also capable of utilizing very minimal concentrations of essential nutrients to demineralize and/or utilize carbon derived from the microbial community to produce fluorescing material. It is notable that conditions containing no introduced glucose-DOC still produced substantial fluorescence signatures over the experimental period (that is, 11.3, 21.5, and 28.6 QSU for Peaks T, C, and C+ in high nutrient, no DOC conditions at 48 h) which, while lower than the 58, 332.6 and 612.7 QSU for Peaks T, C, and C+ seen in high nutrient, excess DOC conditions, still represents a significant increase in fluorescence over the experimental period. It is likely that this occurred as a result of DOC delivered into the system from the microbial inoculum in the form of bacterial biomass which was utilized by the community as an organic substrate to generate fluorescing compounds. The introduction of bioavailable DOC from the microbial community may have occurred as a result of a number of factors; for example, cell death and subsequent cell lysis, or the export of compounds such as iron-scavenging siderophores into the system.

Data presented in **Figure 3** clearly demonstrate that the relationship between AFOM peaks and cell density is not correlated for any conditions within this model system. The intensity of the AFOM produced per bacterial cell varies both throughout the experimental period and between different conditions of nutrients and carbon. By observing these dynamics over time (at hourly intervals between 0 and 8 h) variations in $f_{QSU/CFU}$ are observed between all experimental conditions studied. Peak T was observed in all conditions and always displays an increase in fluorescence intensity between 8 and 16 h. This suggests that while DOC and nutrient availability heavily influence the maximum intensity of the fluorescence peaks produced, ultimately it does not affect the inevitable pattern of AFOM production over time. There are large fluctuations observed in $f_{QSU/CFU}$ during the first 12 h period of all experiments, with Peak T reaching its maximum $f_{QSU/CFU}$ between 0 and 7 h in all conditions, before sharply decreasing thereafter. The sharp increase in maximum $f_{QSU/CFU}$ during the first several hours of the experiment suggests that an increase in Peak T fluorescence intensity may represent a precursor to the start of the exponential growth phase, indicating the upregulated metabolic state the bacterial community is undergoing prior to cell replication. This variable relationship between $f_{QSU/CFU}$ of Peak T, and the increase seen in the $f_{QSU/CFU}$ prior to a period of rapid cell multiplication, strongly supports the use of Peak T as a marker for an active bacterial population under model conditions, as has been evidenced in recent literature (Fox et al., 2017, 2018). As such, this model highlights the complexity of the relationship between bacterial activity and observed fluorescence, underscoring the fact that while Peak T presents a useful tool for monitoring microbial presence in surface waters, there may be challenges associated with using this technique as a direct enumerator for bacterial cells as has been previously reported (Sorensen et al., 2015, 2018), particularly within dynamic systems which are heavily influenced by nutrient influxes. It should be noted that the viable count method used to enumerate bacterial cells in this study does not account for every cell present within the system, for example viable but non-culturable cells. Therefore, while methodological consistency ensures relative accuracy within the study, some of the cells present within that are not represented within the bacterial cell number data, may still be contributing to the observed fluorescence signature.

Peak C/C+ fluorescence also exhibits a non-linear relationship with bacterial cell density over the duration of the experimental period. Following the initial fluctuation in $f_{QSU/CFU}$ between 0 and 12–16 h, the $f_{SU/CFU}$ can be seen to increase, gradually, for the duration of the experiment for all conditions except for high nutrient and limited DOC. This could possibly be caused by the persistence of compounds that comprise Peak C/C+ FOM within the system (i.e., are not acted upon by the bacterial population). This is supported by previous literature which demonstrates the microbial production of less labile, higher molecular weight material (known to fluoresce in the Peak C/C+ region) albeit in the marine environment, from a simple glucose carbon substrate, which exhibited persistence for up to 2 years (Kinsey et al., 2018). Our data shows the *in situ* production of Peaks C and C+ within a freshwater matrix, and their subsequent accumulation and persistence within the system throughout the experimental duration of 48 h. Material that fluoresces in this region has conventionally been associated with allochthonous material that is transported into surface waters from the surrounding catchment, rather than as a result of the direct *in situ* production by microorganisms. While the *in situ* production of this material has previously been seen in marine environments, to our knowledge, our study is the first to show this phenomenon in a controlled laboratory environment using a representative SFW matrix. Further work is required to determine the relative recalcitrance of the presumed higher molecular weight FOM that is produced, by monitoring the fluorescence in this region over longer periods of time and in the presence of a more diverse microbial community. Recent literature has suggested that the origin of Peak C+ is partly derived from extracellular microbial products (Sorensen et al., 2020; Fox et al., 2021) However, to date, the overwhelming consensus is that Peaks C and C+ in freshwater environments are associated with material that is allochthonous in origin (Coble et al., 2014).

Effects of DOC and Nutrients (NO_3^- and PO_4^{3-}) on AFOM Production and Processing

The concentration of DOC, nitrate, and phosphate was found to have an impact on the production and processing of AFOM by the bacterial community within the SFW models studied here. The data presented in **Table 4** show that higher concentrations of DOC resulted in higher maximum $f_{CFU/QSU}$ values (sum of Peaks T, C, and C+). For all low nutrient conditions, the sum of the maximum $f_{QSU/CFU}$ is higher with increasing DOC conditions. Similarly, for high nutrient conditions, incremental increases of the maximum $f_{CFU/QSU}$ are observed. This shows that with higher DOC availability, bacteria are capable of producing increased quantities of AFOM per bacterial cell. This suggests that carbon availability represents a limiting factor to AFOM production within the model system studied. This further supports the notion that AFOM observed in the natural environment will be a direct consequence of the activity of the bacterial cells present and the quantity and availability of a carbon substrate from which to produce AFOM.

While increased DOC availability results in overall increases to the maximum $f_{QSU/CFU}$, there are substantial differences in the relative contribution of each of the studied peaks to the f_{total}. Moreover, the DOC concentration appears to have an influence on the effect of nutrient additions on AFOM production. In experimental conditions containing no added DOC and 5 mg L^{-1} DOC, the addition of nutrients results in an increase in Peak T fluorescence and a decrease in Peaks C and C+. However, in high nutrient and excess DOC conditions, there is a substantial decrease in Peak T fluorescence, and an increase in the production of Peaks C and C+, in comparison to the observed fluorescence exhibited in low nutrient, excess DOC conditions. This suggests that when the availability of carbon substrate in the system is a limiting factor, the production of

Peak T takes precedent within the system. Peak T is considered to represent intracellular structural and functional compounds such as amino acids, which are essential for cell growth and replication (Coble, 2007) and therefore may take priority when carbon is limited, or in high demand, to the bacteria within the system. However, when carbon is available in excess, additional nutrient resources may be diverted to the production of higher molecular weight compounds such as Peaks C and C+. This may suggest that the community is producing a pool of more recalcitrant compounds to store carbon while DOC is available in excess. Conversely, when DOC is available in excess but nutrient resources are limited, the ability to produce these higher molecular-weight compounds may be compromised, leading to an excess production of smaller, simpler proteinaceous material. By providing a nutrient-limited baseline which can be incrementally manipulated to study the effects of controlled nitrate, phosphate, and DOC loading on the system, we have been able to demonstrate that the availability of these nutrients has a significant impact on the fluorescence production by the bacterial species present within our controlled model system. This further supports previous findings that fluorescence intensity measurements cannot be used as a surrogate measure of bacterial enumeration. When monitoring fluorescence within natural systems, it may be important to consider the effect of changing environmental conditions such as nutrient and DOC availability on the intensity and ratios of fluorescence peaks present to obtain an insight into the functioning of a system.

The DOC availability within the system is also seen to influence the normalized fluorescence intensity per bacterial cell ($f_{QSU/CFU}$). Greater variations were observed in high-nutrient, excess DOC conditions than in any other experimental condition (**Figure 2**) in relation to Peaks C and C+. This is possibly because organic matter produced by *P. aeruginosa* is known to fluoresce in the Peak C+ region, which also corresponds to the observed fluorescence properties of the siderophore pyoverdine (Wasserman, 1965). Pyoverdine is an extracellular iron-scavenging metabolite, and is strongly pigmented (Meyer, 2000). It is possible that the rapid production of Peak C+ shown in our data can be attributed to the production and exporting of pyoverdine from the bacterial cells. The production of pigmented, water-soluble extracellular siderophores by *Pseudomonas* species has long been known to be influenced by a range of environmental factors (Cornelis et al., 2002). The differential expression of these fluorescent pigments as a result of external factors such as nutrient availability could suggest that under high-nutrient conditions, external factors controlling the rate of fluorescence production may be affecting the system, resulting in the variability seen only within the high-nutrient, excess DOC conditions. The variability in the expression of fluorescent pigments by bacteria as a result of nutrient and DOC availability further highlights the complexities associated with using fluorescence intensity as a predictor for bacterial enumeration, but could support its application as a useful biomarker for a metabolically active microbial population, particularly in relation to its responses to changing environmental conditions in natural waters. The observed high variations in Peak C/C+ fluorescence intensities within the high nutrient, excess DOC conditions could be attributed to metabolic differences between independent biological populations of the same species. Observed variations between individual fluorescence measurements within experimental repeats are much lower, eliminating instrumental variability. Therefore, we postulate that the variations in exported humic-like AFOM are driven by metabolic variations between discrete populations of *P. aeruginosa*. This is further supported by the $f_{QSU/CFU}$ data which demonstrates that the measured fluorescence values are independent of cell numbers. In addition, while pyoverdine fluoresces in the humic-like region, it is not considered to represent humic-like material. Siderophores are usually considered a group of low molecular weight compounds, often between 500 and 1,500 Daltons (Da; Hider and Kong, 2010). Pyoverdine has a molecular weight of 1335.4 Da which, while still considered to be low molecular weight, does represent a higher molecular weight than glucose, at 180 Da. This suggests the possible production of higher molecular weight compounds (pyoverdine) from a simple and labile carbon source (glucose) is occurring.

In the future, further investigation into the relationship between microbial metabolism and AFOM production would be required to help develop our understanding, including an investigation of a broader range of species to obtain a more representative bacterial community inoculum. In addition, changes could be made toward the development of a more environmentally representative model. This may include investigating bacterial AFOM production under ambient environmental temperature conditions, or employing a range of environmentally representative nutrient and DOC conditions. It would also be of merit to investigate the continued processing of AFOM over a longer experimental period (i.e., weeks) to determine the relative recalcitrance of the material produced. A limitation of this study is the lack of data pertaining to the levels of nitrate, phosphate and DOC within the system throughout the experimental time period. Future work will incorporate these measurements to further delineate the relationship between nutrient availability and AFOM production. Furthermore, the inclusion of a mixed-community model encompassing planktonic bacteria along with biofilm and algal communities would be more relevant to systems observed in the natural environment. In addition, while the relationship between AFOM production and bacterial metabolism is postulated in this study, further work would be required to verify this experimentally. This may include the addition of direct measurements of metabolic rate or bacterial production alongside fluorescence and enumeration measurements to determine the relationship.

CONCLUSION

- *Pseudomonas aeruginosa* is capable of producing a range of AFOM including Peaks T, C, and C+ from a simple carbon source within a SFW model system. This includes the production of material which fluoresces in the allochthonous region, which is conventionally associated with higher molecular weight material within freshwater systems.

- The relationship between fluorescence intensity and bacterial cell number is nonlinear over the experimental time period. During times of known upregulated metabolism, e.g., the exponential bacterial growth phase, higher $f_{QSU/CFU}$ is observed, supporting the use of fluorescence as a marker for upregulated microbial activity rather than enumeration.
- Both fluorescence intensity and fluorescence peak ratios are influenced by the concentration of nitrate, phosphate, and DOC within a SFW model system. While higher DOC concentrations result in higher total fluorescence, this also influences the response of the bacterial community to the introduction of nutrients.

DATA AVAILABILITY STATEMENT

The original contributions presented in the study are included in the article/supplementary material, further inquiries can be directed to the corresponding author.

AUTHOR CONTRIBUTIONS

EP, DR, and RT: conceptualization and methodology. EP: data curation, investigation, and writing—original manuscript draft. EP, DR, RT, and SS: formal analysis. DR, RT, and JA: funding acquisition. EP and DR: project administration. DR, RT, SS, and JA: supervision. SS, RT, and DR: manuscript writing, reviewing, and editing. JA: manuscript review only. All authors contributed to the article and approved the submitted version.

FUNDING

This study received partial funding from Chelsea Technologies Ltd., who were not involved in the study design, collection, analysis, interpretation of data, or the writing of this article (manuscript reviewing only) nor the decision to submit it for publication. Other funding was provided by the University of the West of England, Bristol (PhD funding) and the Natural Environment Research Council, UKRI as part of delivering grant NE/R003106/1.

ACKNOWLEDGMENTS

The authors acknowledge the assistance of Bethany Fox for providing the custom Python™ script (Python Software Foundation) used for the normalization of fluorescence data to QSU and the generation of EEM optical maps.

REFERENCES

Anderson, T. R., Rowe, E. C., Polimene, L., Tipping, E., Evans, C. D., Barry, C. D. G., et al. (2019). Unified concepts for understanding and modelling turnover of dissolved organic matter from freshwaters to the ocean: the UniDOM model. *Biogeochemistry* 146, 105–123. doi: 10.1007/s10533-019-00621-1

Asmala, E., Kaartokallio, H., Carstensen, J., and Thomas, D. N. (2016). Variation in riverine inputs affect dissolved organic matter characteristics throughout the estuarine gradient. *Front. Mar. Sci.* 2:125. doi: 10.3389/FMARS.2015.00125/BIBTEX

Baker, A., and Spencer, R. G. M. (2004). Characterization of dissolved organic matter from source to sea using fluorescence and absorbance spectroscopy. *Sci. Total Environ.* 333, 217–232. doi: 10.1016/j.scitotenv.2004.04.013

Berggren, M., Gudasz, C., Guillemette, F., Hensgens, G., Ye, L., and Karlsson, J. (2020). Systematic microbial production of optically active dissolved organic matter in subarctic lake water. *Limnol. Oceanogr.* 65, 951–961. doi: 10.1002/lno.11362

Coble, P. G., Spencer, R. G. M., Baker, A., and Reynolds, D. M. (2014). *Aquatic Organic Matter Fluorescence*. Cambridge University Press.

Coble, P. G. (2007). Marine optical biogeochemistry: the chemistry of ocean color. *Chem. Rev.* 107, 402–418. doi: 10.1021/CR050350

Cornelis, P., and Matthijs, S. (2002). Diversity of siderophore-mediated iron uptake systems in fluorescent pseudomonads: not only pyoverdines. *Environ. Microbiol.* 4, 787–798. doi: 10.1046/J.1462-2920.2002.00369.X

Cole, J. J., Prairie, Y. T., Caraco, N. F., McDowell, W. H., Tranvik, L. J., Striegl, R. G., et al. (2007). Plumbing the global carbon cycle: integrating inland waters into the terrestrial carbon budget. *Ecosystems* 10, 172–185. doi: 10.1007/s10021-006-9013-8

Directive 2000/60/EC of the European Parliament and of the Council of 23 October 2000 establishing a framework for community action in the field of water policy (2000). Official Journal L 327, EUR-Lex, 0001-0073. Available at: https://eur-lex.europa.eu/legal-content/EN/TXT/?uri=CELEX:32000L0060 (Accessed October 01, 2019).

Downing, J. A. (2008). Emerging global role of small lakes and ponds: little things mean a lot. *Limnetica* 29, 9–24. doi: 10.23818/limn.29.02

Elliott, S., Lead, J. R., and Baker, A. (2006). Characterisation of the fluorescence from freshwater, planktonic bacteria. *Water Res.* 40, 2075–2083. doi: 10.1016/J.WATRES.2006.03.017

European Environment Agency (2018). European waters – Assessment of status and pressures 2018 [online]. Luxembourg: Publications Office of the European Union. Available at: eea.europea.eu (Accessed January 15, 2021)

Fox, B. G., Thorn, R. M. S., Anesio, A. M., Cox, T., Attridge, J. W., and Reynolds, D. M. (2018). Microbial processing and production of aquatic fluorescent organic matter in a model freshwater system 11:10. doi: 10.3390/w11010010

Fox, B. G., Thorn, R. M. S., Anesio, A. M., and Reynolds, D. M. (2017). The in situ bacterial production of fluorescent organic matter; an investigation at a species level. *Water Res.* 125, 350–359. doi: 10.1016/j.watres.2017.08.040

Fox, B. G., Thorn, R. M. S., and Reynolds, D. M. (2021). Laboratory in-situ production of autochthonous and allochthonous fluorescent organic matter by freshwater bacteria. *Microorganisms* 9:1623. doi: 10.3390/MICROORGANISMS9081623

Gao, Y., Yang, T., Wang, Y., and Yu, G. (2017). Fate of river-transported carbon in china: implications for carbon cycling in coastal ecosystems. *Ecosyst. Heal. Sustain.* 3:e01265. doi: 10.1002/EHS2.1265

Guillemette, F., and del Giorgio, P. A. (2012). Simultaneous consumption and production of fluorescent dissolved organic matter by lake bacterioplankton. *Environ. Microbiol.* 14, 1432–1443. doi: 10.1111/j.1462-2920.2012.02728.x

Hedges, J. I. (1992). Global biogeochemical cycles: progress and problems. *Mar. Chem.* 39, 67–93. doi: 10.1016/0304-4203(92)90096-S

Hider, R. C., and Kong, X (2010). Chemistry and biology of siderophores. *Nat. Prod. Rep.* 27, 637–657. doi: 10.1039/B906679A

Hudson, N., Baker, A., and Reynolds, D. (2007). Fluorescence analysis of dissolved organic matter in natural, waste and polluted waters—a review. *River Res. Appl.* 23, 631–649. doi: 10.1002/rra.1005

Hudson, N., Baker, A., Ward, D., Reynolds, D. M., Brunsdon, C., Carliell-Marquet, C., et al. (2008). Can fluorescence spectrometry be used as a surrogate for the biochemical oxygen demand (BOD) test in water quality assessment? An example from south West England. *Sci. Total Environ.* 391, 149–158. doi: 10.1016/j.scitotenv.2007.10.054

Jiao, N., Herndl, G. J., Hansell, D. A., Benner, R., Kattner, G., Wilhelm, S. W., et al. (2011). The microbial carbon pump and the oceanic recalcitrant dissolved organic matter pool. *Nat. Rev. Microbiol.* 9:555. doi: 10.1038/nrmicro2386-c5

Kinsey, J. D., Corradino, G., Ziervogel, K., Schnetzer, A., and Osburn, C. L. (2018). Formation of chromophoric dissolved organic matter by bacterial degradation of phytoplankton-derived aggregates. *Front. Mar. Sci.* 4:430. doi: 10.3389/fmars.2017.00430

Koch, B. P., Kattner, G., Witt, M., and Passow, U. (2014). Molecular insights into the microbial formation of marine dissolved organic matter: recalcitrant or labile? *Biogeosciences* 11, 4173–4190. doi: 10.5194/bg-11-4173-2014

Kominoski, J. S., Rosemond, A. D., Benstead, J. P., Gulis, V., and Manning, D. W. P. (2018). Experimental nitrogen and phosphorus additions increase rates of stream ecosystem respiration and carbon loss. *Limnol. Oceanogr.* 63, 22–36. doi: 10.1002/lno.10610

Kramer, G. D., and Herndl, G. J. (2004). Photo- and bioreactivity of chromophoric dissolved organic matter produced by marine bacterioplankton. *Aquat. Microb. Ecol.* 36, 239–246. doi: 10.3354/AME036239

Leenheer, J. A., and Croué, J.-P. (2003). Peer reviewed: characterizing aquatic dissolved organic matter. *Environ. Sci. Technol.* 37, 18A–26A. doi: 10.1021/es032333c

Manning, D. W. P., Rosemond, A. D., Gulis, V., Benstead, J. P., and Kominoski, J. S. (2018). Nutrients and temperature additively increase stream microbial respiration. *Glob. Chang. Biol.* 24, e233–e247. doi: 10.1111/gcb.13906

McKnight, D. M., Boyer, E. W., Westerhoff, P. K., Doran, P. T., Kulbe, T., and Andersen, D. T. (2001). Spectrofluorometric characterization of dissolved organic matter for indication of precursor organic material and aromaticity. *Limnol. Oceanogr.* 46, 38–48. doi: 10.4319/lo.2001.46.1.0038

Meyer, J. M. (2000). Proverdines: pigments, siderophores and potential taxonomic markers of fluorescent pseudomonas species. *Arch. Microbiol.* 174, 135–142. doi: 10.1007/s002030000188

Milbrandt, E. C., Coble, P. G., Conmy, R. N., Martignette, A. J., and Siwicke, J. J. (2010). Evidence for the production of marine fluorescent dissolved organic matter in coastal environments and a possible mechanism for formation and dispersion. *Limnol. Oceanogr.* 55, 2037–2051. doi: 10.4319/LO.2010.55.5.2037

Mostofa, K. M. G., Liu, C. Q., Mottaleb, M. A., Wan, G., Ogawa, H., Vione, D., et al. (2013). Dissolved organic matter in natural waters. *Environ. Sci. Eng.* 1–137. doi: 10.1007/978-3-642-32223-5_1

Noacco, V., Wagener, T., Worrall, F., Burt, T. P., and Howden, N. J. K. (2017). Human impact on long-term organic carbon export to rivers. *J. Geophys. Res. Biogeosci.* 122, 947–965. doi: 10.1002/2016JG003614

Shimotori, K., Omori, Y., and Hama, T. (2010). Bacterial production of marine humic-like fluorescent dissolved organic matter and its biogeochemical importance. *Aquat. Microb. Ecol.* 58, 55–66. doi: 10.3354/ame01350

Sigee, D. C. (2004). "Biodiversity and dynamic interactions of microorganisms in the aquatic environment," in *Freshwater Microbiology*. John Wiley & Sons Ltd., 1–524.

Smith, E. J., Davison, W., and Hamilton-Taylor, J. (2002). Methods for preparing synthetic freshwaters. *Water Res.* 36, 1286–1296. doi: 10.1016/S0043-1354(01)00341-4

Sorensen, J. P. R., Diaw, M. T., Pouye, A., Roffo, R., Diongue, D. M. L., Faye, S. C., et al. (2020). In-situ fluorescence spectroscopy indicates total bacterial abundance and dissolved organic carbon. *Sci. Total Environ.* 738:139419. doi: 10.1016/j.scitotenv.2020.139419

Sorensen, J. P. R., Lapworth, D. J., Marchant, B. P., Nkhuwa, D. C. W., Pedley, S., Stuart, M. E., et al. (2015). In-situ tryptophan-like fluorescence: a real-time indicator of faecal contamination in drinking water supplies. *Water Res.* 81, 38–46. doi: 10.1016/j.watres.2015.05.035

Sorensen, J. P. R., Vivanco, A., Ascott, M. J., Gooddy, D. C., Lapworth, D. J., Read, D. S., et al. (2018). Online fluorescence spectroscopy for the real-time evaluation of the microbial quality of drinking water. *Water Res.* 137, 301–309. doi: 10.1016/j.watres.2018.03.001

Tranvik, L. J., Downing, J. A., Cotner, J. B., Loiselle, S. A., Striegl, R. G., Ballatore, T. J., et al. (2009). Lakes and reservoirs as regulators of carbon cycling and climate. *Limnol. Oceanogr.* 54, 2298–2314. doi: 10.4319/lo.2009.54.6_part_2.2298

Trimmer, M., Grey, J., Heppell, C. M., Hildrew, A. G., Lansdown, K., Stahl, H., et al. (2012). River bed carbon and nitrogen cycling: state of play and some new directions. *Sci. Total Environ.* 434, 143–158. doi: 10.1016/j.scitotenv.2011.10.074

Tsuji, A., Kaneko, Y., Takahashasi, K., Ogawa, M., and Goto, S. (1982). The effects of temperature and pH on the growth of eight enteric and nine glucose non-fermenting species of gram-negative rods. *Microbiol. Immunol.* 26, 15–24. doi: 10.1111/J.1348-0421.1982.TB00149.X

Wasserman, A. E. (1965). Absorption and fluorescence of water-soluble pigments produced by four species of *Pseudomonas*. *Appl. Microbiol.* 13, 175–180. doi: 10.1128/am.13.2.175-180.1965

Woodward, G., Gessner, M. O., Giller, P. S., Gulis, V., Hladyz, S., Lecerf, A., et al. (2012). Continental-scale effects of nutrient pollution on stream ecosystem functioning. *Science* 336, 1438–1440. doi: 10.1126/science.1219534

Yamashita, Y., Jaffé, R., Maie, N., and Tanoue, E. (2008). Assessing the dynamics of dissolved organic matter (DOM) in coastal environments by excitation emission matrix fluorescence and parallel factor analysis (EEM-PARAFAC). *Limnol. Oceanogr.* 53, 1900–1908. doi: 10.4319/lo.2008.53.5.1900

Yamashita, Y., and Tanoue, E. (2004). *In situ* production of chromophoric dissolved organic matter in coastal environments. *Geophys. Res. Lett.* 31, 2–5. doi: 10.1029/2004GL019734

Conflict of Interest: JA is employed by Chelsea Technologies Ltd. who provided partial funding for this study. The funder Chelsea Technologies Ltd. had the following involvement with the study—reviewing of final manuscript only.

The remaining authors declare that the research was conducted in the absence of any commercial or financial relationships that could be construed as a potential conflict of interest.

Publisher's Note: All claims expressed in this article are solely those of the authors and do not necessarily represent those of their affiliated organizations, or those of the publisher, the editors and the reviewers. Any product that may be evaluated in this article, or claim that may be made by its manufacturer, is not guaranteed or endorsed by the publisher.

Appendix II

Stakeholder Water Quality Report

The Implementation of a fluorescence-based sensor for improved understanding of river catchment quality as a function of land-use: A case study from South-West England and Abisko, Sweden

Eva Perrin
Professor Darren Reynolds
Dr Robin Thorn
Dr Stephanie Sargeant
Dr John Attridge

Executive Summary

The characterisation of aquatic fluorescent organic matter of river catchments using a newly developed V-Lux fluorosensor (Chelsea Technologies Ltd) was assessed. Rivers situated in **1.** Cornwall, South West of England (UK) and; **2.** Abisko National Park, North-West Sweden were sampled and the water quality monitored. For river catchments located in the South-West England, UK, the River Deer and the River Claw (situated within the Tamar Upper Catchment area) was sampled and monitored on two separate occasions. Firstly, between the 14th and the 16th of August, 2019 and also between the 8th and 11th of October, 2019 following a heavy precipitation event. Sample sites were identified along the River Deer (S1 to S7) and the River Claw (S8 to S12). Water quality assessment undertaken in 2015 revealed that in this catchment area 16 water bodies were deemed as being either "moderate" or "poor" in quality whilst only 5 water bodies achieved "good" status. The main pressures in this catchment arise predominantly from agricultural and wastewater pollution. For the river catchments investigated in Northern Sweden, i.e. the *Abiskojakka* and *Mjellajokka* monitoring was undertaken between 9th and 12th of September 2019. Sample sites were located mainly within the *Abiskojakka* (A1 to A10) but sites located within the *Mjellajokka* catchment (A11 to A13) were also investigated. The *Abiskojakka* catchment is approximately 600km^2 in size and has headwaters that drain Meyers, tundra, mountainous and glaciated regions, eventually forming large water bodies with wide rivers & streams. The *Mjellajokka* catchment is considerably smaller at approximately 52km^2 and is comprised mainly of headwaters draining tundra regions down to birch forest. The catchments located in North West Sweden provided examples of headwater streams, with water regions above and below the treeline, originating from the main Arctic sub-regions. Not taking into account climate change which is known to affect all rivers globally the systems studied here such are near pristine in quality and exhibiting natural environmental gradients and little or no localised impacts. This study provided the opportunity to characterise the water quality in a range of unperturbed and perturbed aquatic environments. This contrast is useful for comparing the aquatic fluorescent organic matter characteristics from catchments directly impacted by agricultural land use and catchment that experience little or no impact. Ultimately work like this will lead to the development of robust representative datasets that inform the implementation of a fluorescence-based sensor for improved understanding of river catchment quality as a function of land-use. The data collected concluded that;

- All rivers and streams studied in Abisko National park exhibited ultra-low fluorescence characteristics (EEMs and V-Lux sensing) when compared to rivers studied in the UK
- On average Peak T was 4.5 times lower in Arctic systems than in SW UK systems.
- On average Peak C (C+^{2}) was on average 234 times higher in SW UK systems.

- Natural gradients in the fluorescence characteristics were observed across the various sub-arctic aquatic environments (headwaters that drain Meyers, tundra, mountainous and glaciated regions). Such gradients were not observed in the South West of England catchments.
- All Abisko aquatic systems studied were oligotrophic in nature in contrast to the South West of England systems.
- All SW UK aquatic systems studied exhibited higher levels of DOC in contrast to the Swedish systems.
- All Abisko aquatic systems studied exhibited low levels of microbes in contrast to South West of England systems
- All Abisko aquatic systems studied exhibited low levels of metabolic activity as a function of Peak T when compared to South West of England systems.

Reporting of Optical Regions

The fluorescence characteristics from both Abiskojakka and Mjellajokka catchments have been collated. For characterisation purposes, the optical regions reported conform to the peak nomenclature defined by Coble *et al.,* 2014. These include Peaks T, M, B, C, and $C^{+(1\&2)}$. The optical orientation of these peaks are displayed in Figure x. The wavelengths associated with these optical regions are shown in Table 2. Caution is advised when interpreting direct comparisons between Aqualog-derived fluorescence intensity measurements and sensor-derived measurements due to intrinsic differences in optical arrangements of the instruments. The optical regions interrogated by the V-Lux sensor are illustrated in red. The V-Lux has two fluorescence channels, TRYP FL (Peak T) & CDOM aligned with the region $C+^{2}$ (collectively termed Peak C).

Table 1.6.3.1 Optical regions for Aqualog peak-picking (derived from Coble et al., 2014) and from the Chelsea Technologies V-Lux fluorescence sensor

		Assigned Peak Nomenclature as defined by Coble *et al.* 2014					
		T	**B**	**M**	**C**	**$C+^{1}$**	**$C+^{2}$**
Optical Region *λex/λem* (nm)	**Coble *et al.,* 2014**	275/340	275/305	300/370-420	350/420-470	400/470-505	250/470-505
	V-Lux	280/350-375	-	-	-	-	280/425-575

1 South-West England (UK)

1.1 Aims

To investigate the use of *in-situ* fluorescence measurements for water quality monitoring in the Tamar Upper catchment. Specifically, sampling was undertaken along the rivers Deer and Claw with the aim of investigating changes in water quality as a function of land-use. Specifically, this included the following objectives:

1. To characterise the fluorescence of the system
2. To obtain V-Lux fluorescence sensing data for the rivers; Deer and Claw
3. Undertake river transects
4. Undertake initial physical and chemical assessment

1.2 The South West River Basin District

According to the South West River Basin Management Plan which was last updated in 2015, the South West river basin district (Figure 2) covers over 21,000km^2. It includes Cornwall, Devon, Dorset and parts of Somerset, Hampshire and Wiltshire. The Isles of Scilly, a group of islands 25 miles south west of Cornwall, and Lundy Island are included in the district. In total over 5.3 million people live and work in the south west, with a resident population fluctuating due to seasonal tourism. The south west has the lowest population density of any English region and includes urban areas such as Exeter, Plymouth, Torquay, Bournemouth and Poole.

The South West river basin district has a rich diversity of wildlife and habitats, supporting many species of global and national importance. Freshwater habitats within the river basin district are very important for wintering wildfowl, and reservoirs, rivers, estuaries and coastal water bodies support fisheries and shellfish waters. Coastal waters are also very important and SW river basin district has over half of the country's designated bathing waters.

There are *9 operational management catchments* that make up the SW river basin district that include many interconnected rivers, lakes, groundwater and coastal waters. These catchments range from the shallow aquifers and rocky rivers in Cornwall and Devon to lowland chalk rivers in Dorset. Around 80% of the river basin district is rural, with dairy farming being the most common land use. This, and the legacy of mineral extraction, shape much of the landscape. In addition, the popularity of the district as a holiday destination means tourism makes a significant contribution to the local economy.

1.2.1 Water Quality Stressors

The main causes of deteriorating water quality in the river basin district have been identified as;

• *Pollution from rural areas - affecting 44% of water bodies in this river basin district*

Some approaches to land management have increased the amount of soils and sediment run-off from surrounding land subsequently carrying phosphorus into aquatic systems that can lead to excessive algae growth called 'eutrophication'. A changing climate means that more intense rainfall is likely to occur, increasing the risk of impacts further. Nitrate from fertilisers has built up in groundwater over decades and will take a long time to reduce furthermore, nutrients are also present in rivers from this diffuse agricultural pollution. Sedimentation from erosion, forestry practices, saturated and compacted fields and livestock trampling on river banks has affected river ecology by smothering fish spawning grounds. Other impacts include bacteriological contaminations from animal faeces and inappropriately stored and applied livestock slurry being washed off the land, and pesticides from farming, forestry, golf courses and parks. These contaminants pose a particular threat to bathing waters, shellfish waters and drinking water as well as the overall ecological health of affected aquatic systems.

• *Pollution from wastewater – affecting 33% of water bodies in this river basin district*

Wastewater, or sewage, can contain large amounts of nutrients (phosphorus and nitrates), ammonia, bacteria, harmful chemicals and other damaging substances. It can enter water bodies where sewage treatment technology to remove enough of the phosphorus and harmful chemicals doesn't exist, from leakages from privately owned septic tanks and, in wet weather, storm overflows can discharge untreated sewage having a significant impact on bathing waters. Population growth and changes in rainfall patterns are increasing the pressure on the sewer network.

• *Pollution from towns, cities and transport - affecting 4% of water bodies in this river basin district*

Rainwater draining from roofs, roads and pavements carries pollutants, including grit, bacteria, oils, metals, vehicle emissions, detergent and road salt drains to surface water, including estuaries and coastal waters. Many homes and workplaces have 'misconnected' drains, meaning that dirty water often enters surface waters and groundwater rather than foul sewer drains.

1.3 Tamar Upper Catchment

The Tamar catchment area (Figure 1.1) is about 1,800km^2 and is predominantly rural and to the south are the Tamar estuary and the city of Plymouth where the majority of the population is based. There are 19 river water bodies and 2 lakes in this catchment. There are no estuarine & coastal waters or groundwater bodies. The upper River Tamar catchment and its tributaries include the Otter, Kensey,

Carey, Claw and Deer are found within this catchment. The main Tamar rises on Woolley Moor just north of Youlstone, then flows south through rural agricultural land and through Upper Tamar Lakes, which are an important source of public water supply. The Tamar is then joined by the Deer and Claw from the east, before continuing its journey south. Just above the town of Launceston the Tamar is joined by the Ottery and Kensey from the west and the Carey from the east. This area is very agricultural. In 2013, assessment of the water quality of all the 21 water bodies in this catchment area was undertaken (cycle 2). This assessment revealed that 16 water bodies were deemed as being either "moderate" or "poor" in quality whilst only 5 water bodies achieved "good" status. The main pressures in this catchment arise predominantly from agricultural and wastewater pollution.

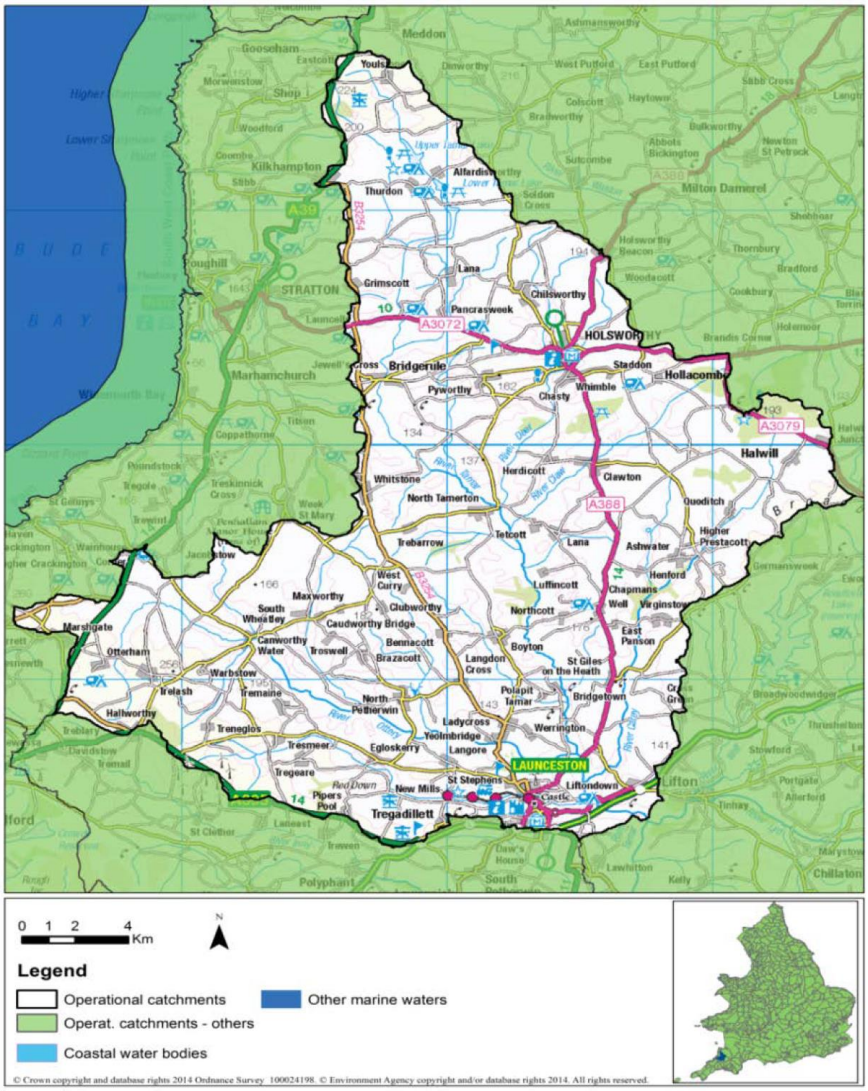

Figure 0.1 Map of the Tamar Upper operational catchment

1.4 Water quality monitoring and sampling sites on the Rivers Deer and Claw

Monitoring was undertaken on two separate occasions, firstly between the 14th and the 16th of August, 2019 (M1) and also between the 8th and 11th of October, 2019 (M2) following a heavy precipitation event. For M1, sample sites (see Figure 2) were identified along the River Deer (S1 to S7) and the River Claw (S8 to S12). For M2, sampling sites S1 to S8 were visited.

At each sampling site the following analyses was undertaken;

i. Preliminary macro-biological assessment (kick-sampling)
ii. Conductivity, Dissolved Oxygen, Temperature and pH
iii. *In situ* fluorescence sensing (V-Lux, Chelsea Technologies Group)

Water samples collected so that the following analysis could be undertaken;

i. Microbial assessment via flow cytometry ~ (2mL in sterile microcentrifuge containing 10µL of 25% glutaraldehyde).
ii. Nutrient analysis (NO_3^-, PO_4^-) using ion chromatography ~ (50mL filtered 0.2µm, sterile Falcon tubes)
iii. Excitation and Emission Matrices, via fluorescence spectroscopy, Aqualog, HORIOBA ~ (50mL filtered 0.2µm, sterile Falcon tubes)

Figure 0.2 Map displaying sampling sites (S1 to S11) within the Tamar Upper catchment on the River Deer and River Claw

1.5 Data

Data shown in Tables 1.2 and 1.3 show monitoring results from M1 and M2 respectively. Data shown in Figure 1.3 shows Excitation-Emission Matrices (EEMs) from sites S1-S6 during M1 and M2.

Table 1.1 Summary of physico-chemical and fluorescence data from sampling sites S1-S11 during monitoring M1.

Site	Physical				Chemical			EEM AFOM Peaks (QSU)						*In situ* sensing measurements (V-Lux)				
	Site Comments	Temp (ºC)	DO (mgL^{-1})	EC (µS)	pH	NO_3^- (mgL^{-1})	PO_4^- (mgL^{-1})	T	M	B	C	C+[1]	C+[2]	Abs AU	Turbidity (AU)	Chl (QSU)	Peak T (QSU)	Peak C (QSU)
S1 *Deer*	Small stream Low flow	16	3.45	222.4	7.17	2.7	ND	6.94	18.52	*	21.9	10.85	38.02	0.27	10.63	2.39	20.97	78.67
S2	Small stream near grazing land	16.4	9.00	250	7.5	3.33	ND	6.78	21.66	*	24.82	12.33	43.68	0.28	3.64	3.18	23.62	93.02
S3	Wide stream Slow flow Near main road	16.4	9.1	257.8	6.81	6.26	0.098	8.39	24.75	*	28.44	13.44	49.47	0.44	19.54	2.18	23.90	90.14
S4	Small tributary stream	16.5	8.5	273.4	6.53	6.48	ND	12.02	31.33	*	34.78	16.70	59.48	0.71	15.28	1.50	27.43	93.73
S5	Close (downstream) to Holsworthy Sewage Treatment Plant	16.3	8.84	276.5	6.5	14.18	1.41	11.58	23.91	1.19	25.99	11.33	44.24	0.40	12.11	0	28.64	103
S6	Near grazing land	16	9.16	280.20	6.35	11.94	1.18	10.65	25.16	0.72	27.83	12.47	47.05	0.24	4.03	2.06	31.38	99.32
S7	Approximately 50m upstream of confluence with Tamar	15.9	9.42	275	7.66	11.97	0.89	11.89	27.46	*	30.01	13.55	51.61	0.29	12.29	2.94	30.10	100.78
S8 *Claw*	Small, shallow, rocky stream	16.7	9.06	208	7.58	2.57	ND	9.75	34.53	*	38.81	18.29	68.81	0.59	12.44	0	19.42	89.65
S9	Near grazing land	16.4	9.75	206	7.55	2.61	ND	7.44	26.10	*	31.46	16.02	52.60	0.41	7.39	0	18.77	89.53
S10	Wide and slow-flowing stream	16.3	9.18	219	6.9	3.90	ND	10.70	31.67	*	35.90	17.42	64.25	0.48	11.07	1.09	23.29	99.87
S11	Approximately 200m upstream of Tamar confluence Heavy grazing	15.8	9	220	7.26	4.527	ND	9.57	29.57	*	33.70	16.29	60.92	0.41	10.58	1.36	22.54	100.27

Table 1.2 Summary of physico-chemical and fluorescence data from sites S1-S1 during monitoring M2.

Site	Physical				Chemical			EEM AFOM Peaks (QSU)						*In situ* sensing measurements (V-Lux)				
	Site Comments	Temp (^oC)	DO (mgL^{-1})	EC (μS)	pH	NO_3^- (mgL^{-1})	PO_4^- (mgL^{-1})	T	M	B	C	C+1	C+2	Abs AU	Turbidity (AU)	Chl (QSU)	Peak T (QSU)	Peak C (QSU)
S1 *Deer*	Small stream Low flow	12.8	9.85	197	6.86	2.109	n/d	6.59	26.90	0	43.77	18.85	56.02	0.2	13.02	0	25.85	132.2
S2	Small stream near grazing land	13	10.25	186.1	7.31	6.764	n/d	7.12	26.59	0	44.59	18.03	53.78					
S3	Wide stream Slow flow Near main road	12.9	10.32	190	7.41	9.819	n/d	8.43	28.77	0	46.57	19.44	57.47	0.41	4	0	25.85	132.2
S4	Small tributary stream	12.7	9.93	194	7.43	11.612	n/d	8.15	34.67	0	48.99	21.70	64.48	0.42	5.43	2.09	25.41	137.01
S5	Close (downstream) to Holsworthy Sewage Treatment Plant	13	10.2	196	7.6	12.09	0.243	8.33	29.91	0	43.33	20.70	56.24					
S6	Near grazing land	13.1	10.34	194	7.4	11.184	0.170	8.34	30.01		43.45	20.88	56.88	0.24	4.03	2.06	31.38	134.26

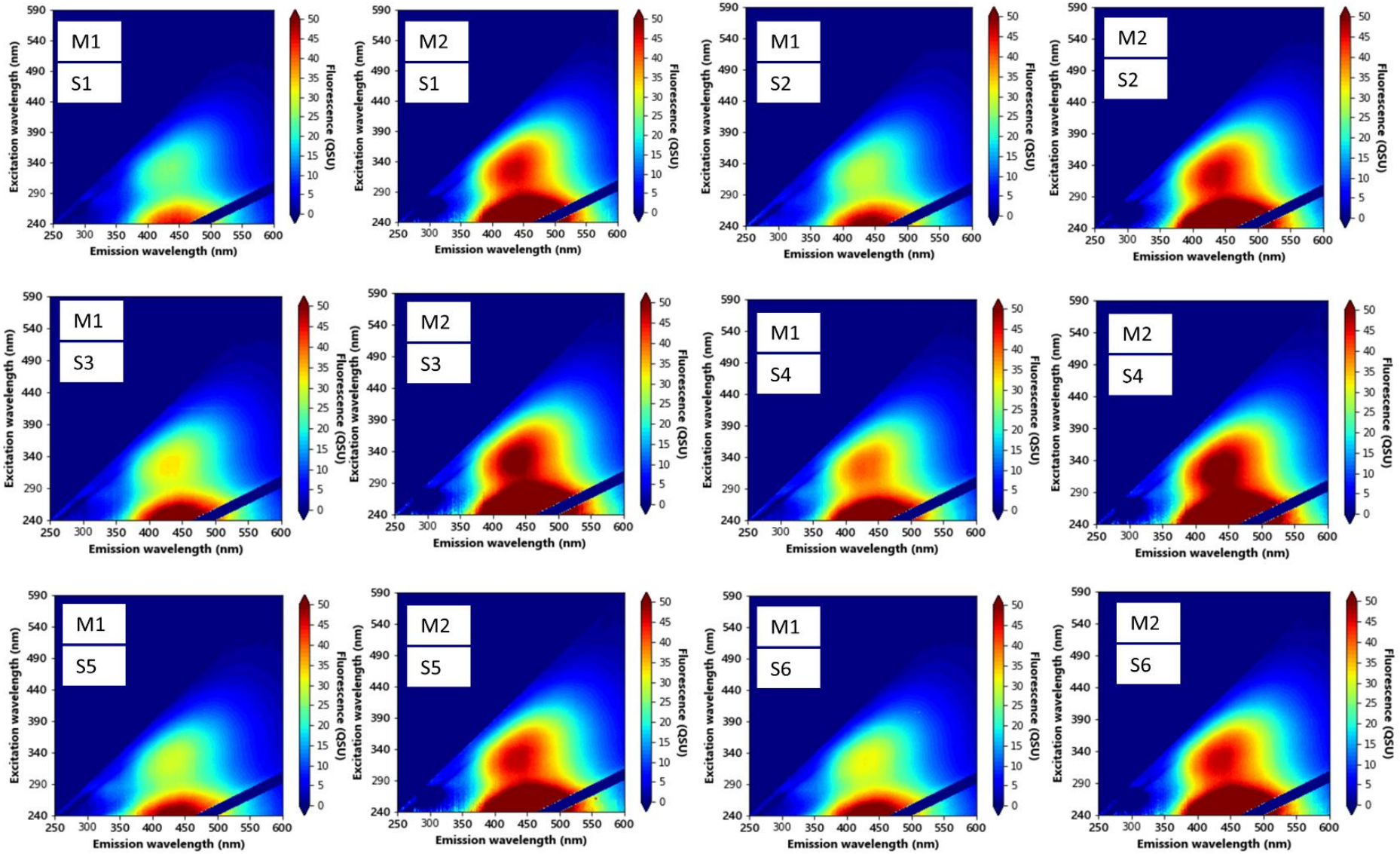

Figure 0.3 Excitation-Emission Matrices (EEMs) from S1-S6 during M1 and M2.

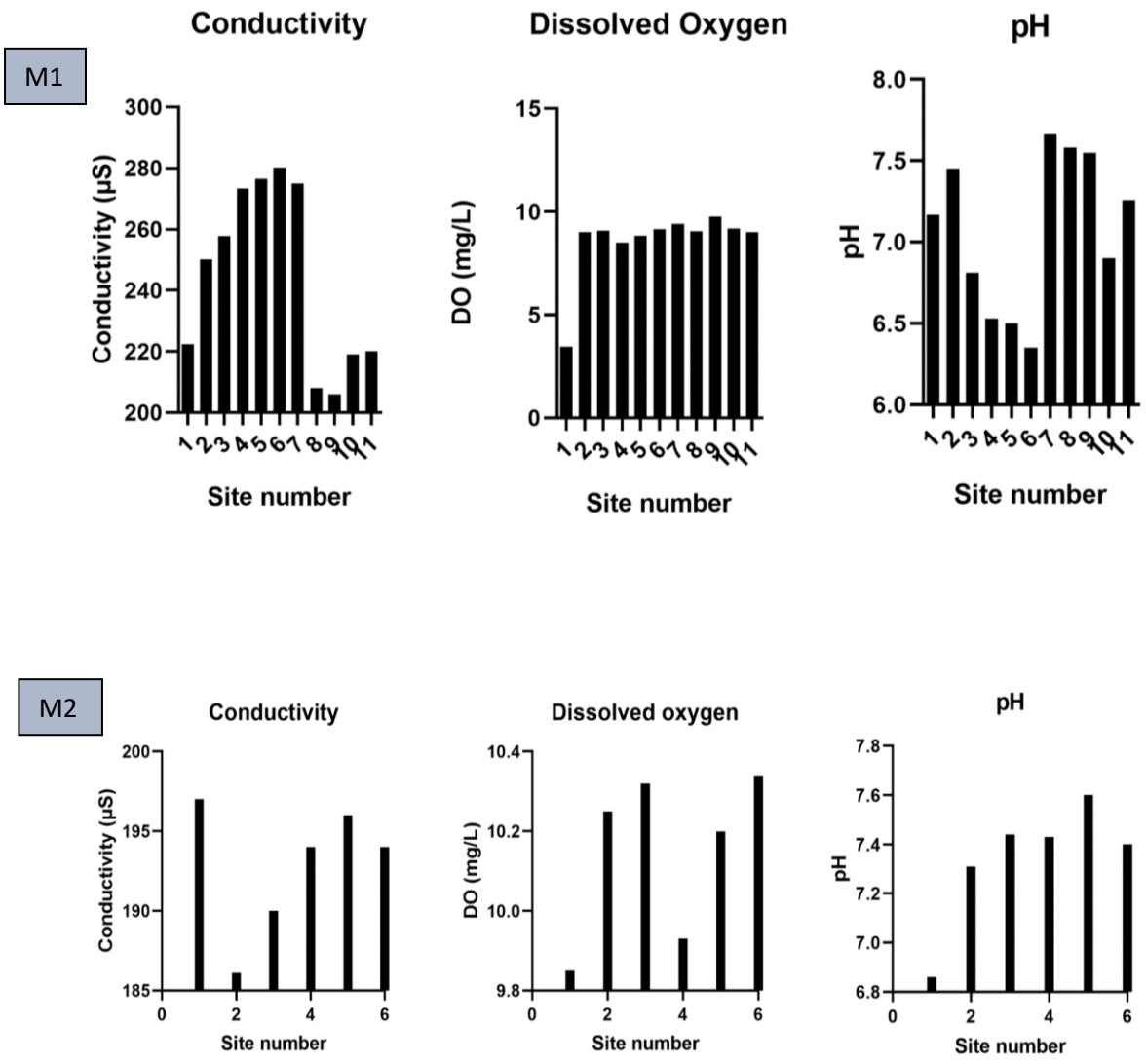

Figure 0.4 Physico-chemical data from sites S1-S11 (M1) and sites S1-S6 (M2)

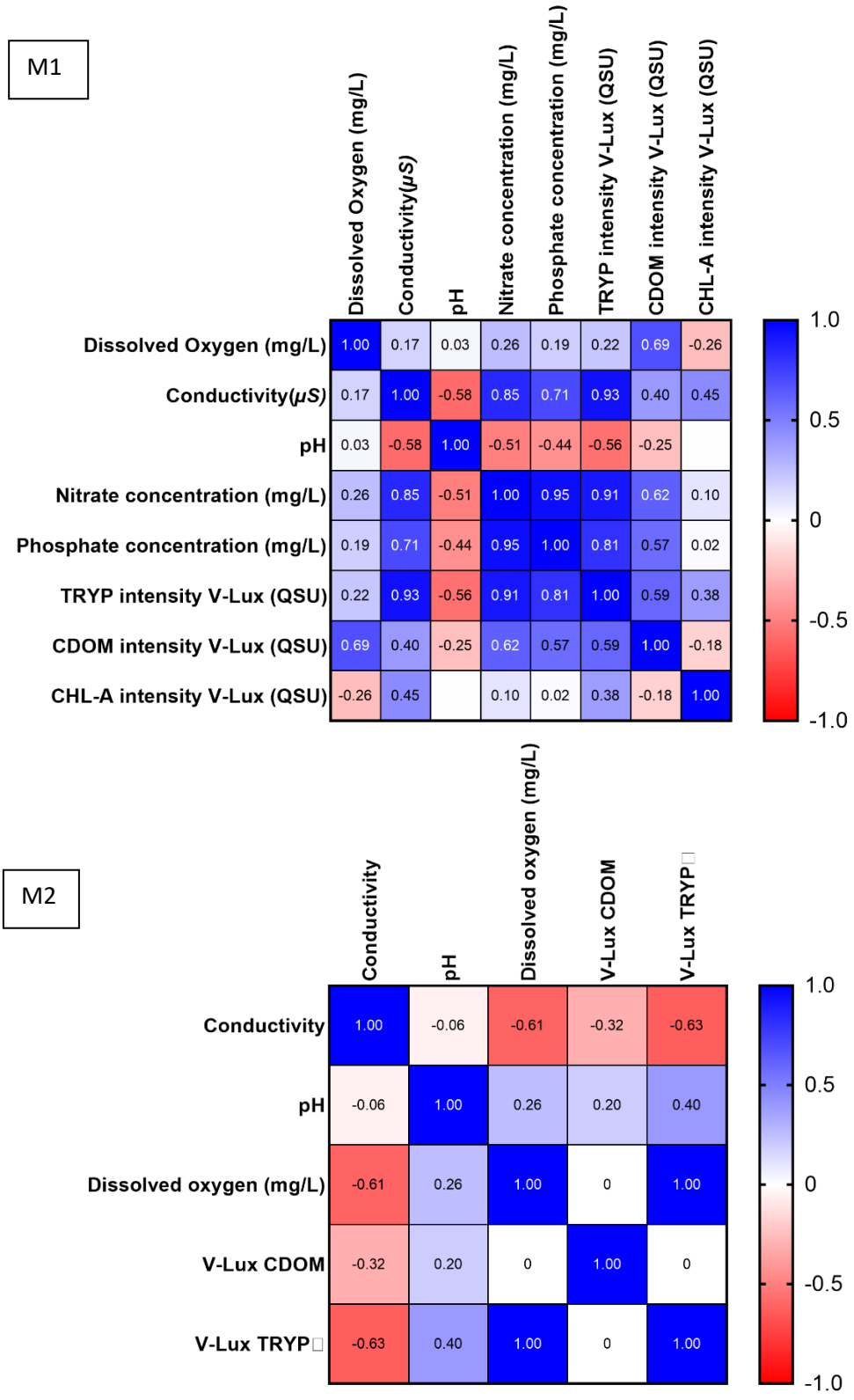

Figure 0.5 Correlation matrix for physico-chemical parameters and fluorescence for M1 and M2

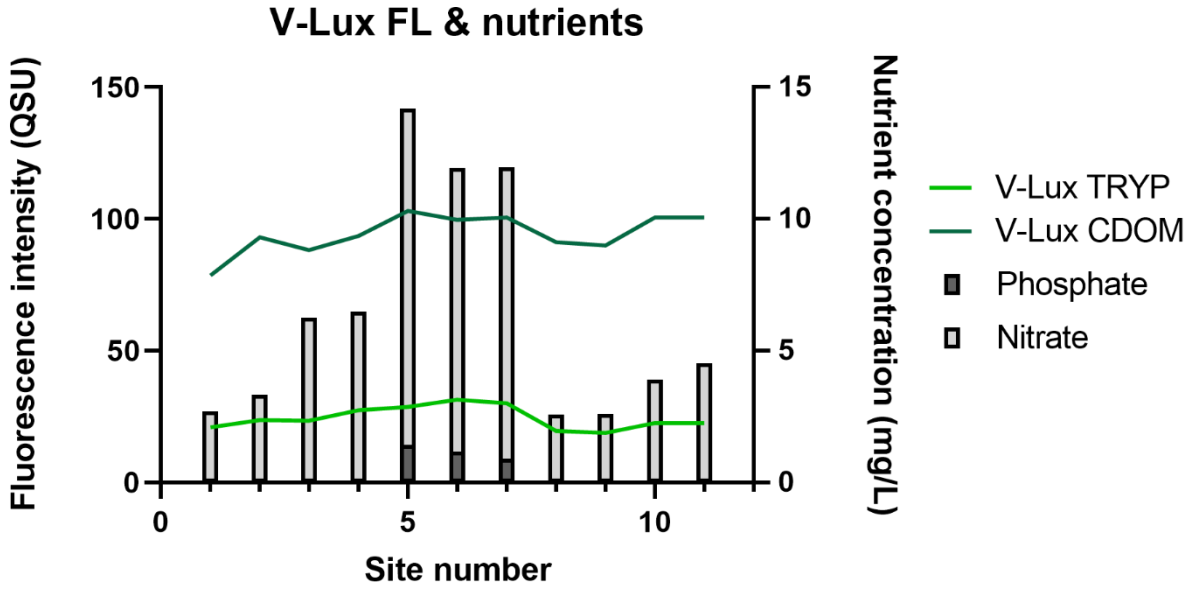

Figure 1.6 Fluorescence intensity from the V-Lux fluorosensor and nutrient concentrations from Monitoring 1 (M1)

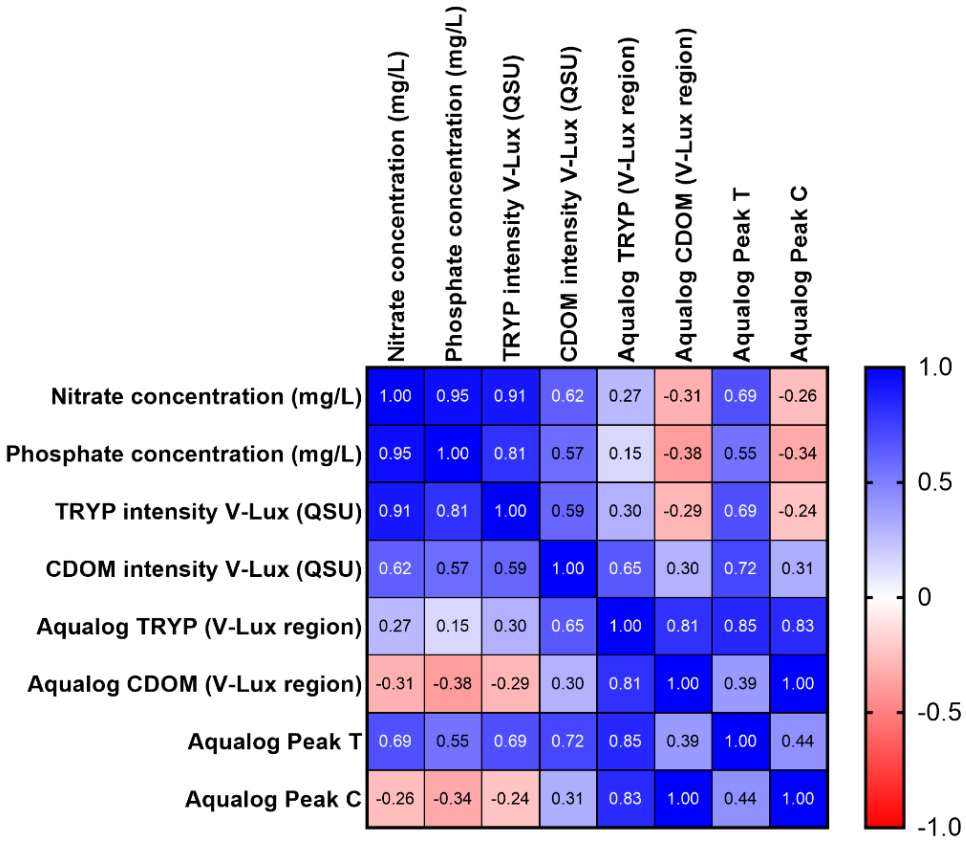

Figure 1.7 Correlation matrix of V-Lux and Aqualog fluorescence data (Using the specified V-lux optical regions)

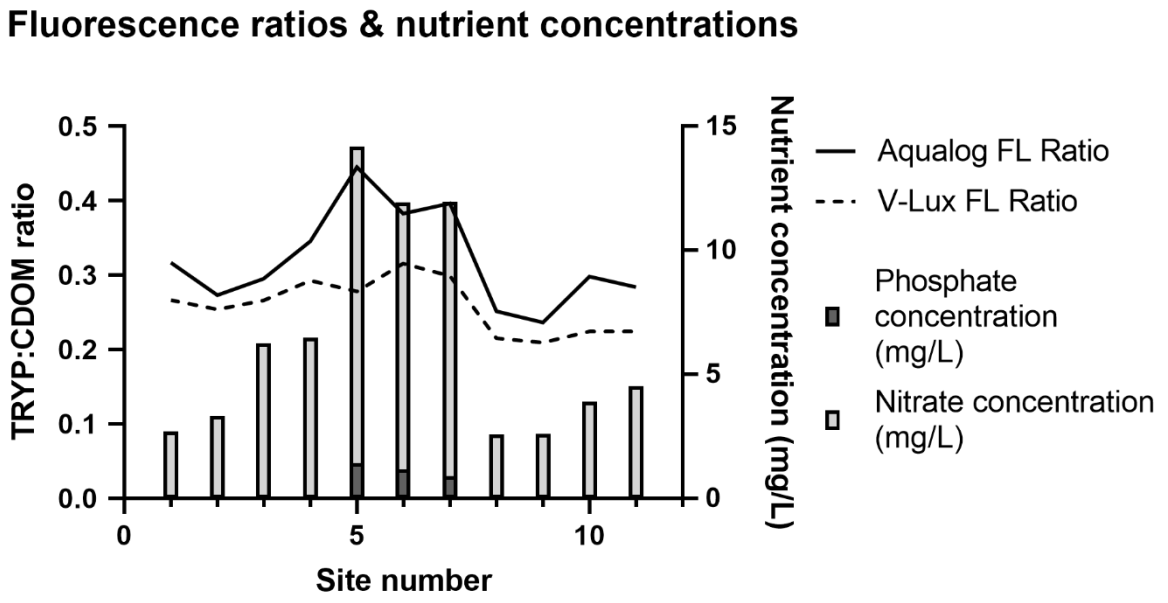

Figure 1.8 Comparison of Tryptophan: CDOM ratios from the V-Lux fluorosensor with nutrient concentrations

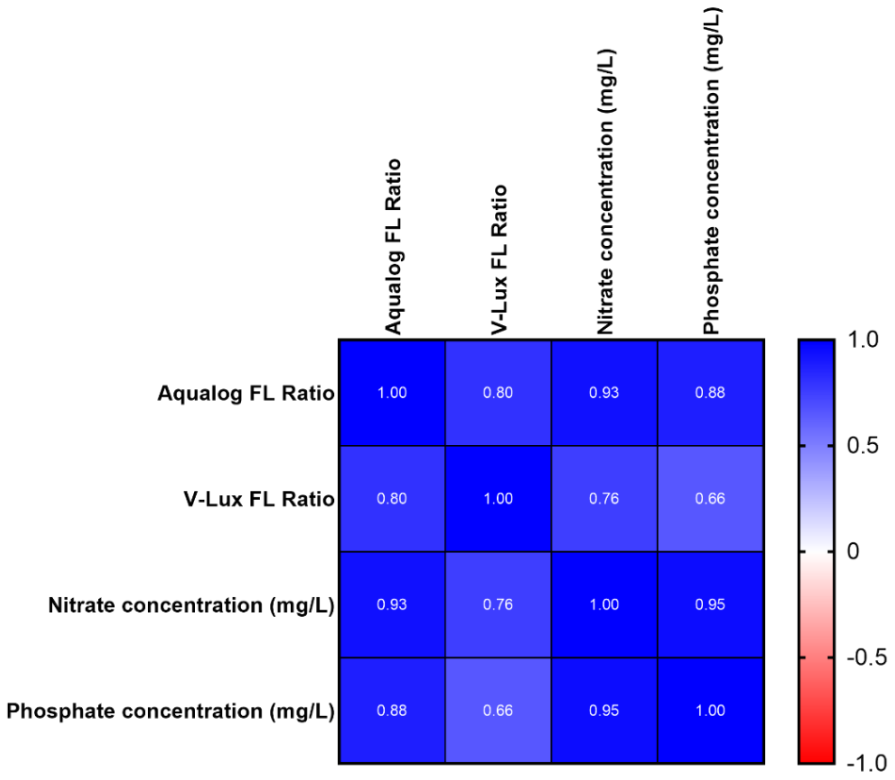

Figure 1.9 Correlation matrix of Peak T to Peak C fluorescence ratios and nutrient concentrations

1.6 Brief Summary

- The ratio of **Peak T** to **Peak C** fluorescence intensities vary across all sites (confirmed from V-Lux and Aqualog data)
- There is a significant correlation between Peak T/Peak C ratios and nitrate and phosphate nutrient concentrations (V-Lux and Aqualog), see Figures 7 and 8.
- At increasing nutrient concentration, the Peak T /Peak C ratio increases

Further work is needed to assess the use of Peak T/Peak C ratios as an indication of microbial activity resulting from increased nutrient loading.

M1

- **Peak T** (Aqualog and V-Lux) was found to have significant positive correlations with concentrations of **nitrate** and **phosphate**, p=0.003 and 0.000113 respectively, see Figure 4a.
- **Peak C** (Aqualog and V-Lux) shows a significant correlation with **phosphate concentration** (p=0.04), but not nitrate concentration.
- **Nitrate** and **Phosphate** have significant positive correlations
- **Phosphate** and **nitrate concentrations** have significant positive correlations with **conductivity** (p=0.004 and 0.001 respectively).
- There is a significant positive correlation between **Peak T** (Aqualog and V-Lux) and Electrical **Conductivity** (p=0.0000295).

M2

- ***No significant*** correlations were found between any parameters.

2 Abisko, Sweden

Two catchments were investigated in Abisko National Park, North-West Sweden, *Abiskojakka* and *Mjellajokka* (Figure 2.1). The *Abiskojakka* catchment is approximately 600km^2 in size and is comprised of headwater that drain Meyers, tundra, mountainous and glaciated regions, moors and heathland, eventually forming large water bodies with wide rivers and streams. The *Mjellajokka* catchment is considerably smaller at 52km^2 and is comprised mainly of headwaters draining tundra regions down to dense broad-leaved forests (predominantly birch). These catchments provide examples of headwater streams, with stream sections both above and below the treeline, originating from the main Arctic sub-regions. This study provided the opportunity to characterise the AFOM characteristics, along with other physical, chemical and microbiological parameters, in a range of environments which experience little to no human-related perturbations at a local level. Ultimately work like this will lead to the development of robust representative datasets that inform the implementation of a fluorescence-based sensor for improved understanding of the relationship between AFOM characteristics and ecosystem health.

2.1 Aim

To better understand the physical, chemical, microbiological and fluorescence properties across natural gradients within oligotrophic, low dissolved organic carbon (DOC), and low productivity arctic aquatic systems. This consisted of the following objectives:

1. Characterise the fluorescence characteristics from a range of unperturbed streams representing different arctic freshwater environments
2. Obtain fluorescence sensing data from unperturbed aquatic environments that are oligotrophic in nature and exhibit low dissolved organic carbon
3. Understand changes in fluorescence characteristics across natural aquatic gradients

2.2 Sampling methodology

Monitoring was undertaken between the 9th and 12th of September, 2019. Sampling sites were identified in the *Abiskojakka* (A1 to A10) and *Mjellajokka* (A11 to A13) catchments. The sample sites chosen for both catchments are shown in Figure 1 below.

At each sampling site the following analyses was undertaken:

i. Conductivity, Dissolved Oxygen, Temperature and pH
ii. *In-situ* fluorescence sensing (V-Lux, Chelsea Technologies Ltd.)

In addition, water samples were collected so that the following analysis could be undertaken:

iii. Microbial analysis via flow cytometry (2mL in sterile microcentrifuge containing 10µL of 25% glutaraldehyde)

iv. Nutrient analysis (NO_3^-, PO_4^-) using ion chromatography (50mL filtered 0.2µm, sterile Falcon tubes)

v. Excitation and Emission Matrices, via fluorescence spectroscopy, HORIBA Aqualog (50mL filtered 0.2µm, sterile Falcon tubes

2.3 Results

All field sites within both the Abiskojakka and Mjellajokka catchments exhibit very low fluorescence intensities (Table 2.1, Figure 2.2). The data from site 2 displays the highest fluorescence intensity both visibly from the EEMs and also quantitatively when referring to already-assigned peak regions. In particular, the humic-like fluorescence region is particularly intense here. This sits in line with the site description of a slow-flowing and boggy stream which was high in both colour and suspended sediment, further supported by the *in-situ* absorbance and turbidity values (1.87 and 3.69 FNU respectively). In contrast, the lowest fluorescence intensity was observed in site A1, a glacial-fed river within the Abiskojakka catchment. The EEM from this site visibly contains little to no fluorescence, in addition to displaying the lowest QSU values for *in-situ* Peak C measurements with the V-Lux fluorimeter, and the second lowest for *in-situ* Peak T measurements.

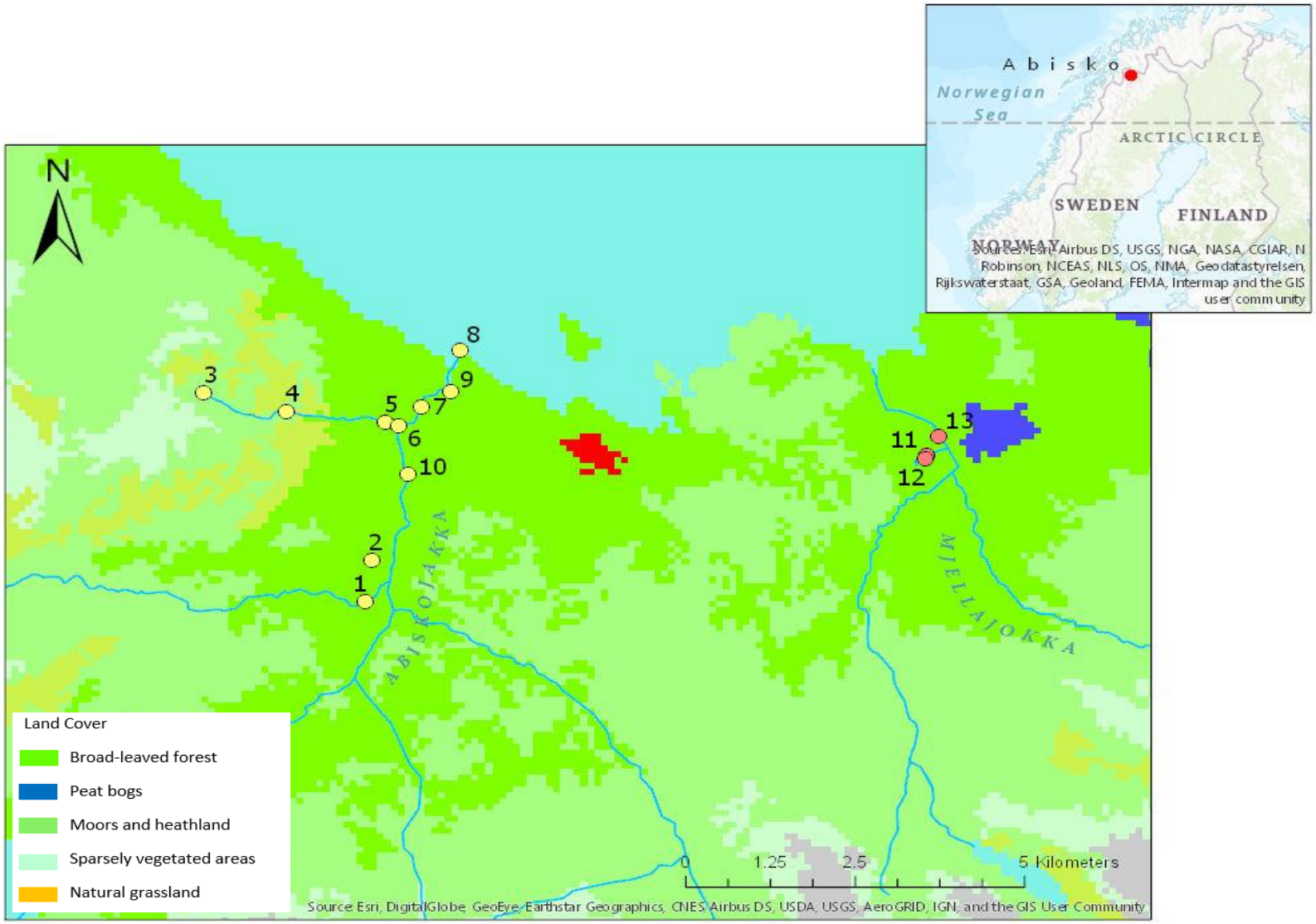

Figure 0.6 Map of sampling sites and land type in Abisko, Sweden

Table 2.1 Physico-chemical, biological and fluorescence data from sites A1-A13 in Abisko, Sweden

Site	Physical				Chemical			Biological	EEM AFOM Peaks (QSU)						*In situ* sensing measurements (V-Lux)				
	Site Comments	Temp (°C)	DO (mgL^{-1})	EC (µS)	pH	NO_3^- (mgL^{-1})	PO_4^- (mgL^{-1})	Bacterial (cells/mL)	T	M	B	C	$C+^1$	$C+^2$	Abs	Turb	Chl (QSU)	Peak T (QSU)	Peak C (QSU)
A1 *Abiskojakka*	Glacial fed, fast flowing	8.8	8.37	53.6	7.9	0.530	n/d	$5.66x10^5$	0	0	0	0	0	0.22	0.08	*	0.1	4.47	0.5
A2	Small order boggy stream , low flowing	8.7	7.32	259	7.99	0.357	n/d	$4.51x10^5$	0	0	0	0	0	0.56	1.87	3.69	0	6.45	0.84
A3	Headwater of catchment, high-altitude	6.2	7.66	79.1	7.75	0.673	n/d	$3.47x10^5$	0	0	0	0	0	0.22	0.14	*	2.7	6.62	10.89
A4	Fast-flowing, above treeline	7.6	7.93	105.4	8.14	0.439	n/d	$1.76x10^5$	0	0	0	0	0	0.12	0.08	*	0	4.05	2.19
A5	Low flow & shallow, after treeline	7.7	8.42	120.7	7.8	0.357	n/d	$1.57x10^5$	0	0	0	0	0	0.09	0.06	1.21	3.77	4.75	8.44
A6	Just after confluence with Abiskojakka	10.3	8.11	49.2	7.69	0.347	n/d	$5.77x10^5$	0	0	0	0	0	0.12	0.07	*	2.88	5.42	9.08
A7	Large canyon, very deep	10.5	8.25	45.7	7.73	0.367	n/d	$7.18x10^5$	0	0	0	0	0	0.13	0.07	*	2.09	5.4	10.08
A8	Wide, near mouth to lake	10.7	8.14	46.1	7.34	0.286	n/d	$1.1x10^6$	0	0	0	0	0	0.14	0.068	*	8.04	4.97	8.04
A9	Very rapid canyon, downstream of Turiststation	13.1	8.2	43.3	7.61	0.347	n/d	$6x10^5$	0	0	0	0	0	0.13	0.07	*	3.56	5.23	8.63
A10	Shallow & wide with dense forest either side	11.1	7.85	42.8	7.45	0.337	n/d	$8.98x10^5$	0	0	0	0	0	0.14	0.06	*	0	5.19	8.86
A11 Mjellajokka	Several hundred meters from groundwater emergence	7.9	7.57	50.6	7.57	0.541	n/d	$1.1x10^6$	0	0	0	0	0	0.35	0.08	*	0	6	17.09
A12	Meyer-draining	7.3	7.7	60	7.59	0.632	n/d	$3.91x10^6$	0	0	0	0	0	0.41	0.07	*	0	5.68	14.97
A13	Fast-flowing	9.8	8.02	51.3	7.57	0.439	n/d	$5.59x10^6$	0	0	0	0	0	0.37	0.08	*	0	7.29	22.35

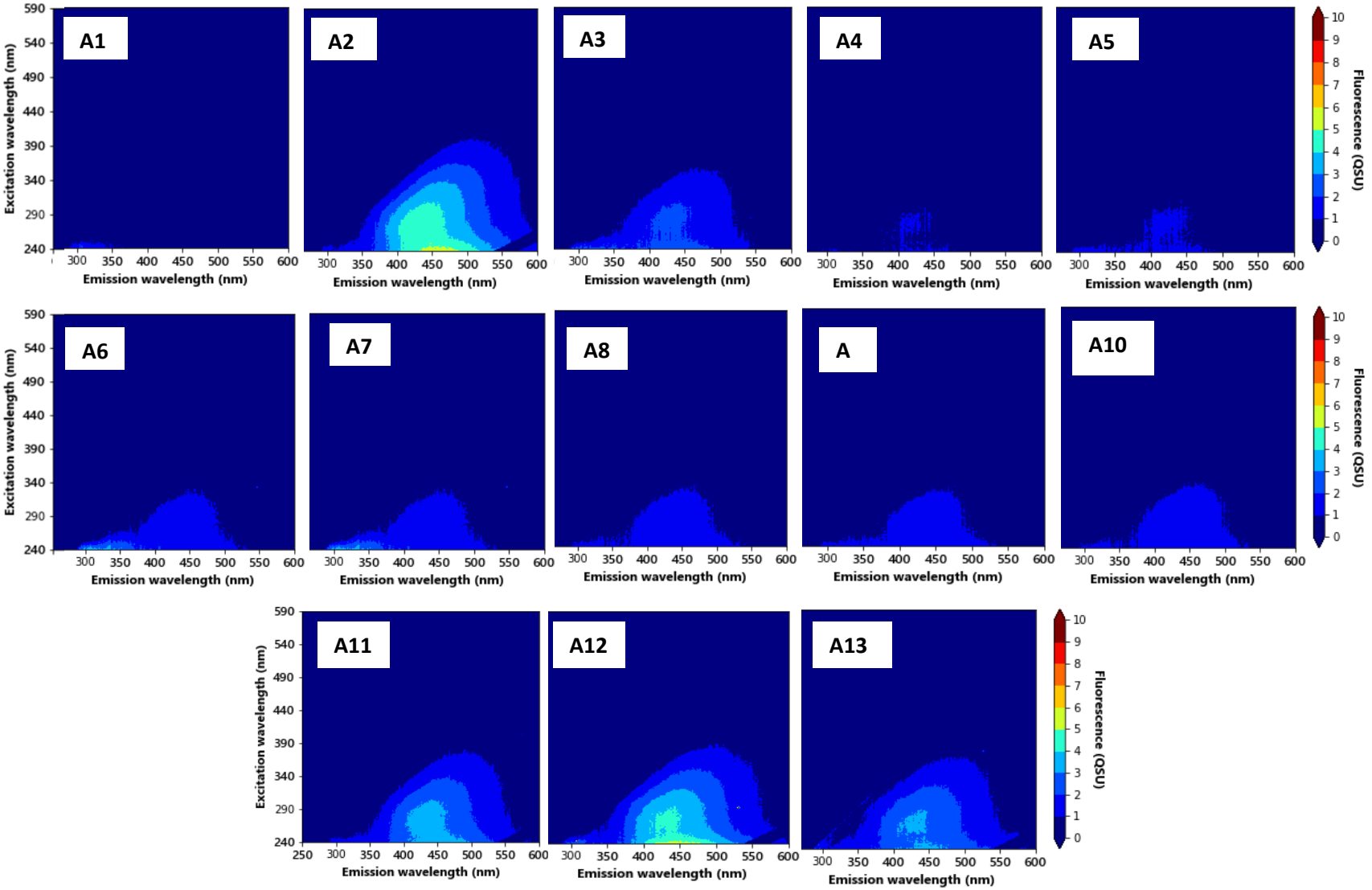

Figure 0.7 Excitation-Emission Matrices (EEMs) from sites A1-A13

Other than for Peak C^{+2} (the most optically similar to the Peak C channel in the V-Lux), all referenced peaks within the EEMs (including Peaks T and C) exhibit fluorescence intensity of 0 QSU. Whilst some caution should be advised due to time between sample collection and Aqualog analysis, all samples were analysed within 24 hours. Therefore, these results could lean towards support for the application of *in-situ* fluorescence sensing for characterising AFOM in intrinsically low-fluorescent environments such as these.

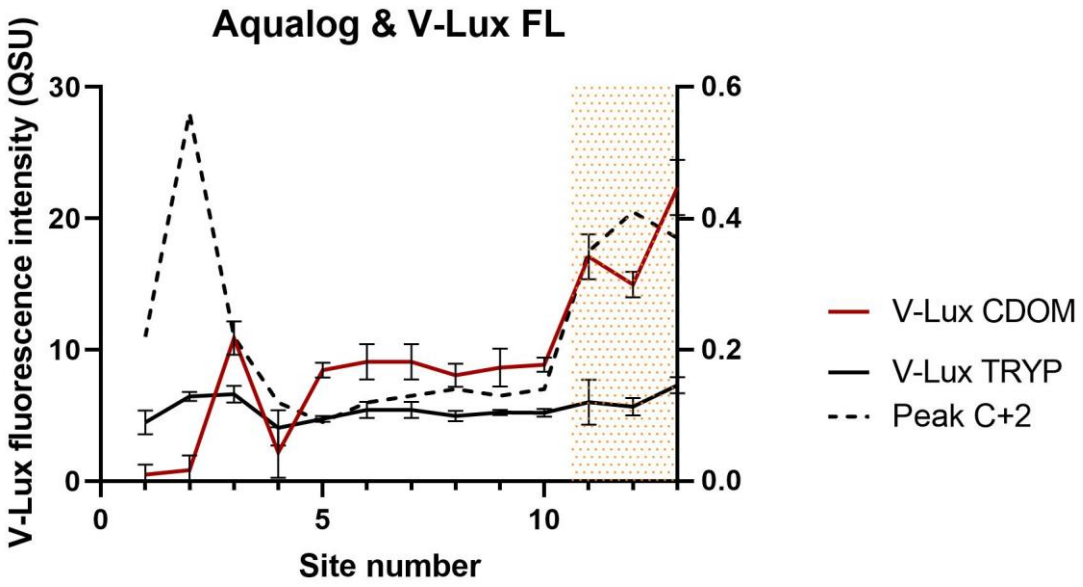

Figure 2.3 Fluorescence intensities from sites A1-A13 from Abiskojakka and Mjellajokka (shaded) catchments, showing Peaks C^{+2} from the Aqualog and in-situ measurements taken from the V-Lux fluorosensor

Whilst fluorescence intensity scales are different on each Y axis, Peak C^{+2} can be seen to mirror the general trend in fluorescence intensities expressed from the V-Lux *in-situ* sensing data. This is supported by the statistically significant correlation between significant correlations between V-Lux Peak T and Aqualog Peak C^{+2} (*p=0.015*).

2.3.1 Analysis of fluorescence against other parameters

A correlation matrix generated using data from all sampling sites within the Abiskojakka and Mjellajokka catchments found several significant correlations between the measured parameters (Figure 2.4). Out of the physico-chemical parameters that were measured, there was a significant positive correlation between conductivity and pH (*p=0.028*). A significant negative correlation can be seen between V-Lux Peak C fluorescence intensity and pH, potentially explained by an increase in

acidity associated with higher concentrations of humic and fulvic acids of allochthonous origin which are known to fluoresce in the Peak C region.

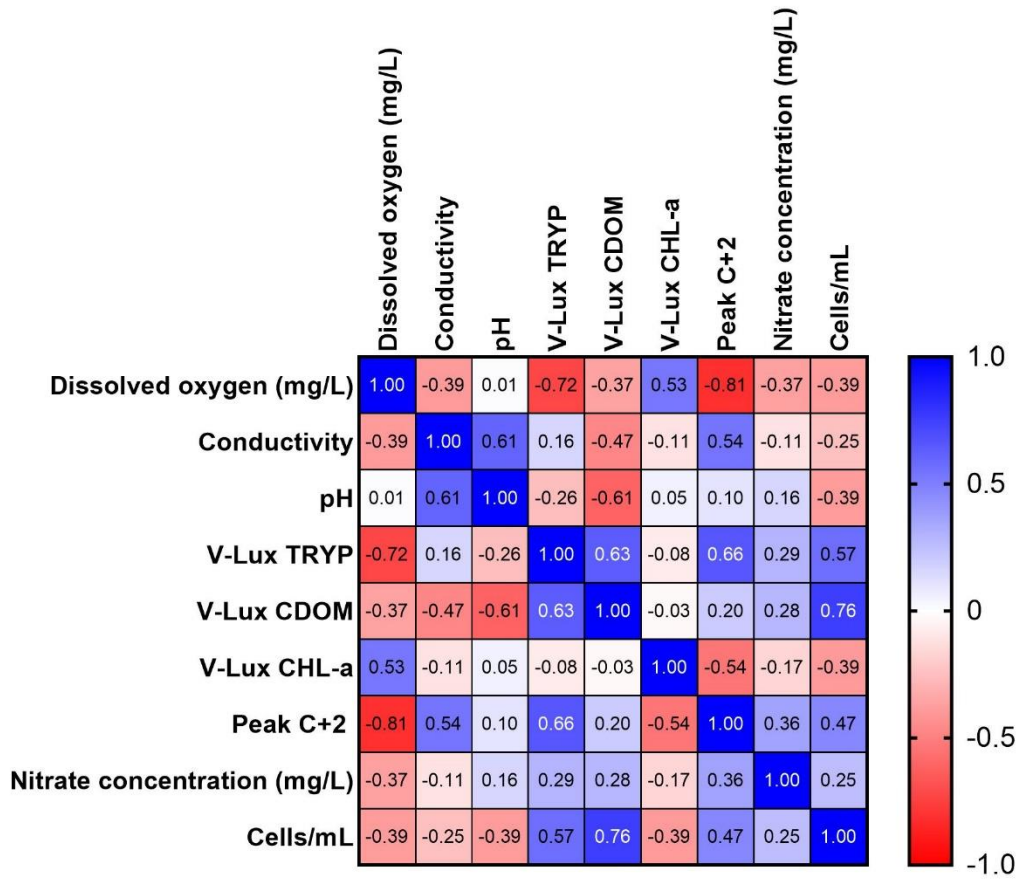

Figure 2.4. Correlation matrix of all measured parameters from sites A1-A13 (excluding parameters where no data was obtained)

A significant negative correlation was also found between dissolved oxygen concentration and Peak T measurements from the V-Lux ($p < 0.005$), and dissolved oxygen concentration and Peak C^{+2} fluorescence intensity measured with the Aqualog ($p < 0.001$). A negative correlation can also be seen between dissolved oxygen concentration and Peak C fluorescence intensity from the V-Lux, however this was not statistically significant.

Other significant correlations identified within the data include relationships between fluorescence intensity and microbial cell density . Both Peak C and Peak T from the V-Lux *in-situ* fluorescence data display positive correlations with cell density (*p=0.003* & *0.044* respectively). Interestingly, the correlation between Peak C and cell density is much stronger (*r=0.76,* Pearson r) than the correlation between Peak T and cell density (*r=0.57*). This is in disagreement with the conventional view that Peak T, or tryptophan-like, fluorescence intensity is autochthonous in origin and acts as a marker for microbial enumeration, or presence, and that Peak C is representative of allochthonous compounds from terrestrial origin exported from the surrounding catchment. The stronger correlation between Peak C and cell density than Peak T could suggest that the allochthonous carbon inputs from the surrounding catchment could be fuelling metabolic activity by stream microorganisms to a more significant degree than is currently considered. With recent publications having demonstrated the *in-situ* production of humic-like compounds by bacteria in laboratory-based model systems, it could be that there is a stronger relationship with Peak C fluorescence and microbial presence and/or activity than is currently known.

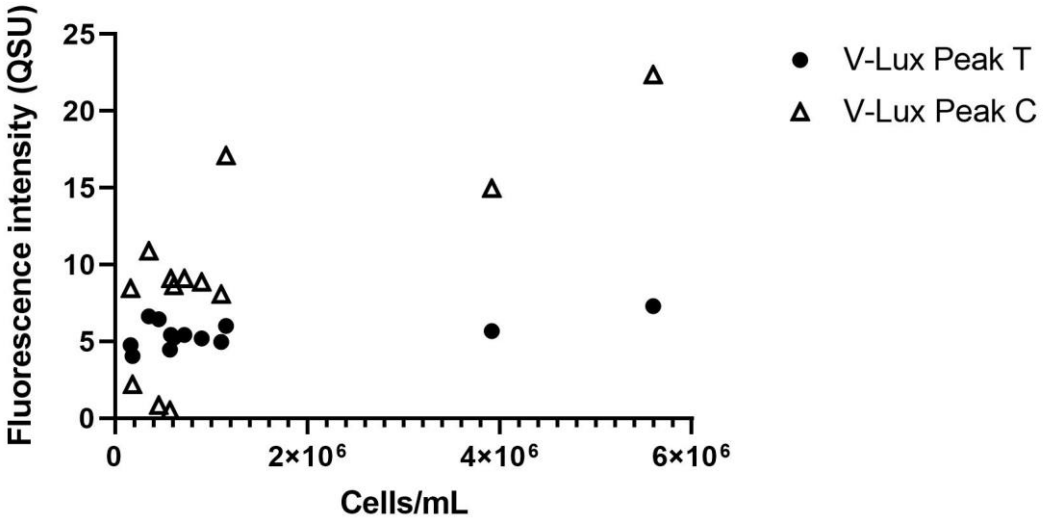

Figure 2.5. Fluorescence intensity collected by the V-Lux in-situ fluorosensor and cell density from all sampling sites within the Abiskojakka and Mjellajokka catchments

2.4 Tamar vs Abisko: Brief summary of fluorescence analysis

- Data from the Tamar Upper catchment exhibited significantly higher fluorescence intensities than data from Abisko catchments (Peak T fluorescence was on average **4.5 times lower** in Abisko sites, and on average Peak $C+^{2}$ was **235 times higher** in Tamar sites)

- This pattern is true for both Aqualog and V-Lux *in-situ* sensing data

- Both Tamar and Abisko exhibit higher Peak C fluorescence than Peak T fluorescence throughout most of the sites, other than sites A1 and A2 in Abisko where very little Peak C fluorescence is visible

- Whilst a fluorescence intensity of 0 QSU is seen from Aqualog Peak T data from Abisko, there is still some Peak T fluorescence seen from the V-Lux *in-situ* sensing data. A similar pattern is seen in Tamar sites, where higher Peak T is reported from the V-Lux than from the Aqualog. Due to the optical regions cropped by peak-picking the Aqualog data vs. the optical bandwidth reported from the V-Lux.

- Whilst there are strong positive correlations between nutrient concentrations and fluorescence intensities from the Tamar sites, nutrient analysis is yet to be undertaken on samples from the Abisko sites. Therefore, this warrants further investigation to determine whether there is a similar relationship between nutrients and fluorescence in what is assumed to be a very nutrient-limited, oligotrophic environment.

Site-specific data (Tamar)

S1 - Vognacott stream, River Deer

Site notes: This site was a small stream located near a road. The water body had very low flow. The sample was taken from underneath a road bridge.

Monitoring (M)	River	GPS location	Dissolved Oxygen (mg/L)	EC (µS)	pH	NO_3^- (mg/L)	PO_4^- (mg/L)	Flow data	Invertebrate data
1	Deer (tributary)	50.8501144, -4.3682892	3.45	222.4	7.17	2.7	n.d.	-	Bullhead, shrimp, cased caddisfly larvae, burrowing mayfly nymph, bloodworms, mosquito larvae
2			9.85	197	6.86	-	-	-	x

Monitoring (M)	V-Lux data					
	Channel	Tryptophan (QSU)	CDOM (QSU)	Chlorophyll a (QSU)	Absorbance	Turbidity
1	**Mean**	20.94	78.58	2.37	0.2	13.02
2		25.85	132.20	0	0.41	4.85
1	**Standard deviation**	1.63	6.60	0.19	0.01	18.72
2		0.24	0.71	0	0.001	1.10
1	**Coefficient of variance %**	7.79	8.40	8.09	5.63	143.76
2		0.93	0.54	0	0.39	22.80

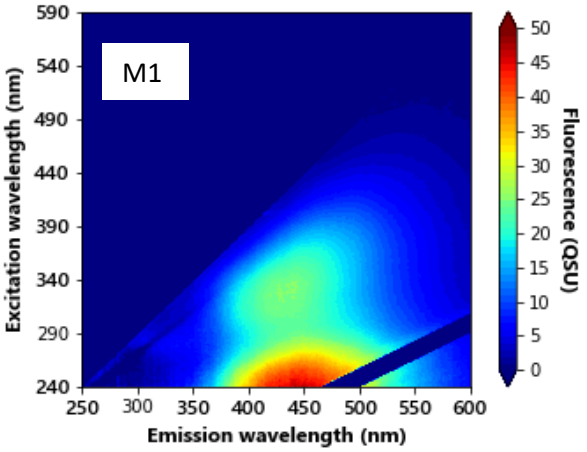

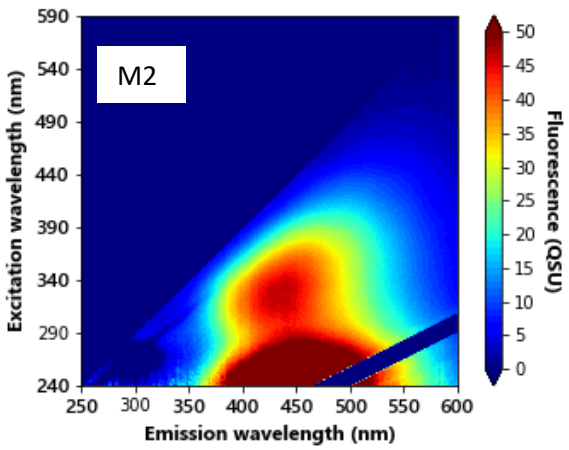

S2 – Chilsworthy, River Deer

Site notes: Sample taken just upstream from a small road bridge. Site is a small stream surrounded by hedgerows and farmland with some grazing.

Monitoring (M)	River	GPS location	Dissolved oxygen (mg/L)	EC (µS)	pH	Nitrate concentration (mg/L)	Phosphate concentration (mg/L)	Flow cytometry data	Invertebrate data
1	Deer	50.8373890, -4.3726082	9	250	7.45	3.335	not detected	n/a	n/a
2			10.25	186.1	7.31	n/a	n/a	n/a	n/a

Monitoring (M)	V-Lux data					
	Channel	Tryptophan (QSU)	CDOM (QSU)	Chlorophyll a (QSU)	Absorbance	Turbidity
1	Mean	23.63	93.02	3.19	0.29	3.67
1	Standard deviation	0.22	0.39	0.06	0.00	0.25
1	Coefficient of variance %	0.95	0.41	1.85	0.00	6.88

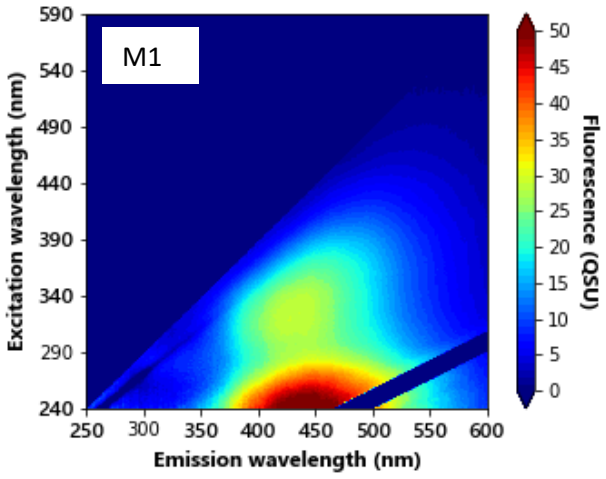

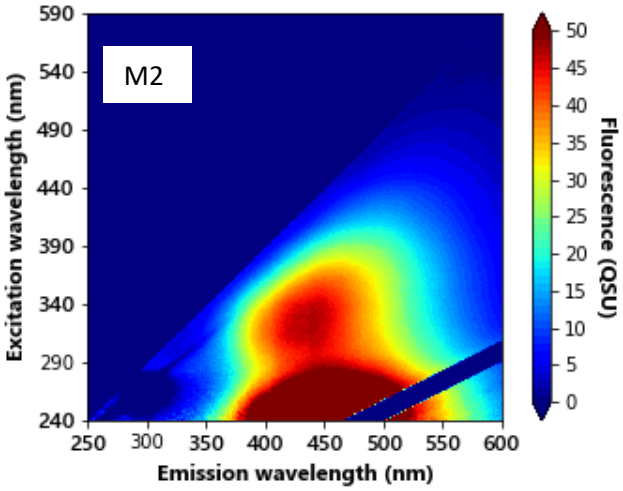

S3 – Gulliver Bridge, River Deer

Site notes: The site is around 2km upstream of Holsworthy and near a main road. The stream widens at this location and becomes very slow flowing. Surrounded by hedgerows and farmland, possibly grazing for some of the year.

Monitoring (M)	River	GPS location	Dissolved oxygen (mg/L)	EC (µS)	pH	Nitrate concentration (mg/L)	Phosphate concentration (mg/L)	Flow cytometry data	Invertebrate data
1	Deer	50.8213437, -4.3639155	9.1	257.8	6.81	6.26	0.098	n/a	n/a
2			10.32	190	7.41	n/a	n/a	n/a	n/a

Monitoring (M)	V-Lux data					
	Channel	Tryptophan (QSU)	CDOM (QSU)	Chlorophyll a (QSU)	Absorbance	Turbidity
1	Mean	23.90	90.15	2.19	0.44	19.54
2		25.85	132.20	0	0.41	4
1	Standard deviation	3.36	13.54	0.25	0.07	25.89
2		0.24	0.71	0	0.001	1.10
1	Coefficient of variance %	14.07	15.02	11.61	15.54	132.47
2		0.93	0.54	0	0.33	22.80

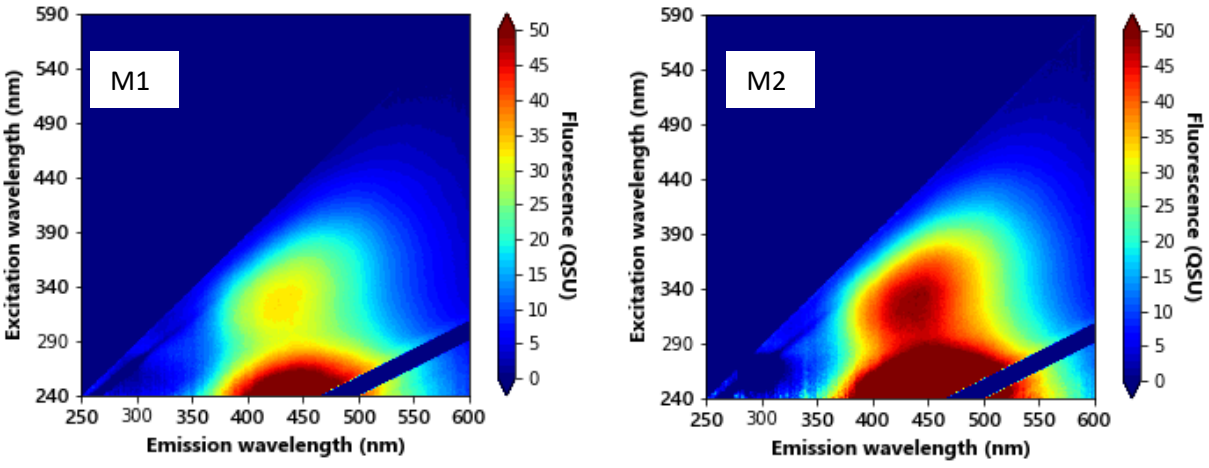

S4 - Lamerton Stream, River Deer

Site notes: Small tributary stream of the Deer. Sample taken from underneath road bridge near a small single-track road, surrounded by farmland and hedgerows. Approx. 1km upstream of Holsworthy.

Monitoring (M)	River	GPS location	Dissolved oxygen (mg/L)	EC (µS)	pH	Nitrate concentration (mg/L)	Phosphate concentration (mg/L)	Flow cytometry data	Invertebrate data
1	Deer (tributary)	50.8180036, -4.3421145	8.5	273.4	6.53	6.483	Not detected	n/a	n/a
2			9.93	194	7.43	n/a	n/a	n/a	n/a

Monitoring (M)	,					
	Channel	Tryptophan (QSU)	CDOM (QSU)	Chlorophyll a (QSU)	Absorbance	Turbidity
1	Mean	27.43	93.74	1.50	0.71	15.28
2		25.41	137.01	2.09	0.42	5.43
1	Standard deviation	0.30	0.85	0.07	0.01	2.08
2		0.21	0.38	1.77	0	0.43
1	Coefficient of variance %	1.11	0.90	4.34	0.71	13.60
2		0.83	0.28	85.57	0.20	7.92

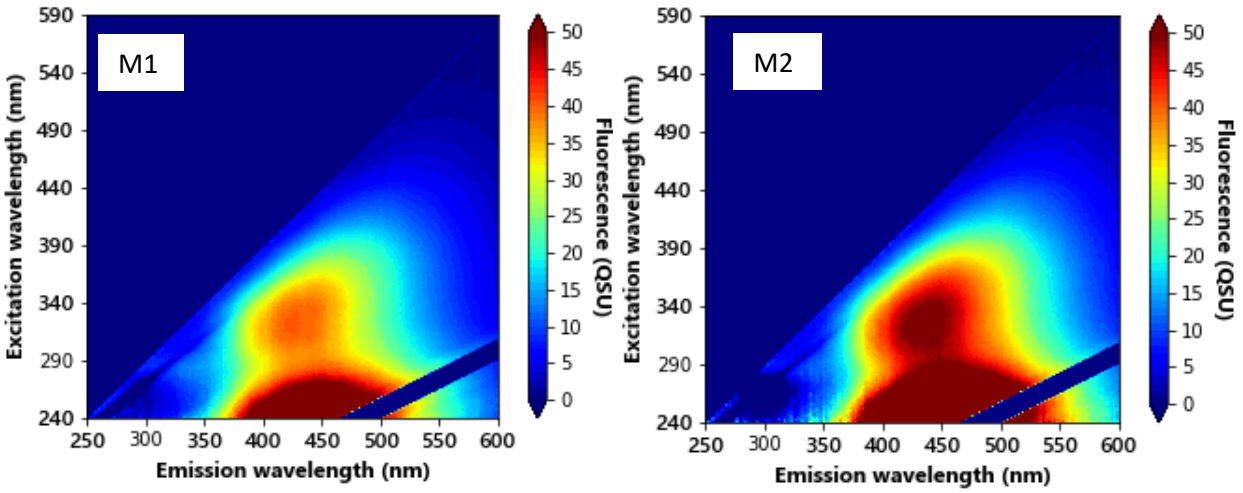

S5 – Deritton, River Deer

Site notes: Main river Deer. The site is surrounded by woodland and some farmland. It is very close (downstream) to the Holsworthy sewage treatment plant.

Monitoring (M)	River	GPS location	Dissolved oxygen (mg/L)	EC (µS)	pH	Nitrate concentration (mg/L)	Phosphate concentration (mg/L)	Flow cytometry data	Invertebrate data
1	Deer	50.80098, -4.363890	8.84	276.5	6.5	14.186	1.414	n/a	Shrimp, cased caddisfly larvae, bloodworms
2			10.2	196	7.6	n/a	n/a	n/a	n/a

Monitoring (M)	V-Lux data					
	Channel	Tryptophan (QSU)	CDOM (QSU)	Chlorophyll a (QSU)	Absorbance	Turbidity
1	Mean	28.63	103	0	0.40	12.19
1	Standard deviation	0.24	0.30	0	0.00	0.54
1	Coefficient of variance %	0.84	0.29	0	0.41	4.46

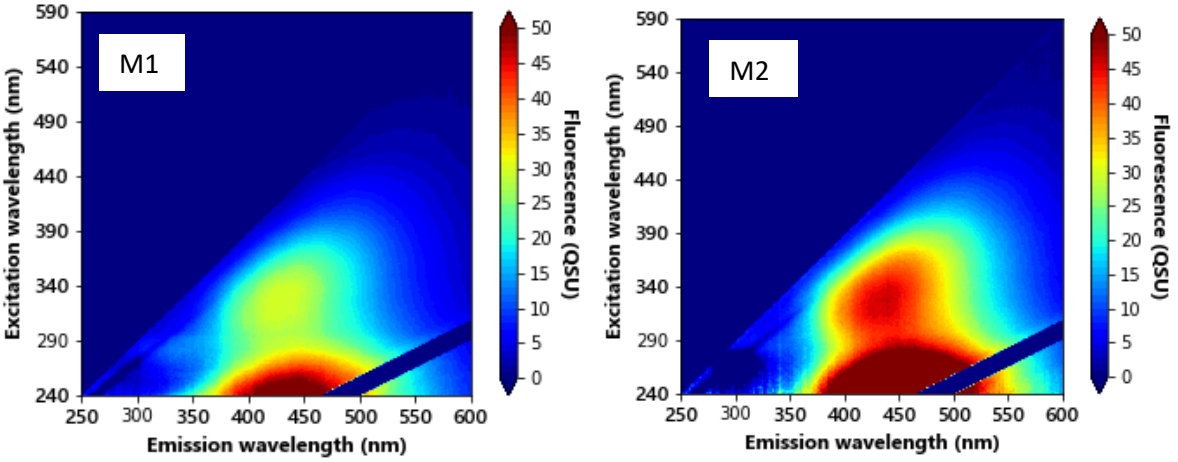

S6 – Winscott Bridge, River Deer

Site notes: Sample taken from underneath road bridge. Site surrounded by trees and hedgerows, some farmland.

Monitoring (M)	River	GPS location	Dissolved oxygen (mg/L)	EC (µS)	pH	Nitrate concentration (mg/L)	Phosphate concentration (mg/L)	Flow cytometry data	Invertebrate data
1	Deer	50.773109, -4.37606	9.16	280.2	6.35	11.939	1.175	n/a	n/a
2			10.34	194	7.4	n/a	n/a	n/a	n/a

Monitoring (M)	V-Lux data					
	Channel	Tryptophan (QSU)	CDOM (QSU)	Chlorophyll a (QSU)	Absorbance	Turbidity
1	Mean	31.38	99.32	2.06	0.24	4.03
2		26.43	134.26	4.70	0.41	16.00
1	Standard deviation	0.24	0.44	1.07	0.00	0.83
2		0.22	0.47	0.06	0.00	0.37
1	Coefficient of variance %	0.76	0.44	51.93	0.63	20.56
2		0.84	0.35	1.43	0.11	2.35

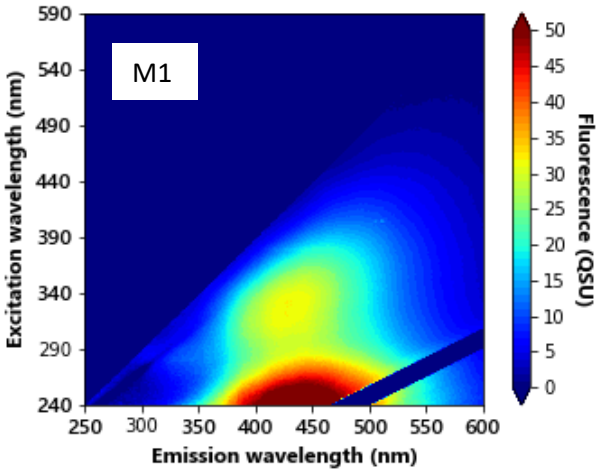

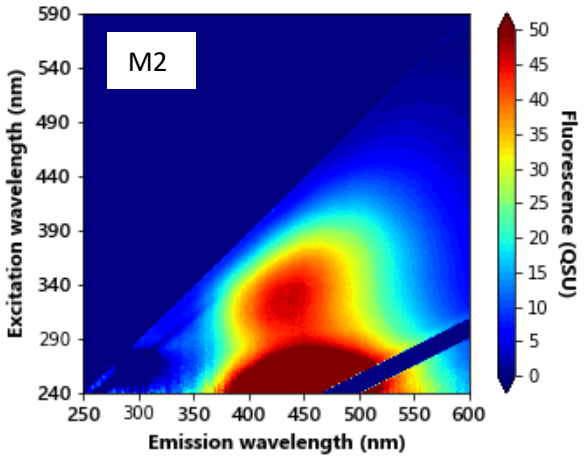

S7 – Deer & Tamar confluence, River Claw

Site notes: Sample was taken from approximately 50m upstream of the confluence of the river Deer with the river Tamar. Sample taken from road bridge.

Monitoring (M)	River	GPS location	Dissolved oxygen (mg/L)	EC (µS)	pH	Nitrate concentration (mg/L)	Phosphate concentration (mg/L)	Flow cytometry data	Invertebrate data
1	Deer	50.751638, -4.383582	9.42	275	7.66	11.973	0.896	n/a	n/a

Monitoring (M)	V-Lux data					
	Channel	Tryptophan (QSU)	CDOM (QSU)	Chlorophyll a (QSU)	Absorbance	Turbidity
1	Mean	30.10	100.78	2.94	0.30	12.29
1	Standard deviation	0.24	0.48	0.18	0.00	2.03
1	Coefficient of variance %	0.78	0.47	6.24	0.17	16.52

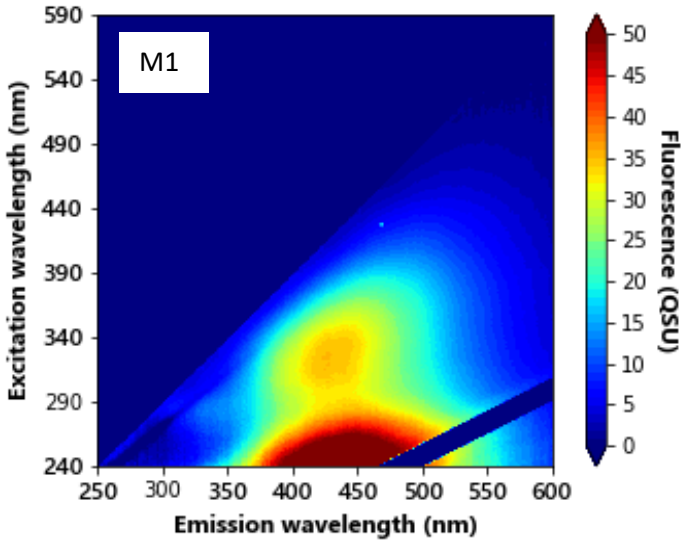

S8 – Higher Claw Bridge, River Claw

Site notes: Sample taken from near a small road bridge. River is small and shallow and rocky here. Surrounded by lots of deciduous woodland and some agricultural land.

Monitoring (M)	River	GPS location	Dissolved oxygen (mg/L)	EC (µS)	pH	Nitrate concentration (mg/L)	Phosphate concentration (mg/L)	Flow cytometry data	Invertebrate data
1	Claw	50.798771, -4.286392	9.06	208	7.58	2.571	Not detected	n/a	n/a

Monitoring (M)	V-Lux data					
	Channel	**Tryptophan (QSU)**	**CDOM (QSU)**	**Chlorophyll a (QSU)**	**Absorbance**	**Turbidity**
1	**Mean**	19.42	89.65	0.00	0.59	12.44
1	**Standard deviation**	0.38	1.88	0.00	0.02	7.55
1	**Coefficient of variance %**	1.95	2.10		2.57	60.72

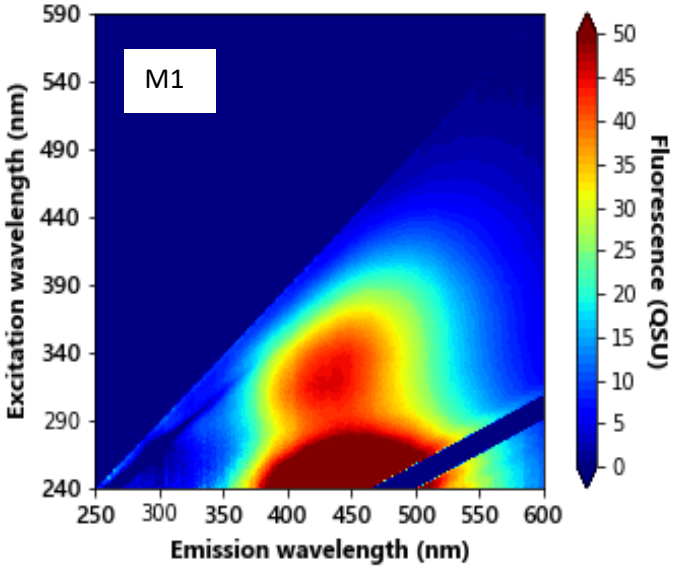

S9 – Claw Bridge, River Claw

Site notes: Sample taken from near a small road bridge. Surrounded by large expanse of fields (possibly grazing) and some hedgerows and woodland

Monitoring (M)	River	GPS location	Dissolved oxygen (mg/L)	EC (µS)	pH	Nitrate concentration (mg/L)	Phosphate concentration (mg/L)	Flow cytometry data	Invertebrate data
1	Claw	50.4755.6, -4.1711.0	9.75	206	7.55	2.606	Not detected	n/a	Dragonfly nymph, cased caddisfly, bullhead, damselfly nymph

Monitoring (M)	V-Lux data					
	Channel	Tryptophan (QSU)	CDOM (QSU)	Chlorophyll a (QSU)	Absorbance	Turbidity
1	**Mean**	18.77	89.53	0.00	0.41	7.40
1	**Standard deviation**	0.22	0.59	0.00	0.00	0.48
1	**Coefficient of variance %**	1.16	0.66		0.13	6.54

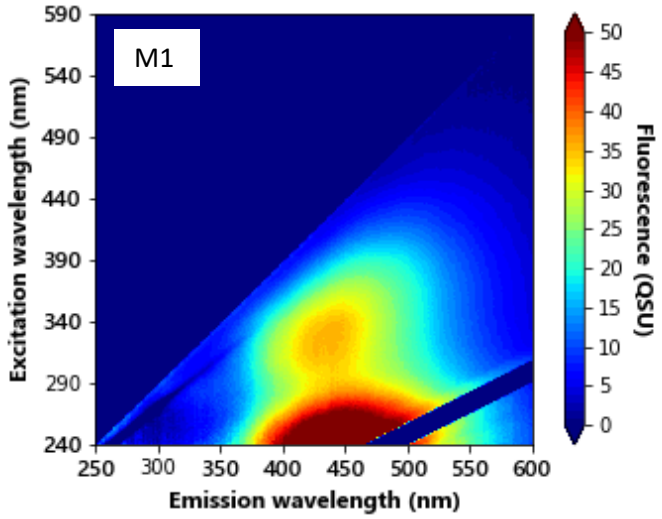

S10 – Clawton, River Claw

Site notes: Just upstream from Clawton village. River is wide and slow-flowing here. Mostly surrounded by hedgerows and grazing fields. Sample taken from bridge of relatively busy road.

Monitoring (M)	River	GPS location	Dissolved oxygen (mg/L)	EC (µS)	pH	Nitrate concentration (mg/L)	Phosphate concentration (mg/L)	Flow cytometry data	Invertebrate data
1	Claw	50.769640, -4.338439	9.18	219	6.9	3.901	Not detected	n/a	n/a

Monitoring (M)	V-Lux data					
	Channel	Tryptophan (QSU)	CDOM (QSU)	Chlorophyll a (QSU)	Absorbance	Turbidity
1	Mean	22.54	100.27	1.36	0.41	10.58
1	Standard deviation	0.30	1.83	0.71	0.03	6.82
1	Coefficient of variance %	0.26	0.37	10.50	1.41	12.88

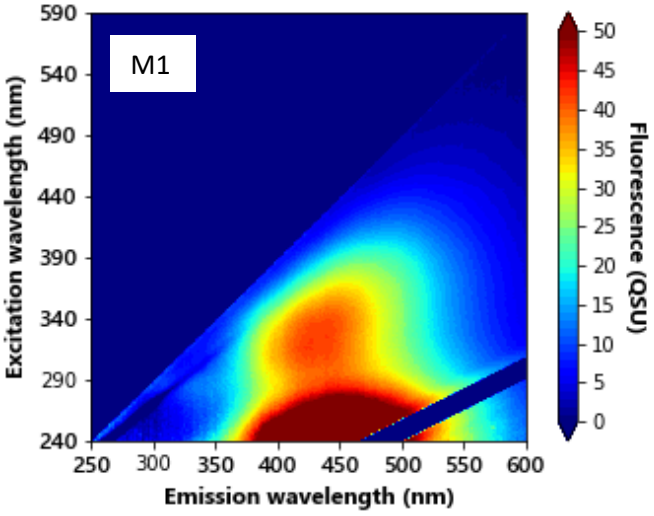

S11 – Northwood (Tetcott), River Deer

Site notes: Approx. 200m upstream of Claw & Tamar confluence. Sample taken from river around 50m from the road. The river was flanked on one side by heavy grazing and heavy runoff from the field, and dense woodland on the other.

Monitoring (M)	River	GPS location	Dissolved oxygen (mg/L)	EC (µS)	pH	Nitrate concentration (mg/L)	Phosphate concentration (mg/L)	Flow cytometry data	Invertebrate data
1	Claw	50.747805, -4.370528	9	220	7.26	4.527	Not detected	n/a	Burrowing mayfly nymph, shrimp, leech, stonefly nymph, caseless caddis

Monitoring (M)	V-Lux data					
	Channel	Tryptophan (QSU)	CDOM (QSU)	Chlorophyll a (QSU)	Absorbance	Turbidity
1	Mean	22.57	100.54	1.02	0.40	9.83
1	Standard deviation	0.28	1.66	0.84	0.02	5.98
1	Coefficient of variance %	1.25	1.65	82.60	6.72	60.85

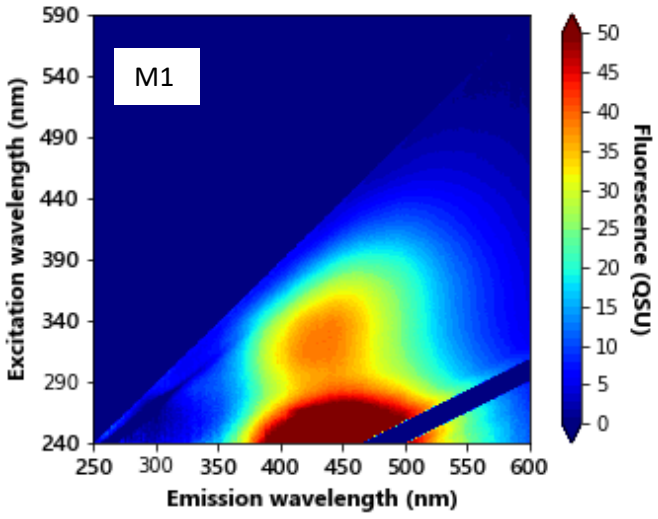

Appendix 2 – Site Specific Data (Abisko)

A1 – Kavsajakka/Gorsajohka

Site notes: Glacial-fed river. Very fast-flowing. Both sides of the bank fairly steep, and one bank covered by birch forest. Riverbed very rocky and very little organic material visible.

River	GPS location	Dissolved oxygen (mg/L)	Conductivity (µS)	pH	Nitrate concentration (mg/L)	Phosphate concentration (mg/L)	Flow cytometry data	Invertebrate data
Kavsajakka/Gorsajohka (Abiskojakka catchment)	681948.9 18.4438.8	8.37	53.6	7.9	n/a	n/a	n/a	n/a

V-Lux data					
Channel	Tryptophan (QSU)	CDOM (QSU)	Chlorophyll a (QSU)	Absorbance	Turbidity
Mean	4.47	0.50	0.10	0.08	-8.46
Standard deviation	0.90	0.74	0.51	0.13	3.99
Coefficient of variance %	20.27	147.91	504.91	157.07	-47.19

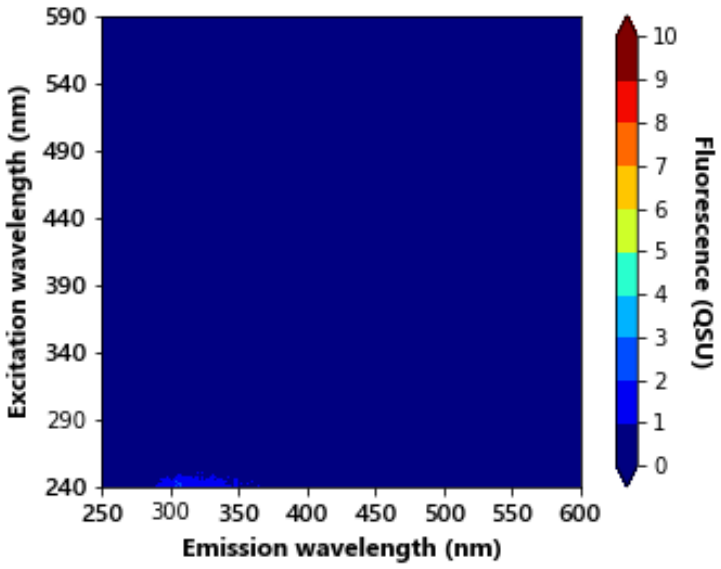

A2 – Small-order boggy stream

Site notes: Very small-order boggy stream. Slow-flowing.

River	GPS location	Dissolved oxygen (mg/L)	Conductivity (µS)	pH	Nitrate concentration (mg/L)	Phosphate concentration (mg/L)	Flow cytometry data	Invertebrate data
Unknown (Abiskojakka catchment)	682010.9 18.4457.3	7.32	259	7.99	n/a	n/a	n/a	n/a

V-Lux data					
Channel	Tryptophan (QSU)	CDOM (QSU)	Chlorophyll a (QSU)	Absorbance	Turbidity
Mean	6.45	0.84	0	1.87	3.69
Standard deviation	0.35	1.12	0	0.00	0.02
Coefficient of variance %	5.50	133.44	0	0.31	0.69

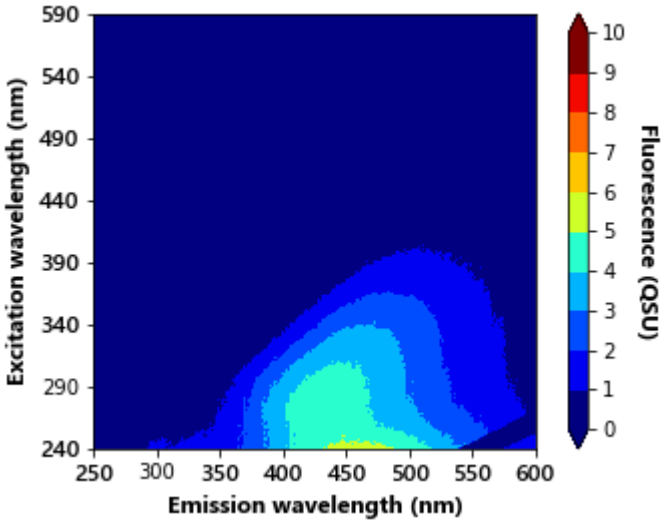

A3 – Njulla/Sloahtta

Site notes – headstream of Rihtonjira river. Sample taken from near a small lake at a plateau in a col between Njulla and Sloahtta mountains. Far above the treeline. Some marshy/boggy land surrounding the lake. Shallow and slow-flowing.

River	GPS location	Dissolved oxygen (mg/L)	Conductivity (µS)	pH	Nitrate concentration (mg/L)	Phosphate concentration (mg/L)	Flow cytometry data	Invertebrate data
Rihtonjira (headstream)	68.21528 18.41376	7.66	79.1	7.75	n/a	n/a	n/a	n/a

V-Lux data					
Channel	Tryptophan (QSU)	CDOM (QSU)	Chlorophyll a (QSU)	Absorbance	Turbidity
Mean	6.62	10.89	2.70	0.14	-0.60
Standard deviation	0.63	1.28	0.59	0.00	0.38
Coefficient of variance %	9.62	11.83	21.91	1.28	-63.38

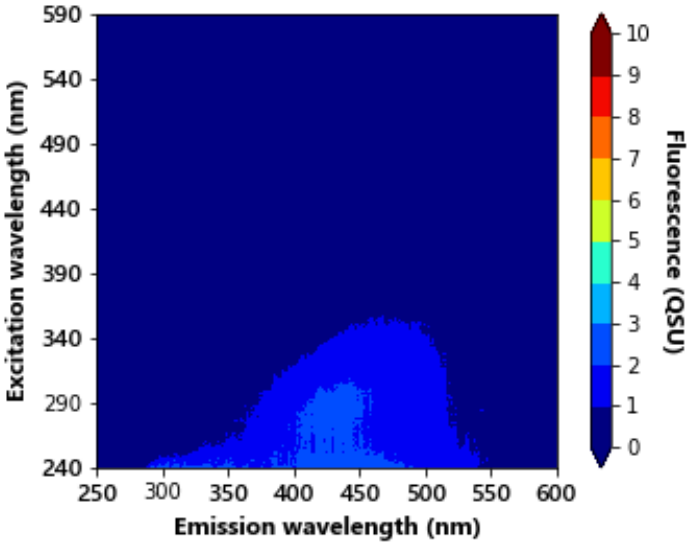

A4 – Aurorastation

Site notes – Steep hillside. Water is visibly clear and very fast-flowing. Rocky riverbed. Still far above the treeline. Shallow stream, approx. 2 meters wide.

River	GPS location	Dissolved oxygen (mg/L)	Conductivity (µS)	pH	Nitrate concentration (mg/L)	Phosphate concentration (mg/L)	Flow cytometry data	Invertebrate data
Rihtonjira (mid)	68.3600903, 18.7271022	7.93	105.4	8.14	n/a	n/a	n/a	n/a

V-Lux data					
Channel	Tryptophan (QSU)	CDOM (QSU)	Chlorophyll a (QSU)	Absorbance	Turbidity
Mean	4.05	2.19	0	0.08	-5.18
Standard deviation	1.35	1.93	0	0.18	5.37
Coefficient of variance %	33.47	88.36	0	214.07	-103.58

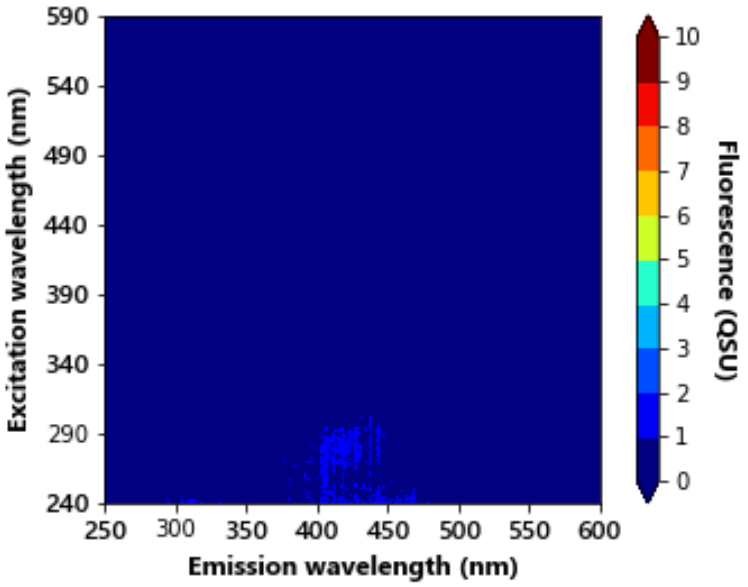

A5 – Rihtonjira lower

Site notes – slow-flowing and shallow. River bed very rocky with some debris from surrounding forest. Just below the treeline.

River	GPS location	Dissolved oxygen (mg/L)	Conductivity (µS)	pH	Nitrate concentration (mg/L)	Phosphate concentration (mg/L)	Flow cytometry data	Invertebrate data
Rihtonjira (lower)	68.3567345 18.7614221	8.42	120.7	7.8	n/a	n/a	n/a	n/a

V-Lux data					
Channel	Tryptophan (QSU)	CDOM (QSU)	Chlorophyll a (QSU)	Absorbance	Turbidity
Mean	4.75	8.44	3.77	0.066	1.21
Standard deviation	0.24	0.58	0.39	0.00	2.98
Coefficient of variance %	5.15	6.97	10.51	1.62	244.35

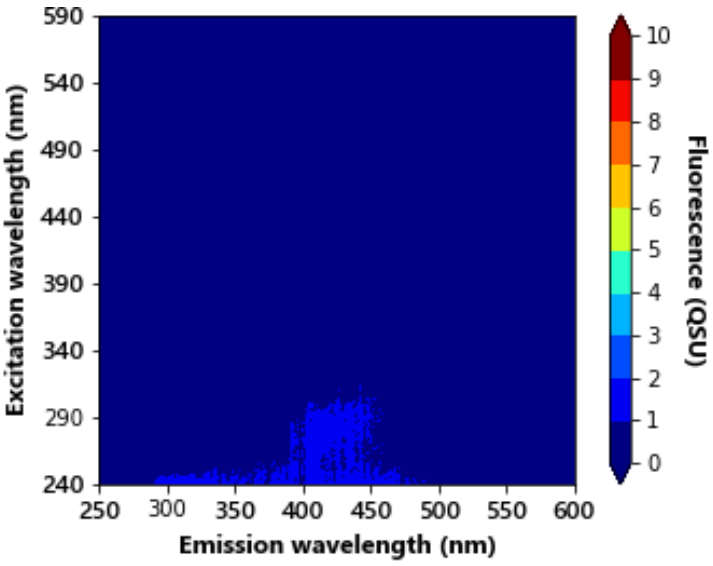

A6 – Abiskojakka/Rihtonjira confluence

Site notes – Sample taken just after confluence of both rivers. Just upstream of the confluence, Rihtonjira goes underground as it is a seasonally dry stream in some places. Site was very fast-flowing and wide with a rocky riverbed.

River	GPS location	Dissolved oxygen (mg/L)	Conductivity (µS)	pH	Nitrate concentration (mg/L)	Phosphate concentration (mg/L)	Flow cytometry data	Invertebrate data
Rihtonjira/Abiskojakka (confluence)	68.21223 18.46026	8.11	49.2	7.69	n/a	n/a	n/a	n/a

V-Lux data					
Channel	Tryptophan (QSU)	CDOM (QSU)	Chlorophyll a (QSU)	Absorbance	Turbidity
Mean	5.42	9.08	2.88	0.07	-5.18
Standard deviation	-0.61	-1.34	-1.74	-0.00	-2.12
Coefficient of variance %	-11.40	-14.81	-60.43	-3.65	40.93

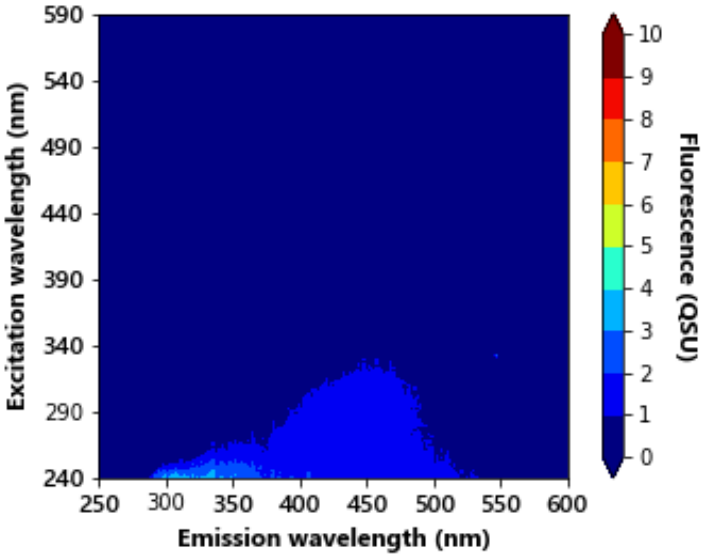

A7 – Abiskojakka lower

Site notes – Sample taken from large canyon that is very deep. Probably very little terrestrial runoff due to steep-sided rocky canyon.

River	GPS location	Dissolved oxygen (mg/L)	Conductivity (µS)	pH	Nitrate concentration (mg/L)	Phosphate concentration (mg/L)	Flow cytometry data	Invertebrate data
Abiskojakka lower	68.21242 18.46176	8.25	45.7	7.73	n/a	n/a	n/a	n/a

V-Lux data					
Channel	Tryptophan (QSU)	CDOM (QSU)	Chlorophyll a (QSU)	Absorbance	Turbidity
Mean	5.42	9.08	2.88	0.07	-5.18
Standard deviation	-0.61	-1.34	-1.74	-0.00	-2.12
Coefficient of variance %	-11.40	-14.81	-60.43	-3.65	40.93

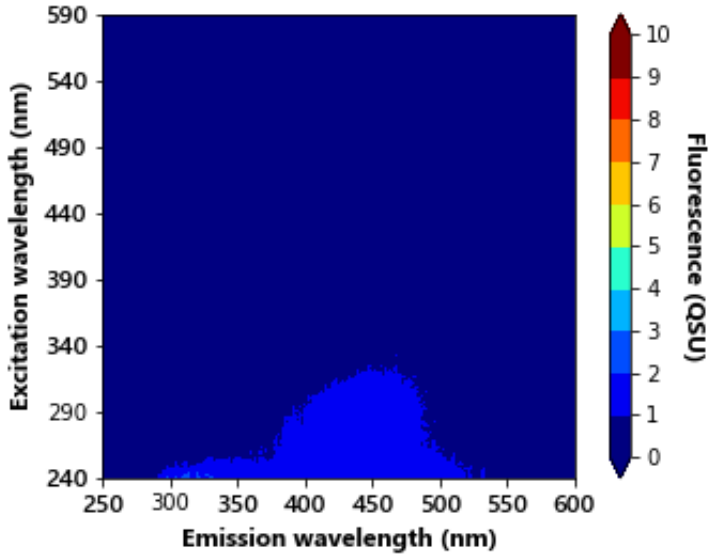

A8 – Abiskojakka mouth

Site notes: Sample taken from near the mouth of Abiskojakka river near Tornetrask lake. Road and Turiststation approx. 500m upstream of here.

River	GPS location	Dissolved oxygen (mg/L)	Conductivity (µS)	pH	Nitrate concentration (mg/L)	Phosphate concentration (mg/L)	Flow cytometry data	Invertebrate data
Abiskojakka mouth	68.366385, 18.791937	8.14	46.1	7.34	n/a	n/a	n/a	n/a

V-Lux data					
Channel	Tryptophan (QSU)	CDOM (QSU)	Chlorophyll a (QSU)	Absorbance	Turbidity
Mean	4.97	8.04	0	0.068	-5.58
Standard deviation	0.41	0.89	0	0.00	0.95
Coefficient of variance %	8.28	11.03	0	1.10	-17.08

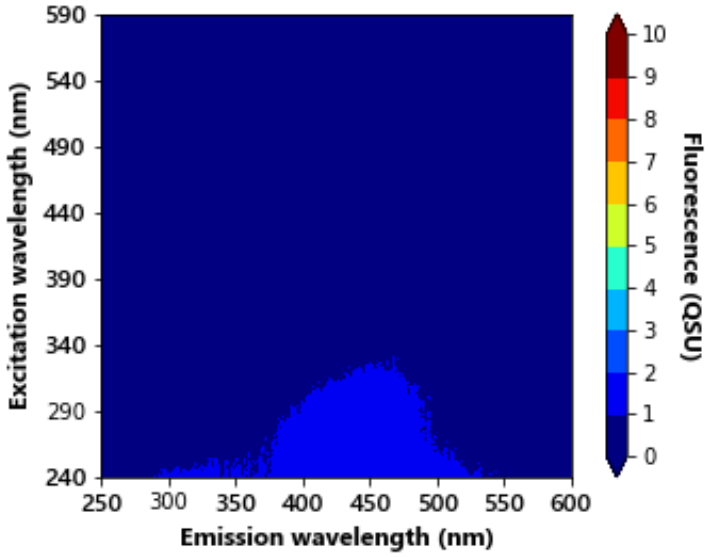

A9 – downstream from Turiststation

Site notes – Very rapid and rocky canyon. Sample taken just downstream from Turiststation with busy main road. Lots of well-trodden paths around.

River	GPS location	Dissolved oxygen (mg/L)	Conductivity (µS)	pH	Nitrate concentration (mg/L)	Phosphate concentration (mg/L)	Flow cytometry data	Invertebrate data
Abiskojakka	68.360361, 18.7863297	8.2	43.3	7.61	n/a	n/a	n/a	n/a

V-Lux data					
Channel	Tryptophan (QSU)	CDOM (QSU)	Chlorophyll a (QSU)	Absorbance	Turbidity
Mean	5.23	8.63	3.56	0.07	-1.98
Standard deviation	0.20	1.45	1.94	0.00	3.58
Coefficient of variance %	3.98	16.87	54.48	3.21	-180.58

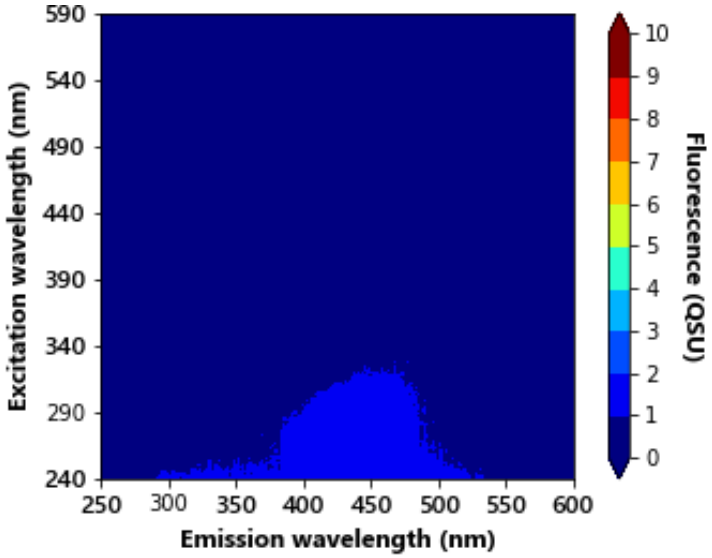

A10 – Abiskojakka upstream of Rihtonjirra confluence

Site notes – River very wide, slow and shallow here. No longer canyon-like. Dense birch forest on either side and some heavily trodden paths.

River	GPS location	Dissolved oxygen (mg/L)	Conductivity (µS)	pH	Nitrate concentration (mg/L)	Phosphate concentration (mg/L)	Flow cytometry data	Invertebrate data
Abiskojakka	68.20550, 18.45590	7.85	42.8	7.45	n/a	n/a	n/a	n/a

V-Lux data					
Channel	Tryptophan (QSU)	CDOM (QSU)	Chlorophyll a (QSU)	Absorbance	Turbidity
Mean	5.19	8.86	0	0.06	-6.50
Standard deviation	0.31	0.55	0	0.00	0.70
Coefficient of variance %	5.99	6.28	0	0.97	-10.86

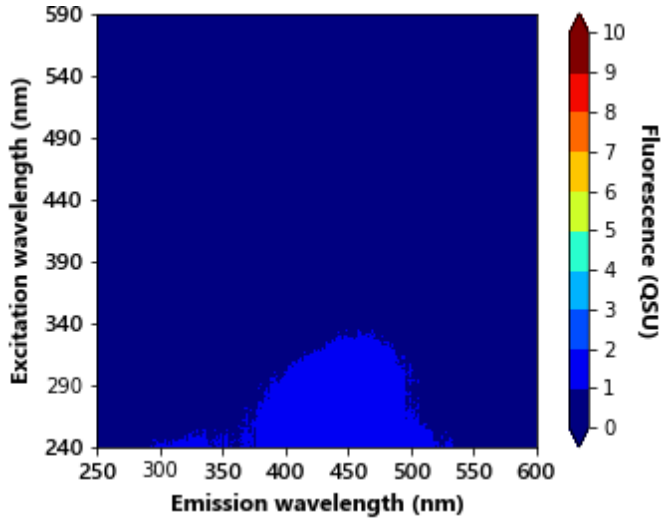

A11 – Birch stream forest

Site notes – visibly more brown than previous sites within the Abiskojakka catchment. Surrounded by dense birch forest. Only several hundred meters after emerging from groundwater.

River	GPS location	Dissolved oxygen (mg/L)	Conductivity (µS)	pH	Nitrate concentration (mg/L)	Phosphate concentration (mg/L)	Flow cytometry data	Invertebrate data
Mjellajoka catchment		7.44	50.6	7.57	n/a	n/a	n/a	n/a

V-Lux data					
Channel	Tryptophan (QSU)	CDOM (QSU)	Chlorophyll a (QSU)	Absorbance	Turbidity
Mean	6.00	17.09	0	-6.47	0.08
Standard deviation	1.71	1.71	0	0.45	0.00
Coefficient of variance %	11.01	10.01	0	-7.07	0.34

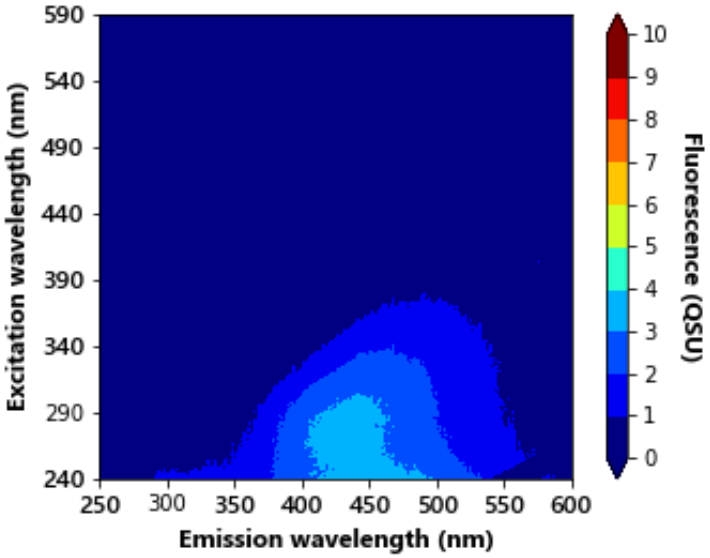

A12 – Birch stream forest (meyer-draining)

Site notes – this stream directly drains from Meyers further upstream so organic load expected to be very high. The site has a high temperature threshold to change and remains cool during summer and relatively warm during winter.

River	GPS location	Dissolved oxygen (mg/L)	Conductivity (µS)	pH	Nitrate concentration (mg/L)	Phosphate concentration (mg/L)	Flow cytometry data	Invertebrate data
Mjellajoka catchment	68.20313 18.56587	7.7	60	7.59	n/a	n/a	n/a	n/a

V-Lux data					
Channel	Tryptophan (QSU)	CDOM (QSU)	Chlorophyll a (QSU)	Absorbance	Turbidity
Mean	5.68	14.97	0	-10.42	0.07
Standard deviation	0.67	0.98	0	0.46	0.00
Coefficient of variance %	11.92	6.58	0	-4.43	0.44

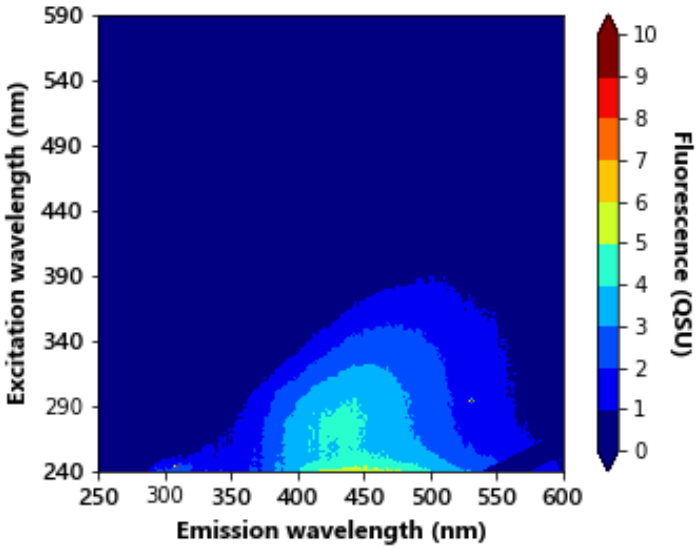

A13 – Main stream draining Mjellajoka

Site notes – Sample taken from nearby main road. This is a large, fast-flowing stream which is the main steam draining this catchment. Relatively shallow. Thick biofilm formation on riverbed.

River	GPS location	Dissolved oxygen (mg/L)	Conductivity (µS)	pH	Nitrate concentration (mg/L)	Phosphate concentration (mg/L)	Flow cytometry data	Invertebrate data
Mjellajoka catchment	68.345231, 18.9550699	7.57	51.3	7.57	n/a	n/a	n/a	n/a

V-Lux data					
Channel	Tryptophan (QSU)	CDOM (QSU)	Chlorophyll a (QSU)	Absorbance	Turbidity
Mean	7.29	22.35	0	-7.21	0.08
Standard deviation	0.61	2.11	0	4.12	0.00
Coefficient of variance %	8.42	9.47	0	-57.18	3.528